

Bone marrow endothelial transmigration of prostate carcinoma cells

A thesis submitted to the University of Manchester for the degree of
PhD Oncology
in the Faculty of Medical and Human Sciences

2008

Jo-An Roulson

School of Medicine

ProQuest Number: U504484

All rights reserved

INFORMATION TO ALL USERS

The quality of this reproduction is dependent upon the quality of the copy submitted.

In the unlikely event that the author did not send a complete manuscript and there are missing pages, these will be noted. Also, if material had to be removed, a note will indicate the deletion.



ProQuest U504484

Published by ProQuest LLC (2019). Copyright of the Dissertation is held by the Author.

All rights reserved.

This work is protected against unauthorized copying under Title 17, United States Code
Microform Edition © ProQuest LLC.

ProQuest LLC.
789 East Eisenhower Parkway
P.O. Box 1346
Ann Arbor, MI 48106 – 1346

(EUW25)

Th 32534



THE
JOHN FRYL
UNIVERSITY
LIBRARY

Contents

List of figures.....	6
List of tables.....	10
List of video clips and animations.....	11
Abbreviations.....	12
Abstract.....	13
Declaration and copyright statement.....	14
Acknowledgements.....	15
The author.....	16
<i>1 Introduction.....</i>	<i>17</i>
1.1 Prostate carcinoma	17
1.1.1 Incidence	17
1.1.2 Problems in patient management	17
1.1.3 Natural history	18
1.2 Metastasis	20
1.2.1 Metastasis	20
1.2.2 Steps in metastasis of prostate carcinoma to bone	21
1.2.3 Homing to bone	22
1.3 Mechanisms of metastasis	23
1.3.1 Endothelial barrier.....	23
1.3.1.1 Endothelial cells	23
1.3.1.2 Endothelial cell-cell junctions	23
1.3.1.2.1 Tight junctions.....	24
1.3.1.2.2 Adherens junctions	25
1.3.1.2.3 Other endothelial junctional proteins	26
1.3.1.3 Vascular basement membrane.....	27
1.3.2 Cell adhesion to the endothelium.....	28
1.3.2.1 Leukocytes.....	28
1.3.2.2 Malignant cells	29
1.3.2.3 Prostate carcinoma	29
1.3.2.3.1 Integrins.....	31
1.3.2.3.2 Integrins and prostate carcinoma.....	32
1.3.3 Endothelial Transmigration.....	35
1.3.3.1 Leukocytes.....	35
1.3.3.2 Melanoma and other malignant cells.....	36
1.3.3.2.1 Melanoma.....	36
1.3.3.2.2 Breast carcinoma and other malignant cells.....	38
1.3.3.3 Prostate carcinoma	40
1.3.4 Tissue invasion and colony formation.....	40
1.4 Cell motility and metastasis	41
1.4.1 Cell motility.....	41
1.4.1.1 Collective cell movement.....	42
1.4.1.2 Mesenchymal motility	42
1.4.1.3 Amoeboid motility	43
1.4.1.4 Switching between modes of motility	44
1.4.2 Motility and metastasis.....	45
1.4.2.1 Motility transitions and metastasis.....	46
1.5 Modelling metastasis and invasion.....	47
1.5.1 Invasion through matrices	47

1.5.2	Invasion chambers.....	47
1.5.3	Co-culture systems.....	48
1.5.4	<i>In vivo</i> systems.....	48
1.5.5	Imaging.....	49
1.5.5.1	Light microscopy.....	49
1.5.5.1.1	Fluorescence.....	51
1.5.5.2	Scanning electron microscopy.....	51
1.5.5.2.1	Basic SEM.....	51
1.5.5.2.2	SEM for migration and invasion.....	52
1.6	Aims and hypotheses.....	54
2	<i>Materials and methods</i>	55
2.1	Materials.....	55
2.1.1	Antibodies.....	55
2.1.2	Inhibitors.....	55
2.2	Methods.....	55
2.2.1	Cell lines and culture.....	55
2.2.1.1	Cell lines.....	55
2.2.1.1.1	PC-3 and PC-3-GFP.....	55
2.2.1.1.2	PNT2-C2.....	56
2.2.1.1.3	BMEC.....	56
2.2.1.2	Primary cells.....	56
2.2.1.2.1	Human bone marrow stroma.....	56
2.2.1.2.2	Human bone marrow endothelial cells.....	56
2.2.1.3	Culture conditions.....	57
2.2.1.3.1	PC-3 and PC-3-GFP.....	57
2.2.1.3.2	PNT2-C2.....	57
2.2.1.3.3	BMEC and human primary bone marrow endothelial cells.....	57
2.2.1.3.3.1	Coating flasks for endothelial cell culture.....	57
2.2.1.3.4	Human bone marrow stroma.....	57
2.2.1.3.4.1	Preparation of BMSCM.....	57
2.2.1.4	Passaging of cell cultures.....	58
2.2.1.4.1	PC-3 and PC-3-GFP.....	58
2.2.1.4.2	PNT2-C2.....	58
2.2.1.4.3	BMEC and human primary bone marrow endothelial cells.....	58
2.2.2	Synchronisation.....	58
2.2.2.1	Serum starvation/temperature shock and FACS analysis.....	58
2.2.2.1.1	Serum starvation/temperature shock.....	58
2.2.2.1.2	Analysis of cell cycle by flow cytometry and propidium iodide staining.....	59
2.2.2.2	Cell cycle sorting by flow cytometry and Hoechst staining.....	59
2.2.3	Invasion Assay.....	59
2.2.3.1	Invasion assay with BMEC.....	60
2.2.3.1.1	Immunocytochemical staining for cytokeratins.....	61
2.2.3.2	Invasion assay with inhibitors.....	61
2.2.4	Permeability assay.....	61
2.2.5	Statistics.....	62
2.2.6	Light microscopy and immunofluorescence.....	62
2.2.6.1	Time lapse video microscopy.....	62
2.2.6.2	Immunofluorescence microscopy of fixed cells.....	62
2.2.6.2.1	Fixation for immunofluorescence.....	62

2.2.6.2.1.1	Methanol.....	62
2.2.6.2.1.2	Formalin/Triton X-100	63
2.2.6.2.2	Antibody staining of fixed cells	63
2.2.6.2.2.1	3-step method	63
2.2.6.2.2.2	2-step method	64
2.2.6.2.2.3	Zenon® antibody labelling and staining	64
2.2.6.3	Live cell co-culture studies.....	65
2.2.6.3.1	Confocal invasion study	65
2.2.6.3.1.1	Confocal invasion with inhibitors	65
2.2.6.3.2	Confocal invasion studies using 24 well plate insert and Transwell chambers.....	65
2.2.6.3.2.1	Confocal invasion studies using 24 well plate insert and Transwell chambers with inhibitors	66
2.2.6.3.3	Time lapse video microscopy invasion studies	66
2.2.6.3.3.1	Time lapse invasion with inhibitors	66
2.2.7	Scanning electron microscopy.....	66
2.2.7.1	Fixation and processing.....	66
2.2.7.2	Immunogold labelling	67
2.2.7.3	Critical point drying	67
2.2.7.4	Sputter coating.....	67
2.2.7.5	Scanning electron microscopy.....	68
3	<i>Results</i>	69
3.1	Cell cycle synchronisation, analysis and invasion	69
3.1.1	Synchronisation by serum starvation/temperature shock	69
3.1.2	Synchronisation by Hoechst and FACS	73
3.2	Characterisation of cell lines	75
3.2.1	Light microscopy.....	75
3.2.1.1	PC-3 and PC-3-GFP cells.....	75
3.2.2	Time lapse video microscopy.....	75
3.2.2.1	PC-3 and PC-3-GFP cells.....	75
3.2.3	Scanning Electron Microscopy (SEM) examination of cell morphology	92
3.2.3.1	PC-3 and PC-3-GFP cells.....	92
3.2.4	Immunophenotyping	94
3.2.4.1	PC-3 and PC-3-GFP cells.....	94
3.3	Bone marrow endothelial cell line (BMEC) culture optimisation and characterisation.....	98
3.3.1	Media and substrate test	98
3.3.1.1	Time lapse video microscopy.....	99
3.3.1.2	Substrate test.....	103
3.3.1.3	SEM analysis of BMEC morphology.....	104
3.3.2	Comparison of cell lines.....	107
3.3.2.1	Light microscopy.....	109
3.3.2.2	Time lapse video microscopy.....	109
3.3.2.3	Immunofluorescence	112
3.4	Co-culture studies.....	119
3.4.1	Time lapse video microscopy live invasion studies	119
3.4.2	Confocal live invasion studies.....	128
3.4.2.1	Confocal invasion studies using 24 well plate insert and Transwell chambers	136

3.4.2.1.1	Development of the plate insert.....	136
3.4.2.1.2	Invasion studies using the plate insert.....	138
3.4.3	SEM invasion studies.....	140
3.5	Inhibitor studies.....	147
3.5.1	Invasion through basement membrane.....	147
3.5.2	Cell motility in 2D monoculture	152
3.5.2.1	Amoeboid motility inhibitors.....	152
3.5.2.1.1	Y-27632.....	152
3.5.2.1.2	Blebbistatin.....	156
3.5.2.2	Mesenchymal movement inhibitors	161
3.5.2.2.1	Rac1 inhibitor.....	161
3.5.2.2.2	GM6001.....	162
3.5.2.3	Inhibitor washout studies.....	162
3.5.3	Effect of inhibitors on the BMEC monolayer	163
3.5.3.1	Time lapse video microscopy studies.....	163
3.5.3.2	Immunofluorescent staining of tight junctions.....	163
3.5.3.3	Permeability studies	164
3.5.4	Invasion through endothelial cells.....	167
3.5.4.1	Amoeboid motility inhibitors.....	167
3.5.4.1.1	Y-27632.....	167
3.5.4.1.2	Blebbistatin.....	169
3.5.4.2	Mesenchymal motility inhibitors.....	171
3.5.4.2.1	Rac1 inhibitor.....	171
3.5.4.2.2	GM6001.....	173
3.5.5	Invasion through BMEC monolayer	177
3.5.6	Invasion through BMEC monolayer and basement membrane.....	178
4	<i>Discussion</i>	181
4.1	Development of the in vitro model.....	181
4.2	Migration of prostate carcinoma cells through bone marrow endothelium ...	194
4.2.1.1	Overview of migration	207
4.3	Summary and future work.....	209
5	<i>References</i>	212
6	<i>Appendix: video clips and animations</i>	221

Word count: 58,000

List of figures

Figure 1-1: Anatomy of the prostate gland	18
Figure 1-2: Gleason grading of prostate carcinoma	19
Figure 1-3: Metastasis via the bloodstream.....	21
Figure 1-4: Endothelial cell-cell junctions	24
Figure 1-5: Structure of a tight junction.....	25
Figure 1-6: Structure of an adherens junction	26
Figure 1-7: Stages of endothelial transmigration of malignant cells.....	37
Figure 1-8: Types of cell motility.....	45
Figure 1-9: Diagram of an invasion chamber.....	48
Figure 1-10: Laser scanning confocal microscope.....	50
Figure 1-11: Scanning electron microscope.....	52
Figure 3-1: Typical FACS plots of cell cycle distribution in PC-3-GFP cells.....	70
Figure 3-2: Results of starvation/temperature shock treatment on cell cycle of PC-3 and PC-3-GFP cells	71
Figure 3-3: Effects of recovery on the cell cycle of PC-3 cells	72
Figure 3-4: Results of invasion assay using PC-3-GFP cells after starvation synchronisation and recovery	73
Figure 3-5: Defining stages of the cell cycle by Hoechst 33342 staining.....	73
Figure 3-6: Invasion assay using PC-3-GFP cells post FACS sorting for phases of the cell cycle.....	74
Figure 3-7: Morphology of PC-3 and PC-3GFP cells under phase contrast microscopy	77
Figure 3-8: PC-3 cells in culture	79
Figure 3-9: PC-3 cell showing fibroblastic movement	83
Figure 3-10: PC-3 cell switching from a fibroblastic mode of movement to amoeboid movement	84
Figure 3-11: PC-3 cell undergoing mitosis	85
Figure 3-12: PC-3-GFP cells showing blebbing and amoeboid movement.....	86
Figure 3-13: PC-3-GFP cells showing fibroblastic movement	87
Figure 3-14: PC-3-GFP cells in culture.....	88
Figure 3-15: PC-3 cells cultured in BMSCM.....	88
Figure 3-16: PC-3 cells cultured in BMSCM.....	89
Figure 3-17: PC-3 cells showing escape from a cell cluster	90
Figure 3-18: PC-3 cells showing amoeboid movement	91
Figure 3-19: PC-3-GFP cells cultured in BMSCM.....	92
Figure 3-20: PC-3-GFP cells cultured in BMSCM showing cell clusters	92
Figure 3-21: Typical appearances of PC-3 and PC-3-GFP cells on SEM.....	93
Figure 3-22: Immunophenotype of PC-3 cells.....	96
Figure 3-23: Immunophenotype of PC-3-GFP cells	97
Figure 3-24: Typical appearances of BMEC on tissue culture plastic in different culture media	99
Figure 3-25: BMEC cultured in M199 showing fibroblastic movement	100
Figure 3-26: BMEC cultured in M199 showing spontaneous apoptosis.....	101
Figure 3-27: BMEC cultured in BMSCM showing slow fibroblastic movement across the substrate.....	102
Figure 3-28: BMEC cultured in BMSCM with cell dividing.....	102
Figure 3-29: Confluent BMEC monolayer cultured in BMSCM.....	103

Figure 3-30: Typical appearances of BMEC cultured in BMSCM on different substrates	106
Figure 3-31: Charging artefacts on SEM	106
Figure 3-32: Appearances of BMEC on SEM.....	108
Figure 3-33: Appearances of BMEC and primary endothelial cells on different substrates	110
Figure 3-34: Primary human bone marrow endothelial cells cultured in BMSCM .	111
Figure 3-35: Primary human bone marrow endothelial cell undergoing mitosis.....	111
Figure 3-36: Primary human bone marrow endothelial cells	112
Figure 3-37: Immunophenotype of BMEC cultured in BMSCM	116
Figure 3-38: Immunophenotype of primary human bone marrow endothelial cells cultured in BMSCM	117
Figure 3-39: Results of staining with antibody to ZO-1 using different techniques to reduce non-specific staining	118
Figure 3-40: Results of immunofluorescent staining of PNT2-C2 cells	118
Figure 3-41: Time taken for PC-3 and PC-3-GFP cells to complete invasion across a BMEC monolayer.....	120
Figure 3-42: Percentage of PC-3 and PC-3-GFP cells completing invasion at different time points	121
Figure 3-43: Live cell invasion study using time lapse video microscopy	122
Figure 3-44: PC-3 cell invading through a BMEC monolayer	123
Figure 3-45: BMEC monolayer after invasion of PC-3 cells.....	124
Figure 3-46: BMEC monolayer with PC-3-GFP cells	124
Figure 3-47: PC-3-GFP cell migrating over a BMEC monolayer.....	125
Figure 3-48: PC-3-GFP cell invading through a BMEC monolayer.....	126
Figure 3-49: BMEC monolayer with PNT2-C2 cells.....	127
Figure 3-50: BMEC monolayer with PNT2-C2 cells.....	127
Figure 3-51: Effect of cell culture medium on invasiveness of PNT2-C2 cells through Matrigel	128
Figure 3-52: Live cell invasion study using confocal microscope	129
Figure 3-53: PC-3-GFP cell invading a BMEC monolayer	130
Figure 3-54: PC-3-GFP cell migrating across a BMEC monolayer.....	132
Figure 3-55: PC-3-GFP cell invading a BMEC monolayer	134
Figure 3-56: Transwell chambers with plastic and glass bottomed 24 well plates ..	137
Figure 3-57: Methods of holding Transwells in a glass bottomed 24 well plate	137
Figure 3-58: Confocal invasion study using Transwell chamber and glass bottomed 24 well plate	138
Figure 3-59: PC-3-GFP cell invading through Matrigel and Transwell membrane pore.....	139
Figure 3-60: SEM images of BMEC monocultures and BMEC + PC-3 co-cultures showing potential artefacts.....	141
Figure 3-61: SEM images of 10nm gold labelled BMEC/PC-3 cell co-culture specimens	143
Figure 3-62: SEM images of a PC-3 cell invading a BMEC monolayer	145
Figure 3-63: Tilted SEM images of PC-3 cells invading a BMEC monolayer.....	146
Figure 3-64: Effect of the ROCK inhibitor Y-27632 on PC-3-GFP invasion through Matrigel	148
Figure 3-65: Effect of blebbistatin on PC-3-GFP invasion through Matrigel.....	149
Figure 3-66: Effect of Rac1 inhibitor on PC-3-GFP invasion through Matrigel	149
Figure 3-67: Effect of GM6001 on PC-3-GFP invasion through Matrigel.....	150

Figure 3-68: Effect of inhibitors on PC-3 cells invading through Matrigel.....	151
Figure 3-69: PC-3 cells cultured on tissue culture plastic in the presence of Y-27632	153
Figure 3-70: PC-3 cells cultured on tissue culture plastic in the presence of Y-27632	153
Figure 3-71: PC-3 cells cultured on tissue culture plastic in the presence of Y-27632	154
Figure 3-72: PC-3-GFP cells cultured on tissue culture plastic in the presence of Y-27632	155
Figure 3-73: PC-3-GFP cells cultured on tissue culture plastic in the presence of Y-27632	156
Figure 3-74: PC-3 cells cultured on tissue culture plastic in the presence of blebbistatin	157
Figure 3-75: PC-3 cells cultured on tissue culture plastic in the presence of blebbistatin	159
Figure 3-76: PC-3-GFP cells cultured on tissue culture plastic in the presence of blebbistatin	159
Figure 3-77: PC-3-GFP cells cultured on tissue culture plastic in the presence of blebbistatin	160
Figure 3-78: PC-3 cells cultured on tissue culture plastic in the presence of Rac1 inhibitor	161
Figure 3-79: PC-3-GFP cell cultured on tissue culture plastic in the presence of Rac1 inhibitor	162
Figure 3-80: ZO-1 staining in BMEC after 24 hours incubation with inhibitors.....	164
Figure 3-81: A typical standard curve for FITC-dextran dilutions	165
Figure 3-82: Permeability of the BMEC monolayer to FITC-dextran in the presence of inhibitors or PC-3 cells after 6 hours incubation	165
Figure 3-83: Permeability of the BMEC monolayer to FITC-dextran in the presence of inhibitors or PC-3 cells after 24 hours incubation	166
Figure 3-84: BMEC monolayer with PC-3 cells in the presence of Y-27632	167
Figure 3-85: BMEC monolayer with PC-3 cells in the presence of Y-27632	168
Figure 3-86: BMEC monolayer with PC-3-GFP cells in the presence of Y-27632	168
Figure 3-87: BMEC monolayer with PC-3-GFP cells in the presence of Y-27632	168
Figure 3-88: BMEC monolayer with PC-3 cells in the presence of blebbistatin.....	169
Figure 3-89: BMEC monolayer with PC-3 cells in the presence of blebbistatin.....	170
Figure 3-90: BMEC monolayer with PC-3 cells in the presence of blebbistatin.....	170
Figure 3-91: BMEC monolayer with PC-3-GFP cells in the presence of blebbistatin	171
Figure 3-92: BMEC monolayer with PC-3-GFP cells in the presence of blebbistatin	171
Figure 3-93: BMEC monolayer with PC-3 cells in the presence of Rac1 inhibitor.	172
Figure 3-94: BMEC monolayer with PC-3-GFP cells in the presence of Rac1 inhibitor	173
Figure 3-95: BMEC monolayer with PC-3 cells in the presence of GM6001	174
Figure 3-96: BMEC monolayer with PC-3-GFP cells in the presence of GM6001.	175
Figure 3-97: Migration of PC-3 cells through a BMEC monolayer in the presence of motility inhibitors	176
Figure 3-98: Migration of PC-3-GFP cells through a BMEC monolayer in the presence of motility inhibitors.....	176

Figure 3-99: Effect of inhibitors on invasion of PC-3 cells through a BMEC monolayer.....	177
Figure 3-100: Effect of inhibitors on invasion of PC-3-GFP cells through a BMEC monolayer.....	178
Figure 3-101: Effect of inhibitors on invasion of PC-3 cells through a confluent BMEC monolayer with an underlying Matrigel layer.....	179
Figure 3-102: Effect of inhibitors on invasion of PC-3-GFP cells through a confluent BMEC monolayer with an underlying Matrigel layer.....	180

List of tables

Table 1-1: TNM staging of prostatic adenocarcinoma (6 th edition).....	20
Table 1-2: Cell adhesion molecules/signalling pathways in prostate carcinoma metastasis to bone.....	22
Table 1-3: Cell adhesion molecules known or suggested to be involved in leukocyte migration across endothelium	29
Table 1-4: Cell adhesion molecules involved in binding of malignant prostate cells to endothelium	30
Table 1-5: Cell adhesion molecule alterations in malignancy	32
Table 1-6: Integrin subunit expression in prostate epithelial cells	34
Table 1-7: Cell adhesion molecules involved in malignant cell interactions with endothelium	39
Table 1-8: Characteristics of mesenchymal and amoeboid motility	44
Table 1-9: Genes involved in cell motility associated with cancer cell invasion and metastasis.....	46
Table 3-1: Morphology and behaviour of PC-3 and PC-3-GFP cells in HAMS F12 as observed by time lapse video microscopy.....	80
Table 3-2: Morphology and behaviour of PC-3 and PC-3-GFP cells in BMSCM as observed by time lapse video microscopy.....	81
Table 3-3: Immunophenotype of PC-3 and PC-3-GFP cells.....	94
Table 3-4: Characteristics of BMEC cultured in different media	98
Table 3-5: Immunophenotype of BMEC when cultured in BMSCM.....	113
Table 3-6: Immunophenotype of primary human bone marrow endothelial cells in BMSCM	114
Table 3-7: Blocking techniques used with immunofluorescent staining	115
Table 3-8: Results of live invasion study using time lapse video microscopy	119
Table 3-9: Morphological characteristics of PC-3 cells and BMEC on SEM.....	142
Table 3-10: Cell motility inhibitors.....	151

List of video clips and animations

Video clips and animations are on the DVD in the appendix.

Video clips and animations are supplied as PowerPoint presentations and as mpeg or avi files on the DVD. Clips within PowerPoint will start playing when the picture is clicked. Video clip files are all within the same folder and can also be played in Windows media player, Apple QuickTime player etc. Section numbers associated with clips refer to the corresponding sections in the report and still frames from the clips and animations are also in the corresponding sections.

Section 3.2. Characterisation of cell lines

- Clips 1-5 PC-3 cells cultured in HAMS F12
- Clips 6-9 PC-3-GFP cells cultured in HAMS F12
- Clips 10-16 PC-3 cells cultured in BMSCM
- Clips 17-20 PC-3-GFP cells cultured in BMSCM

Section 3.3. BMEC culture optimisation and characterisation

- Clips 21-23 BMEC cultured in M199
- Clips 24-27 BMEC cultured in BMSCM
- Clips 28-29 Primary human bone marrow endothelial cells cultured in BMSCM

Section 3.4. Co-culture studies

- Clips 30-36 Time lapse invasion study using PC-3 cells
- Clips 37-41 Time lapse invasion study using PC-3-GFP cells
- Clips 42-43 Time lapse study using PNT2-C2 cells
- Clips 44-48 Confocal invasion study using PC-3-GFP cells
- Clip 49 Transwell chamber confocal invasion using PC-3-GFP cells

Section 3.5. Inhibitor studies

- Clips 50-54 PC-3 and PC-3-GFP cells with Y-27632
- Clips 55-58 PC-3 and PC-3-GFP cells with blebbistatin
- Clips 59-60 PC-3 and PC-3-GFP cells with Rac1 inhibitor
- Clips 61-62 PC-3 and PC-3-GFP cells with GM6001
- Clips 63-66 BMEC with all inhibitors
- Clips 67-70 BMEC with Y-27632 and PC-3 or PC-3-GFP cells
- Clips 71-75 BMEC with blebbistatin and PC-3 or PC-3-GFP cells
- Clips 76-77 BMEC with Rac1 inhibitor and PC-3 or PC-3-GFP cells
- Clips 78-79 BMEC with GM6001 and PC-3 or PC-3-GFP cells

Abbreviations

BMS	Bone marrow stroma
BMSCM	Bone marrow stroma conditioned medium
BSA	Bovine serum albumin
CAR	Coxsackie and adenovirus receptor
CEA	Carcinoembryonic antigen
DAB	Diaminobenzidine
DMEM	Dulbecco's modified Eagle's medium
ECM	Extracellular matrix
EMT	Epithelial to mesenchymal transition
ESAM	Endothelial cell selective adhesion molecule
FAK	Focal adhesion kinase
FITC	Fluorescein isothiocyanate
GFP	Green fluorescent protein
HUVEC	Human umbilical vein endothelial cells
ICAM	Intercellular cell adhesion molecule
IGF	Insulin like growth factor
IL	Interleukin
JAM	Junctional adhesion molecule
MLCK	Myosin light chain kinase
MMP	Matrix metalloproteinase
PBS	Phosphate-buffered saline
PECAM-1	Platelet endothelial cell adhesion molecule 1
PSA	Prostate-specific antigen
ROCK	Rho-associated kinase
SCLC	Small-cell lung carcinoma
SDF-1	Stromal derived factor 1
SEM	Scanning electron microscopy
sLeX	Sialyl Lewis X
TCP	Tissue culture plastic
TGF	Transforming growth factor
TNF	Tumour necrosis factor
TRAMP	Transgenic adenocarcinoma of the mouse prostate
TURP	Transurethral resection of the prostate
VCAM	Vascular cell adhesion molecule
VEGF	Vascular endothelial growth factor
ZO	Zona occludens

Abstract of thesis submitted by Jo-An Roulson for the degree of PhD oncology and entitled:

Bone marrow endothelial transmigration of prostate carcinoma cells

December 2008

Prostate carcinoma is the most common cancer in men in the UK and the second most common cause of cancer death. Bone metastases are the most common cause of morbidity and mortality for these patients, with over 85% of men dying of prostate cancer having bone metastases at the time of death. Tumour cells spread to bone via the peripheral blood and must cross the endothelial lining of vessels to enter the bone marrow. Both benign and malignant prostate epithelial cells bind preferentially to bone marrow endothelium and grow in co-culture with bone marrow stroma. However only malignant cells are able to migrate across the endothelial layer indicating that this is the crucial step in bone metastasis.

The aim this series of studies is to examine the process of migration across the bone marrow endothelial cell barrier by prostate carcinoma cells. In order to study this an *in vitro* model of endothelial transmigration has been developed. This model system utilises the prostate carcinoma cell lines PC-3 and PC-3-GFP, derived from a bone metastasis and BMEC, an immortalised human bone marrow endothelial cell line. Bone marrow stroma conditioned medium was used to provide an environment similar to that experienced by bone marrow endothelial cells *in vivo*. Using this system prostate cancer cells were observed completing migration across the bone marrow endothelium in a mean time of 249 \pm 48 minutes (PC-3 cells) and 291 \pm 52 minutes (PC-3-GFP cells). Virtually all malignant cells completed invasion through the BMEC monolayer. This model provides a useful *in vitro* system for studying the process of endothelial transmigration.

Using this model PC-3 cells manifested both amoeboid and mesenchymal motility during the endothelial transmigration process. Amoeboid motility appeared to be used during endothelial transmigration with a switch to mesenchymal motility after spreading on the underlying substrate. The amoeboid motility inhibitors Y-27632 (an inhibitor of ROCK) and blebbistatin (an inhibitor of myosin II), and mesenchymal motility inhibitors Rac1 inhibitor and GM6001 (a broad spectrum proteinase inhibitor), were used to investigate motility during transmigration. Both Y-27632 and blebbistatin inhibited migration of prostate carcinoma cells across an endothelial monolayer but Rac1 inhibitor and GM6001 had no effect. Rac1 inhibitor and GM6001 lead to a significant reduction in prostate carcinoma cell invasion through Matrigel but Y-27632 and blebbistatin produced little inhibition of invasion. These results suggest that amoeboid motility pathways are needed for prostate cell migration through the bone marrow endothelial cell layer and that PC-3 cells preferentially use amoeboid motility for endothelial transmigration and mesenchymal motility for extracellular matrix invasion.

Understanding the endothelial transmigration process could lead to the development of antimetastatic therapy with potential benefits for large numbers of patients. These findings may be useful for the development of these therapies.

Declaration

No portion of the work referred to in the thesis has been submitted in support of an application for another degree or qualification of this or any other university or institute of learning.

Copyright statement

- i. The author of this thesis (including appendices) owns any copyright in it (the "Copyright") and she has given The University of Manchester the right to use such Copyright for any administrative, promotional, educational and/or teaching purposes.
- ii. Copies of this thesis, either full or in extracts, may be made **only** in accordance with the regulations of the John Rylands University Library of Manchester. Details of these regulations may be obtained from the Librarian. This page must form part of any such copies made.
- iii. The ownership of any patents, designs, trade marks and any and all other intellectual property rights except for the Copyright (the "Intellectual Property Rights") and any reproductions of copyright works, for example graphs and tables ("Reproductions"), which may be described in this thesis, may not be owned by the author and may be owned by third parties. Such Intellectual Property Rights and Reproductions cannot and must not be made available for use without the prior written permission of the owner(s) of the relevant Intellectual Property Rights and/or Reproductions.
- iv. Further information on the conditions under which disclosure, publication and exploitation of this thesis, the Copyright and any Intellectual Property Rights and/or Reproductions described in it may take place is available from the Head of School of Medicine (or the Vice-President).

Acknowledgements

Many people have helped me in my transition from pathologist to student, from my first attempts to organise a PhD to my latest set of results. Sue Pritchard first told me about the Robin Dodge Fellowship and subsequent help from Drs Menasce, Banerjee and Shanks in the Christie Hospital histopathology department secured part of the funding from the money given by Dr Dodge. With help from Graham Cowling, Terry Allen and Noel Clarke the project and rest of the funding all fell into place and with the support of the North Western Postgraduate Deanery I stepped off the training rotation and into the world of research.

My supervisors, Mick Brown and Noel Clarke, have pointed me in the right direction and provided much advice and help. Mick deserves a special mention for his efforts to improve my writing skills, and both he and Noel provided much useful advice in the preparation of this thesis. Claire Hart helped me find my feet in the lab and taught me about all the lab and cell culture techniques I needed. Terry Allen, Steve Murray and Sandra Rutherford shared their electron microscopy expertise and also introduced me to the wonderful and addictive world of time lapse video microscopy. Steve Bagley taught me about confocal and fluorescence microscopy and showed me how to use light microscopes more technologically advanced than a histopathology trainee is normally allowed near. Ehsan Gazi, Pete Gardner and Nick Lockyer explained some of the mysteries of FTIR and ToF-SIMS but unfortunately in the end I was not able to include these techniques in my study. Jeff Barry and Mike Hughes taught me about flow cytometry and undertook the task of sorting my cells. My excellent advisor, Angeliki Malliri, provided not only her signature on numerous forms, but discussions giving a different perspective on my work and suggestions for future work. I am also grateful to Tom Stringfellow for helping me to construct the cable tie Transwell supports and for taking the photographs of the 24 well plate insert, plate and Transwell chambers.

Many thanks are also due to my colleagues and friends at home and at work for their support and encouragement, enabling me to keep going when everything seemed to be going wrong, and for putting up with me spending numerous weekends working or writing. I could not have done it without them.

The author

I qualified in medicine in 1998 at the University of Dundee and am currently a specialist registrar in histopathology in the North Western Deanery. In 1995 I was awarded the degree of Bachelor of Medical Science in forensic medicine at the University of Dundee. For this degree I completed a laboratory-based research project on post-mortem drug degradation by bacteria. After graduating in medicine I worked as a house officer in medicine and surgery before becoming a senior house officer and working in several surgical specialties, as well as spending some time as an anatomy demonstrator. I started training in histopathology in 2002.

1 Introduction

1.1 Prostate carcinoma

1.1.1 Incidence

Prostate carcinoma is the most prevalent cancer in men worldwide, with over 670,000 new cases diagnosed in the year 2002 [1]. It is the most common cancer in men in the UK, with over 30,000 new cases diagnosed in 2001 and the second most common cause of cancer death in men in the UK [2]. The UK has, in common with many other European countries, one of the highest mortality rates from prostate carcinoma in the world [1]. The pathological incidence of the disease increases with age, with over 75% of men over age 85 having histological evidence of cancer, although the cumulative risk of being diagnosed with carcinoma by age 85 is 20% or less [3], suggesting that many cases diagnosed histologically are clinically insignificant. With increased awareness of the disease among men, the increased use of biopsy, incidental diagnoses made after trans-urethral resection of the prostate (TURP), and increasing use of PSA (prostate specific antigen) testing, more men are being diagnosed at a younger age and with lower stage tumours. Incidence is also increasing due to a reduced death rate from other causes [3]. These factors can increase the number of cases of potentially clinically insignificant cancer being diagnosed and may lead to overtreatment of patients.

1.1.2 Problems in patient management

Carcinoma which is localised to the prostate can lead to symptoms of lower urinary tract obstruction, but these can usually be controlled by procedures such as TURP. Other therapeutic options such as radical prostatectomy and radiotherapy are potentially curative for localised disease, but may be unsuitable for some patients, especially elderly patients or those with other medical problems. They have potentially serious complications and side effects, which must be weighed against the potential for cure and the fact that many of these patients will die of other causes.

Active surveillance (watchful waiting) is a potential management strategy for older men with lower stage tumours and/or significant comorbidities [4]. However for younger patients, and those with higher grade or stage tumours, the potential for cure must be balanced against the risks associated with potentially curative treatment and the chance of progression, which is difficult to predict for individual patients.

Although many patients live with localised disease for years, the development of metastases indicates disease progression and a poor prognosis: only 50% of patients are alive 2 years after presentation with bone metastases [5]. Prostate cancer preferentially metastasises to the bone marrow, with over 85% of patients dying of prostate cancer having bone lesions [6]. Bone metastases have a significant adverse effect on quality of life, leading to problems such as pain, bone marrow suppression and anaemia, fractures and spinal cord compression.

1.1.3 Natural history

Prostate adenocarcinoma initially develops within the prostate gland, most commonly in the peripheral zone (see Figure 1-1). There may be a long latent period between development of the disease and clinical presentation, which may not occur until metastases are already present. The most common site for metastases is the bone marrow particularly the axial skeleton. Lymph node metastases are also seen and less commonly, spread can occur to the brain and other viscera. The tumour can also invade locally to involve adjacent structures such as the seminal vesicles, bladder and rectum. The natural history of the disease is not well-defined, but tends to be long, and many patients die with rather than of their disease [7].

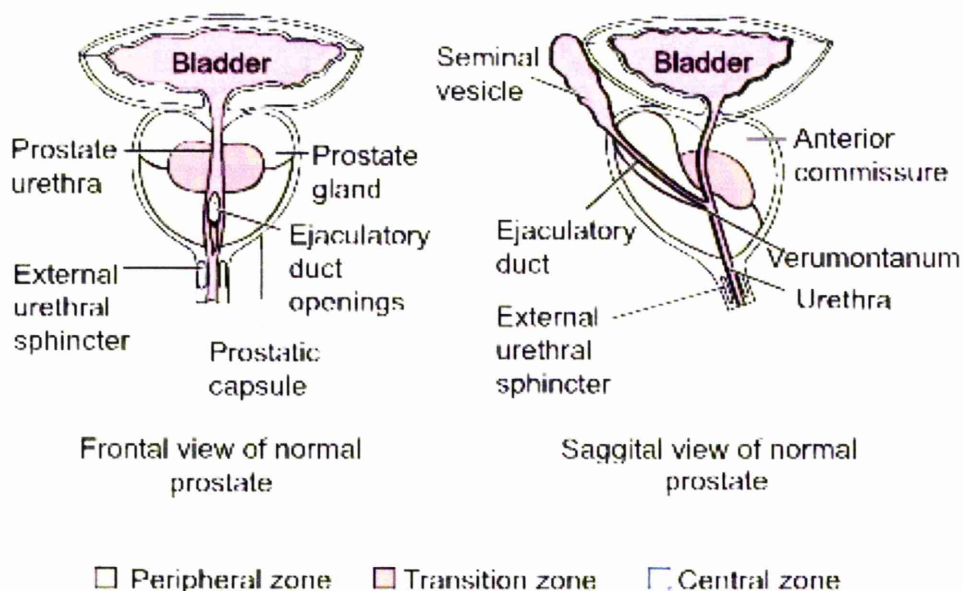


Figure 1-1: Anatomy of the prostate gland
(www.prostateline.com)

Two important factors in predicting prognosis are the Gleason grade and tumour stage. The Gleason grade (see Figure 1-2) is a histological grade based on the glandular architecture of the tumour with 5 grades from grade 1, the most well-differentiated, to grade 5, the most poorly-differentiated. The two predominant grades are combined to give a Gleason score from two to ten.

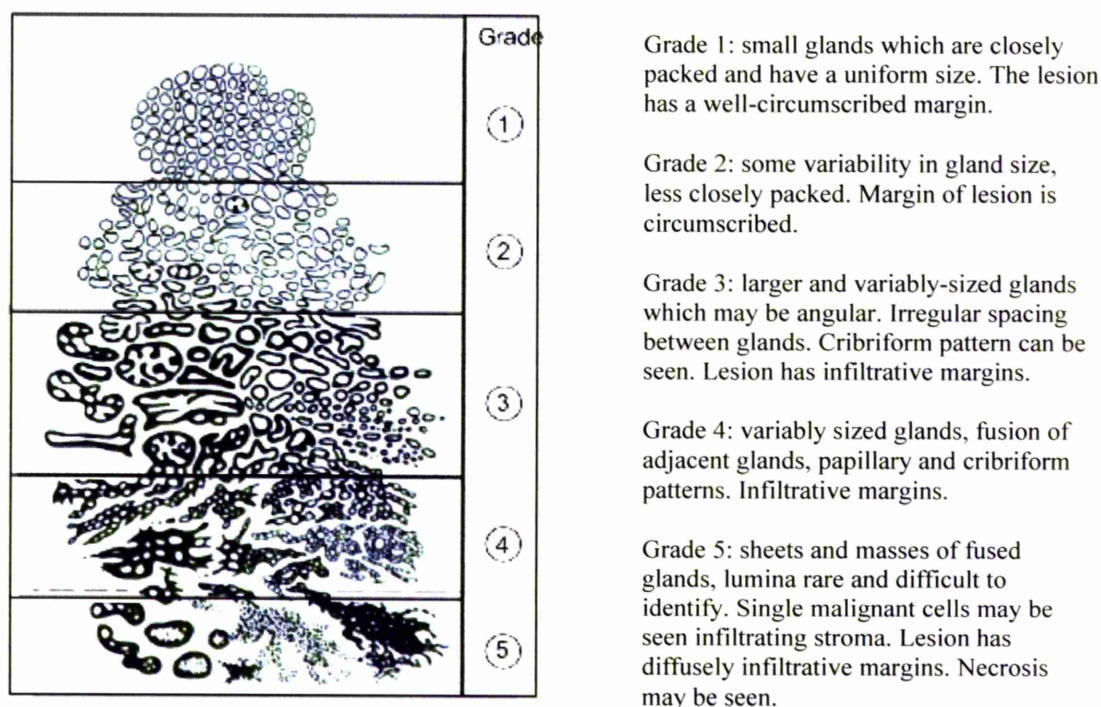


Figure 1-2: Gleason grading of prostate carcinoma
(www.prostateline.com)

The most widely used staging system for tumours is the TNM system, which describes how advanced a tumour is in terms of local disease (the “T” stage), lymph node spread (N) and metastases (M). Staging is determined using a combination of clinical, radiological and pathological information. TNM stages for prostate carcinoma are shown in Table 1-1.

Although Gleason scores and staging systems can be used to predict prognosis, there is still much uncertainty for individual patients. Patients with lower Gleason scores and lower stage tumours show a lesser tendency to develop progressive disease, but 3% to 41% of patients with stage T1 or T2 disease (carcinoma confined within the prostate) will still develop bone metastases within 10 years of diagnosis, as will 3% to 10% of patients with well-differentiated (Gleason score 2-4) tumours [6].

Table 1-1: TNM staging of prostatic adenocarcinoma (6th edition)

	Primary tumour
T0	No evidence of primary tumour
T1	Clinically inapparent tumour not palpable or visible by imaging T1a Tumour incidental histological finding in 5% or less of tissue resected T1b Tumour incidental histological finding in more than 5% of tissue resected T1c Tumour identified by needle biopsy
T2	Tumour confined within prostate gland T2a Tumour involves one half of one lobe or less T2b Tumour involves more than half of one lobe but not both lobes T2c Tumour involves both lobes
T3	Tumour extends through prostatic capsule T3a Extracapsular extension (unilateral or bilateral) T3b Tumour invades seminal vesicle(s)
T4	Tumour is fixed or invades adjacent structures e.g. bladder, rectum, pelvic wall
	Regional lymph nodes (those below bifurcation of common iliac artery)
Nx	Lymph nodes cannot be assessed
N0	No regional lymph node metastasis
N1	Regional lymph node metastasis present
	Distant metastasis
Mx	Distant metastasis cannot be assessed
M0	No metastasis
M1	Metastasis to other sites (includes metastasis to non-regional lymph nodes) M1a Non-regional lymph node(s) M1b Bone(s) M1c Other site(s)

1.2 Metastasis

1.2.1 Metastasis

Several malignancies including prostate, kidney, breast and lung carcinoma commonly metastasize to bone. Production of growth factors in the bone stimulates invasion and motility in prostate carcinoma cells [8], although direct contact with stromal cells may be needed for growth [9]. In the case of breast carcinoma there are interactions between malignant cells and the bone microenvironment which lead to release of growth factors that enhance tumour growth [10]. In order to spread to the bone marrow, tumour cells must first escape the primary tumour and invade through

the walls of blood vessels to enter the peripheral blood. They arrest in vessels within the bone marrow, then invade through the endothelium into the stroma, and multiply to form a metastasis (see Figure 1-3).

1.2.2 Steps in metastasis of prostate carcinoma to bone

Escape from the primary tumour is necessary for the formation of metastases, but it is not the only step required. Malignant prostatic epithelial cells are released into the circulation during surgery to the prostate [11] and have the opportunity to travel to other sites via the bloodstream. Despite this, TURP has not been associated with an adverse effect on survival in patients who have prostate carcinoma [12], so other factors are involved. A variety of molecules have been implicated in this process (see Table 1-2).

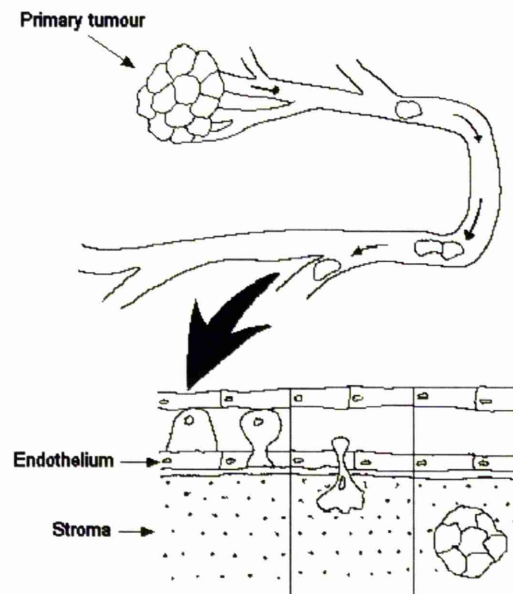


Figure 1-3: Metastasis via the bloodstream

Malignant cells escape from the primary tumour and travel through vessels. They reach the microvasculature of the target organ and must bind to and migrate through the vascular endothelium into the stroma.

Benign and malignant prostate epithelial cells show increased binding to bone marrow endothelium compared to endothelia from the lung and umbilical vein [13-15]. Both also bind to bone marrow stroma more strongly than they bind to prostate fibroblasts [16] and they also grow to a significantly greater extent in co-culture with bone marrow stroma than with prostate fibroblasts [9]. Although benign and malignant prostate epithelial cells bind to endothelium and grow in co-culture with

stroma, Hart *et al* (2005) [17] showed that it is only malignant cells which are able to migrate across the endothelium. Endothelial transmigration is therefore the crucial step in the formation of bone metastases.

Table 1-2: Cell adhesion molecules/signalling pathways in prostate carcinoma metastasis to bone

Adhesion molecule	Ligand	Role
β_1 integrin		binding of PC-3 to bone marrow endothelium [13]
PSA		binding of C4-2b (but not PC-3) to bone marrow endothelium [14]
$\alpha_2\beta_1$ integrin		binding of prostate epithelial cells to bone marrow stroma [16]
β_3 integrin		β_3 integrin on PC-3 cells important in late stages of transmigration, possibly interacting with the ECM [18]
CXCR4	CXCL12	invasion of PC3 cells [17] growth of prostate carcinoma bone metastases [19] binding of prostate carcinoma cells to bone marrow endothelium [20] transmigration across endothelium [20] enhanced tumour cell expression of β_3 integrin [21]
Galectin-3		binding of PC-3 cells to bone marrow endothelium [15]
$\alpha_{IIb}\beta_{IIIa}$ integrin	fibrinogen, platelets	arrest in the circulation [8]
$\alpha_v\beta_3$ integrin	vitronectin, endothelium	arrest in the circulation [8]

1.2.3 Homing to bone

The CXCL12/CXCR4 axis is involved in the homing of haematopoietic stem cells to the bone marrow. The CXCR4 receptor and its ligand, the chemokine CXCL12 (SDF-1) has been implicated in the metastasis of prostate carcinoma to bone [20], small cell lung carcinoma (SCLC) [22] and breast carcinoma [23]. CXCL12 is produced by bone marrow endothelial cells and bone marrow stroma. Prostate carcinoma and benign prostate epithelial cells express CXCR4, and both bind to bone marrow endothelium [17]. However only malignant cells can be stimulated to invade across basement membranes and endothelial layers *in vitro* by CXCL12 [20]. The CXCL12/CXCR4 interaction lead to increased expression of α_5 and β_3 integrins, and increased integrin-mediated adhesion to HUVEC, by prostate

carcinoma cells [21]. The CXCR4/CXCL12 axis plays only a minor role in attracting prostate epithelial cells to the bone marrow [17] suggesting that there may be other stimulatory factors involved. SCLC cells express CXCR4 and can adhere to bone marrow stroma by CXCR4-dependent interactions [22]. This system has also been linked to chemotaxis and pseudopod formation in cells of breast carcinoma [23], another tumour that commonly spreads to the skeleton.

1.3 Mechanisms of metastasis

1.3.1 Endothelial barrier

The main components of the endothelial barrier are the endothelial cells and their basement membrane.

1.3.1.1 Endothelial cells

Endothelial cells line blood vessels and act as a specialized barrier controlling passage of fluid and molecules between blood and tissues. They participate in the active migration of leukocytes and are involved in regulation of blood clotting, platelet adhesion, modulation of blood flow and vascular tone. They produce a wide variety of substances such as inflammatory mediators, growth factors, anti- and procoagulant substances, extracellular matrix components and vasoactive substances [24]. They also respond to environmental stimuli such as pH, hypoxia, temperature, and shear stress [25].

Endothelial cells are specialized for the particular vessel they inhabit. Cells from different parts of the vascular system differ in size, shape and thickness, and their orientation can be affected by the direction of blood flow [26]. Intercellular junctions are also different in different types of vessel.

1.3.1.2 Endothelial cell-cell junctions

Endothelial cells possess both tight and adherens junctions (see Figure 1-4), as well as gap junctions which are involved in cell-cell communication. However they do not have classical desmosomes [27].

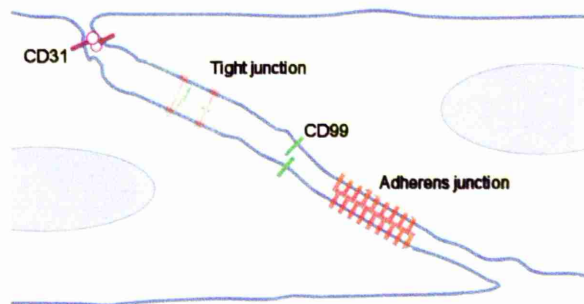


Figure 1-4: Endothelial cell-cell junctions

Cells overlap each other and specialised junctional structures as well as simpler adhesion molecules are present. The distribution of tight and adherens junctions is not polarised.

The cells often overlap each other with tight and adherens junctions intermingled along the cell junction region, rather than adopting the polarised distribution seen in many epithelial cells [28, 29]. Endothelial cells in the brain microvasculature have highly developed tight junctions which form the blood-brain barrier, whereas post-capillary venules have poorly organised cell-cell junctions, allowing for the trafficking of fluid and cells that occurs in these vessels [27]. Endothelial cells from different sites express cell surface antigens which are both endothelial and organ specific [30]. These site-specific differences between endothelial cells are thought to contribute to homing of leukocytes to specific tissues [31] and to the preferential metastasis of tumours to particular secondary sites [32].

1.3.1.2.1 Tight junctions

Tight junctions (see Figure 1-5) are complex structures formed of strands which link the membranes of adjacent cells. They are composed of the proteins occludin and claudins, with associated intracellular multi-protein complexes and other proteins. Both occludin and the claudins are composed of two extracellular loops and four transmembrane domains. Tight junctions are involved in regulating passage of small molecules and ions via the paracellular route and increased expression of occludin correlates with reduced permeability of the endothelium [27]. The claudin family contains numerous members, but claudin-5 is specific to endothelial cells [28]. Various components of the tight junction complex such as ZO-1 interact with signal transduction molecules such as G-proteins including Rho and Ras and protein kinases A and C [27].

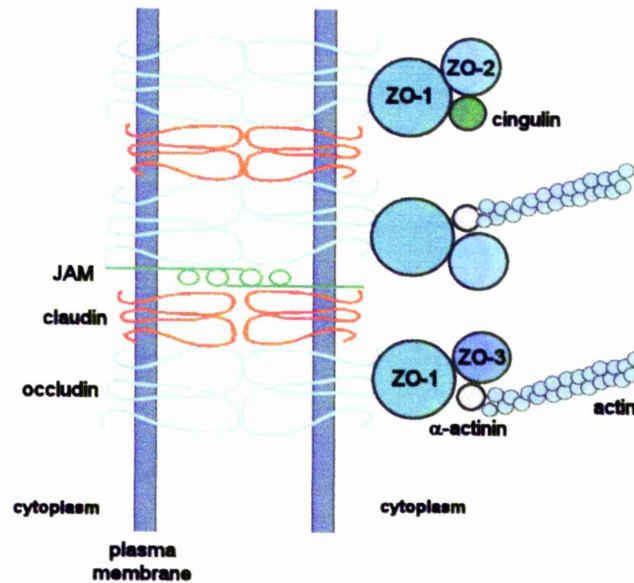


Figure 1-5: Structure of a tight junction

Claudins, occludin and junctional adhesion molecules (JAMs) span the plasma membrane to form junctions between adjacent cells. They are connected to the actin cytoskeleton by other junction associated proteins such as ZO-1.

Junctional adhesion molecules (JAMs) are localized at tight junctions of endothelial and epithelial cells and are also expressed by leukocytes and platelets [33]. JAM-A, JAM-B, and JAM-C can all bind homophilically and heterophilic interactions have been reported between JAM-B and JAM-C. They associate with the tight junction protein zona occludens-1 (ZO-1) and there is some evidence that they may contribute to cell-cell adhesion [33]. JAMs are also associated with leukocyte integrins (see Table 1-3) and may be involved in leukocyte migration across the endothelium [27, 34].

Other molecules have been identified at tight junctions, including the coxsackie and adenovirus receptor (CAR), endothelial cell-selective adhesion molecule (ESAM) and JAM4, all of which are members of the immunoglobulin superfamily [33].

1.3.1.2.2 Adherens junctions

Adherens junctions (see Figure 1-6) are composed mostly of vascular endothelial cadherin (VE-cadherin), a cadherin specific to endothelial cells. It is thought that VE-cadherin mediated adhesion is the most important element contributing to the strength of endothelial cell-cell junctions [35]. VE-cadherin forms dimers laterally and interacts with VE-cadherin dimers on adjacent cells to mediate

homophilic adhesion. Cadherins mainly form homophilic interactions, although they can form heterophilic interactions with different cadherins [36]. The cytoplasmic tail of VE-cadherin is linked to the actin cytoskeleton via β -catenin, α -catenin and plakoglobin (γ -catenin). Vinculin and α -actinin have also been implicated in VE-cadherin binding to actin [27].

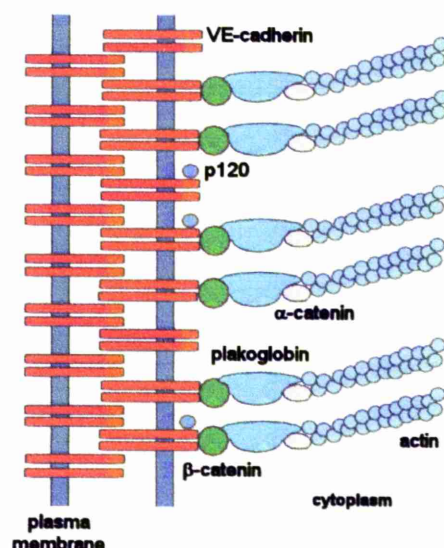


Figure 1-6: Structure of an adherens junction

VE-cadherin dimers on adjacent cells bind to each other to form an adherens junction. Associated proteins such as β -catenin connect them to the actin cytoskeleton.

In addition to their adhesive functions, zonula adherens are involved in cell signalling. They play a crucial role in contact inhibition, endothelial growth and regulation of apoptosis [27]. VE-cadherin is involved in cell signalling pathways [27] e.g. by regulating the cellular response to vascular endothelial growth factor (VEGF). β -catenin and other intracellular proteins associated with VE-cadherin are able to translocate to the nucleus and regulate gene transcription. The protein p120 binds to VE-cadherin but does not interact with α -catenin. It seems to be essential for cell surface expression of cadherin and is involved in regulation of endothelial barrier function [37].

1.3.1.2.3 Other endothelial junctional proteins

Endothelial cells, like platelets and leukocytes, also express PECAM-1 (platelet endothelial cell adhesion molecule 1) which is a member of the immunoglobulin superfamily. It is present at interendothelial cell contact regions, but

not confined to specific junctional complexes [38]. It can form homophilic adhesive contacts between endothelial cells and is involved in leukocyte transmigration across the endothelium [27, 34]. It is also able to mediate heterophilic adhesion, for example by binding to $\alpha_v\beta_3$ integrin [27]. PECAM-1 is able to interact with intracellular signalling pathways via SHP-2 and β -catenin and may be involved in modulating endothelial cell migration [27]. CD99 is another adhesion molecule found at cell-cell contacts where it mediates homophilic binding between endothelial cells and transmigrating leukocytes [39].

Other molecules have been described at interendothelial cell junctions, such as S-endo-1, endoglin, and nectin; all of which appear to mediate homophilic interactions between endothelial cells [27]. N-cadherin is also expressed diffusely on the surface of endothelial cells, but does not form part of a junctional complex. Its function in endothelial cells is unclear, but it may be important in interactions between endothelial cells and adjacent cells such as pericytes and smooth muscle cells [27]. Other as yet unidentified cadherins also appear to be expressed on endothelial cells [40].

1.3.1.3 Vascular basement membrane

Endothelial cells secrete, and are supported by, a basement membrane composed of a combination of extracellular matrix components. The exact composition of the basement membrane varies with the type of endothelium but the major components are typically laminins, collagen type IV, nidogens and heparan sulphate proteoglycans. Other components include fibronectin, thrombospondin and osteonectin [41]. Collagen is important for providing structural stability and proteoglycans have a variety of functions including cross-linking collagen and laminins and contributing to the filtration properties of the membrane [41]. Fibronectin is needed for the formation of blood vessels [41]. The composition of the basement membrane can also affect cellular transmigration; leukocytes preferentially migrate through areas of basement membrane composed of laminins containing α_4 chains instead of α_5 chains [41]. The interaction between endothelial cells and their basement membrane is important for regulating the function of the endothelium [41].

The bone marrow endothelial basement membrane has some differences from most other vascular basement membranes: studies in mice show it is discontinuous and does not contain heparan sulphate proteoglycans, although it does contain

abundant chondroitin sulphate proteoglycans [42]. This more loosely organised structure of the bone marrow basement membrane may be important in allowing the extensive cell trafficking needed at this site; in addition the abundant CD44 receptor in the form of chondroitin sulphate proteoglycans is important for haematopoiesis [42].

1.3.2 Cell adhesion to the endothelium

1.3.2.1 Leukocytes

The mechanisms leukocytes use to cross the endothelial barrier have been more extensively studied than those used by malignant cells. Leukocyte transmigration occurs primarily by the paracellular route, although neutrophils have been seen to pass directly through endothelial cells *in vivo* [43]. Various cell adhesion molecules are involved in this process (see Table 1-3).

There are three main steps described in the endothelial transmigration of leukocytes:

Rolling

Adhesion

Transmigration

Rolling

Rolling occurs due to weak interactions between leukocyte and endothelial adhesion molecules, which slow the leukocyte and allow it to bind more firmly. Rolling is mediated by molecules including L-selectin and sialyl Lewis X on leukocytes, and P- and E-selectin on endothelial cells [34]. Stimulation of L-selectin as leukocytes roll over the endothelium can induce upregulation of CXCR4 on the leukocyte surface. This receptor can interact with the chemokine CXCL12 (SDF-1) expressed by endothelial cells to induce α_4 integrin expression in the leukocyte, which contributes to adhesion and subsequent transmigration [34].

Adhesion

Adhesion is mediated by integrins and represents firm binding of the leukocyte to the endothelium. Leukocytes express several integrins which are involved in adhesion to the endothelium such as: $\alpha_L\beta_2$ (LFA-1), $\alpha_M\beta_2$ (Mac-1), $\alpha_4\beta_1$

(VLA-4) and $\alpha_5\beta_1$ (VLA-5). These can bind to the endothelial ligands intercellular cell adhesion molecule 1 (ICAM-1), ICAM-2, and vascular cell adhesion molecule 1 (VCAM-1) [34].

Table 1-3: Cell adhesion molecules known or suggested to be involved in leukocyte migration across endothelium

Leukocyte	Endothelium	Role
L-selectin	CD34	Rolling [44]
PSGL-1	P-selectin	Rolling [31]
$\alpha_M\beta_2$ (Mac-1)	ICAM-1 and -2 JAM-C	Adhesion [34] Transmigration [34]
$\alpha_L\beta_2$ (LFA-1)	ICAM-1 and -2 JAM-A	Adhesion [34] Transmigration [34]
$\alpha_4\beta_1$ (VLA-4)	VCAM-1 JAM-B	Adhesion [34] Transmigration [34]
CD99	CD99	Transmigration [34]
PECAM-1	PECAM-1	Transmigration [34]

1.3.2.2 Malignant cells

Malignant epithelial cells have been shown to bind to endothelial cells in an integrin dependent manner. Price *et al* (1996) [45] showed that β_1 integrin expressed by both endothelial and malignant cells was involved in binding of a breast carcinoma cell line to human umbilical vein endothelial cells (HUVEC). They noted that carcinoma cells adhered preferentially to endothelial cell-cell junctions and also showed that β_1 integrin was involved in binding of melanoma cells to HUVEC. Malignant cells, including malignant prostate cells, have been observed showing both rolling like motion before firm adhesion and stable adhesion without rolling within the microvasculature [46, 47].

1.3.2.3 Prostate carcinoma

There are several studies examining the involvement of different molecules in adhesion of prostate carcinoma cells to endothelium, some of which have produced conflicting results.

Malignant cells bind preferentially to bone marrow endothelial cells rather than to exposed ECM components [48] or to bone marrow stromal cells [49]. They

also bind preferentially at endothelial cell-cell junctions [17]. Binding of C4-2b malignant prostate cells (which express PSA) to bone marrow endothelium was inhibited by antibodies to PSA, while these had no effect on PC-3 cell binding, which do not express PSA [14]. Work by Scott *et al*, (2001) [13] showed that binding of PC-3 cells to bone marrow endothelium could be inhibited by antibodies to β_1 integrin, but not by antibodies to integrins β_4 , α_2 , α_4 , α_5 , or sialyl Lewis X (sLeX) on PC-3 cells, or to endothelial P-selectin, PECAM-1 (CD31) or VCAM-1. PC-3 binding to bone marrow endothelium was inhibited by antibodies to galectin-3, LFA-1 ($\alpha_L\beta_2$), CD11a (α_L), CD18 (β_2) and PECAM-1 (CD31) [15], when these were incubated with endothelial cells. Galectin-3 may be involved in the initial docking of epithelial cells before firm adhesion to endothelium [50]. Romanov and Goligorsky (1999) [51] showed that antibodies against α_3 , α_5 , β_1 , and $\alpha_V\beta_3$ inhibited binding of several prostatic cell lines, particularly PC-3 and DU145 (a cell line derived from a brain metastasis), to human umbilical vein endothelium (HUVEC). These results are summarised in Table 1-4.

Table 1-4: Cell adhesion molecules involved in binding of malignant prostate cells to endothelium

	α_2	α_3	α_4	α_5	α_6	α_L	$\alpha_V\beta_3$	β_1	β_2	β_4	galectin-3	sLeX	VCAM-1	P-selectin	LFA-1	PECAM-1
PC-3 [13] using BMEC	-		-	-				+		-		-	-	-		-
PC-3 [15] using HBME1						+			+		+				+	+
PC-3 [51] using HUVEC		+	-	+	+		+	+								-
DU145 [51] using HUVEC		+	-	+	+		+	+								-

+ Binding was inhibited by antibody to the adhesion molecule

- Binding unaffected by antibody

BMEC – human bone marrow endothelial cell line

HBME-1 – human bone marrow endothelial cell line

HUVEC – human umbilical vein endothelial cells

Soluble factors released from bone marrow stroma may be involved in stimulating binding of malignant prostate cells to bone marrow endothelium *in vivo*, possibly by modulating the adhesion molecules expressed by bone marrow endothelial cells [50]. Different cell lines also seem to respond differently to other

factors such as cytokines, e.g. TGF- β treatment of bone marrow endothelial cells reduced the adhesion of prostate epithelial cells; treatment of LNCaP cells (a cell line derived from a lymph node metastasis) also reduced their binding to bone marrow endothelium, but treatment of PC-3 cells did not affect their binding [52].

The results of some of these studies are conflicting, possibly due to heterogeneity in binding among different cell lines (including different endothelial cells), samples of primary tissue from different patients [16] and differences in specificity and epitope recognition by different antibodies. It is also the case that, in a similar way to leukocytes, several different adhesion molecules are likely to be involved in the process of binding and transmigration, with initial interactions via selectins [47] and firm adhesion via integrins [53].

1.3.2.3.1 Integrins

Integrins are transmembrane adhesion molecules composed of two non-covalently bonded proteins: an α subunit and a β subunit. A large number of different subunits have been described which can pair up and bind to specific ligands. Not all α subunits can pair with all β subunits so altered expression of one subunit can lead to changes in other integrins [54]. Integrin receptor distribution, surface expression and ligand-binding affinity are mediated by their cytoplasmic tails [54]. Many integrins have been implicated in the development and progression of cancer (see Table 1-5), with changes in integrins leading to effects such as altered interactions with the extracellular matrix (ECM), which can activate cell signalling pathways that lead to altered motility, binding, survival and proliferation. Integrins are also involved in altering and degrading basement membranes and ECM by regulating proteolytic enzymes, for example the integrins $\alpha_2\beta_1$ and $\alpha_v\beta_3$ bind matrix metalloproteinase 1 (MMP-1) and MMP-2 respectively, recruiting these enzymes to sites of cell adhesion to the ECM and promoting its degradation [55]. These effects can promote migration through the primary site and escape from the primary to spread to other sites [56]. Increased expression of β_1 integrin has been linked to increased aggressiveness in breast carcinoma cells [57]. They have also been implicated in binding of malignant cells to and invasion through the endothelium, as well as binding to the stroma of secondary sites [56].

1.3.2.3.2 Integrins and prostate carcinoma

Alterations in integrins are linked to prostate carcinoma development, morphology, Gleason score, migration and motility, invasion and escape from the ECM in the primary tumour [8, 58]. β_{1C} is an alternatively spliced variant of β_1 integrin which inhibits cell proliferation. It is present in normal prostatic epithelial cells [8] and its loss occurs early in malignant transformation [58]. Several integrins also appear to be involved in co-operative binding during interactions between prostate carcinoma cells and endothelial cells [51].

Table 1-5: Cell adhesion molecule alterations in malignancy

Integrin	Ligand	Tumour expression
$\alpha_6\beta_4$	laminin	altered expression in many carcinomas [56] altered location from hemidesmosomes to lamellipodia [56] promotes invasion in colorectal carcinoma [55] expressed in thyroid carcinomas [56]
$\alpha_v\beta_3$	fibronectin, fibrinogen, vitronectin, osteopontin, PECAM-1, L1	upregulated in malignant melanoma [56, 59] involved in activating and localising proteases for ECM degradation [56, 59] increased expression in prostate carcinoma [50]
$\alpha_1\beta_1$	laminin	reduced expression in breast and colon tumours [60]
$\alpha_7\beta_1$	laminin	increased expression in melanoma [60]
$\alpha_6\beta_1$	laminin, epiligrin	increased in breast, liver and non-small cell lung carcinoma [60] promotes invasion in prostate and breast carcinoma [55]
$\alpha_4\beta_1$	VCAM-1, fibronectin	downregulated in breast and colon tumours [60]
$\alpha_5\beta_1$	fibronectin	downregulated in breast and colon tumours [60]
$\alpha_3\beta_1$	fibronectin, collagen, laminin, epiligrin	altered expression or distribution in many malignant tumours [60]
$\alpha_2\beta_1$	collagen, laminin, cell-cell adhesion	altered expression or distribution in many malignant tumours [60] promotes invasion of melanoma [53]
sialyl Lewis antigens	E-selectin	present in squamous carcinoma, absent in normal keratinocytes [53] increased in metastatic breast carcinoma [53] increased in melanoma [53]

Several studies have examined integrin expression on prostatic epithelial cells (see Table 1-6), but results have been somewhat variable, possibly due to the use of different antibodies and methods. Haywood-Reid *et al* (1997) [61] also noted that highly confluent cells downregulated expression of most integrins on their surface.

In general, prostate carcinoma and its metastases show increased levels of integrins β_1 and β_3 (which is not expressed in normal prostate) and decreased levels of integrins α_4 and β_{1C} , although metastases do not always show the same expression patterns as primary tumours, with upregulation of α_2 integrin in metastases compared to primary tumours and upregulation of α_6 in lymph node metastases [54]. The α_6 subunit shows changes in distribution in malignant prostate cells [54].

Table 1-6: Integrin subunit expression in prostate epithelial cells

	Ref	α_1	α_2	α_3	α_4	α_5	α_6	α_v	α_{11b}	β_1	β_2	β_3	β_4	β_5	β_6
PNT-1A non-tumorigenic SV40 transformed cells	25	+	+	++	+	+	++	+	-	++	-	-	-		
PNT-1B non-tumorigenic SV40 transformed cells	25	-	+	++	+	+	+	+	-	++	-	-	-		
PPC-1 cell line derived from/contaminated by PC-3 [62]	25	-	++	++	-	+	++	+	-	++	-	-	+		
DuPro-1 cell line derived from/contaminated by PC-3 [62]	25	+	+++	++	-	+	++	+	-	++	-	-	++		
DUI45 cell line derived from a brain metastasis	24	+	+++	++	-	++	++	+	-	+++	-	+	+	+	
PC-3 cell line derived from a bone metastasis	25	+++	+++	+++	-	+	+++	+	-	+++	-	-	++	+	
PZ-HPV-7 transformed normal peripheral zone prostate epithelial cells	24			++		+		+		+++		+		+	
PrE primary normal prostate epithelial cells	24			++				+		+++		+			
BPH-1 immortalised cells from BPH	24			++		+		+		++		+		-	
P69 poorly tumorigenic prostate epithelial cell line	26	+	++++	++++	++	++	++	++	+	++	+	+	++	+	++
LNCaP cell line derived from lymph node metastasis	26	+	+	+	+	+	+	++	+	++	-	+	+	+	+
C4 poorly tumorigenic prostate epithelial cell line	26	+	+	+	+	++	++	++	+	++	-	+	+	++	+
C4-2 more tumorigenic cell line derived from C4	26	+	++	+	+	+	++	++	+	++	-	+	+	++	+
C4-2B4 more tumorigenic cell line than C4-2	26	+	++	+	+	+	+	++	+	++	+	+	+	++	+

- no expression
+ some expression
+++ high level of expression

1.3.3 Endothelial Transmigration

1.3.3.1 Leukocytes

The intercellular junctions and adhesion molecules between endothelial cells form barriers to the passage of leukocytes and other cells. Transmigration or diapedesis is the process by which leukocytes pass through the endothelial barrier. It occurs rapidly *in vitro*, each cell taking around five minutes [63] and causes minimal disruption of the endothelium. During paracellular transmigration, it is known that sequential homophilic interactions between PECAM-1 and CD99 on leukocytes and endothelial cells are important for transmigration, with the CD99 dependent step occurring distal to the PECAM-1 dependent step [38]. There is evidence for endothelial JAM proteins being involved in transmigration by interacting with leukocyte integrins [34, 64].

During transmigration, monocytes have been observed extending pseudopodia into the endothelial junction region and then migrating through a passage approximately 5µm in diameter in between endothelial cells. In a study by Sandig *et al*(1997), LFA-1 was found to be concentrated within the contact region between the monocyte and endothelial cell, but did not co-localise with ICAM-1 or -2 suggesting that it was interacting with an alternative ligand [65].

In a study using real-time imaging of transmigration, Shaw *et al* (2001) [63] showed that VE-cadherin was removed from endothelial cell junctions at the site of leukocyte transmigration with leukocytes moving through the gaps formed, which then re-sealed, possibly by lateral diffusion, within five minutes. Since VE-cadherin is linked to the cytoskeleton, they suggested that in order to form gaps, it may have to be uncoupled from the cytoskeleton, or that cytoskeletal changes were responsible for the movement of VE-cadherin away from the junction. There is also evidence that signalling via endothelial ICAM-1 can lead to cytoskeletal alterations and opening of endothelial cell junctions [34]. Although PECAM-1 is important in leukocyte transmigration, including passage through the basement membrane [66], any role it may have in signalling during transmigration is not clear [34]. Neutrophil adhesion to endothelial cells has been shown to induce removal of VE-cadherin and its associated catenins from endothelial cell contact regions, but without endothelial retraction or a change in the distribution of PECAM-1. These effects could be blocked by preventing adhesion of neutrophils to endothelium with anti- β_2 integrin

antibodies [67]. Neutrophil and monocyte adhesion has also been shown to induce a rise in endothelial cell intracellular calcium, which was associated with a rearrangement of the endothelial cytoskeleton [68]. The rise in calcium occurs only in cells adjacent to the transmigrating leukocyte [39] and is essential for transmigration, but not for adhesion of neutrophils to the endothelium [69]. The rise in Ca^{2+} could be blocked by pre-treating neutrophils with antibodies to sialyl Lewis X. Monocytes were unable to induce a rise in Ca^{2+} when treated with antibodies against VLA-4 ($\alpha_4\beta_1$) [68]. Treatment of endothelial layers with antibodies to the sialyl Lewis X receptors E-selectin and P-selectin, and the VLA-4 receptor VCAM-1 induced a rise in endothelial Ca^{2+} and actin stress fibre formation leading to gap formation [68]. A rise in free calcium within the endothelium can stimulate myosin light chain kinase (MLCK), which leads to phosphorylation of myosin regulatory light chains and consequently to contraction of endothelial cells [70]. This is dependent on the calcium binding protein calmodulin. Neutrophil transmigration induces formation of organised networks of actin and myosin filaments in endothelial cells which could be prevented by calcium chelating agents, calmodulin antagonists, and MLCK inhibitors. These agents also prevented transmigration of neutrophils across the endothelium, but not their adhesion to it [71]. These results suggest that neutrophil transmigration depends on calcium/calmodulin and MLCK mediated mechanisms associated with cytoskeletal reorganisation in endothelial cells and that signalling between leukocytes and endothelial cells via receptors involved in rolling and adhesion is essential for transmigration [34].

1.3.3.2 Melanoma and other malignant cells

Invasion of tumour cells through endothelium is a crucial step in the formation of distant metastases. Tumour cells must first cross the endothelial barrier to enter the peripheral blood and then cross it again to leave and enter the secondary site. The most well studied tumour-endothelial cell transmigration is in melanoma. However, recently other tumours have been studied.

1.3.3.2.1 Melanoma

Endothelial transmigration has been more extensively studied in melanoma than other malignancies. Invasion takes around five hours *in vitro* and progresses through five stages (see Figure 1-7) described by Voura *et al* [72, 73]:

- I Melanoma cells settle on the endothelium, initially they show a smooth surface.
- II Melanoma cells produce membrane blebs at the surface adjacent to the endothelial cells and begin to extend pseudopodia.
- III Pseudopodia extend into the endothelial cell-cell junction regions and endothelial cells begin to retract.
- IV Melanoma cells move into gaps between retracting endothelial cells, but maintain membrane contact with endothelial cells.
- V Melanoma cells spread on the underlying substrate and endothelial cells begin to seal the gap by spreading over the surface of them.

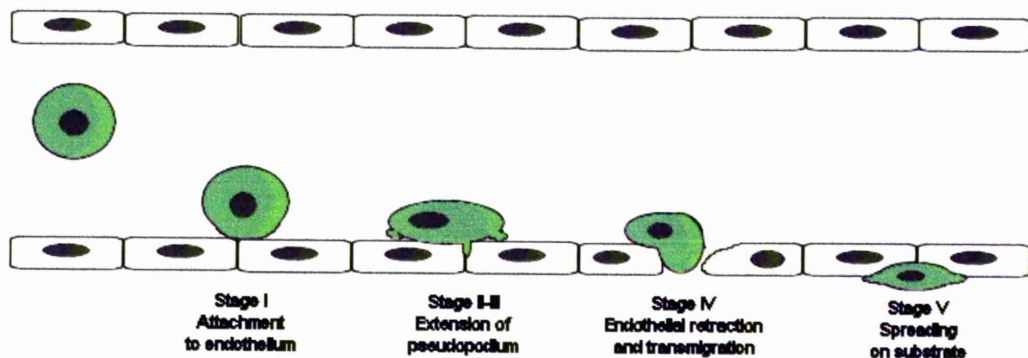


Figure 1-7: Stages of endothelial transmigration of malignant cells

During transmigration the melanoma cell remains in constant contact with the endothelial cell. Endothelial cells have actin filaments which extend to the sites of contact with the melanoma cell at stage II. Taken together with the maintenance of membrane contact between cells during transmigration, this suggests that both cell types are actively involved in interactions during the transmigration process [72]. These interactions may occur through signalling via cell surface receptors, but another possible means of communication between malignant cells and endothelial cells is via gap junctions, which have been demonstrated between some melanoma cell lines and endothelial cells *in vitro* [74, 75]. Formation of these gap junctions precedes transmigration [75]. It has also been shown that invasive melanomas show increased expression of the gap junction component connexin 26 *in vivo* [74].

Both VE-cadherin and PECAM-1 were lost from the endothelial cell junctions below bound melanoma cells as pseudopodia were extended into this

region [40, 76]. Addition of anti-PECAM-1 antibodies to endothelial cells did not affect transmigration, suggesting that, in contrast to leukocytes, PECAM-1 is not needed for melanoma transmigration [76]. However N-cadherin, which is expressed by some tumour cells [77, 78] as well as endothelial cells, was present at these contacts and blocking N-cadherin delayed, but did not prevent transmigration [40].

Integrins also play a role in transmigration of melanoma cells. Membrane blebs and pseudopodia of melanoma cells appear to have a higher concentration of $\alpha_v\beta_3$ integrin than other regions of the cell membrane, and $\alpha_v\beta_3$ integrin is also concentrated in regions of contact with the adjacent endothelial cell during transmigration. Blocking $\alpha_v\beta_3$ integrin on melanoma cells, or using $\alpha_v\beta_3$ negative melanoma variants markedly reduced transmigration, whereas blocking endothelial $\alpha_v\beta_3$ had no effect on transmigration. The binding of melanoma to endothelial cells was not affected by blocking the integrin on either cell type [79]. L1 is a cell adhesion molecule which can form homophilic and heterophilic contacts with $\alpha_v\beta_3$. It is a member of the immunoglobulin superfamily and is expressed on neurones, leukocytes, epithelial cells, some malignant cells [80] and on human microvascular endothelial cells [79]. Blocking endothelial L1 led to a small reduction in transmigration, with more pronounced effects on blocking both L1 and $\alpha_v\beta_3$, suggesting that melanoma cell $\alpha_v\beta_3$ interacts with endothelial L1 during transmigration, but not adhesion [79]. L1 is secreted by melanoma cells [79] and is also found at the invasive front of colonic adenocarcinoma, where shedding of the molecule into the stroma has been suggested to be involved in invasion of malignant cells [80].

1.3.3.2.2 Breast carcinoma and other malignant cells

Transmigration of MCF-7 breast carcinoma cells has been shown to be associated with a transient rise in Ca^{2+} concentration within endothelial cells and endothelial retraction, but only in those cells that were directly interacting with tumour cells. Benign breast epithelial cells were unable to induce either retraction or a change in endothelial Ca^{2+} levels. The rise in Ca^{2+} was tyrosine kinase-dependent and preceded endothelial retraction. Blocking this rise in Ca^{2+} prevented endothelial transmigration [81]. On adhesion of MCF-7 cells, endothelial cells showed a loss of VE-cadherin from cell junction regions, being redistributed to intracytoplasmic sites. At the same time, vinculin was redistributed from endothelial cell contact regions to

focal adhesion plaques on the basal side of the endothelial cells [82]. However, benign breast epithelial cells did not produce these effects. The loss of endothelial cell to cell adhesion was not prevented by metalloproteinase and serine protease inhibitors, suggesting that enzymatic digestion of adhesion molecules was not involved. The VE-cadherin/ β -catenin/ α -catenin/plakoglobin complex did not dissociate on endothelial dissociation and malignant transmigration, but was redistributed away from endothelial cell junctions and showed an increased level of phosphorylation [82]. Phosphorylation of VE-cadherin and catenins produced by vascular endothelial growth factor (VEGF) has been linked to increased endothelial permeability [82].

Table 1-7: Cell adhesion molecules involved in malignant cell interactions with endothelium

Endothelial adhesion molecule	Malignant cell adhesion molecule	Tumour type
E-selectin	sialyl Lewis antigens	colon, renal carcinoma [53] melanoma [83]
CEA	CEA	colon, breast carcinoma [53]
VCAM-1	$\alpha_4\beta_1$ integrin α_4 integrins	melanoma, sarcoma [53], SCLC [22] renal carcinoma [53]
α_6 integrins	$\alpha_6\beta_1$	melanoma [53]
β_1 integrins		small cell carcinoma [53] melanoma, breast carcinoma [45] prostate carcinoma [13, 51]
Thrombospondin	Tsn receptors	MCF7 breast carcinoma cells [53]
CXCL12 (bone marrow stroma and endothelium)	CXCR4	small cell lung carcinoma [22] activation of migration in ovarian carcinoma [55] chemotaxis and metastasis of breast carcinoma [23]
	$\alpha_v\beta_3$	expression correlates with increased ability to migrate across HUVEC monolayer in certain cell lines of breast, lung and renal carcinoma, melanoma [84]

In contrast to the breast carcinoma studies which found that direct interaction between live tumour cells and endothelial cells was required rather than fixed cells [81, 82], isolated malignant cell membranes [81] or tumour-conditioned medium

[82], the production and secretion of soluble factors by pancreatic carcinoma cell lines has been reported to induce endothelial retraction [85]. Endothelial cell E-selectin activation by colon carcinoma cells has been shown to be important in opening endothelial cell-cell junctions [86]. Molecules involved in malignant interaction with the endothelium are shown in Table 1-7.

1.3.3.3 Prostate carcinoma

Prostate carcinoma migrates across the endothelium in similar stages to those described for melanoma [17] (see Figure 1-7) with malignant cells binding in around 90 minutes (stage 1), achieving partial invasion (stage 2) in around two hours and total invasion (stage 5) in 232 \pm 43 minutes [17]. After binding to endothelial cells, malignant prostate cells show membrane blebbing and extend a pseudopodium into the endothelial junction [17, 18]. Prominent actin stress fibres have been observed in endothelial cells during transmigration [18] and contact is maintained between the epithelial and the retracting endothelial cells during the process [17, 18]. A rise in endothelial intracellular calcium on contact with the malignant prostate cell line LNCaP has been demonstrated [87]. These observations support the idea that endothelial transmigration occurs by similar mechanisms in several tumour cells.

Bone marrow endothelium provides a strong stimulus for prostate carcinoma invasion *in vitro*. Matrigel invasion studies with the prostate epithelial cell line PC-3 showed that bone marrow endothelium induces invasion at a similar level to bone marrow stroma. Both bone marrow stroma and bone marrow endothelial cells induced significantly more invasion than either HUVEC or tissue culture plastic [13]. However primary malignant cells invaded towards bone marrow stroma more readily than towards endothelium [17]. Benign cells showed no ability to invade in response to endothelium [13], therefore the ability of epithelial cells to invade through endothelial layers is related to their metastatic potential [88].

1.3.4 Tissue invasion and colony formation

Once through the endothelium, malignant cells must invade the tissue and proliferate to form clinically apparent metastases. Prostate epithelial cells can adhere to bone marrow stroma via integrins, e.g. $\alpha_2\beta_1$. Bone marrow contains growth factors including transforming growth factor β (TGF- β), insulin-like growth factor 1 (IGF-1), interleukin 6 [50, 89] and other factors which promote invasion e.g. collagen type I (a ligand for $\alpha_2\beta_1$ and $\alpha_3\beta_1$ integrins) [8]. TGF- β produced by osteoblasts stimulates

expression of integrins and migration by PC-3 cells [8]. Metastatic prostate carcinoma cells can produce bone morphogenetic proteins which can stimulate osteoblastic differentiation in bone marrow mesenchymal cells [8]. Malignant prostatic cells secrete enzymes such as matrix metalloproteinases and urokinase plasminogen activator which can degrade stroma and facilitate invasion. These enzymes also show increased expression in the stroma adjacent to tumour deposits, suggesting interaction between the malignant cells and stroma [90].

1.4 Cell motility and metastasis

1.4.1 Cell motility

The ability of cells to move within their environment is essential in order for them to migrate to other sites in the body. Cell migration occurs during embryonal development, leukocyte migration and cancer metastasis.

There are five basic steps in cell movement [91]:

- 1) Polarisation and pseudopod protrusion
- 2) Adhesion to extracellular matrix at leading edge of cell. Focal adhesions are formed
- 3) Proteases may be recruited to degrade extracellular matrix
- 4) Cell contraction produces translocation of cell body
- 5) Detachment and retraction of trailing edge

This system of cell movement is dynamic and can be adapted by the cell depending on the environment to allow cell movement under different conditions [92]. Some investigators have noted that migrating cells go through stationary phases during the migration cycle, but these phases are used by the cells to build pseudopodia, attach and reorient themselves within the matrix, making them active parts of cell migration [93].

Cytoskeletal elements, including the cortex, are vital for the shape changes and cell contraction required for cell movement. The cortex is a part of the cytoskeleton under the plasma membrane; it contains actin filaments, myosin II and associated proteins [94]. These are essential for the formation of cell protrusions observed during movement: pseudopodia (tubular), lamellipodia (broad and

flattened) or filopodia (narrow or spike-shaped) [95]. Several different types of cell motility have been described [92].

1.4.1.1 Collective cell movement

This occurs when a group of cells connected by cell-cell junctions migrate together; this can be seen in well differentiated epithelial tumours and melanoma. The cell-cell junctions are maintained by adhesion molecules such as cadherins and integrins but cells take on differing roles in order to allow movement of the group. Cells at the leading edge extend pseudopodia and form new adhesions to the matrix, as well as producing some matrix degradation. Cells at the trailing edge detach from the matrix to allow forward movement and cells inside the cluster maintain cohesion [91]. Collective cell migration is shown in Figure 1-8.

In melanoma cells migrating in this way, thicker F-actin bundles have been found to be oriented mainly towards the leading edge of the cluster and distribution of actin fibres throughout the cell cluster was asymmetric. The authors suggested that a degree of supracellular organisation of the cytoskeleton was necessary for collective migration [96]. They noted that β_1 -integrins, the major collagen receptors, were clustered at the leading edge although they were also present at cell-cell junctions. Blocking β_1 -integrin function with antibodies lead to cell cluster dissociation and a switch to single cell migration [96].

1.4.1.2 Mesenchymal motility

Mesenchymal motility is the type of motility typically demonstrated by fibroblasts. The cells adopt an elongated morphology with a broad lamellipodium at the leading edge and go through the five stages of movement described in section 1.4.1. This form of motility is associated with degradation of the extracellular matrix by the cell, in order to move through it, and by the use of integrins to adhere to the surrounding matrix. Clustering of surface proteases with integrins at cell-matrix contacts is important for degradation of matrix in specific regions. Clustering of integrins at sites of ECM attachment also leads to recruitment of other proteins and formation of more stable attachments called focal contacts. The focal contacts formed are turned over slowly so the speed of migration is slow: around 0.1-1 $\mu\text{m}/\text{min}$ [97]. Detachment of the rear of the cell from the ECM can be accompanied by shedding of membrane fragments with integrins and other adhesion molecules,

known as 'migration tracks'. These may occur as part of the tail retraction process but may also provide a system for guiding other migrating cells [98].

The signalling molecule Rac1 is important for producing the membrane protrusions at the leading edge of the cell [99] and has been shown to be upregulated in metastasis [95].

1.4.1.3 Amoeboid motility

Amoeboid motility is the type typically shown by leukocytes [92]. The cells take on a rounded shape and use pseudopodial extensions to squeeze through the extracellular matrix, pushing collagen fibres aside [100]. Proteases are not required for this form of cell movement [100]. Contacts formed with the extracellular matrix are weak and short-lived and mature focal contacts are not seen. The cell undergoes rapid shape changes in order to migrate through the matrix and enzymes are not used to degrade the matrix. Amoeboid movement is characterised by contraction of myosin at the trailing edge and polymerisation of actin at the leading edge, there is also a cycle of membrane uptake from the plasma membrane with extension of membrane at the leading edge [101].

Amoeboid movement is associated with membrane blebbing which occurs where the plasma membrane becomes focally detached from the actin cortex and forms rounded protrusions on the cell surface. Although blebbing also occurs during cytokinesis and apoptosis, its function is not known. It has been suggested that blebbing is a method of rapidly generating new cortex when the cell needs to expand its cortical area to accommodate rapid shape change [94]. Blebbing is an active process requiring actin, myosin II [101] and ROCK (Rho-associated kinase) activity [102]. It appears that blebbing is important for producing rapid membrane protrusion and retraction and therefore contributes to the speed of movement of cells using amoeboid motility [101]. Blebbing seems to be needed for this membrane extension and cortical actin remodelling also appears to be involved in amoeboid motility [101].

Cells that move with an amoeboid type of motility associated with blebbing can be blocked from invading the ECM by inhibition of Rho or ROCK [99], indicating the importance of this signalling pathway for amoeboid movement. ROCK is important in the production of force needed to deform the ECM [100]. There also seems to be a tendency for tumour cells that show a rounded morphology to have a

greater metastatic potential [99] and ROCK1 has been shown to be upregulated in metastasis [95, 103]. A comparison of amoeboid and mesenchymal motility is shown in Table 1-8.

Table 1-8: Characteristics of mesenchymal and amoeboid motility

Mesenchymal	Amoeboid
MMP dependent	MMP independent
ROCK independent	ROCK dependent
Greater integrin dependence	Lesser integrin dependence
Stronger matrix adhesion	Weaker matrix adhesion
Higher surface expression of $\alpha_2\beta_1$ integrin	Lower surface expression of $\alpha_2\beta_1$ integrin
Degradation of matrix to produce a path for movement	Squeezing through matrix gaps to find a path for movement
Autophosphorylation of FAK	Reduced autophosphorylation of FAK
Calpain dependent invasion [104]	Calpain independent invasion [104]
Src dependent invasion [104]	Src independent invasion [104]
Slow speed (0.1-1 $\mu\text{m}/\text{min}$)	Faster speed (up to 4 $\mu\text{m}/\text{min}$)

1.4.1.4 Switching between modes of motility

The mode of movement adopted by cells is determined by the interaction of factors including the extracellular matrix, the intrinsic activity of signalling pathways within the cell, and chemoattractant gradients [99]. Different types of cell motility are shown in Figure 1-8. *In vitro* experiments have shown that cell movement on a 2D substrate is not a good predictor of how the same cells move in a 3D environment [99].

A reduction in cell-cell adhesion promotes a switch from collective to mesenchymal cell motility and a reduction in both cell-cell and cell-matrix adhesion promotes a switch to amoeboid motility. A more pliable ECM seems to favour amoeboid movement [99]. Cells can be induced to switch from mesenchymal to amoeboid motility by blocking matrix degradation with protease inhibitors [99]. Blocking signalling molecules involved in amoeboid motility *in vitro* can also induce cells to switch from amoeboid to mesenchymal motility [105]. The ability of cells to adopt different modes of motility in response to environmental stimuli is dependent on factors intrinsic to the cell; migration of breast cancer cells of low tumourigenicity could be reduced by Rac1 inhibitor alone, while more aggressive breast cancer cells

showed an increase in migration and an increase in RhoA activity under the same conditions [106]. These breast cancer cells also adopted a rounded morphology [106], suggesting they may have switched to amoeboid motility.

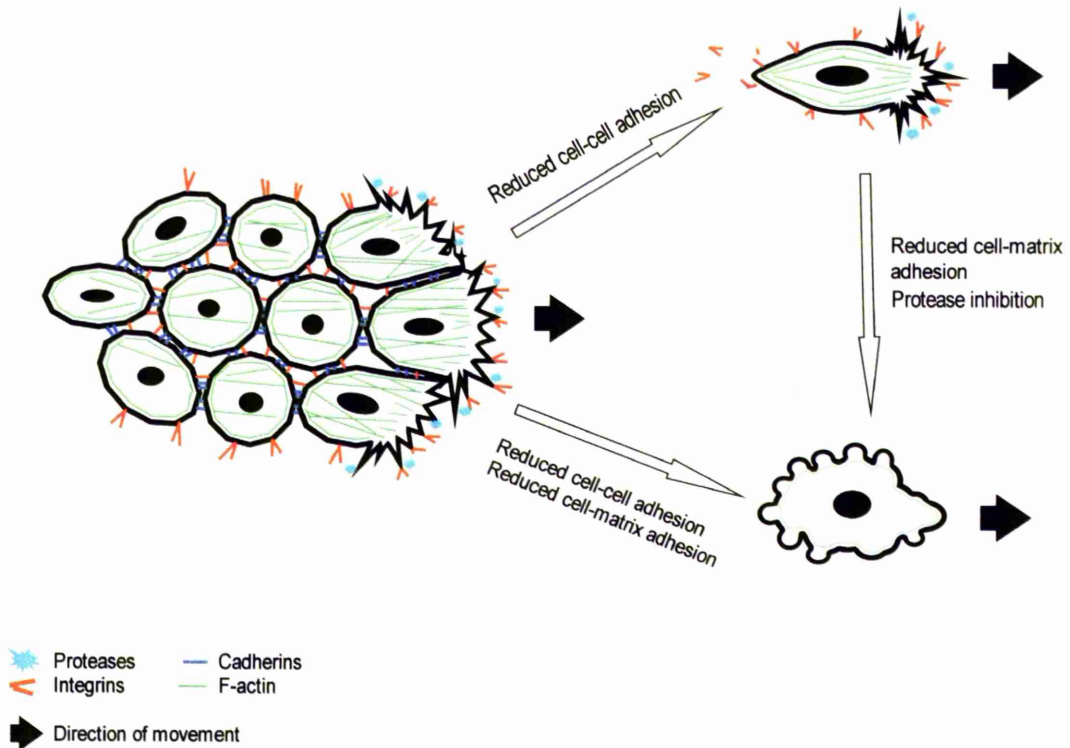


Figure 1-8: Types of cell motility

In collective cell motility (left), cells move as a cluster using integrins to adhere to the ECM and proteases to degrade it. Cadherins and other adhesion molecules including integrins bind the cells together. In mesenchymal motility (top right) single cells use integrins to adhere to the ECM and proteases to degrade it. Integrins (and other adhesion molecules) are often shed into the ECM forming a track which can allow other cells to follow. In amoeboid motility (bottom right) cell-matrix contacts are weak and matrix degradation is not prominent. The cell has a rounded shape and membrane blebs are seen where the plasma membrane has become detached from the underlying actin cortex.

1.4.2 Motility and metastasis

The ability of cells to migrate is crucial for the formation of metastases. Malignant cells must migrate into and out of blood and lymphatic vessels and through tissues in order to spread to other sites. Although many normal cells have the ability to migrate, this is tightly regulated. Changes in gene expression due to mutations lead to aberrant behaviour and can enhance motility in malignant cells [97]. Some of these are shown in Table 1-9. Tumour microenvironment, including

the presence of fibroblasts and macrophages, influences cancer cell motility and motile cells may be found only in localised areas within tumours [97].

Table 1-9: Genes involved in cell motility associated with cancer cell invasion and metastasis

Gene	Alteration	Role
c-fos fra-1	Over expression	Both are genes from the fos family. Involved in invasion through basement membranes [107]
RhoA RhoC	Over expression	Generation of contractile force during cell motility [97]
ROCK	Over expression	Generation of contractile force during cell motility [97] Promotion of cell dissemination from solid tumours [108]
Cdc42 Rac1	Over expression	Formation of actin-rich cell protrusions during motility [97]
u-PA u-PAR	Over expression	Proteases used for degrading ECM [97]
Cathepsins	Over expression	Proteases used for degrading ECM [97]
MMPs	Over expression	Proteases used for degrading ECM [97]
nm23	Reduced expression	Indirectly inhibits cell motility [97]

1.4.2.1 Motility transitions and metastasis

During malignant transformation of epithelial cells, one of the processes that occurs is the transition from a static epithelial phenotype to a migratory mesenchymal phenotype. This is known as the epithelial-mesenchymal transition (EMT) and is characterised by alterations in cell shape such as elongated or spindle shaped morphology, loss of epithelial cadherins and expression of mesenchymal markers e.g. vimentin [109]. This alteration in phenotype allows the cells to invade through the ECM, however the expression of a phenotype suggesting a cell has undergone EMT cannot always be used to predict whether a tumour is able to metastasise [110]. The ability to migrate may occur in the absence of a demonstrable EMT [109]. It is also the case that there may be reversion to an epithelial phenotype after invasion or metastasis, so the transition between these phenotypes appears to be dynamic and reversible [109]. Motility may be acquired by a different transition, that to amoeboid motility. This may occur either from a mesenchymal or epithelial

phenotype and is also likely to be a dynamic and reversible process. The nature of the interactions between the cell and its environment also change with a transition from one phenotype to another, and the environment may influence the phenotype of the cell [109]. Tumour cells seem to need changes both within the cell and in the environment in order to produce a motile phenotype [97]. The ability of malignant cells to change their phenotype in response to their environment may allow them to survive and spread in different microenvironments within the body.

1.5 Modelling metastasis and invasion

Some simple methods for the assessment of cell motility are available such as the wound healing or scratch assay. In this technique cells are grown to confluence before a needle or similar implement is used to scratch part of the cell layer away. The “healing” of the cell layer is then observed, and occurs by a combination of cell division and migration [111]. This technique can be used to study cell migration, but as it is a 2D technique it is difficult to relate the results to cell migration in a 3D *in vivo* environment.

1.5.1 Invasion through matrices

Invasion through ECM can be studied using ECM substitutes such as collagen gels [112], Matrigel or complex custom-made combinations of different matrix components [113]. Matrices can be produced in varying thicknesses to simulate tissue or thinner basement membranes. Malignant cells can be added to these systems, either onto the surface of the matrix or within it, and their behaviour and invasiveness assessed. The ECM gels can be multilayered, with different cell types within each layer [114].

1.5.2 Invasion chambers

Specially designed invasion chambers have been used to study migration across basement membranes and endothelial layers [53, 78]. Malignant cells can be added to the upper chamber and their migration across a basement membrane and/or endothelial barrier assessed in relation to chemotactic factors or specific cell cultures in the lower chamber [13, 20]. The bottom of the upper chamber is composed of a membrane with pores which are smaller than the cells being studied, so that cells must actively migrate through them. A typical invasion chamber is shown in Figure 1-9.

These chambers are useful for assessing the ability of cells to invade through the ECM or a cellular barrier, but they do not allow visualisation of cell-cell or cell-matrix interactions during invasion.

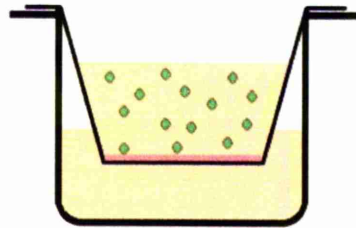


Figure 1-9: Diagram of an invasion chamber

The bottom of the upper chamber is composed of a membrane with pores of a defined diameter. This can be coated with basement membrane components and/or a layer of cells cultured on it to provide a barrier. Chemoattractants can be placed in the lower chamber and cell migration from the upper chamber to the underside of the membrane or into the lower chamber assessed.

1.5.3 Co-culture systems

Co-culture systems can be used to study the interactions between different types of cell e.g. malignant cells and stromal or endothelial cells. 2D and 3D culture systems have been developed to allow the study of many aspects of tumour biology [115]. Co-culture systems have been used to examine the interactions between malignant cells and endothelial cells including melanoma [73] and prostate carcinoma [17]. These *in vitro* systems allow careful control of the environment as well as analysis using a variety of techniques, and can include a variety of extracellular matrices or tissue samples such as explanted veins [116] or bladder wall [117]

1.5.4 *In vivo* systems

Animal models are available for many tumours including prostate cancer [118] and allow the study of metastases and the effects of potential therapies. Rats have been used as a model for prostate carcinoma as they spontaneously develop prostate carcinoma, although the disease in rats has some differences from human disease. Mouse models of spontaneous prostate carcinoma have been developed, but these still show some differences from human disease [118]. Other *in vivo* systems use transplantable tumours; immunocompromised animals are injected with tumour cells which can be derived from their own species or a different species (e.g. human

tumour cells). The cells can be injected directly into the bloodstream to produce metastases directly, or into the tissue to produce a primary tumour which may go on to metastasise [119]. Tumours produced *in vivo* can be imaged non-invasively or examined after sacrifice of the animal. Although green fluorescent protein is widely used *in vitro* for imaging, the problems of tissue autofluorescence at the same wavelength and absorption of GFP emission by tissues have made it less useful for *in vivo* imaging. Other fluorophores and new techniques for imaging GFP *in vivo* have allowed the use of fluorophores for *in vivo* work [120] and GFP labelled PC-3 prostate carcinoma cells have been used in mouse studies of bone metastasis using whole body fluorescence for imaging [121]. Bioluminescent imaging using reporter molecules such as luciferase is a sensitive technique due to the low intrinsic bioluminescence of mammalian tissues and has been used to study bone micrometastases produced by breast carcinoma cells transfected with luciferase [122].

1.5.5 Imaging

To study invasion *in vitro* there are various techniques allowing visualisation of fixed or living cells. Some of these techniques are only suitable for imaging of fixed cells but light microscopy can be used with fixed or living cells and can be used to image living cells over time.

1.5.5.1 Light microscopy

Confocal light microscopy allows examination of a 3 dimensional specimen by varying the focal plane to image different levels within the specimen (see Figure 1-10). The confocal aperture excludes light from out-of-focus planes within the specimen to give a high quality image. The lateral resolution (x,y) is around 180nm and axial resolution (z) around 500nm [123]. In combination with scanning across the specimen laterally, the axial information collected can be used to create a 3D reconstruction of the specimen.

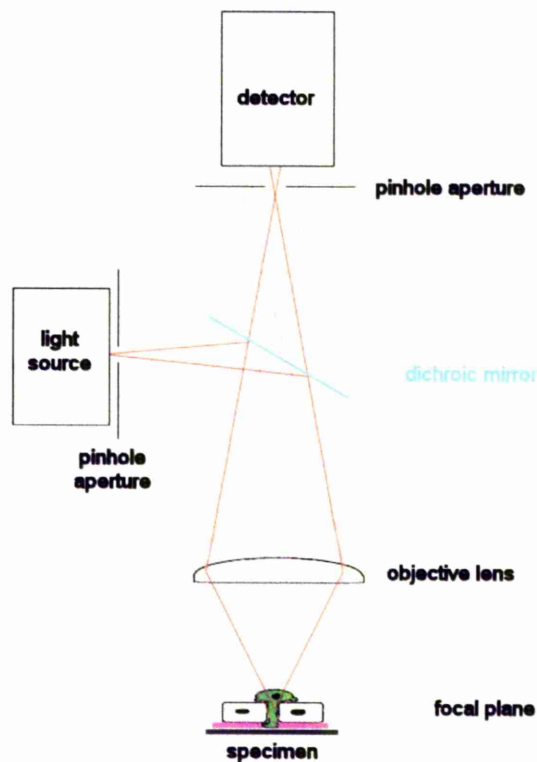


Figure 1-10: Laser scanning confocal microscope

Out of focus light (pink) is excluded by the pinhole aperture so only light from the selected focal plane (red) reaches the detector.

Confocal microscopy has been used to study endothelial transmigration of leukocytes [63] and malignant cells [18, 82]. Interactions can be observed in real time, following labelled cells as they migrate across the endothelial layer, or cultures can be fixed at different time points during the invasion process and labelled with immunofluorescent antibodies. These techniques can show co-localisation and changes in the distribution of junctional proteins, cytoskeletal components and adhesion molecules [40, 65].

Voura *et al* (1997 and 1998) [72, 73] used laser scanning confocal microscopy to investigate interactions between melanoma cells and a layer of endothelial cells. They defined the different stages of transmigration and determined the morphological changes occurring in cells during transmigration. Using fluorescent staining of cell components in fixed specimens, they showed marked changes in actin organisation within transminating melanoma cells and adjacent endothelial cells. Using similar techniques, Sandig *et al* (1997) [40] showed that VE-

cadherin disappeared from endothelial cell-cell contacts at the site of melanoma transmigration. In a similar study using breast carcinoma cells, Lewalle *et al* (1997) [82] also showed a loss of VE-cadherin from endothelial cell contacts adjacent to transmigrating malignant cells.

Real time imaging of live cells by confocal light microscopy was used by Hart *et al* (2005) [17] to follow green fluorescent protein labelled PC-3 cells (PC-3-GFP) as they migrated across a layer of bone marrow endothelium. This occurred in stages similar to those described for melanoma cells.

1.5.5.1.1 Fluorescence

The use of fluorescence allows the identification of cell types and cellular proteins by labelling them with fluorophores which can be visualized by light microscopy. Antibodies conjugated to fluorophores can be used to specifically label proteins of interest or cell surface markers; fluorophores can be used to stain cell membranes non-specifically or transfected into cells to be expressed in the cytoplasm or tagged to specific molecules. These techniques allow visualization of cells and molecules in both live and fixed cultures. The combination of fluorescence and brightfield imaging with confocal microscopy provides a powerful technique for studying biological specimens.

Fluorescence can also be used for *in vivo* imaging in small animal studies to assess metastases and even micrometastases. This is a sensitive technique which allows the development of metastases to be detected at an early stage before significant symptoms are apparent, and because it is non-invasive the same animal can be imaged repeatedly, potentially reducing the total number of animals required [120].

1.5.5.2 Scanning electron microscopy

1.5.5.2.1 Basic SEM

Scanning electron microscopy (SEM) produces static images of the surfaces of cells by using a beam of electrons to scan the surface of a metal-coated, dried specimen. It is capable of both low and high magnification (from around x20 to x150,000) with a resolution of around 1nm [124].

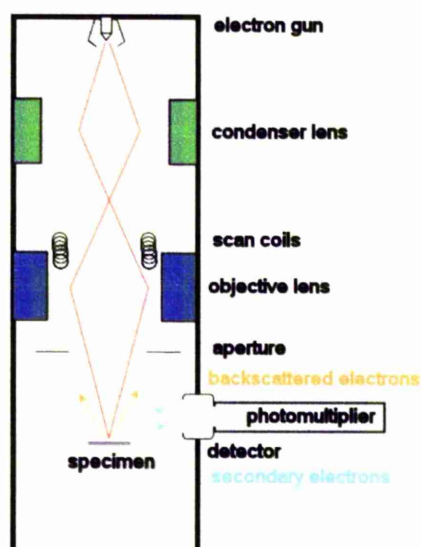


Figure 1-11: Scanning electron microscope

The electron beam is focussed onto the sample where electrons are scattered by the sample's metal coating and these secondary electrons are detected by a photomultiplier to form the image. When gold labelling is used, the gold particles cause backscattering of electrons that interact with them and these backscattered electrons can be detected separately to show the location of the gold particles.

When the specimen is bombarded with electrons in the SEM, low energy secondary electrons are emitted from the surface of the specimen which are responsible for forming the image. High energy backscattered electrons are produced when beam electrons are scattered back out of the specimen; this depends on the atomic number of the specimen and these are electrons can be used to localise immunogold labelled molecules.

It can show relationships between cells in three dimensions and structures on the cell surface such as integrins and selectins. These can be identified by immunogold labelling and their distribution studied [125]. Fracturing specimens allows imaging of intracellular structures such as the cytoskeleton, and it is particularly useful for large and complex structures such as this, which can be visualised without the limitations of the thin sections needed for transmission electron microscopy.

1.5.5.2.2 SEM for migration and invasion

Because of its ability to produce high resolution images of surfaces at both low and high magnifications, SEM is useful for studying cell-cell interactions. It has been used to visualise membrane blebs, lamellipodia and endothelial retraction during migration of malignant cells across endothelial layers *in vitro* [82, 126].

Lewalle *et al* (1997) [82] used SEM in combination with light microscopy to demonstrate endothelial retraction of HUVEC upon interaction with breast carcinoma cells. Lang *et al* used SEM to study interactions between prostate epithelial cells and bone marrow stroma in an in vitro model of bone colonisation by prostate cancer [9].

1.6 Aims and hypotheses

Hypothesis: that there are specific interactions occurring between malignant prostatic epithelial cells and bone marrow endothelial cells which allow invasion through the endothelium.

Aim: to map the physical and molecular interactions between malignant prostate epithelial cells and bone marrow endothelial cells during invasion by:

1. Defining optimal conditions for prostate epithelial cell tracking during endothelial transmigration
2. Image mapping of intercellular interactions within the endothelial cell-cell junction during prostate epithelial cell invasion
3. Determining the signalling pathways involved in prostate epithelial cell transendothelial migration

2 Materials and methods

2.1 Materials

All plasticware was from Becton-Dickinson (Oxford, UK) unless otherwise stated. Laboratory reagents were from Sigma-Aldrich (Gillingham, UK) unless otherwise stated.

2.1.1 Antibodies

Mouse monoclonal antibodies to VE-Cadherin (cadherin-5, CD144), α 5-integrin (CD49e), VCAM-1 (CD106), PECAM-1 (CD31), β 4-integrin (CD104), α 4-integrin (CD49d), P-selectin (CD62P), CD99, Occludin, and Sialyl Lewis X (CD15s) were from BD Biosciences (Oxford, UK). Mouse monoclonal antibodies to ZO-2 and claudin-5, and rabbit polyclonal antibodies to ZO-3 and claudin-12 were from Zymed (CA, USA). Mouse monoclonal antibodies to E-Cadherin and N-Cadherin, rabbit anti-mouse biotin, rabbit anti-mouse-FITC, swine anti-rabbit-FITC and streptavidin-FITC were from Dako (Ely, UK). Mouse monoclonal antibodies to β 1-integrin were from Santa-Cruz (CA, USA). Mouse anti-pancytokeratin antibody (clone C-11) was from Sigma. Goat anti-mouse 10nm gold antibodies were from Amersham Biosciences (Buckinghamshire, UK).

Zenon® Alexa Fluor® antibody labelling kits and image-iT FX signal enhancer were from Invitrogen (Paisley, UK). Vectastain ABC kit was from Vector Labs (Peterborough, UK)

2.1.2 Inhibitors

Y-27632, Rac-1 inhibitor, GM6001 and blebbistatin were from Merck Biosciences (Nottingham, UK). Y-27632 and Rac1 inhibitor were made up in sterile water at 6.75mg/ml and 5mg/ml respectively, GM6001 was made up in dimethyl sulphoxide at 5mg/ml and blebbistatin was made up in methanol at 3.65mg/ml.

2.2 Methods

2.2.1 Cell lines and culture

2.2.1.1 Cell lines

2.2.1.1.1 PC-3 and PC-3-GFP

PC-3 cells were originally isolated from a vertebral metastasis of a poorly differentiated prostate adenocarcinoma [127]. They are androgen independent; have

a population doubling time of around 33 hours and are tumourigenic in mice. PC-3-GFP cells are a GFP-transfected variant of PC-3 [128] which express GFP diffusely in the cytoplasm.

2.2.1.1.2 PNT2-C2

The PNT2-C2 cell line is derived from normal human prostatic epithelial cells transfected with SV40 [129]. They have a doubling time of 36 hours, are serum dependent, non-tumourigenic and express cytokeratins 8 and 18 which are typical of luminal prostatic epithelium.

2.2.1.1.3 BMEC

The BMEC cell line is a cell line derived from normal human primary bone marrow endothelial cells transformed by SV40 large T antigen [130]. These cells were a gift from Dr Graca Almeida-Porada (University of Nevada at Reno, NV, USA)

2.2.1.2 Primary cells

2.2.1.2.1 Human bone marrow stroma

Primary human bone marrow from ribs donated, with informed consent and after ethical approval, by patients undergoing renal surgery for non-malignant disease was extracted by flushing the marrow cavity with long term culture medium (Iscove's modified Dulbecco's medium (Gibco, Paisley, UK) with 10% FCS (Cambrex Bioscience, Nottingham, UK), 10% horse serum (Invitrogen, Paisley, UK) and 5×10^{-7} M hydrocortisone). Isolated cells were seeded at 2×10^7 cells in a 25cm^2 tissue culture flask in long term culture medium. Cultures were incubated at 33°C in 5% CO_2 in air. Cells were used post observation of haemopoietic activity [131].

2.2.1.2.2 Human bone marrow endothelial cells

These cells had been previously extracted from normal primary human bone marrow using a method developed by Masek and Sweetenham [132] modified by Scott *et al* [13]. This method used bone marrow aspirates which were washed and underwent red cell lysis before endothelial cells were separated using magnetic beads coupled to Ulex europaeus agglutinin-1. The cells were stored under liquid nitrogen.

2.2.1.3 Culture conditions

2.2.1.3.1 *PC-3 and PC-3-GFP*

PC-3 cells were cultured in HAMS F12 with 7% FCS and 2mM L-glutamine, PC-3-GFP cells were cultured as above with the addition of 0.15mg/ml Hygromycin B (PAA Laboratories, UK). Cultures were incubated at 37°C in 5%CO₂ in air.

2.2.1.3.2 *PNT2-C2*

Cells were cultured in RPMI 1640 (Cambrex Bioscience) with 10% FCS and 2mM L-glutamine. Cultures were incubated at 37°C in 5%CO₂ in air.

2.2.1.3.3 *BMEC and human primary bone marrow endothelial cells*

Both cell lines were cultured in flasks coated with either fibronectin (50µg/ml in PBS) or neat attachment factor (TCS Cellworks, UK). Cells were cultured in BMSCM (undiluted bone marrow stroma conditioned medium, see section 2.2.1.3.4.1) unless otherwise stated. Cultures were incubated at 37°C in 5%CO₂ in air.

2.2.1.3.3.1 Coating flasks for endothelial cell culture

Tissue culture treated plastic flasks were used for endothelial cell culture. Flasks were coated with either neat Attachment factor or fibronectin 50µg/ml in PBS (1ml in a 25 cm² flask or 2ml in a 75cm² flask). Flasks were then incubated at 37°C for 1 hour. Excess liquid was then removed before cells were seeded into flasks.

2.2.1.3.4 *Human bone marrow stroma*

Bone marrow stroma was cultured in Iscove's modified Dulbecco's medium with 10% horse serum, 10% FCS and 5 x 10⁻⁷ M hydrocortisone. Half the volume of medium was removed once weekly and replaced with an equal volume of fresh medium. Cultures were incubated at 33°C in 5%CO₂ in air.

2.2.1.3.4.1 Preparation of BMSCM

Growth media from 2 week old bone marrow stromal cultures was collected and filtered through a 0.2µm pore diameter membrane before being frozen at -80°C until required.

2.2.1.4 Passaging of cell cultures

2.2.1.4.1 *PC-3 and PC-3-GFP*

Cells were passaged one to two times weekly when at approximately 70% confluence (judged visually) by removing medium, washing twice with 5ml PBS and using 1ml trypsin-EDTA (0.5g/l porcine trypsin with 0.2g/l EDTA·4Na in Hanks balanced salt solution with phenol red) at 37°C over 2-3 minutes to detach cells from the flask. Cells were placed in fresh medium and split 1:3.

2.2.1.4.2 *PNT2-C2*

Cells were passaged once weekly when at approximately 70% confluence (judged visually) by removing medium, washing twice with 5ml PBS and using trypsin-EDTA (as for PC-3 and PC-3-GFP cells, section 2.2.1.4.1) at 37°C over 5-6 minutes to detach cells from the flask. Cells were placed in fresh medium and split 1:20.

2.2.1.4.3 *BMEC and human primary bone marrow endothelial cells*

Cells were passaged when at approximately 70% confluence (judged visually) by removing medium, washing twice with 5ml PBS and using trypsin for endothelial cells (Sigma-Aldrich) at 37°C over 5-6 minutes to detach cells from the flask. Cells were washed out of the flask using PBS, centrifuged at 600g for 5 minutes to remove trypsin and resuspended in culture medium before being seeded into fibronectin coated flasks (see section 2.2.1.3.3.1). Cells were split 1:3.

2.2.2 Synchronisation

2.2.2.1 Serum starvation/temperature shock and FACS analysis

2.2.2.1.1 *Serum starvation/temperature shock*

PC-3 or PC-3-GFP cells were seeded into 25cm² tissue culture flasks in their standard medium (5x10⁵ cells per flask for flasks due to be incubated at 37°C and 1x10⁶ cells per flask for all other flasks). Cells were incubated at 37°C overnight. Medium was removed and cells washed four times with PBS. Standard PC-3 or PC-3-GFP medium was added to “control”, “room temperature” and “4°C” flasks, and starvation medium (L-glutamine-free RPMI 1640 for PC-3 cells, and L-glutamine free RPMI 1640 with Hygromycin B at 0.15mg/l for PC-3-GFP cells) added to “starvation”, “starvation/room temperature” and “starvation/4°C” flasks. “Control”

and “starvation” flasks were incubated for 48 hours at 37°C. “Room temperature” and “starvation/room temperature” flasks were incubated at room temperature on the laboratory bench for 48 hours. “4°C” and “starvation/4°C” flasks were incubated for 1 hour at 4°C. After incubation for the appropriate time, cells were either prepared for cell cycle analysis by flow cytometry immediately, or allowed to recover. Media was removed, cells were washed four times with PBS and standard medium was added to the flasks, which were incubated at 37°C for either 24 or 48 hours to allow cells to recover, before cell cycle analysis by flow cytometry.

2.2.2.1.2 Analysis of cell cycle by flow cytometry and propidium iodide staining

Cells were trypsinized, washed twice in PBS (centrifuge at 800g for 5 minutes, brake rate 3) and fixed in 500µl of ice-cold 70% ethanol for 15 minutes. Fixed cells could be used immediately or stored at 4°C in 70% ethanol until needed. Cells were then washed twice in PBS (centrifuge at 800g for 5 minutes, brake rate 3). After the second wash, the supernatant was removed and 100µl of RNase I reaction buffer (New England Biolabs, Hitchin, UK) (10µl 10x buffer and 90µl PBS) added, before 1µl of RNase I (New England Biolabs) was added and incubated for 5 minutes at room temperature. 30µl of propidium iodide at 500µg/ml was added and incubated at room temperature for 30 minutes in the dark. 400µl of PBS was added and cells were analysed on a FACSCalibur flow cytometer (Becton Dickinson) with an excitation wavelength of 488nm.

2.2.2.2 Cell cycle sorting by flow cytometry and Hoechst staining

Cells were trypsinized, washed once in PBS (centrifuge at 800g for 5 minutes, brake rate 3) and resuspended in PBS with 2% FCS at 1×10^6 cells/ml. Hoechst 33342 was added to give a final concentration of 5µM and cells were incubated for 30 minutes at 37°C on a shaking platform in the dark. Cells were then sorted into G₀/G₁ and G₂/M phases on a FACSVantage cell sorter (Becton Dickinson). Sorted cells were washed once in PBS before use.

2.2.3 Invasion Assay

For invasion assays utilising bone marrow stroma, stroma was cultured in long term culture medium in selected wells of a 24-well tissue culture plate for approximately 2 weeks until confluent and haematopoiesis was occurring.

Transwell chambers (8µm pore size) were prepared by coating the membrane with 100µl of Matrigel diluted 1:25 in DMEM (Gibco) or RPMI 1640 and allowed to set at 37°C for 2 hours. 60µl of excess medium was then removed to leave a thin layer of Matrigel on the chamber membrane.

Bone marrow medium was removed and bone marrow stromal cultures washed twice with PBS. 1ml of DMEM containing 0.1% BSA (PAA laboratories, UK) and 2mM L-glutamine or RPMI 1640 with 0.1% BSA and 2mM L-glutamine was added to the experimental wells containing bone marrow stroma as well as control wells with tissue culture plastic only. Prepared Transwell chambers were placed in the experimental wells and a suspension of 1×10^5 cells in 250µl DMEM or RPMI 1640 containing 0.1% BSA 2mM L-glutamine were added to the chamber. Each well was carried out in duplicate.

Plates were incubated at 37°C in 5%CO₂ in air for 18 hours to allow invasion of cells through the Matrigel. After 18 hours, chambers were rinsed with PBS and the internal surface of the chamber membrane was wiped with a dry cotton bud and then rinsed with a cotton bud moistened with PBS. The chamber membrane was stained with crystal violet for 10 minutes and rinsed in water until clean before allowing it to dry. The number of cells present on the underside of the central part of the membrane was then counted using an eyepiece graticule.

2.2.3.1 Invasion assay with BMEC

For these assays, Transwell chambers were coated with Matrigel or fibronectin (100µl of fibronectin 50µg/ml in PBS) in the same way as that described for the standard invasion assay (section 2.2.3). After removal of excess liquid, 4×10^5 BMEC were added to the chamber and cultured in BMSCM for 1-2 days until confluent. The chambers containing BMEC were rinsed in PBS to remove traces of BMSCM immediately before being used in the invasion assay in the same way as for the standard invasion assay. After 18 hours, Transwell chambers were rinsed with PBS and the internal surface of the chamber membrane was wiped with a dry cotton bud and then rinsed with a cotton bud moistened with PBS. Transwell chambers were then fixed in methanol:acetone 1:1 for a minimum of 30 minutes, air-dried, and then stained using an immunocytochemical method for cytokeratin (see section 2.2.3.1.1).

2.2.3.1.1 Immunocytochemical staining for cytokeratins

Methanol:acetone fixed Transwell chambers were blocked using a blocking serum of 10% rabbit serum and 1% BSA in PBS for 30 minutes before application of mouse anti-pancytokeratin antibody (1 in 200 in PBS with 1% BSA). Primary antibody was incubated at room temperature for 2 hours and the Transwell chambers were rinsed 3 times in PBS before incubation with 0.3% peroxide for 10 minutes. The chambers were then rinsed 3 times in PBS. Chambers were then incubated with rabbit anti-mouse biotin antibody (1 in 400 in PBS with 1% BSA) for 40 minutes and then rinsed three times in PBS prior to incubation with Vectastain ABC complex for 25 minutes and a further 3 rinses in PBS. Chambers were incubated for 5-15 minutes in DAB solution until a brown staining could be seen. Transwells were then rinsed 3 times in water and counterstained with haematoxylin.

2.2.3.2 Invasion assay with inhibitors

These assays were set up in the same way as the standard invasion assay (section 2.2.3) or invasion assay with BMEC (section 2.2.3.1), but with the addition of the required inhibitor to the PC-3 or PC-3-GFP cell suspension immediately before addition of the cell suspension to the Transwell chamber. The concentration of inhibitor varied depending on the experiment.

2.2.4 Permeability assay

Duplicate Transwell chambers with 1µm pores were coated with fibronectin and seeded with 4×10^5 BMEC in BMSCM. They were cultured for two days until BMEC were confluent. Control wells containing either Transwells in culture medium or Transwells coated with fibronectin in culture medium were also set up. Agents were added to the medium in the experimental Transwell chambers (to a final concentration in the chamber of Y-27632 at 40µM, blebbistatin at 75µM, Rac1 inhibitor at 75µM or GM6001 at 20µM). The BMEC were cultured with inhibitors present for 6 or 24 hours, or with PC-3 cells (1×10^5 cells in 250µl medium per Transwell chamber) present for 6 or 24 hours. Then 12.5µl FITC-dextran (molecular weight 40,000) at 1mg/ml in PBS was added to the Transwell chambers and allowed 30 minutes to diffuse. The Transwell chambers were then removed from the plate and the medium in the lower well was examined using a fluorescent plate reader (BMG Labtech). In order to assess the percentage of FITC-dextran passing through the endothelial layer, a series of standards were produced by adding FITC-dextran to

BMSCM and performing a serial dilution by taking half the FITC-dextran solution from the first standard well and adding it to an equal volume of BMSCM in a second well. This was repeated to produce a series of FITC-dextran concentrations which could be correlated with fluorescence readings. This produced a standard curve which could be used to calculate the amount of FITC-dextran which had diffused into the lower well from the fluorescence readings taken.

2.2.5 Statistics

Invasion assay data and permeability assay data were compared using a two tailed student's t-test with unequal variance (which is suitable for normally distributed data), and a Mann-Whitney U test (which is suitable for non-parametric data). For both tests a p value of less than 0.05 was taken to be significant.

2.2.6 Light microscopy and immunofluorescence

2.2.6.1 Time lapse video microscopy

Cells were seeded into a 12.5cm² tissue culture flask in growth medium (HAMS F12, 7% FCS, 200mM L-glutamine for PC-3, the same medium with the addition of Hygromycin B for PC-3-GFP cells. BMEC were cultured on fibronectin in BMSCM unless stated otherwise), gassed with 5%CO₂ in air and allowed to settle overnight before being placed on the microscope stage of a modified version of the time lapse video microscopy unit. which has been previously described [133]. This consisted of an inverted microscope with environmental chamber heated to 37°C surrounding the stage. A microscope mounted camera recorded images to a tape and the camera, light source and video recorder were controlled by an animation control unit. Two frames of footage were recorded every 20 seconds. Total magnification was x100. Footage was recorded onto analogue tape, captured using a Dazzle Fusion video capture device and imported into Pinnacle Studio 9 (Pinnacle Systems) for editing.

2.2.6.2 Immunofluorescence microscopy of fixed cells

2.2.6.2.1 Fixation for immunofluorescence

2.2.6.2.1.1 Methanol

Cells were cultured on 22x22mm glass coverslips in 6-well culture plates to the desired confluence: 100% for isolated endothelial cells and 25-50% for isolated

PC-3 and PC-3-GFP cells. Coverslips were coated with fibronectin 50µg/ml in PBS for 1 hour at 37°C before adding endothelial cells. Culture medium was removed, coverslips washed twice with PBS and fixed for 5 minutes in methanol at -20°C. The methanol was then removed and coverslips were air-dried and stored at -20°C until required

2.2.6.2.1.2 Formalin/Triton X-100

Endothelial cells were cultured on 22x22mm diameter glass coverslips or 22mm diameter Thermanox coverslips (Science Services, UK) to 100% confluence. Coverslips or Thermanox pieces were coated with fibronectin 50µg/ml in PBS for 1 hour at 37°C before adding endothelial cells. Culture medium was removed; coverslips were washed twice in PBS and fixed for 10 minutes in 4% formalin in PBS at room temperature. Formalin was removed, coverslips were washed twice with PBS and then permeabilized in 0.05% or 0.5% Triton X-100 in PBS for 5 minutes at room temperature before being washed twice in PBS. Cover slips were then air-dried and stored at -20°C until required.

2.2.6.2.2 Antibody staining of fixed cells

2.2.6.2.2.1 3-step method

Previously fixed and frozen coverslips in 6-well plates were defrosted at room temperature for 5 minutes and wax applied to the well to surround the coverslip. Coverslips were rehydrated with blocking serum (10% serum from the secondary antibody host with 1% BSA in PBS) for 30 minutes at room temperature. Blocking serum was removed and 200µl of the appropriate primary antibody solution in 1% BSA was added and incubated for 1 hour at room temperature. Primary antibody was removed and the coverslip washed three times in PBS. 200µl of secondary biotin-conjugated antibody (1:200 in 1% BSA in PBS) was added to the coverslip and incubated for 40 minutes. Coverslips were washed three times in PBS and then 200µl of streptavidin-FITC (1:20 in 1% BSA in PBS) was applied to the coverslip and incubated for 1 hour in the dark. Coverslips were washed three times in PBS and mounted onto glass slides using fluorescence mounting medium. Clear nail polish was applied to seal the edges of the coverslip and allowed to dry in the dark before examination of slides.

2.2.6.2.2.2 2-step method

Previously fixed and frozen coverslips in 6-well plates were defrosted at room temperature for 5 minutes and wax applied to the well to surround the coverslip. Coverslips were rehydrated with blocking serum (2% serum from the secondary antibody host with 2% BSA in PBS) for 30 minutes at room temperature. Blocking serum was removed and 200µl of the appropriate primary antibody solution in 1% BSA was added and incubated for 1 hour at room temperature. Primary antibody was removed and the coverslip washed three times in PBS. 200µl of secondary FITC-conjugated antibody (1:20 in 1% BSA in PBS) was applied and incubated for 45 minutes in the dark. Coverslips were then washed three times in PBS and mounted onto glass slides using fluorescence mounting medium. Clear nail polish was applied to seal the edges of the coverslip and allowed to dry in the dark before examination of slides.

2.2.6.2.2.3 Zenon® antibody labelling and staining

Preparation of Zenon®-labelled primary antibodies

The appropriate amount of primary antibody to produce the required final antibody concentration in 200µl total volume of solution was used. Zenon® labelling reagent was added at 5µl per 1µg of antibody and incubated for 5 minutes at room temperature. Zenon® blocking reagent was then added at 5µl per 1µg of antibody and incubated for 5 minutes at room temperature. 1% BSA in PBS was added to make up the volume to 200µl of antibody solution (enough for 1 coverslip). Labelled antibodies were used within 30 minutes.

Immunofluorescent staining using Zenon®-labelled antibodies

Previously fixed and frozen coverslips in 6-well plates were defrosted at room temperature for 5 minutes and wax applied to the well to surround the coverslip. Coverslips were rehydrated with PBS for 10-15 minutes and then blocked with 4 drops of Image-iT-FX® signal enhancer for 30 minutes. Coverslips were washed three times with PBS before Zenon®-labelled primary antibody was added and incubated in the dark for 1 hour at room temperature. Antibody was removed and coverslips were washed three times in PBS. Coverslips were fixed in 4% formalin in PBS for 15 minutes in the dark and again washed three times in PBS. Coverslips were mounted onto glass slides using fluorescence mounting medium. Clear nail

polish was applied to seal the edges of the coverslip and allowed to dry in the dark before examination of slides.

2.2.6.3 Live cell co-culture studies

2.2.6.3.1 Confocal invasion study

A confluent monolayer of BMEC was cultured in a quartz glass bottomed dish (IWAKI, Japan) coated with fibronectin (50µg/ml in PBS). Culture medium was removed from the BMEC monolayer and replaced with medium (BMSCM) containing 5×10^5 PC-3-GFP cells. The co-cultures were incubated at 37°C for 1 hour to allow binding of PC-3-GFP cells to BMEC. Medium was then removed and replaced with fresh BMSCM. Co-cultures were placed on the microscope stage within an environmental chamber (Solent Scientific, UK) maintained at 37°C and observed using a custom built confocal microscope based on a Zeiss inverted 200M with an ASI scanning stage. Brightfield and fluorescence images were captured at 30 minute intervals over 22-24 hours, for 5-10 different stage (x,y) positions with a stack of vertical (z) images at intervals of 3µm over a 24-30µm distance at each stage position. Total magnification was x400. Images were captured using Metamorph (Molecular Devices) and processed using Imaris (Bitplane AG).

2.2.6.3.1.1 Confocal invasion with inhibitors

This was set up in a similar way to the standard confocal invasion study but with the addition of the required inhibitor both to the PC-3-GFP cell suspension before addition to the BMEC monolayer, and also to the fresh BMSCM applied after the 1 hour cell binding period.

2.2.6.3.2 Confocal invasion studies using 24 well plate insert and Transwell chambers

Transwell chambers were prepared by coating with either Matrigel alone, Matrigel with BMEC, or fibronectin with BMEC as for invasion assays with and without BMEC (sections 2.2.3 and 2.2.3.1). The 24 well plate insert was rinsed in 100% ethanol and allowed to dry in a tissue culture cabinet before being placed onto a glass bottomed 24 well plate (IWAKI) and secured in position using adhesive tape. The experimental wells were filled with 750µl of BMSCM and the prepared Transwells lowered into them and secured onto the plate insert using adhesive tape. A suspension of 2×10^4 PC-3-GFP cells in BMSCM was added to the Transwell

chamber and the 24 well plate lid was secured in place with adhesive tape. The experimental wells were then observed using a custom built confocal microscope based on a Zeiss inverted 200M with an ASI scanning stage. Brightfield and fluorescence images were captured at 30 minute intervals over 22-24 hours, from the centre of each experimental well, with a stack of vertical (z) images at intervals of 3-10µm over a 100-150µm distance. Total magnification was x200. Images were captured using Metamorph (Molecular Devices) and processed using Imaris (Bitplane AG).

2.2.6.3.2.1 Confocal invasion studies using 24 well plate insert and Transwell chambers with inhibitors

These were set up the same way as the standard confocal invasion assay (section 2.2.6.3.2) except that the required inhibitors were mixed with the PC-3-GFP cell suspension before addition to the Transwell chamber.

2.2.6.3.3 Time lapse video microscopy invasion studies

BMEC were seeded into a 12.5cm² tissue culture flask in BMSCM, gassed with 5%CO₂ in air and cultured until confluent before being placed in the recess of the microscope stage. 2 frames of footage were recorded every 20 seconds (section 2.2.6.1) for at least 3 hours before the addition of 6.25x10⁵ PC-3, PC-3-GFP or PNT2-C2 cells in BMSCM. The flask was immediately replaced on the microscope stage and footage recorded as before for a further period of 24 hours. Total magnification was x100 throughout the recording. Footage was recorded onto analogue tape, captured and imported into Pinnacle Studio 9 for editing as before.

2.2.6.3.3.1 Time lapse invasion with inhibitors

These were set up in the same way as the standard time lapse video microscopy studies (section 2.2.5.3.3) but the required inhibitors were mixed with the cell suspension before addition to the BMEC monolayer.

2.2.7 Scanning electron microscopy

2.2.7.1 Fixation and processing

Cells were cultured on 5x5mm silicon wafers (Agar Scientific Ltd., Stanstead, UK) for PC-3 and PC-3-GFP cells, or fibronectin coated Thermanox plastic coverslips cut to 5x5mm for BMEC, in 6-well culture plates to the desired confluence: 100% for isolated endothelial cells and 25-50% for isolated PC-3 and

PC-3-GFP cells. Culture medium was removed and wafers were washed twice in Sorenson's buffer and then fixed in 3% glutaraldehyde in Sorenson's buffer for 1 hour at room temperature or overnight at 4°C. Wafers/coverlips were washed twice for 5 minutes in Sorenson's buffer and then post-fixed with 1% osmium tetroxide (Agar Scientific) in Sorensen's buffer for 1 hour at room temperature. They were washed twice for 5 minutes in double distilled water and then dehydrated for 3 minutes each in sequential solutions of ethanol in double distilled water (30%, 50%, 70%, 95%, 95%, 100%, 100%, 100%). Specimens could be critical point dried from 100% ethanol or ethanol was exchanged for Arklone® (Taab laboratory supplies, Reading, UK) by two immersions of 3 minutes each. Specimens were then critical point dried from Arklone®.

2.2.7.2 Immunogold labelling

Cultures on Thermanox pieces were washed 3 times in PBS, fixed in 4% paraformaldehyde in PBS for 15 minutes and then washed 3 times in PBS. Primary antibody was applied in PBS with 1% BSA and allowed to bind for 1 hour at room temperature or overnight at 4°C. Specimens were washed 3 times in PBS and secondary goat anti-mouse antibody conjugated to 10nm gold was added (1 in 10 in PBS with 1% BSA) and allowed to bind for 1 hour. Specimens were washed 3 times in PBS and then fixed in 3% glutaraldehyde before being post-fixed and processed as described in section 2.2.6.1 above.

2.2.7.3 Critical point drying

Silicon wafers or Thermanox pieces in ethanol or Arklone® were critical point dried via carbon dioxide in a Baltec 030 critical point dryer (Baltec, Lichtenstein) and stored under vacuum until required.

2.2.7.4 Sputter coating

Critical point dried specimens on silicon wafers were sputter coated with a 4nm layer of chromium in an Edwards 306 Autocryo coating unit (Edwards, Crawley, UK). Specimens on Thermanox were mounted onto aluminium stubs (Agar Scientific) using Acheson ElectroDAG 1415M conducting adhesive (Agar Scientific) and sputter coated with 8nm platinum-palladium 80/20 for unlabelled specimens; or 6nm chromium for gold labelled specimens.

2.2.7.5 Scanning electron microscopy

Chromium-coated specimens on silicon wafers were examined in an ABT DS130-F dual stage field emission scanning electron microscope (ABT, Japan) at an accelerating voltage of 30kV. Platinum-palladium or chromium coated Thermanox specimens were examined at 20-30kV and 10nm gold particles were detected using a backscatter detector (KE Developments, Cambridge, UK) at an accelerating voltage of 30kV.

3 Results

3.1 Cell cycle synchronisation, analysis and invasion

3.1.1 Synchronisation by serum starvation/temperature shock

An initial aim of the project was to synchronise the cell cycles of the prostate cancer cell lines PC-3 and the PC-3 derivative PC-3-GFP. This was done with the aim of achieving synchronised invasion through the endothelial layer and so enabling the visualisation of invasion by 3D microscopy. PC-3 and PC-3-GFP cells were subjected to the following synchronisation protocols:

1	Control	48 hours culture in PC-3 or PC-3-GFP growth medium at 37°C
2	Control - recovery	48 hours culture in PC-3 or PC-3-GFP growth medium with a further 24 hours culture in growth medium at 37°C
3	Temperature shock 4°C	1 hour of culture in PC-3 or PC-3-GFP growth medium at 4°C
4	Temperature shock 4°C and recovery	1 hour of culture in PC-3 or PC-3-GFP growth medium at 4°C with 24 hours recovery in PC-3 or PC-3-GFP growth medium at 37°C
5	Serum starvation plus temperature shock 4°C	1 hour of culture in PC-3 or PC-3-GFP serum-free medium at 4°C
6	Serum starvation plus temperature shock 4°C and recovery	1 hour of culture in PC-3 or PC-3-GFP serum-free medium at 4°C with 24 hours recovery in PC-3 or PC-3-GFP growth medium at 37°C
7	Serum starvation	48 hours culture in PC-3 or PC-3-GFP serum-free medium at 37°C
8	Serum starvation and recovery	48 hours culture in PC-3 or PC-3-GFP serum-free medium at 37°C with 24 hours recovery in PC-3 or PC-3-GFP growth medium at 37°C
9	Temperature shock (room temperature)	48 hours culture in PC-3 or PC-3-GFP growth medium at room temperature
10	Temperature shock (room temperature) and recovery	48 hours culture in PC-3 or PC-3-GFP growth medium at room temperature with 24 hours recovery in PC-3 or PC-3-GFP growth medium at 37°C
11	Serum starvation plus temperature shock (room temperature)	48 hours culture in PC-3 or PC-3-GFP serum-free medium at room temperature
12	Serum starvation plus temperature shock (room temperature) and recovery	48 hours culture in PC-3 or PC-3-GFP serum-free medium at room temperature with 24 hours recovery in PC-3 or PC-3-GFP growth medium at 37°C

PC-3 growth medium: Hams F-12 with 7% FCS and 2mM L-glutamine

PC-3 starvation medium: RPMI 1640 (L-glutamine free)

PC-3-GFP medium was the same as PC-3 medium but with the addition of Hygromycin B

Typical FACS plots of PC-3-GFP cells are shown in Figure 3-1. Figure 3-1a shows a plot of control (unsynchronised) cells with 56% in G_0/G_1 . After 48 hours of culture in starvation medium 73% of cells were in G_0/G_1 (Figure 3-1b). Cells cultured

in serum-free medium for 48 hours followed by 24 hours recovery in growth medium (Hams F-12 with 7% FCS and 2mM L-glutamine) showed a marked shift into S phase (Figure 3-1c) with 38% of cells in this phase.

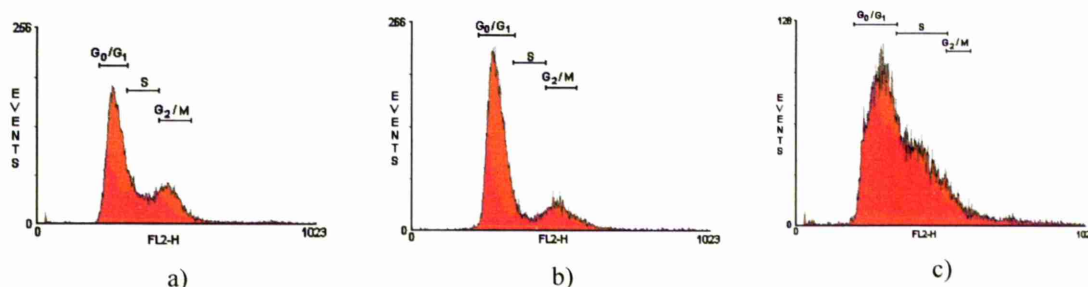
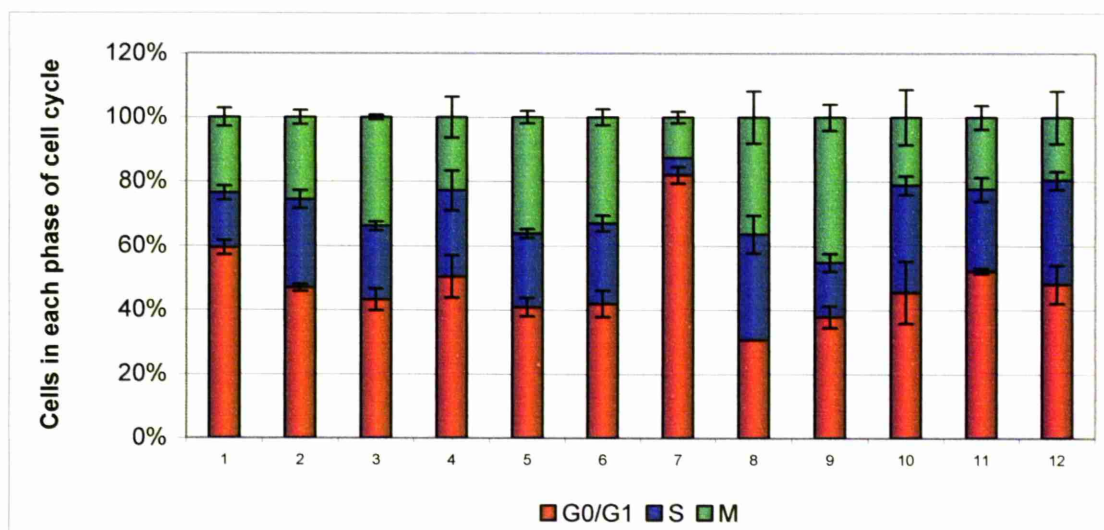


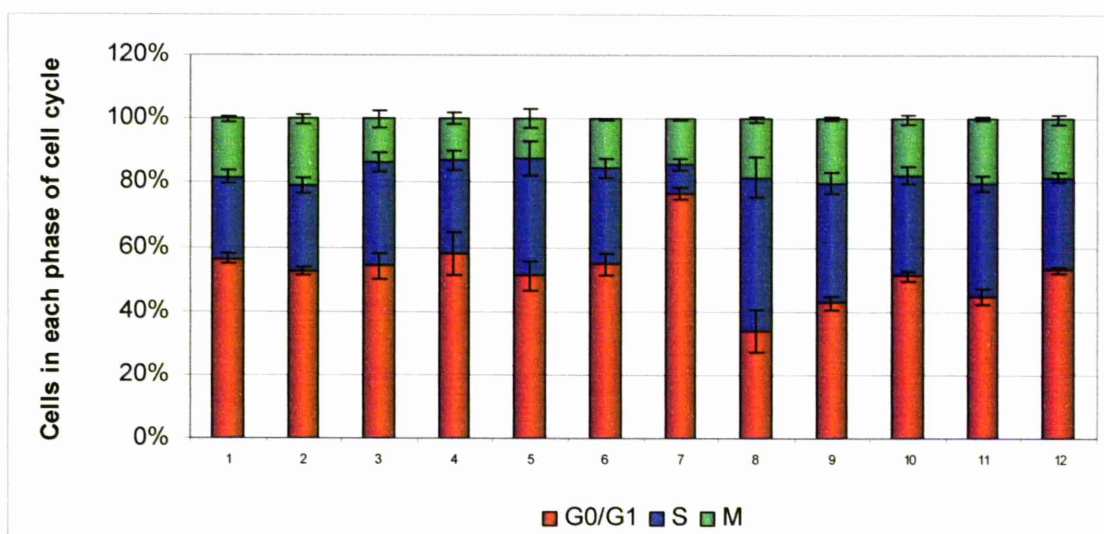
Figure 3-1: Typical FACS plots of cell cycle distribution in PC-3-GFP cells

Typical FACS plots of PC-3-GFP cells stained with propidium iodide: **a)** unsynchronised cells **b)** after 48 hours incubation in serum-free medium at 37°C. Cells show a shift into G₀/G₁ phase **c)** after 48 hours in serum-free medium followed by 24 hours recovery in PC-3-GFP growth medium both at 37°C. Cells show a shift into S phase.

Both cell lines showed a similar response to the synchronisation treatments as shown in Figure 3-2. Cell cycle analysis of control cells showed that 42% to 56% of cells were in G₀/G₁ and 17% to 23% were in G₂/M. Incubation at 4°C or room temperature shifted PC-3 cells into G₂/M (up to 43% in G₂/M at room temperature) but had a less pronounced effect on PC-3-GFP cells which showed only a slight shift into S phase. For both cell lines incubation in serum-free medium for 48 hours at 37°C achieved the most effective synchronisation with up to 76±4% of PC-3 and 73±3% of PC-3-GFP cells in G₀/G₁ as compared to 51±8% in controls. The increase in the proportion of cells in G₀/G₁ phase was significant ($p=0.003$ for PC-3 and $P=0.0007$ for PC-3-GFP cells). After 24 hours recovery in growth medium, PC-3-GFP cells showed a marked shift into S phase (42% of cells). A similar shift into S phase was seen after 16 hours recovery in PC-3 cells (see Figure 3-3).



a) PC-3



b) PC-3-GFP

Figure 3-2: Results of starvation/temperature shock treatment on cell cycle of PC-3 and PC-3-GFP cells

Proportion of **a) PC-3** and **b) PC-3-GFP** cells in each stage of the cell cycle after treatment with starvation and/or temperature shock, with or without 24 hours recovery. Results shown as mean of 3 experiments, each experiment performed in duplicate.. Bars show standard error of the mean.

1, 2: controls incubated in PC-3 or PC-3-GFP growth medium at 37°C.

3: 1 hour of culture at 4°C

4: 1 hour of culture at 4°C + 24 hours recovery at 37°C

5: 1 hour of culture in serum-free medium at 4°C

6: 1 hour of culture in serum-free medium at 4°C + 24 hours recovery in growth medium at 37°C

7: 48 hours culture in serum-free medium at 37°C

8: 48 hours culture in serum-free medium at 37°C + 24 hours recovery in growth medium at 37°C

9: 48 hours culture at room temperature

10: 48 hours culture at room temperature + 24 hours recovery at 37°C

11: 48 hours culture in serum-free medium at room temperature

12: 48 hours culture in serum-free medium at room temperature + 24 hours recovery in growth medium at 37°C

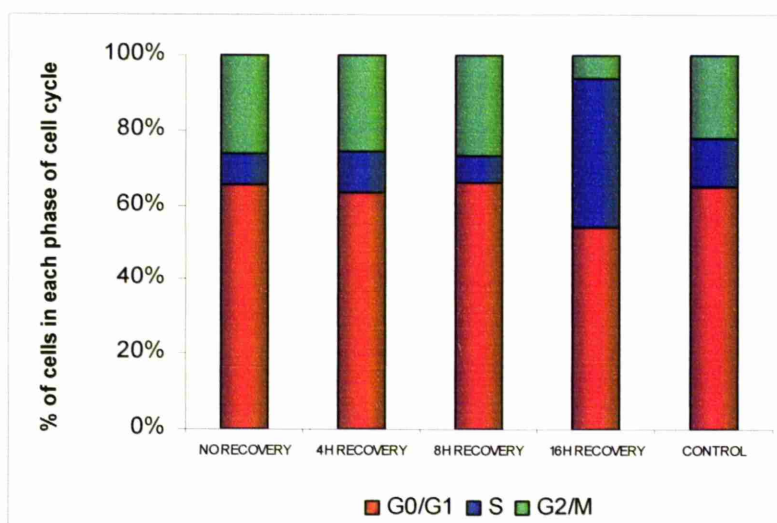


Figure 3-3: Effects of recovery on the cell cycle of PC-3 cells

Proportion of PC-3 cells in different phases of the cell cycle at different points during recovery in growth medium after 48 hours of culture in serum-free medium. All cells were incubated in serum-free medium at 37°C for 48 hours. No recovery: cells analysed immediately. 4h/8h/16h recovery: cells incubated in PC-3 growth medium at 37°C for 4, 8 or 16 hours before analysis. Results shown are of two experiments, each experiment performed in duplicate.

Since 48 hours incubation in serum-free medium was the most effective treatment to synchronise cells in G₀/G₁, cells synchronised by this method with or without 24 or 48 hours of recovery in growth medium were used in an invasion assay to assess their ability to invade, over 18 hours, through a layer of Matrigel. Figure 3-4 shows the results of an assay using PC-3-GFP cells. Although cells showed significantly more invasion towards bone marrow stroma than towards tissue culture plastic under all conditions, the invasive ability of synchronised cells was significantly less than that of unsynchronised cells, with maximal invasion occurring 24 hours post recovery with 238±29 cells invading towards bone marrow stroma compared with 777±64 control cells (T-test $p=0.0001$, Mann-Whitney U test $p=0.0022$). This is similar to the level of invasion towards tissue culture plastic in unsynchronised cells at 175±13 ($p=0.09$).

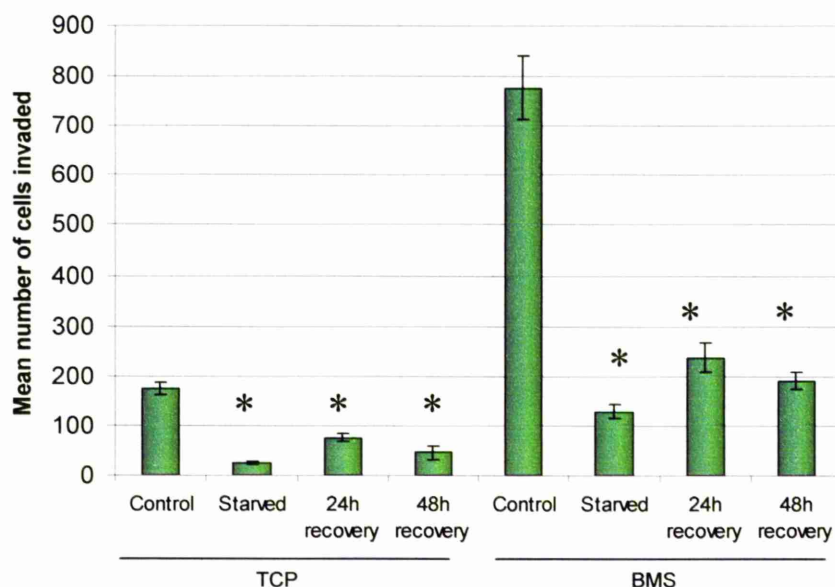


Figure 3-4: Results of invasion assay using PC-3-GFP cells after starvation synchronisation and recovery

1×10^5 PC-3-GFP cells pre-treated by synchronisation by starvation for 48 hours (starved) with or without a recovery period of either 24 (24h recovery) or 48 hours (48h recovery). PC-3-GFP cells were seeded onto Matrigel coated Transwell chambers over tissue culture plastic (TCP) controls or human bone marrow stroma (BMS). PC-3-GFP cells showed significantly less invasion towards TCP after all treatments compared to TCP control ($p < 0.05$ for all conditions on both T-test and Mann-Whitney U test). PC-3-GFP cells showed significantly less invasion towards BMS after all treatments compared to BMS control ($p < 0.05$ for all conditions on both T-test and Mann-Whitney U test). Bars show standard error (results shown as mean of 3 experiments, each experiment performed in duplicate). Asterisks indicate significance at $p < 0.05$ for both T-test and Mann-Whitney U test.

3.1.2 Synchronisation by Hoechst and FACS

As starvation reduced the invasive ability of the prostate cells, FACS sorting was used as a method of obtaining cells within the same stage of the cell cycle. Cells were stained with Hoechst 33342 and sorted by FACS. Hoechst 33342 is a nucleic acid stain which can be used on live cells.

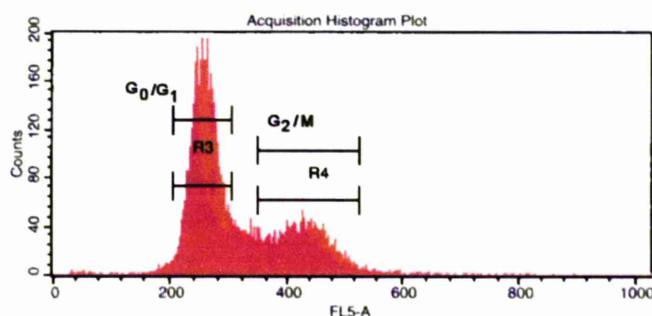


Figure 3-5: Defining stages of the cell cycle by Hoechst 33342 staining

A typical FACS plot produced during cell cycle sorting of PC-3-GFP cells. PC-3-GFP cells were cultured in medium based on HAMS-F12 and stained with Hoechst 33342 at $5 \mu\text{M}$ for 30 minutes before being sorted by FACS into two fractions: G_0/G_1 (R3) and G_2/M (R4).

Measuring the intensity of fluorescence allows cells to be sorted by the relative amount of DNA they contain, with cells in G₀/G₁ containing one copy of each chromosome, those in G₂/M containing 2 copies and those in S phase containing an intermediate amount of DNA. This allows cells to be sorted by cell cycle phase. Figure 3-5 shows a typical FACS plot obtained during sorting with the cell cycle stages defined. Hoechst 33342 treated and FACS sorted cells were also used in an invasion assay to assess their invasive ability; the results are shown in Figure 3-6.

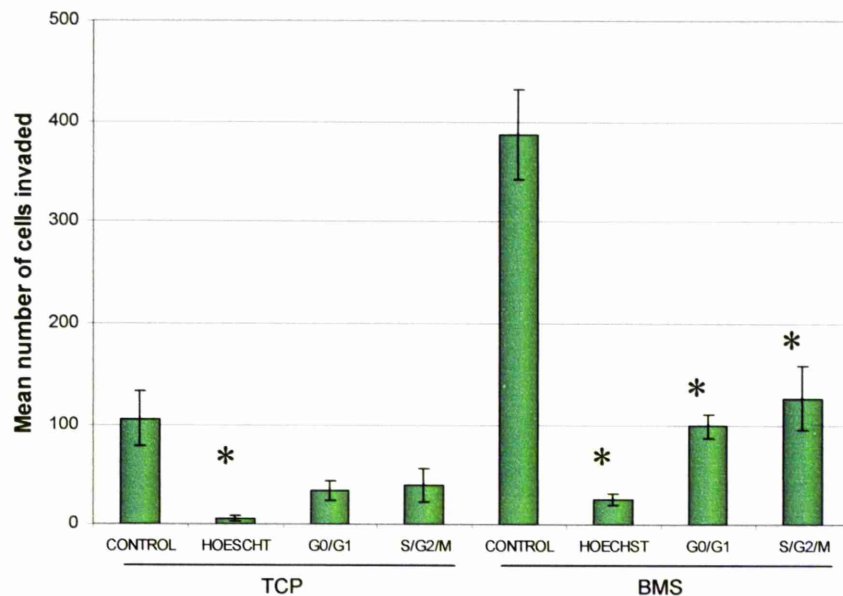


Figure 3-6: Invasion assay using PC-3-GFP cells post FACS sorting for phases of the cell cycle
 1 X 10⁵ PC3-GFP cells invading through Matrigel towards either tissue culture plastic (TCP) or bone marrow stroma (BMS) after treatment with Hoechst 33342 only or synchronisation by Hoechst 33342 staining and FACS sort. PC-3-GFP cells showed significantly less invasion towards BMS after all treatments compared to BMS control ($p < 0.05$ for all conditions on both T-test and Mann-Whitney U test). PC-3-GFP cells showed significantly less invasion towards TCP after Hoechst 33342 treatment compared to TCP control ($p < 0.05$ on both T-test and Mann-Whitney U test) but the results did not achieve significance for invasion towards TCP after sorting into either G₀/G₁ or G₂/M phase. Bars show standard error (results shown as mean of 3 experiments, each experiment performed in duplicate). Asterisks indicate significance at $p < 0.05$ for both T-test and Mann-Whitney U test.

Hoechst 33342 stained FACS sorted cells showed a significantly reduced invasive ability compared to unsynchronised control cells (Figure 3-6) with 484 ± 49 control cells invading towards bone marrow stroma compared to 127 ± 32 G₂/M sorted cells (T-test $p = 0.0003$, Mann-Whitney U test $p = 0.0023$); although they still showed more invasion towards bone marrow stroma than tissue culture plastic. Unsorted Hoechst 33342 treated cells also showed a significantly reduced invasive

ability towards both tissue culture plastic (T-test $p=0.003$, Mann-Whitney U test $p=0.002$) and bone marrow stroma (T-test $p=0.000005$, Mann-Whitney U test $p=0.0001$).

Due to the lack of invasive ability demonstrated by Hoechst 33342 treated synchronised cells, unsynchronised cells were used for further studies.

3.2 Characterisation of cell lines

3.2.1 Light microscopy

3.2.1.1 PC-3 and PC-3-GFP cells

Isolated cultures of PC-3 and PC-3-GFP cells were observed by light microscopy to assess their morphology in the absence of other cells before co-culture studies were started, and to compare the morphology of the two cell lines.

A range of morphology was observed for both cell lines including flattened and polygonal epithelioid cells (Figure 3-7b and g), spindle shaped fibroblastic (Figure 3-7c and f) and rounded amoeboid cells (Figure 3-7d and h). Cells did not form organised colonies and single cells were seen frequently. Some cells formed membrane contacts with adjacent cells (Figure 3-7c and g). Areas of membrane ruffling were visible as phase dark portions of the peripheral cell membrane and were also seen on time lapse video microscopy (section 3.2.2.1).

3.2.2 Time lapse video microscopy

3.2.2.1 PC-3 and PC-3-GFP cells

Isolated cultures of PC-3 and PC-3-GFP cells were observed using time lapse video microscopy to assess their movement and behaviour in the absence of other cells before co-culture studies were commenced. Cells were cultured in their standard medium and also in bone marrow stroma conditioned medium (BMSCM, see section 2.2.1.3.4.1) which was used for co-culture studies.

PC-3 and PC-3-GFP cells in tissue culture flasks in either their growth medium (HAMS F12 with 7% FCS and 2mM L-glutamine) or BMSCM were observed in the time lapse video microscopy unit for 3 to 7 days. Two frames of footage were recorded every 20 seconds, giving a 250x increase in speed compared with real time. Two experiments were done with a single field of view observed for each. The results are shown in Table 3-1 for cells in HAMS F12 and Table 3-2 for cells cultured in BMSCM. Frames from time lapse videos are shown in Figure 3-8 to

Figure 3-11 for PC-3 cells in HAMS F12, Figure 3-12 to Figure 3-14 for PC-3-GFP cells in HAMS F12, Figure 3-15 to Figure 3-18 for PC-3 cells cultured in BMSCM and Figure 3-19 to Figure 3-20 for PC-3-GFP cells cultured in BMSCM. The corresponding video clips can be found on the accompanying DVD in presentation 3.2.

PC-3 and PC-3-GFP cells had similar morphology and exhibited the same types of movement, but PC-3-GFP cells were more motile overall (over 70% of PC-3-GFP cells migrated across the substrate compared to under 20% of PC-3 cells) and showed a greater tendency to amoeboid movement. PC-3-GFP cells continued to migrate as confluence increased, while PC-3 cells became more static with increasing confluence. PC-3-GFP cells showed prominent membrane blebbing which was not related to apoptosis. Post-mitotic cells sometimes became detached from the substrate and floated away or became adherent to another cell (Figure 3-7d) where they could remain rounded for several hours before re-attaching to the substrate. Both cell lines showed prominent membrane ruffling and extension and retraction of processes.

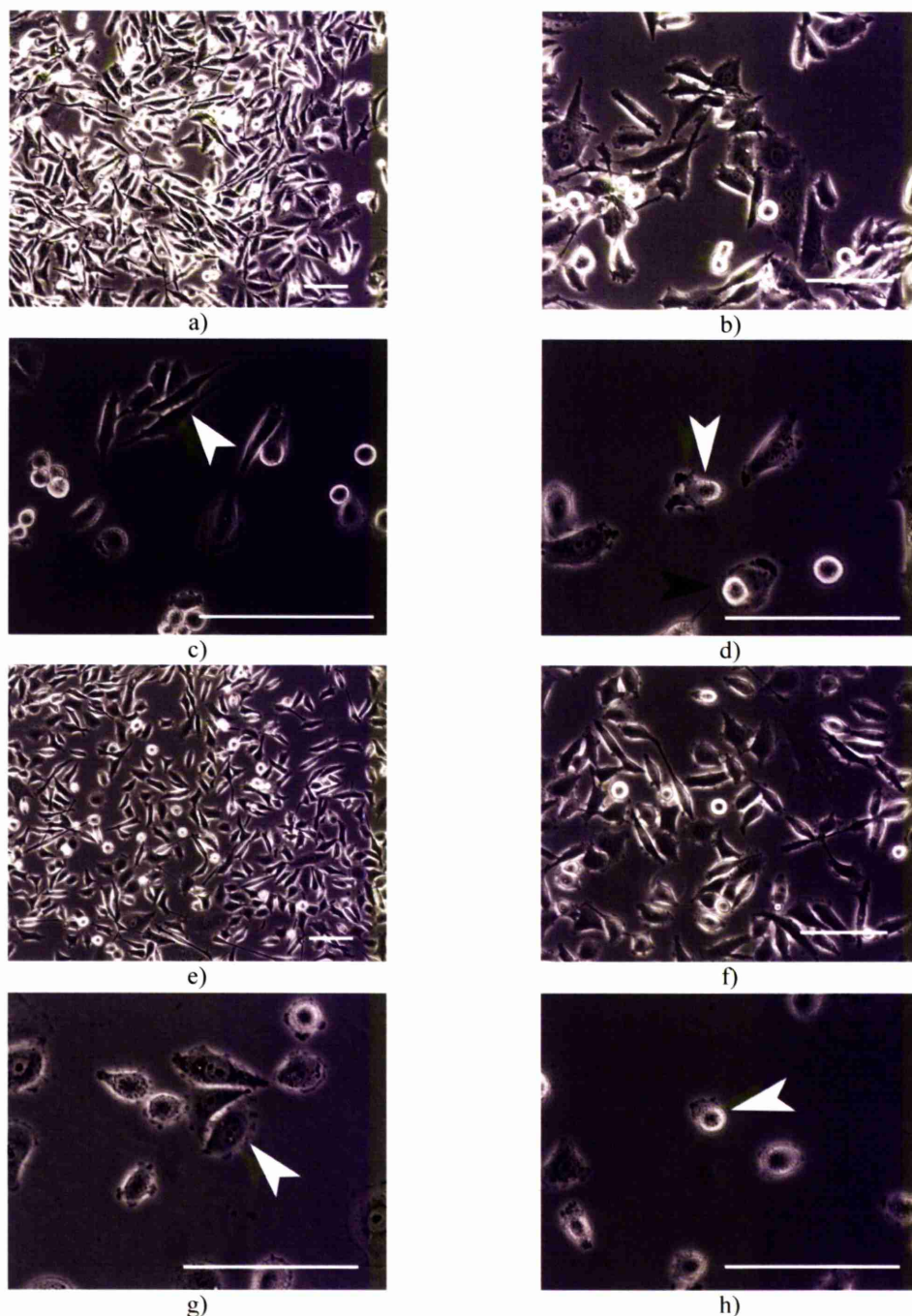


Figure 3-7: Morphology of PC-3 and PC-3GFP cells under phase contrast microscopy

Cells were cultured in tissue culture treated plastic flasks in HAMS F12 with 7% FCS, 2mM L-glutamine and Hygromycin B for PC-3-GFP cells.

a-d) PC-3 cells **e-h)** PC-3-GFP cells

a) and e) cells in culture did not form organised colonies

b) and f) cells exhibited a range of morphology with flattened epithelioid, fibroblastic and rounded cells. Phase dark areas at cells edges are sites of membrane ruffling

c) and g) membrane contacts were seen between some adjacent cells (groups of cells arrowed).

d) and h) amoeboid cells (white arrows) with lamellipodia are present in the centre of the images. In image **d)** a rounded cell is seen adherent to the surface of a flattened cell (black arrow) in the lower part of the image

Phase contrast images taken using a Zeiss Axiovert 35M. Scale bars represent 200µm.

Video clip 1 and Figure 3-8b show a more confluent culture of PC-3 cells showing reduced cell migration compared to that seen in less confluent cultures such as in video clip 2 in which a large cell can be seen migrating across the substrate. Cells in both clips can be seen extending and retracting processes and ruffling their membranes. Some cells showed a greater tendency to migrate than others and continued to move across the substrate as confluence increased, a cell of this type can be seen in Figure 3-9 and video clip 3. This cell can be followed for several hours during the period of filming. It shows fibroblastic movement and extends processes under other cells as it moves (Figure 3-9 time 00:59). Although most motile PC-3 cells exhibited fibroblastic movement, some cells were able to change to an amoeboid type of movement, as seen in Figure 3-10 and video clip 4. The cell is initially spindle-shaped and polarised with a lamellipodium at one end. It then becomes rounded but continues to move with a short lamellipodium at its leading edge. During mitosis cells frequently divided perpendicular to the substrate as seen in Figure 3-11 and video clip 5. The cell divides vertically and the lower daughter cell spreads on the substrate before the upper daughter cell re-attaches to the substrate. PC-3-GFP cells also showed division perpendicular to the substrate, as seen in video clip 6. Rounded post-mitotic cells sometimes remained attached to another cell for some time before spreading on the substrate as seen in Figure 3-13 and video clip 8 where PC-3-GFP cells can also be seen showing fibroblastic movement. These cells showed more amoeboid movement and membrane blebbing (seen in Figure 3-12 and video clip 7) than PC-3 cells. In more confluent cultures, PC-3-GFP cells continued to migrate but showed fibroblastic rather than amoeboid movement, shown in Figure 3-14 and video clip 9.

PC-3 and PC-3-GFP cells cultured in BMSCM showed some differences from those in medium based on HAMS F12. Cellular morphology was similar, particularly in subconfluent cultures (see Figure 3-15a and video clip 10) although PC-3 cells showed more blebbing, shown in Figure 3-15b and video clip 11, than the same cells cultured in HAMS F12 and more cells appeared rounded and showed amoeboid movement. Figure 3-15 a) shows a subconfluent culture with cells morphologically identical to those seen in HAMS F12 (see also video clip 10). In Figure 3-15 b) a spindle shaped cell has a rounded cell attached to it and a large cell exhibits membrane blebbing (see video clip 11). As confluence increased, clusters of

rounded cells that were loosely attached to the substrate were seen (Figure 3-15c and video clips 12 and 16). Cells within clusters were able to undergo mitosis (Figure 3-16 and video clip 13) and escape from the cluster to spread on the substrate (Figure 3-17 video clip 14). PC-3 cells also showed more amoeboid movement, illustrated in Figure 3-18 and video clip 15, than when cultured in HAMS F12. PC-3-GFP cells showed very similar features, although with a larger proportion of cells exhibiting amoeboid movement, seen in Figure 3-19 and video clips 17 and 18. They also showed fibroblastic movement, seen in video clip 19, and formed clusters of cells, seen in Figure 3-20 and video clip 20. A summary of the morphology and behaviour of these cells is shown in Table 3-1 and Table 3-2.

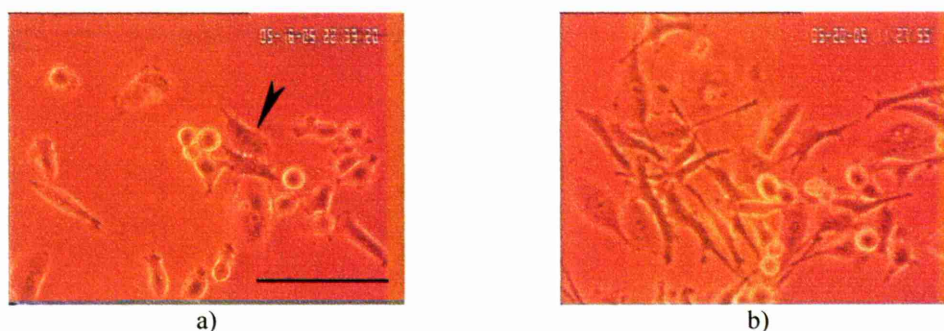


Figure 3-8: PC-3 cells in culture

a) cells forming membrane contacts (arrowhead) in a subconfluent culture. Amoeboid, epithelioid and fibroblastic cells are present. **b)** a more confluent culture with numerous fibroblastic and epithelioid cells.

Cells were cultured in growth medium (HAMS F12 with 7% FCS and 2mM L-glutamine). Scale bar represents 100µm.

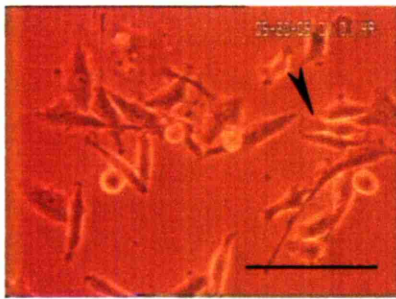
See also video clip 1

Table 3-1: Morphology and behaviour of PC-3 and PC-3-GFP cells in HAMS F12 as observed by time lapse video microscopy
Observations based on two experiments with a single field of view each. One field typically contained 15-50 cells depending on confluence.

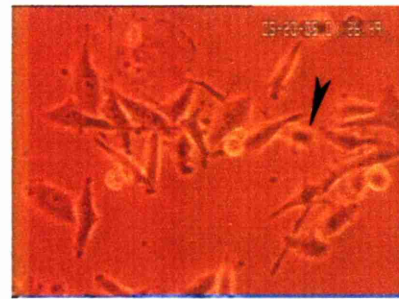
CELL LINE/ MEDIUM	MORPHOLOGY	MIGRATION	EXTENSION OF PROCESSES	MEMBRANE RUFFLING	MITOSES	CELL-CELL CONTACTS	OTHER
PC-3/ HAMS F12	A range of morphology is seen. Initially more cells are polarised, spindle shaped and migratory. Cells tend to become more flattened and polygonal or flattened and elongated with increasing confluence	Some cells (<20%) constantly migrating across substrate. Most cells show slow and gradual movement. Cell movement reduces with increasing confluence. Some cells alternate between being static and migrating. <5% of cells show short-lived intermittent amoeboid movement in cultures under 50% confluent	Over 90% of cells frequently extend and retract processes	Cells exhibit almost constant membrane ruffling	Almost all occur vertically (perpendicular to the substrate). Post-mitotic cells often remain rounded up for over 1 hour before spreading on the substrate. Some cells become detached from the substrate during mitosis and may float in the medium or attach to another cell	Rarely seen but can last for several hours. Filopodia are seen extending between adjacent cells	Inter-mitotic interval 22-27 hours. Occasional cells exhibit blebbing which does not lead to apoptosis
PC-3-GFP/ HAMS F12	A range of morphology is seen. Initially cells are often rounded with a lamellipodium or polarised and spindle shaped, and migrate across the substrate. Around 20% of cells are rounded. Cells tend to become more flattened and polygonal or elongated with increasing confluence	Most cells (>70%) migrate across the substrate. 5-10% of cells show intermittent amoeboid movement in cultures under 50% confluent. Cells mostly continue to migrate as confluence increases. Some cells alternate between being static and migrating	Over 90% of cells frequently extend and retract processes	Cells exhibit almost constant membrane ruffling	Almost all occur vertically (perpendicular to the substrate). Post-mitotic cells often remain rounded up for over 1 hour before spreading on the substrate. Some cells become detached from the substrate during mitosis and may float in the medium or attach to another cell	Not seen during filming but can be seen between cells in culture	Inter-mitotic interval could not be assessed as cells tended to migrate out of the field of view frequently. More prominent blebbing occurs than seen in PC-3-cells, but rarely leads to apoptosis

Table 3-2: Morphology and behaviour of PC-3 and PC-3-GFP cells in BMSCM as observed by time lapse video microscopy
Observations based on two experiments with a single field of view each. One field typically contained 15-50 cells depending on confluence.

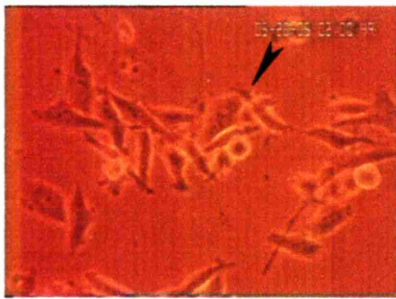
CELL LINE/ MEDIUM	MORPHOLOGY	MIGRATION	EXTENSION OF PROCESSES	MEMBRANE RUFFLING	MITOSES	CELL-CELL CONTACTS	OTHER
PC-3/ BMSCM	Similar to that seen in HAMS F12 except that cells were more often rounded. As confluence increased, clusters of rounded cells formed which were loosely attached to the substrate. Cells were able to divide while in these clusters and could escape them and spread on the substrate	A similar proportion of cells are motile compared to HAMS F12 but more of the motile cells show amoeboid movement (up to 10% of all cells)	Over 90% of cells frequently extend and retract processes	Cells exhibit almost constant membrane ruffling	Similar mitoses to those seen in HAMS F12. Pre and post-mitotic cells were more loosely attached to the substrate and showed a greater tendency to float away. Cells were able to divide when forming part of a cluster and not apparently attached to the substrate	One possible cell-cell contact was seen	Cells showed more prominent blebbing than seen in HAMS F12. Inter-mitotic interval could not be assessed as cells tended to float away or become lost in cell clusters
PC-3-GFP/ BMSCM	Similar to that seen in HAMS F12 except that more cells are rounded (approximately 50% compared to 20% in HAMS). As confluence increased, clusters of rounded cells formed which were loosely attached to the substrate. Cells were able to divide while in these clusters and could escape them and spread on the substrate	Over 70% of cells migrate across the substrate. Around 50% of all cells show amoeboid movement	Over 90% of cells frequently extend and retract processes	Cells exhibit almost constant membrane ruffling	Similar mitoses to those seen in HAMS F12. Pre and post-mitotic cells were more loosely attached to the substrate and showed a greater tendency to float away	Not seen	Blebbing similar to that seen in HAMS F12. Inter-mitotic interval could not be assessed as cells tended to float away or become lost in cell clusters



00:00



00:25



00:59



01:18



01:36



01:54



02:12



02:56



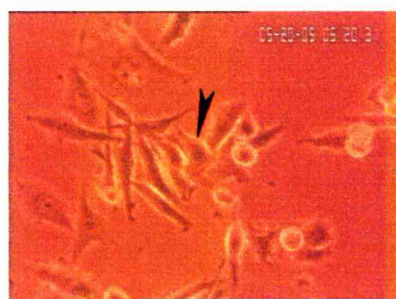
03:17



03:39



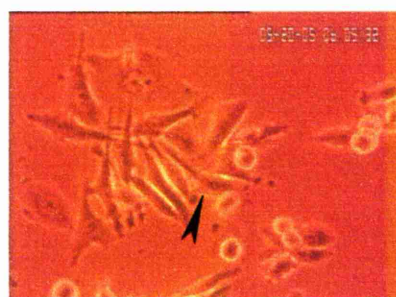
03:59



04:14



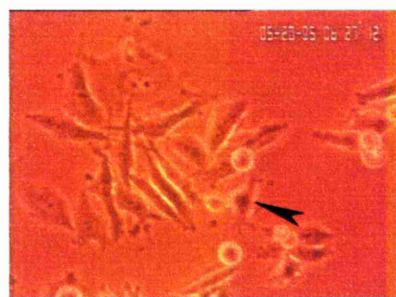
04:40



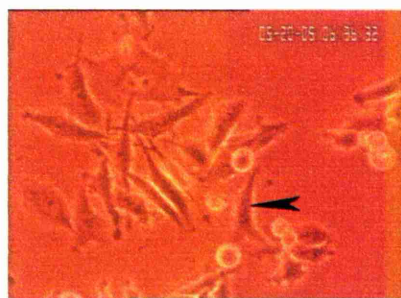
05:04



05:18



05:26



05:35



05:47



05:53

Figure 3-9: PC-3 cell showing fibroblastic movement

A migrating cell (arrowhead) can be followed through a sequence lasting 5 hours 53 minutes. Cells were cultured in growth medium (HAMS F12 with 7% FCS and 2mM L-glutamine). Times are shown as hours and minutes after the first image at 00:00. Scale bar represents 100 μ m. *See also video clip 3*

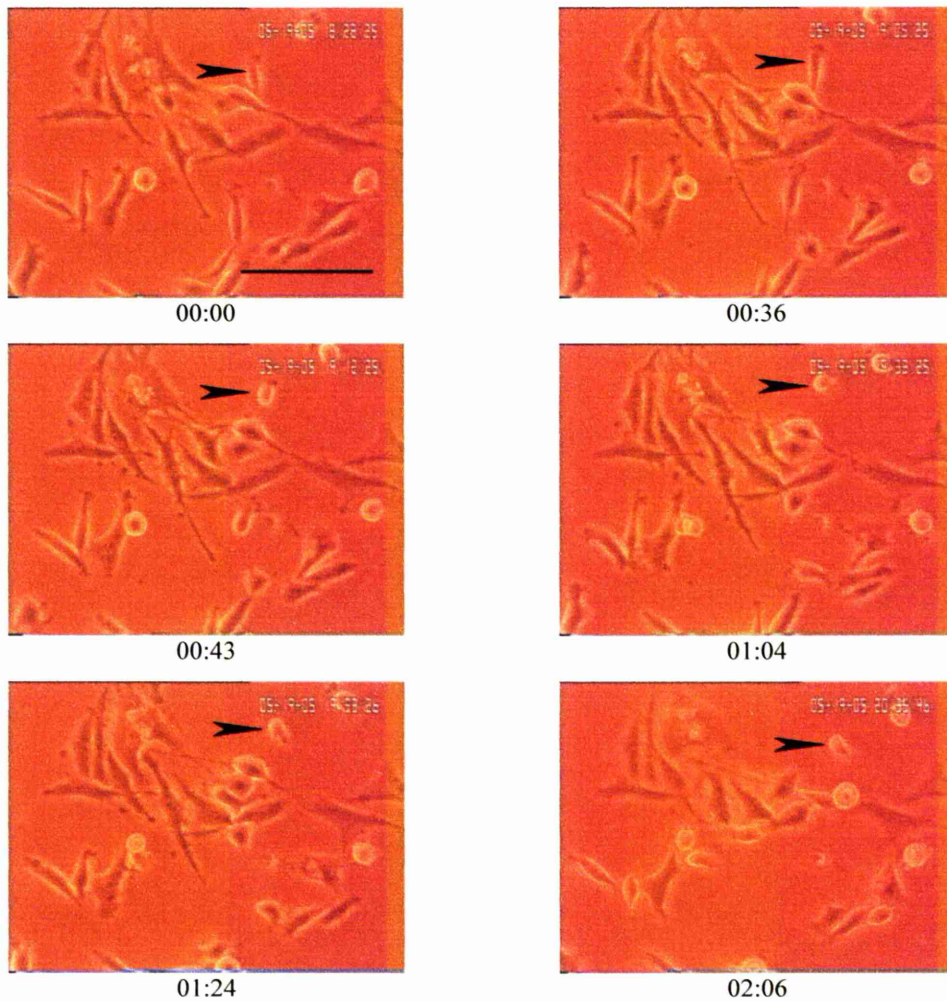


Figure 3-10: PC-3 cell switching from a fibroblastic mode of movement to amoeboid movement

The cell (arrowed) is initially elongated with a lamellipodium at the upper end but then becomes rounded and continues to move. A lamellipodium is still visible. Cells were cultured in growth medium (HAMS F12 with 7% FCS and 2mM L-glutamine). Times are shown as hours and minutes after the first image at 00:00. Scale bar represents 100 μ m.

See also video clip 4

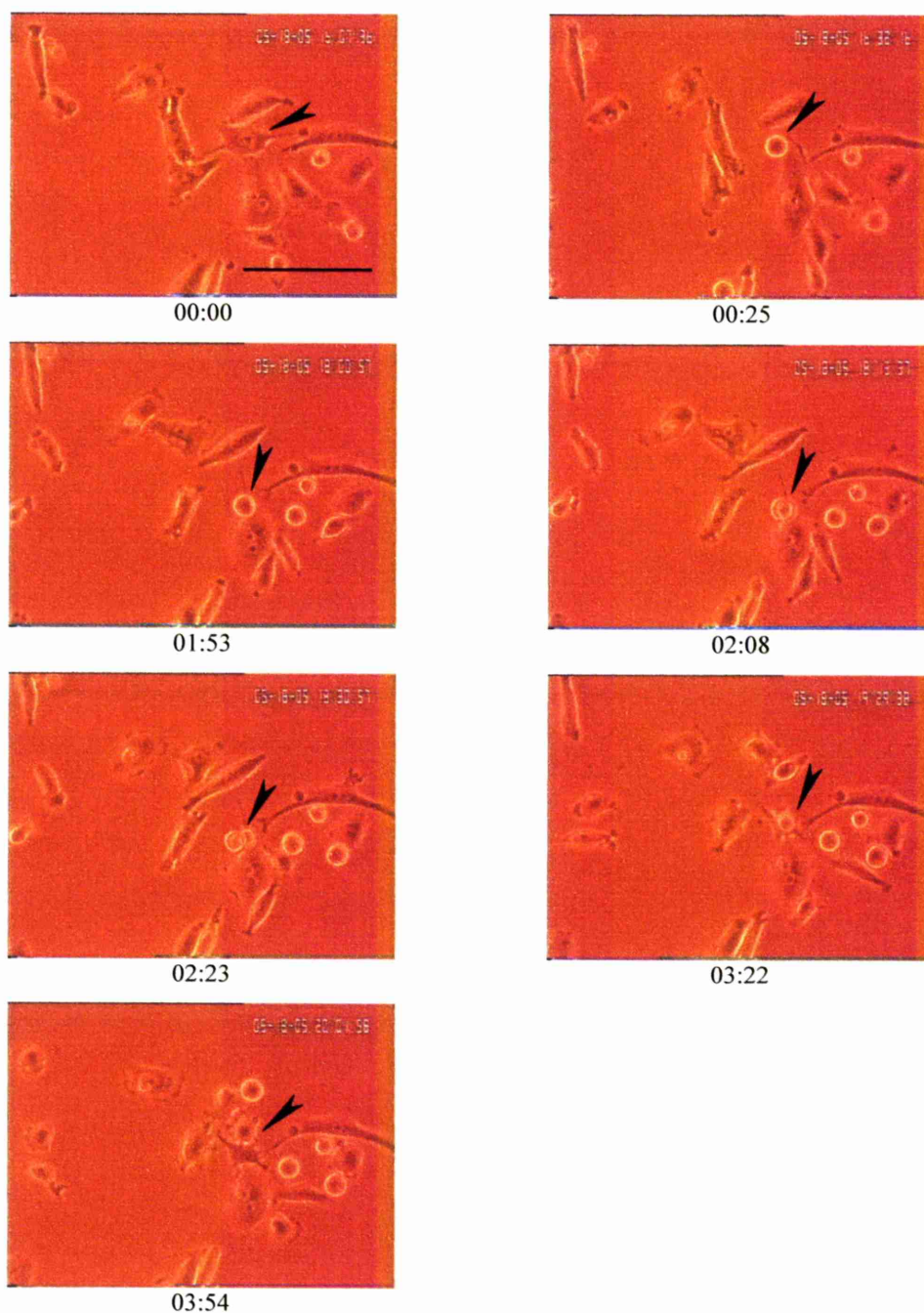


Figure 3-11: PC-3 cell undergoing mitosis

PC-3 cell (arrowed) showing division perpendicular to the substrate. The lower daughter cell spreads on the substrate at 03:22 and the upper daughter cell at 03:54. Cells were cultured in growth medium (HAMS F12 with 7% FCS and 2mM L-glutamine). Times are shown as hours and minutes after the first image at 00:00. Scale bar represents 100 μ m.

See also video clip 5

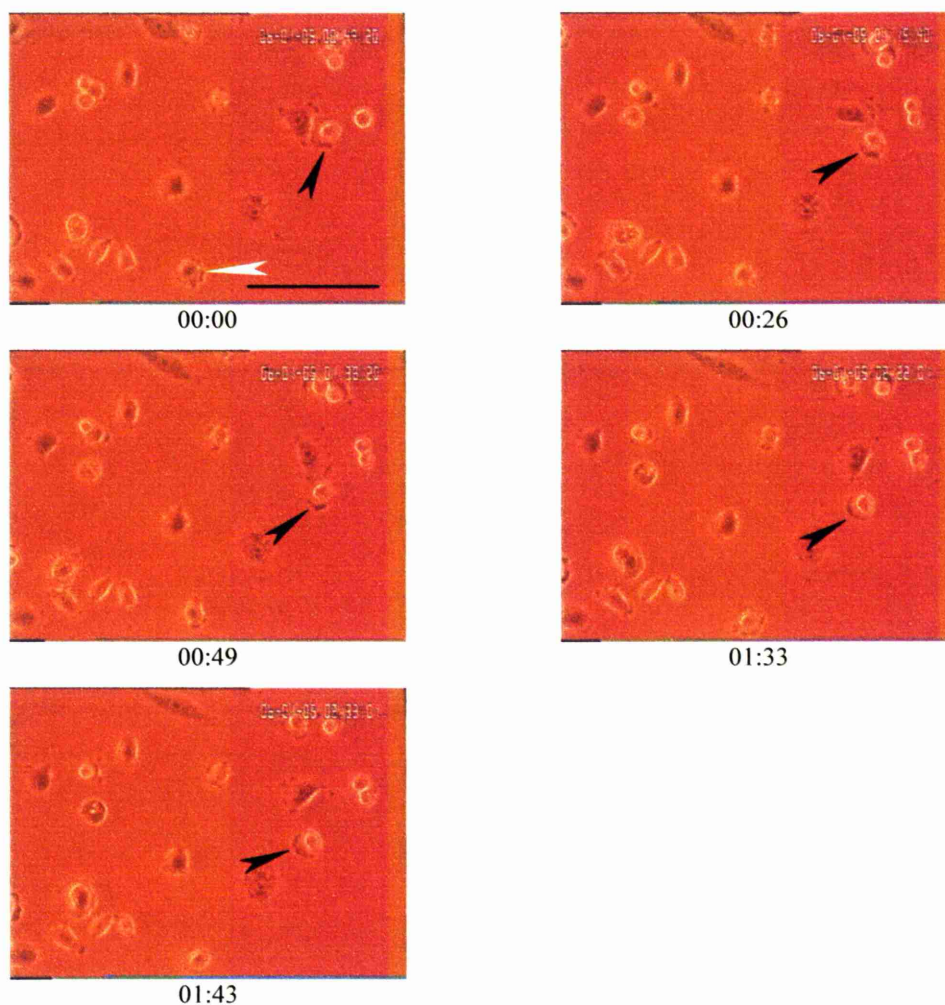


Figure 3-12: PC-3-GFP cells showing blebbing and amoeboid movement

One cell (white arrowhead) shows prominent blebbing. Another cell (black arrowhead) shows amoeboid movement. Cells were cultured in growth medium (HAMS F12 with 7% FCS and 2mM L-glutamine).

Times are shown as hours and minutes after the first image at 00:00. Scale bar represents 100 μ m.

See also video clip 7

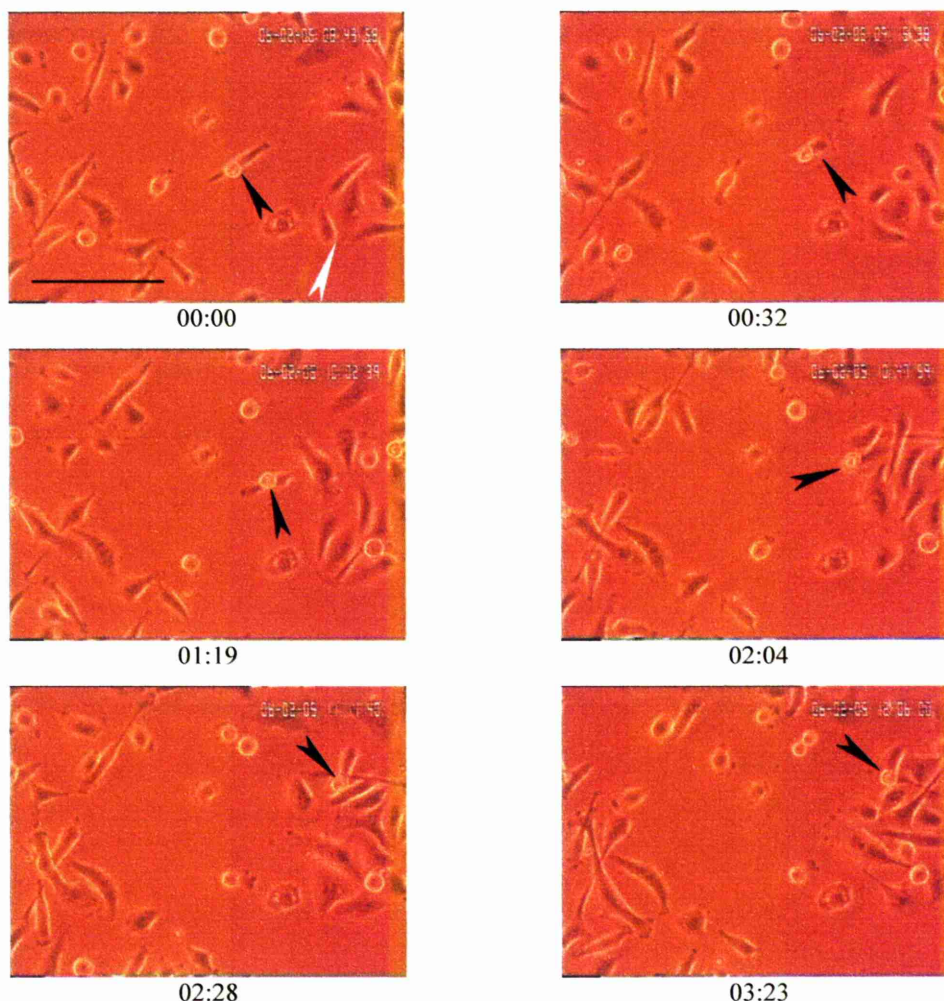


Figure 3-13: PC-3-GFP cells showing fibroblastic movement

A cell (black arrowhead) migrates across the substrate showing fibroblastic movement and carrying an adherent rounded cell which detaches as the cell migrates into the group of epithelioid cells on the right of the field of view (white arrowhead). Cells were cultured in growth medium (HAMS F12 with 7% FCS and 2mM L-glutamine). Times are shown as hours and minutes after the first image at 00:00. Scale bar represents 100µm.

See also video clip 8



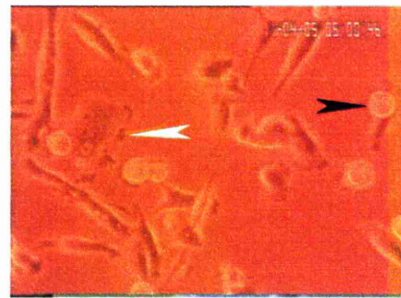
Figure 3-14: PC-3-GFP cells in culture

When cells become more confluent the majority of cells adopt a fibroblastic morphology but continue to migrate. Cells were cultured in growth medium (HAMS F12 with 7% FCS and 2mM L-glutamine). Scale bar represents 100 μ m.

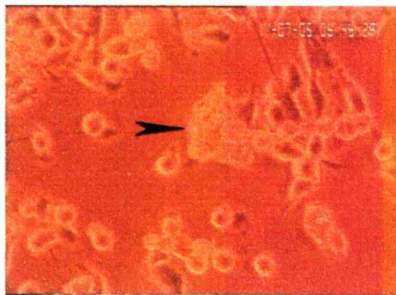
See also video clip 9



a)



b)



c)

Figure 3-15: PC-3 cells cultured in BMSCM

a) a subconfluent culture; cells appear similar to those cultured in HAMS F12. b) a large cell shows blebbing (white arrowhead) and a rounded cell is attached to the surface of another cell (black arrowhead). c) the culture is more confluent and cell clusters are present (black arrowhead).

Scale bar represents 100 μ m.

See also video clips 10-12

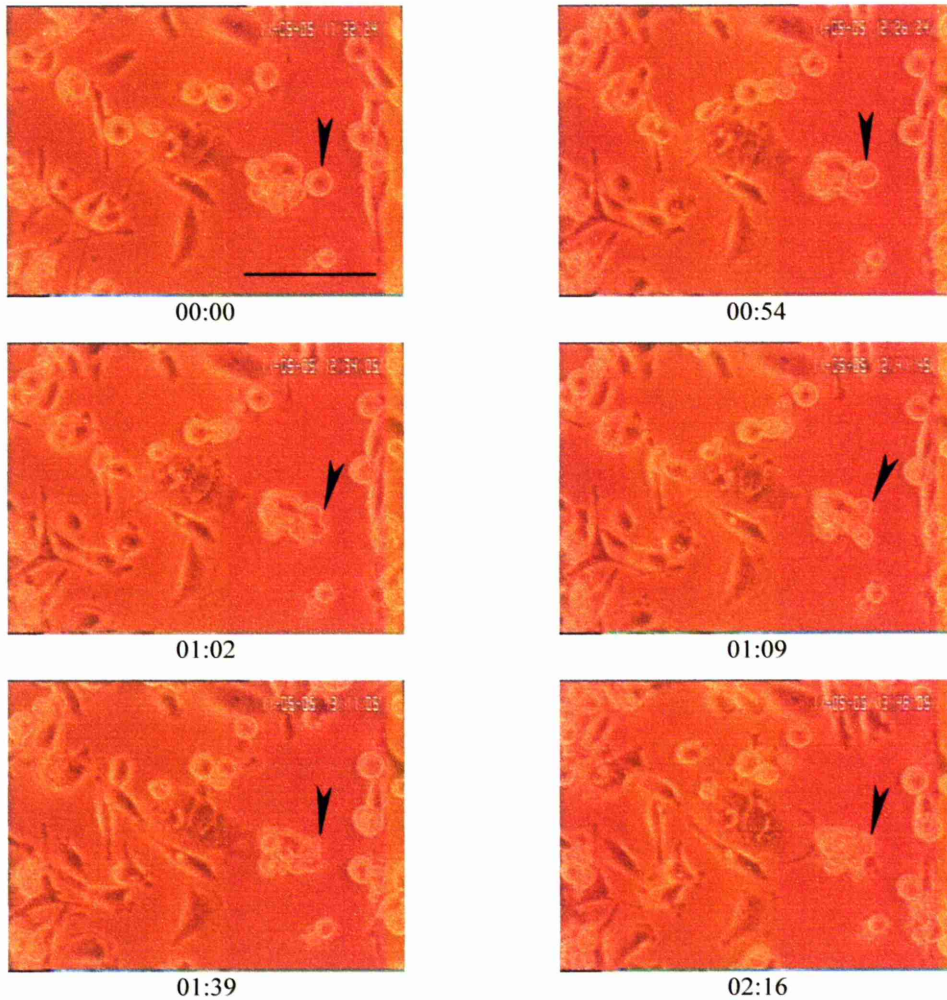


Figure 3-16: PC-3 cells cultured in BMSCM

Cells formed clusters which were loosely attached to the substrate. Cells within the clusters were able to divide. The rounded cell (black arrowhead) undergoes mitosis (image at 01:02) and remains within the cell cluster. Times are shown as hours and minutes after the first image at 00:00. Scale bar represents 100 μ m.

See also video clip 13

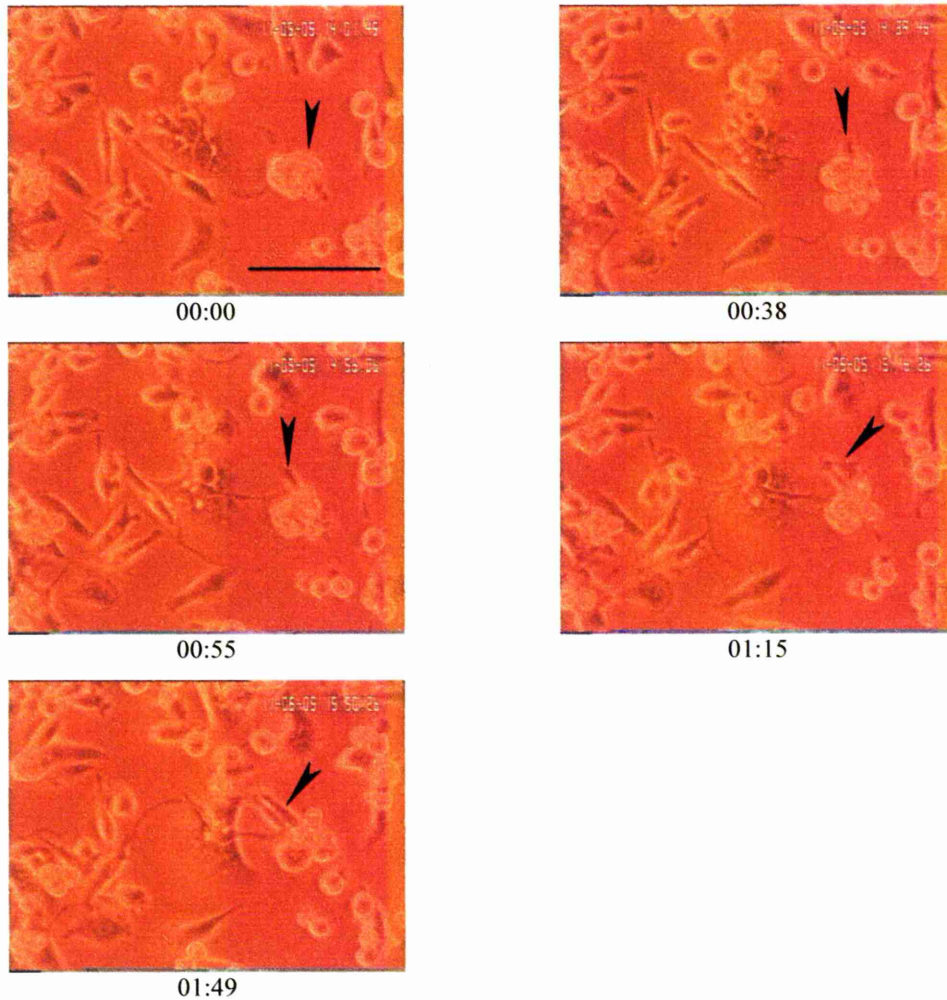


Figure 3-17: PC-3 cells showing escape from a cell cluster

Cells were able to spread on the substrate after being part of a cell cluster. A cell within a cluster (arrowhead) spreads on the substrate and begins to migrate away from the cluster. Cells were cultured in BMSCM. Times are shown as hours and minutes after the first image at 00:00. Scale bar represents 100 μ m.

See also video clip 14

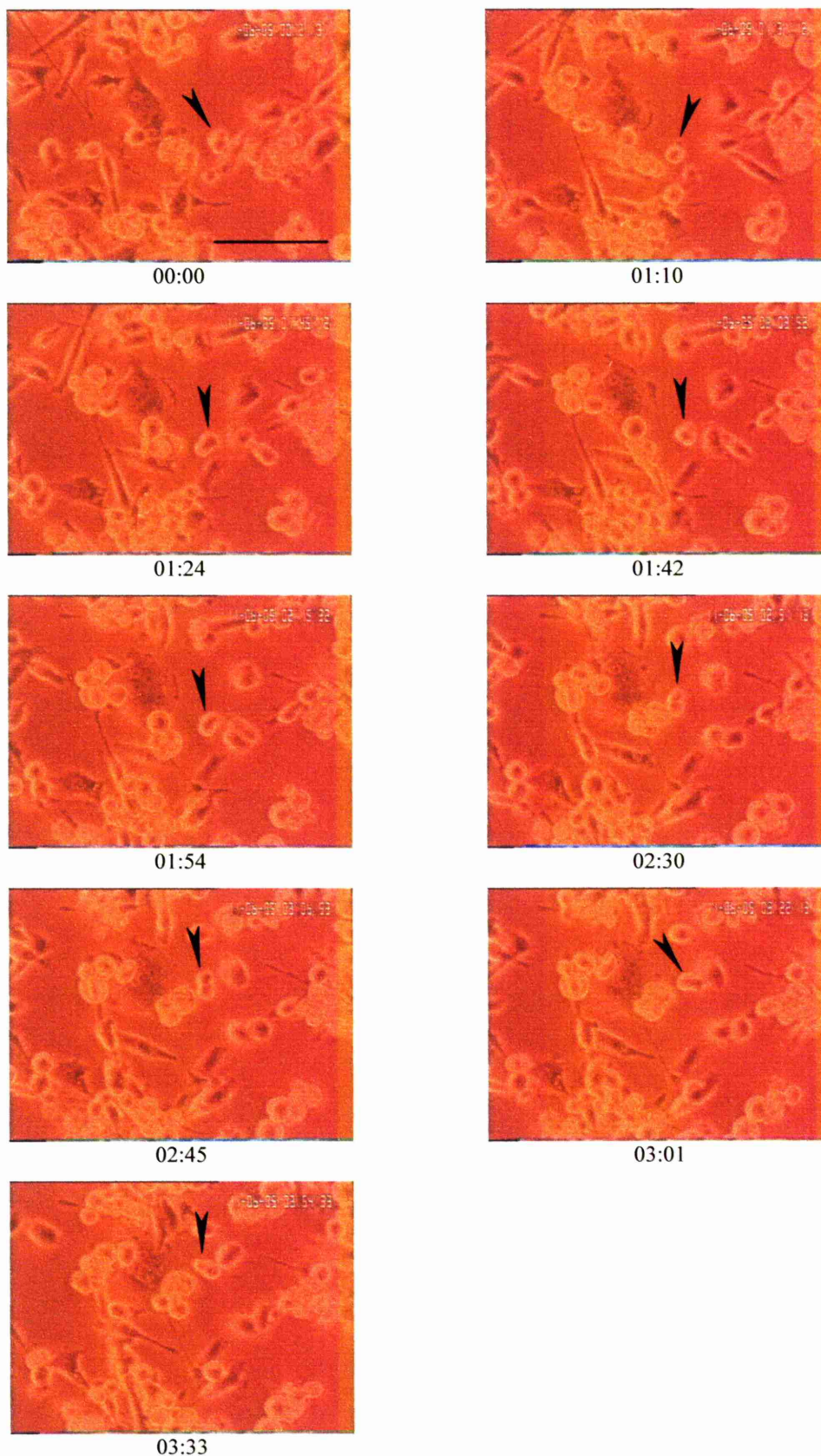


Figure 3-18: PC-3 cells showing amoeboid movement

The cell (black arrowhead) moves across the substrate remaining rounded but with a visible lamellipodium. Cells were cultured in BMSCM. Times are shown as hours and minutes after the first image at 00:00. Scale bar represents 100 μ m. *See also video clip 15*

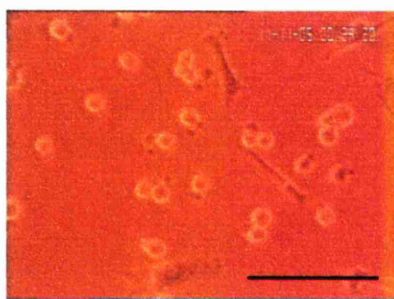


Figure 3-19: PC-3-GFP cells cultured in BMSCM

A large proportion of cells are rounded and showing amoeboid movement. Cells were cultured in BMSCM. Scale bar represents 100µm.

See also video clip 18

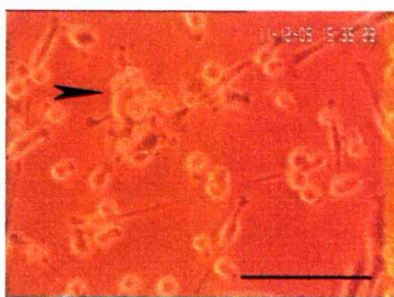


Figure 3-20: PC-3-GFP cells cultured in BMSCM showing cell clusters

PC-3-GFP cells formed rounded clusters in BMSCM (arrowhead). Cells were cultured in BMSCM. Scale bar represents 100µm.

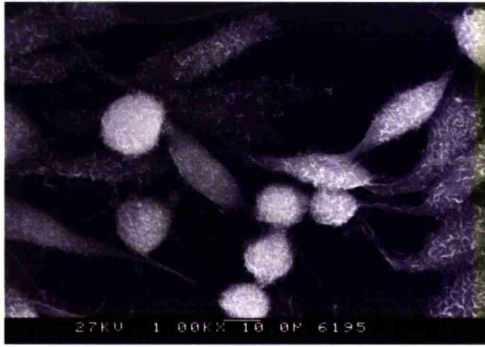
See also video clip 20

3.2.3 Scanning Electron Microscopy (SEM) examination of cell morphology

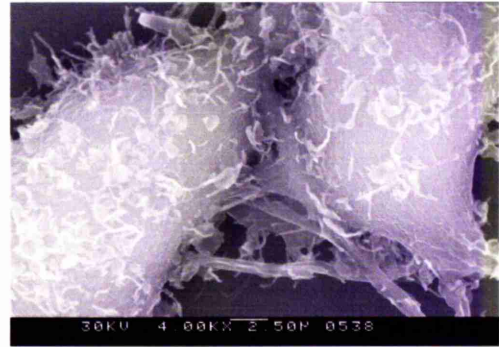
3.2.3.1 PC-3 and PC-3-GFP cells

Cultures of PC-3 and PC-3-GFP cells were examined by SEM to examine and compare their morphology before co-culture studies were commenced.

PC-3 and PC-3-GFP cells were cultured on silicon wafers in Ham's F12, fixed in glutaraldehyde and osmium tetroxide, critical point dried and coated with chromium for examination in the SEM. Representative images of PC-3 and PC-3-GFP cells are shown in Figure 3-21. Both cell lines showed a similar range of morphology to that seen on light and time lapse video microscopy. Spindle-shaped, epithelioid and amoeboid cells were seen, illustrated in Figure 3-21a. Both fibroblastic and amoeboid migrating cells with lamellipodia were seen (see Figure 3-21c, e and f) and both cell lines showed prominent microvillous processes on their surfaces. PC-3-GFP cells displayed more membrane blebbing than PC-3 cells. PC-3 cells could also be seen forming cell-cell contacts (Figure 3-21b).



a)



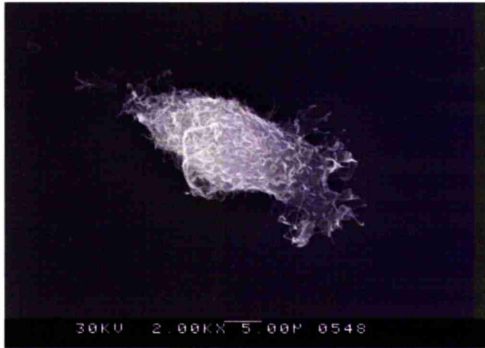
b)

a-c) PC-3 cells

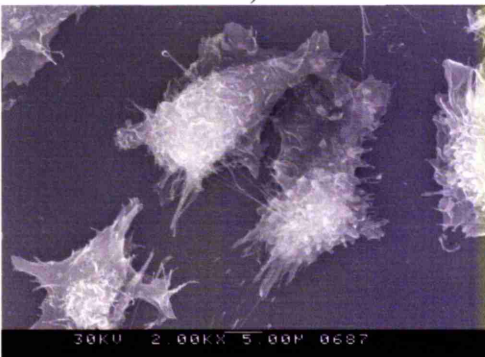
a) spindle shaped, rounded and flattened polygonal cells (x1000)

b) two adjacent epithelioid cells showing microvillous processes and membrane contacts (x4000)

c) fibroblastic migrating cell with flattened lamellipodium (x2000)



c)



d)



e)

d-f) PC-3-GFP cells

d) flattened polygonal cells showing microvillous processes and membrane blebs (x2000)

e) fibroblastic migrating cell with broad lamellipodium (x2000)

f) amoeboid cell with lamellipodium and membrane blebs (x3000)



f)

Figure 3-21: Typical appearances of PC-3 and PC-3-GFP cells on scanning electron microscopy
Cells were cultured on silicon wafers in Ham's F12, fixed with glutaraldehyde and osmium tetroxide, critical point dried and coated with 4nm chromium before examination in the SEM.

3.2.4 Immunophenotyping

3.2.4.1 PC-3 and PC-3-GFP cells

One of the initial aims of the project was to examine the role of a variety of cell junctional components and other adhesion proteins in co-culture invasion studies. Basal expression levels of each cellular component were first assessed in isolation. This also allowed the two cell lines to be phenotyped and compared.

Table 3-3: Immunophenotype of PC-3 and PC-3-GFP cells

MARKER	STAINING
α 2-integrin	Membrane staining more prominent on some cells, possibly negative in some cells
β 1-integrin	Granular membrane staining including filopodia
β 4-integrin	Membrane staining more prominent on some cells, possibly negative in some cells
Claudin-12	Staining of Golgi body, with some staining of membrane ruffles/focal adhesions
N-Cadherin	Membrane staining
Occludin	Surface membrane staining. Concentrated at some cell-cell junctions but not specifically present at leading edges
ZO-1	Staining of cell-cell contacts and nucleoli with focal staining of membrane. No staining apparent at cell-cell junctions
ZO-2	Staining of nucleus but not nucleoli. Focal membrane staining but not at cell-cell junctions
ZO-3	Staining of membrane ruffles with dot-like nuclear staining and vague cytoplasmic staining
E-Cadherin	Negative
VE-cadherin	Negative
Claudin-5	Negative
α 4-integrin	Negative
α 5-integrin	Negative
CD31	Negative
VCAM-1	Negative
P-Selectin	Negative
Sialyl Lewis X (PC-3 only)	Negative

PC-3 and PC-3-GFP cells were cultured on glass coverslips and fixed in methanol. PC-3 cells were stained by a two step method using primary antibody with a FITC conjugated secondary antibody. Primary antibodies labelled using a Zenon Alexa Fluor 555 kit were used to stain PC-3-GFP cells. Where cells showed positive labelling, virtually all cells were positive and no scoring system was used. Negative controls (non-specific mouse or rabbit IgG depending on the primary antibody host) were used in all experiments. For most antibodies a suitable positive control was not known so labelling was performed in batches using the same reagents for all steps

except for the primary antibodies. This allowed the secondary antibody or Zenon reagents to be assessed as long as one of the primary antibodies in the batch under test produced positive labelling. The results are shown in Table 3-3, Figure 3-22 for PC-3 and Figure 3-23 for PC-3-GFP cells. PC-3 and PC-3-GFP cells show an identical immunophenotype for all markers tested on both cell lines.

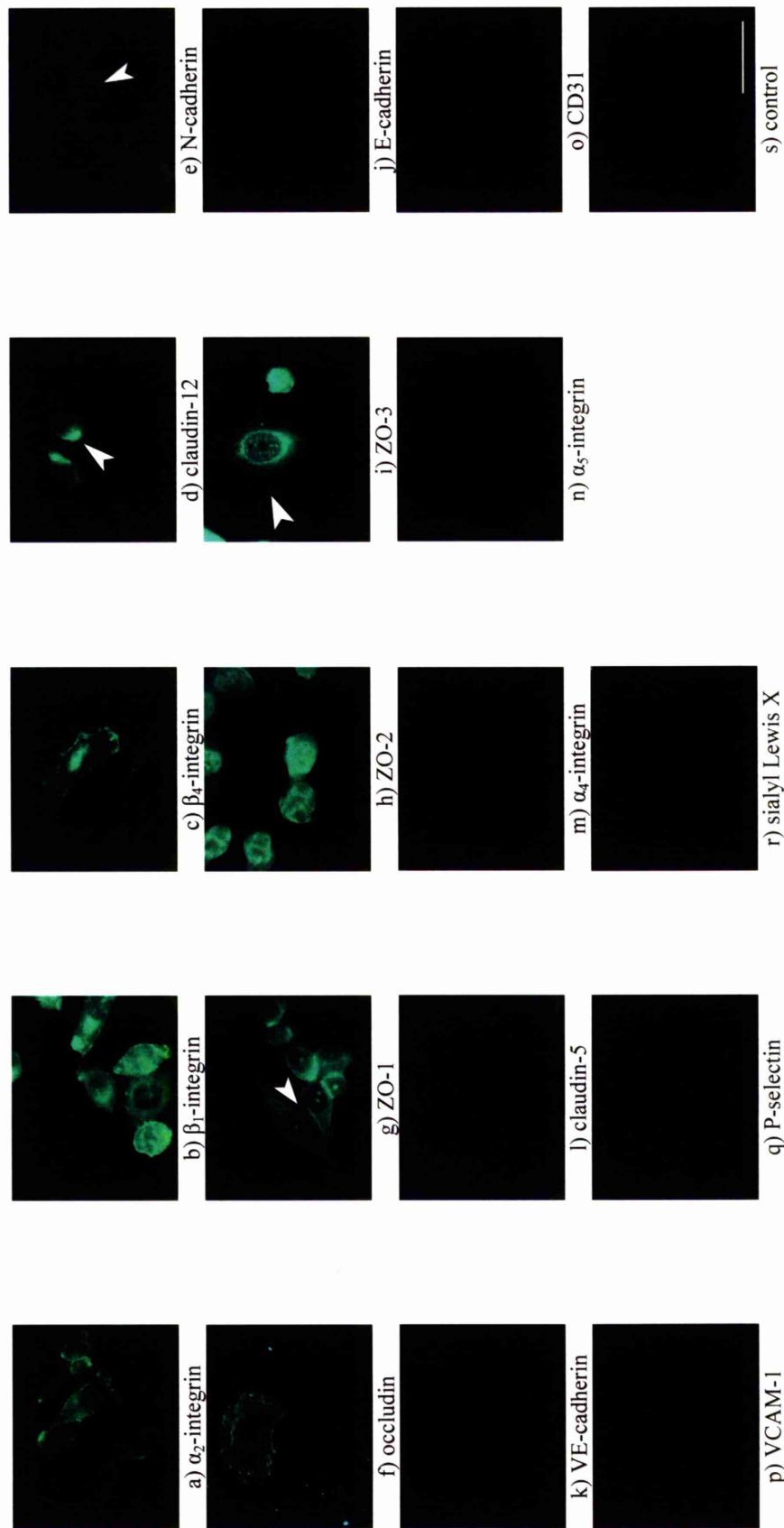


Figure 3-22: Immunophenotype of PC-3 cells

a) – s) Methanol fixed PC-3 cells were stained using primary antibody with FITC-conjugated secondary antibody. Labelling was judged to be negative when the level of fluorescence present was no higher than that seen in the negative control, with the illuminating light at the same intensity. Positive labelling was seen with a) α_2 -integrin, b) β_1 -integrin, c) β_4 -integrin, d) claudin-12 (positive labelling of Golgi body arrowed), e) N-cadherin (membrane labelling arrowed), f) occludin, g) ZO-1 (positive labelling of cell-cell contacts arrowed), h) ZO-2 and i) ZO-3 (positive labelling of membrane ruffles arrowed). Specimens were examined using an Olympus BX51 fluorescence microscope. Scale bar represents 50 μ m.

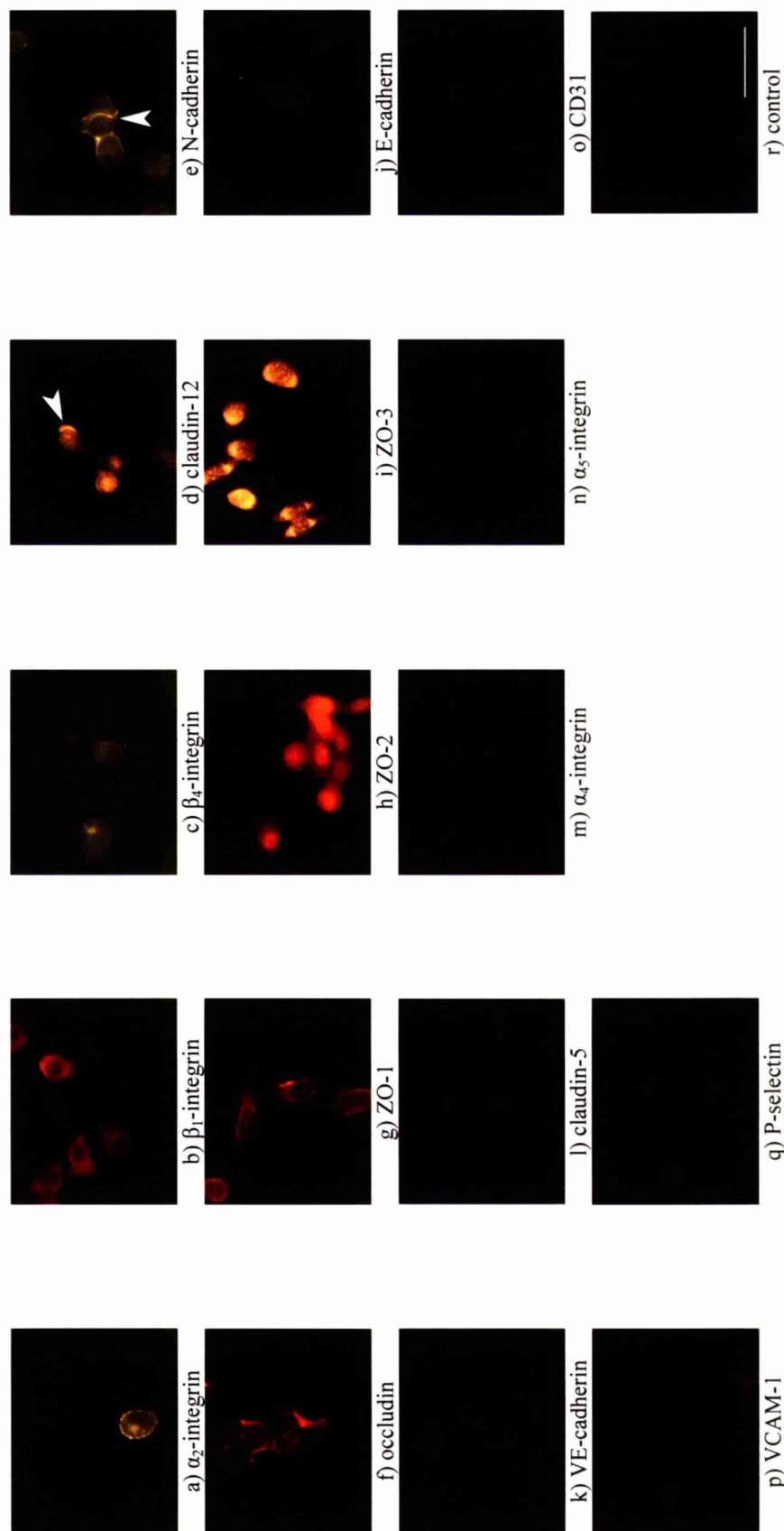


Figure 3-23: Immunophenotype of PC-3-GFP cells

a) – r) methanol fixed PC-3-GFP cells were stained using Zenon Alexa Fluor 555 labelled primary antibody. Labelling was judged to be negative when the level of fluorescence present was no higher than that seen in the negative control, with the illuminating light at the same intensity. Positive labelling was seen with a) α_2 -integrin, b) β_1 -integrin, c) β_4 -integrin, d) claudin-12 (positive labelling of Golgi body arrowed), e) N-cadherin (membrane labelling arrowed), f) occludin, g) ZO-1, h) ZO-2 and i) ZO-3. Specimens were examined using an Olympus BX51 fluorescence microscope. Scale bar represents 50 μ m

3.3 Bone marrow endothelial cell line (BMEC) culture optimisation and characterisation

3.3.1 Media and substrate test

BMEC were initially cultured in EGM-2 (EBM-2 + EGM-2 bullet kit (Cambrex) 15% FCS, 2mM L-glutamine) but many cells appeared apoptotic and cells did not form a confluent monolayer. Other media were tested to find more suitable conditions in which the cells would form a confluent monolayer and produce a model for the bone marrow vascular endothelium. BMEC had previously been successfully cultured in attachment factor coated flasks in a medium based on M199 (M199 with Earle's salts and Glutamax, 15% FCS, 16 U/ml heparin, endothelial cell growth supplement) by Almeida-Porada (personal communication). Medium conditioned by normal human bone marrow stromal cultures was also tested with the aim of providing an environment similar to that experienced by bone marrow endothelial cells *in vivo*. Fibronectin and attachment factor were tested as substrates for growth.

BMEC were cultured in tissue culture treated plastic flasks coated with either fibronectin or attachment factor, in EGM-2, M199 or BMSCM. Table 3-4 shows the characteristics of BMEC cultured in each medium. The growth and morphology of cells was not affected by whether they were cultured on fibronectin or attachment factor. Figure 3-24 shows the typical morphology of BMEC in different media.

Table 3-4: Characteristics of BMEC cultured in different media

MEDIUM	PASSAGING INTERVAL	MORPHOLOGY AND GROWTH	APOPTOSIS/ CELL DEBRIS
EGM-2	5-6 days	Variable size and shape of cells, some spindle shaped and with long processes. Very reluctant to form cell-cell contacts. Cells appear disorganised and become heaped up when confluent. Many cells contain vacuoles	++++
M199	6+ days	Confluent patches of flattened polygonal cells. Some cells are vacuolated. Cells become disorganised and spindle-shaped when over confluent. Growth is variable and unpredictable with cells requiring passaging at intervals of 6 days up to 28 days	++
BMSCM	3-4 days	Confluent monolayer of short spindle-shaped cells. Occasional cells are vacuolated. Appear to form cell-cell contacts. Become crowded when over confluent	-/+

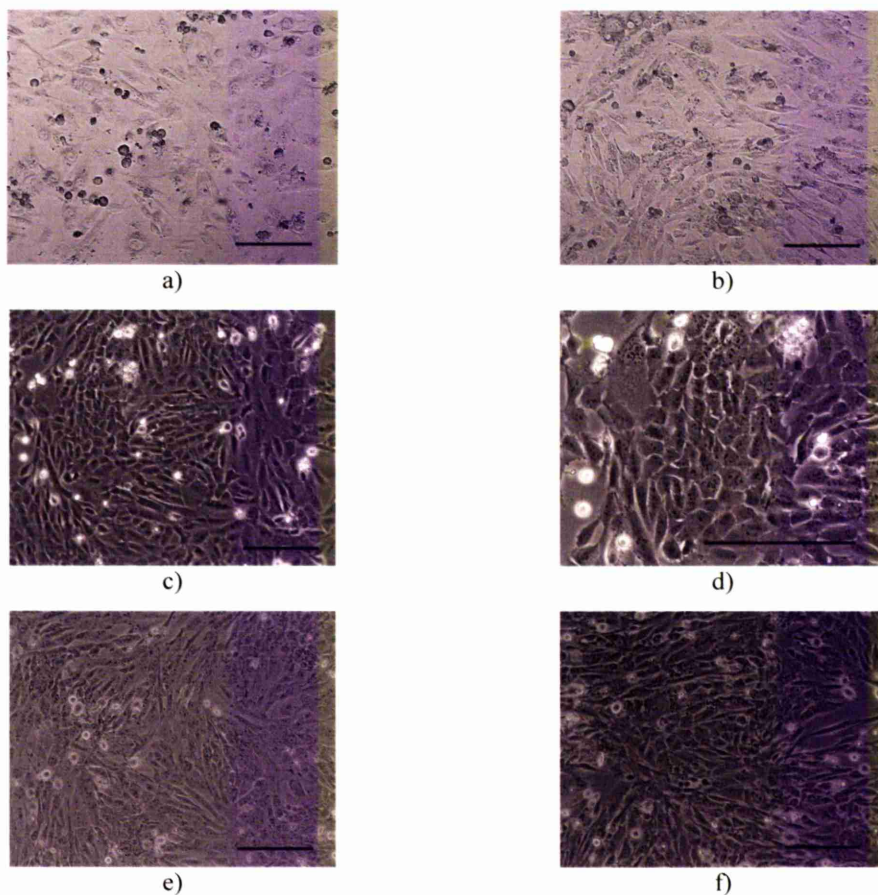


Figure 3-24: Typical appearances of BMEC on tissue culture plastic in different culture media
a) and b) EGM-2: frequent apoptosis was seen (apoptotic cells are rounded, irregular and fragmented or dark)
c) and d) M199: cells show a good “cobblestone” morphology
e) and f) BMSCM: cells form a monolayer of flattened and short spindle shaped cells
 Photographs taken using a Zeiss Axiovert 35M. Scale bars represent 200µm.

BMEC showed frequent apoptosis and poor morphology, and did not form confluent monolayers in EGM-2 so no further work was done using this medium. M199 and BMSCM both produced cells with good morphology, although growth could be slow and unpredictable in M199. The best morphology and growth was obtained in BMSCM.

3.3.1.1 Time lapse video microscopy

Time lapse video microscopy was used to study cell morphology and behaviour, compare BMEC with primary cells and to further assess the reaction of BMEC to the different culture media. M199 and BMSCM were used as both produced good cellular morphology. The corresponding video clips can be found on the accompanying DVD in presentation 3.3.

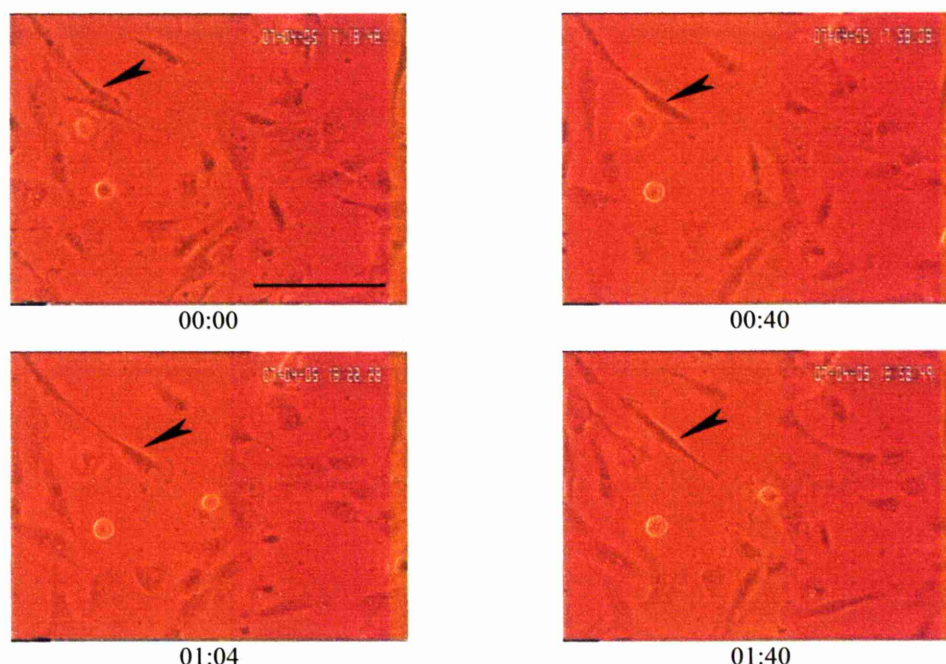


Figure 3-25: BMEC cultured in M199 showing fibroblastic movement

Cells in a subconfluent culture show relatively rapid fibroblastic movement. An elongated cell (arrowhead) moves across the substrate. Times are shown as hours and minutes after the first image at 00:00. Scale bar represents 100 μ m.

See also video clip 21

BMEC cultured in M199 showed a fibroblastic morphology with some cells showing relatively rapid movement across the substrate, shown in Figure 3-25 and video clip 21. Occasional cells within the monolayer also showed spontaneous apoptosis (see Figure 3-26 and video clip 22). In the image at 00:05 a BMEC can be seen retracting from adjacent cells and then undergoing apoptosis, after which the adjacent cells spread laterally to close the gap. A cell undergoing mitosis and then spreading rapidly on the substrate can be seen in video clip 23. This clip also illustrates the disorganised appearance of the monolayer which was observed as cells became increasingly confluent.

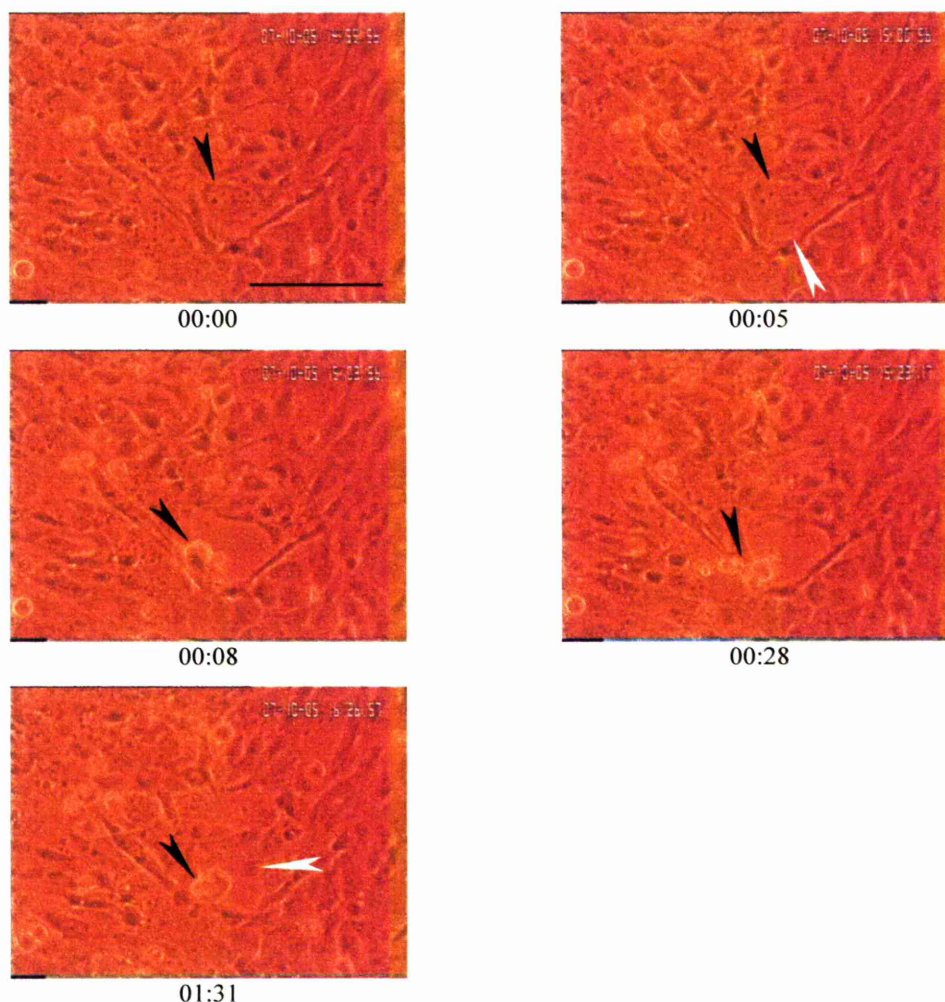


Figure 3-26: BMEC cultured in M199 showing spontaneous apoptosis

A confluent BMEC monolayer cultured in M199. The large cell (black arrowhead) begins to retract (image at 00:05, white arrowhead) and undergoes apoptosis leaving a gap in the monolayer which is gradually filled by other cells (image at 01:31, white arrowhead). Membrane blebbing which does not lead to apoptosis is visible on many of the cells. Times are shown as hours and minutes after the first image at 00:00. Scale bar represents 100µm.

See also video clip 22

In subconfluent cultures BMEC in BMSCM also had a fibroblastic morphology and moved across the substrate slowly, as shown in Figure 3-27 and video clip 24.

A more confluent monolayer is shown in Figure 3-28 and video clip 25. A cell undergoes mitosis and spreads rapidly on the substrate in a similar way to that seen when cells were cultured in M199. In video clip 26 cell-cell junctions can be seen very slowly opening and closing as cells move short distances within the monolayer. Some cells seem to maintain a small gap at their junctions for several hours. As BMEC become confluent they continue to form an organised monolayer,

shown in Figure 3-29 and video clip 27. In both media many cells showed membrane blebbing which can be seen in many of the video clips.

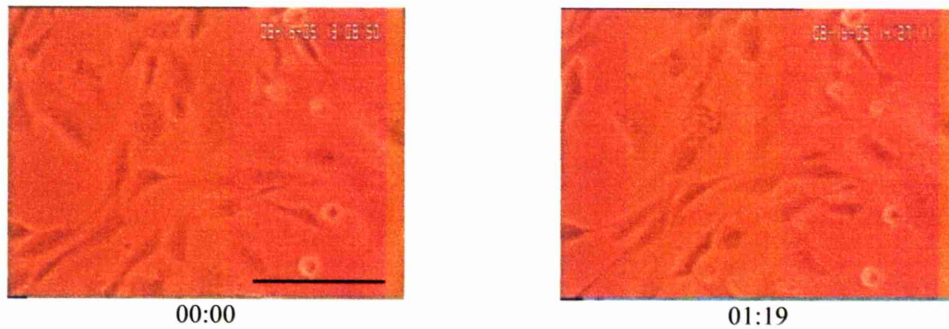


Figure 3-27: BMEC cultured in BMSCM showing slow fibroblastic movement across the substrate

BMEC show only slow movement in BMSCM. The second image is taken 79 minutes after the first and shows that the cells have moved only a small distance in the intervening period. Times are shown as hours and minutes after the first image at 00:00. Scale bar represents 100 μ m.

See also video clip 24

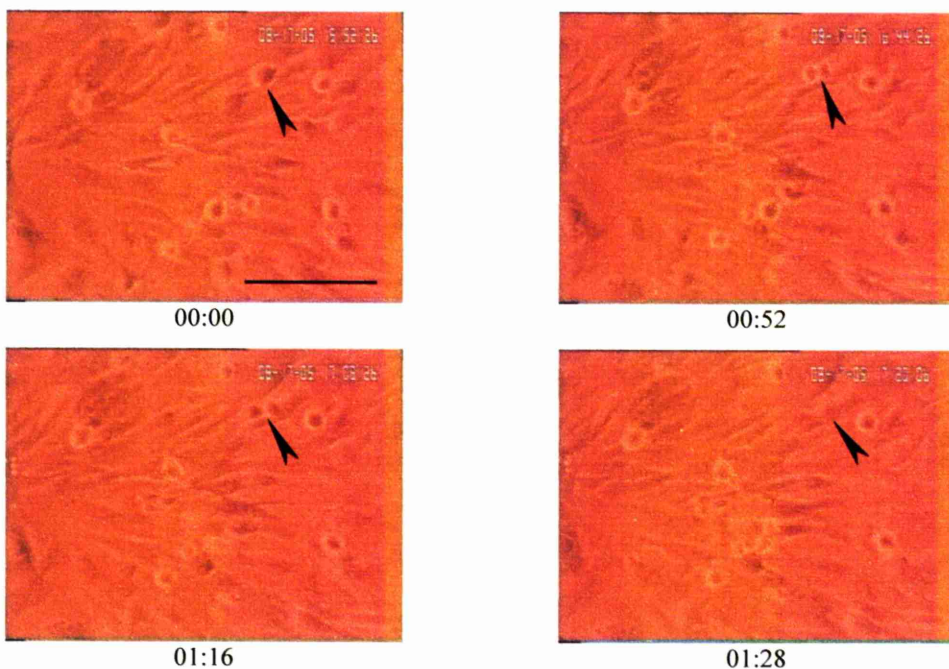


Figure 3-28: BMEC cultured in BMSCM with cell dividing

The cell (arrowhead) divides parallel to the substrate and then rapidly spreads on the substrate. Times are shown as hours and minutes after the first image at 00:00. Scale bar represents 100 μ m.

See also video clip 25



Figure 3-29: Confluent BMEC monolayer cultured in BMSCM

Cells form an organised, confluent monolayer. Membrane blebbing can be seen on some cells. Scale bar represents 100µm.

See also video clip 27

Although both media produced good morphology, cells showed more rapid growth and formed cell-cell contacts more readily in BMSCM than M199. Cells cultured in BMSCM also seemed to produce a more well-organised monolayer. Therefore it was decided to use BMSCM for the culture of BMEC and for primary human bone marrow endothelial cells.

During time lapse video microscopy studies it was noted that BMEC monolayers which had reached 100% confluence as judged visually could continue remain confluent for a further 3 days before the cells began to appear crowded. During these 3 days BMEC could continue to divide and still be accommodated within the monolayer. For this reason, whenever BMEC were cultured to confluence for experimental work they were cultured for a further day after 100% confluence was observed in order to ensure the monolayer was adequately confluent.

3.3.1.2 Substrate test

Although cells grew well and formed a good monolayer in tissue culture treated plastic flasks, they grew in a more disorganised way on glass coverslips, even when these were coated with fibronectin or attachment factor. Coverslips were originally intended to be possible substrates for light microscopy of co-cultures but an alternative was needed that would promote formation of a good monolayer. BMEC were cultured in BMSCM on several different optically suitable substrates (tissue culture treated borosilicate glass, quartz glass and tissue culture treated Thermanox plastic) coated with either fibronectin or attachment factor. The results are shown in Figure 3-30.

On all substrates except quartz glass, the choice of attachment factor or fibronectin coating did not affect cellular morphology. On quartz glass coated with

attachment factor cells attached poorly to the substrate and appeared to detach with increasing time and form rounded masses (Figure 3-30a). When quartz glass was coated with fibronectin, BMEC formed a monolayer with good morphology (Figure 3-30b). They detached and formed rounded masses similar to those seen in Figure 3-30a when cultured on tissue culture treated glass slides coated with either protein (results not shown). On glass coverslips cells formed a disorganized monolayer with cells frequently overlapping and orientated perpendicular to each other (Figure 3-30c) and a slightly disorganized monolayer on Thermanox sterilized with 100% ethanol. They formed a monolayer with typical bone marrow endothelial morphology on Thermanox sterilized with UV and coated with either attachment factor or fibronectin (Figure 3-30d). It was decided to use fibronectin coated quartz glass bottomed dishes for co-culture studies as these were suitable for live cell work and for immunofluorescence.

3.3.1.3 SEM analysis of BMEC morphology

SEM was used to assess the morphology and cell-cell junctions of BMEC, and to compare them with primary bone marrow endothelial cells. Initial attempts to grow BMEC on silicon wafers proved unsuccessful even when wafers were coated with fibronectin or attachment factor. Thermanox tissue culture treated plastic coverslips are resistant to reagents used in processing for SEM, can be used in place of silicon wafers and can be used to culture BMEC (section 3.3.1.2).

BMEC cultures on Thermanox coated with 4nm chromium and examined in the SEM at an accelerating voltage of 30kV produced unusable images (Figure 3-31a) due to specimen charging. This occurs because plastic is nonconductive and allows a negative charge to build up on the specimen during electron bombardment[134]. Lowering the accelerating voltage reduces the charge build up but artefacts are still problematic (Figure 3-31b). Mounting of the Thermanox BMEC cultures on aluminium stubs using ElectroDAG conductive adhesive and examination at a voltage of 20kV partially alleviated these problems, as seen in Figure 3-31. However, charging artefacts are still present, seen as horizontal lines on the image and abnormal contrast between flattened and rounded cells.

To further reduce charging, a coating of 8nm platinum-palladium 80/20 was used instead of chromium on aluminium/ElectroDAG mounted specimens. These specimens showed virtually no charging artefact when examined at an accelerating

voltage of 20kV; therefore this treatment was used for further work on cells cultured on Thermanox. Typical images of BMEC obtained in this way are shown in Figure 3-32.

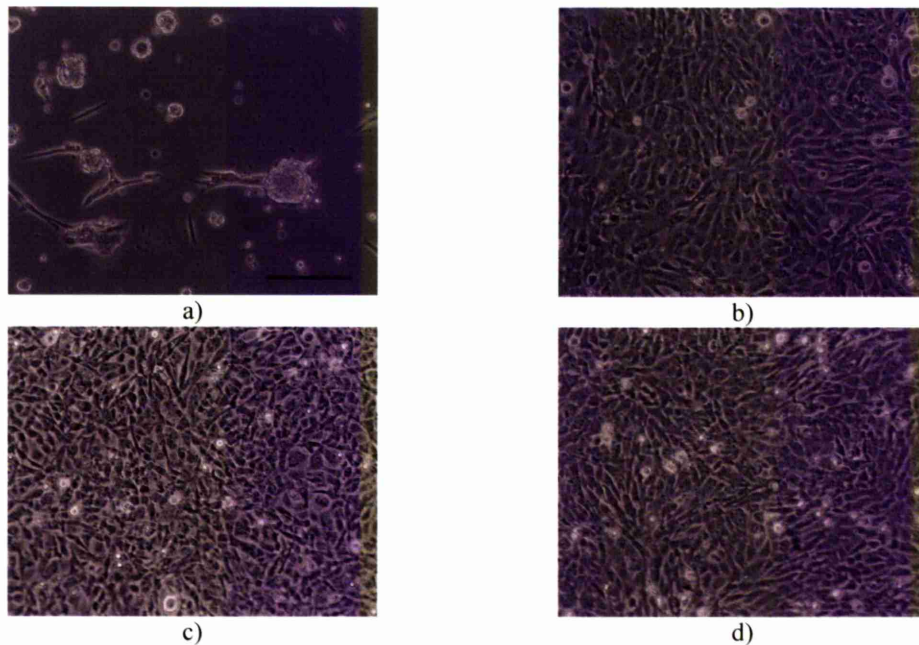


Figure 3-30: Typical appearances of BMEC cultured in BMSCM on different substrates

a) quartz glass bottomed dish coated with attachment factor. Cells detach from the substrate and form rounded clusters.

b) quartz glass bottomed dish coated with fibronectin. Cells form an organised monolayer.

c) glass coverslip sterilized with UV and coated with fibronectin. Cells form a slightly disorganised layer with cells overlapping each other.

d) Thermanox coverslip sterilized with UV and coated with fibronectin. Cells form an organised monolayer.

Phase contrast images taken using a Zeiss Axiovert 35M. Scale bar represents 200 μ m.

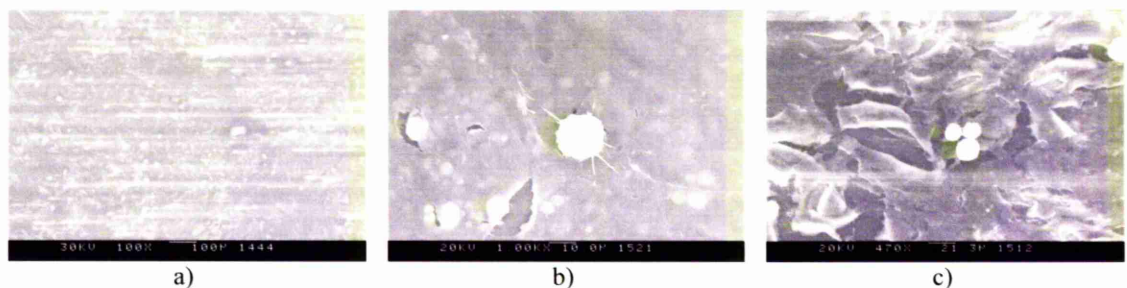


Figure 3-31: Charging artefacts on SEM

SEM images showing charging artefacts: a) horizontal white lines across the image and b) abnormal high contrast seen in the rounded cell which is very white with no detail visible. Both show 4nm chromium coated BMEC on Thermanox pieces at an accelerating voltage of a) 30kV and b) 20kV.

c) horizontal white lines and abnormal contrast. The image shows 4nm chromium coated BMEC on a Thermanox piece mounted on an aluminium stub with ElectroDAG paint at an accelerating voltage of 20kV

At low magnification a monolayer of flattened cells with some rounded cells was seen (Figure 3-32 a and b). Cells undergoing apoptosis and apoptotic debris were present (Figure 3-32d). Most cells have smooth surfaces with occasional short processes, although some have a larger number of surface processes (Figure 3-32e). There are smooth-edged gaps present between cells which may be due to shrinkage during processing. Cell-cell junctions can be seen as irregular structures where cells overlap and often extend narrow processes across the junction (Figure 3-32 e to h).

3.3.2 Comparison of cell lines

To assess the usefulness of BMEC and validate the endothelial model system, BMEC were compared with primary human bone marrow endothelial cells which had been previously extracted using a method developed by Masek and Sweetenham[132] and modified by Scott *et al*[13] (see section 2.2.1.2.2). Their morphology was compared using light, time lapse and scanning electron microscopy; and their immunophenotypes were compared using antibody labelling and fluorescence microscopy.

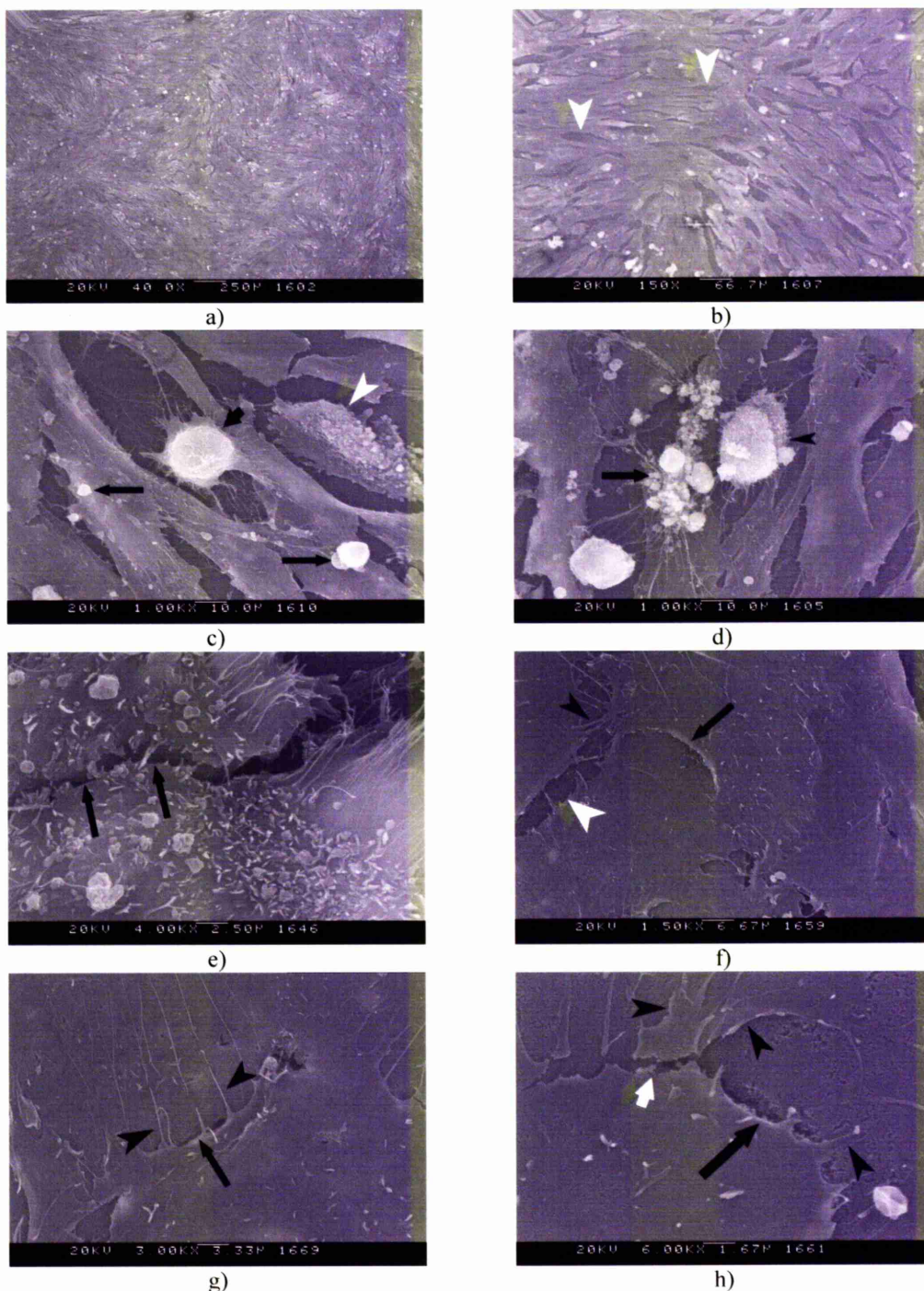


Figure 3-32: Appearances of BMEC on SEM

BMEC were cultured on fibronectin coated Thermanox pieces, fixed, critical point dried and mounted on aluminium stubs with ElectroDAG before coating with platinum-palladium. They were examined in the SEM at 20kV.

a) and b) low power images of BMEC monolayers: some rounded cells are seen and smooth edged gaps (white arrowheads) are present

c) a rounded cell (short arrow) and a blebbing cell (white arrowhead) with adjacent flattened cells and apoptotic debris (black arrows)

d) an apoptotic cell (arrow) with an adjacent rounded cell (arrowhead) which may be undergoing division

e) to h) cell to cell junctions (arrows) showing cell edges overlapping and extension of cell processes across junctions (arrowheads). Drying artefact causing cracking is seen (white arrow)

a) x40, b) x150, c) x1000, d) x1000, e) x4000, f) x1500, g) x3000, h) x6000

3.3.2.1 Light microscopy

Cells cultured in BMSCM on fibronectin coated tissue culture plastic, glass coverslips and Thermanox were compared. As seen in Figure 3-33, both cell types grew well on fibronectin coated tissue culture plastic and Thermanox, exhibiting a spindle-shaped morphology. Primary cells had a more angular shape while BMEC had a short spindle-shaped morphology on tissue culture plastic. On Thermanox both grew with cells orientated parallel to each other and formed a better organised monolayer. Although both cell types grew on fibronectin coated glass coverslips they both showed a disorganised pattern with cells overlapping and orientated perpendicular to each other, illustrated in Figure 3-33 e and f.

3.3.2.2 Time lapse video microscopy

Primary cells were observed in the time lapse video microscopy unit. These cells were almost entirely static but showed occasional very slow movement over short distances (see Figure 3-34 and video clip 28). Cells remained flattened as they moved. The cells showed membrane blebbing and blebs could detach and float away or attach to the substrate and continue to bleb. Where cells were adjacent their cell-cell junctions were not static and slowly opened and closed as cells moved their borders back and forth. Cells divided rapidly and spread rapidly on the substrate after mitosis, as shown in Figure 3-35 and video clip 28. In Figure 3-36 and video clip 29, the cells have become more confluent, although they did not achieve full confluence in culture.

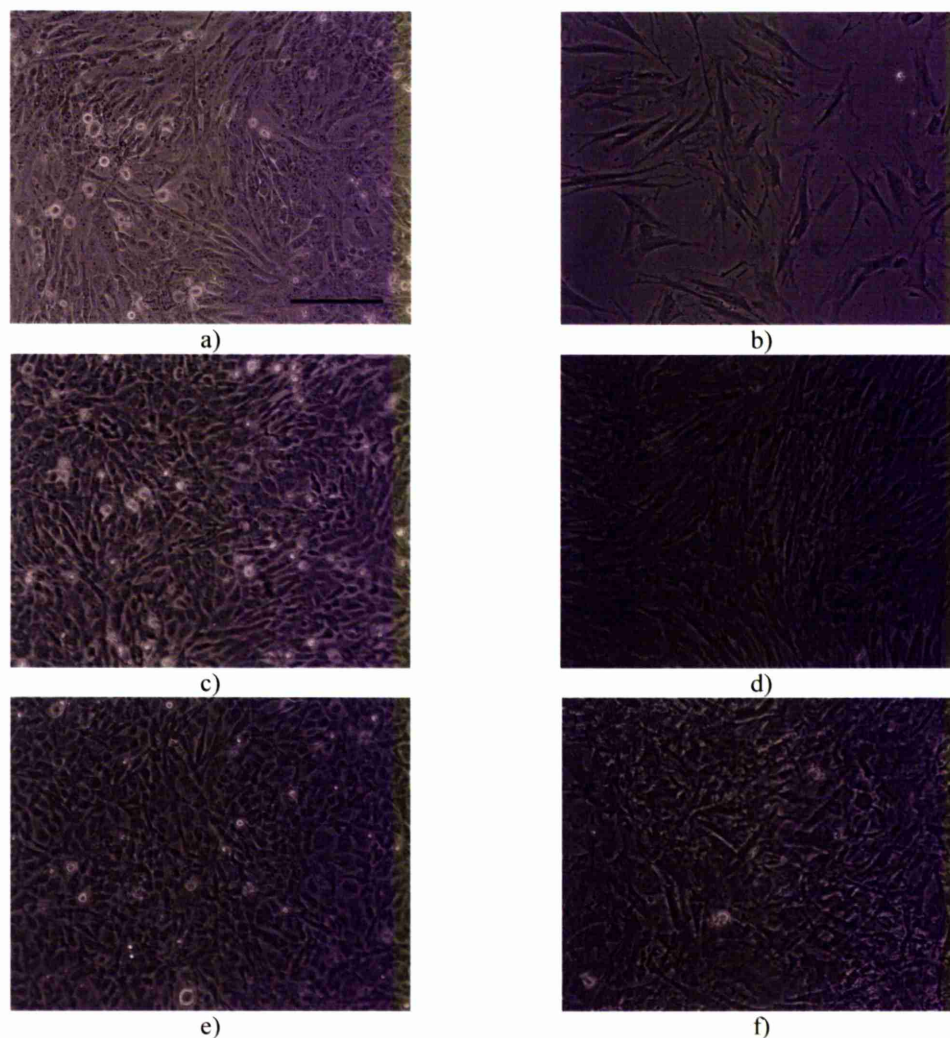
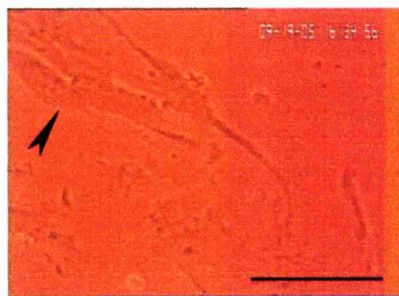


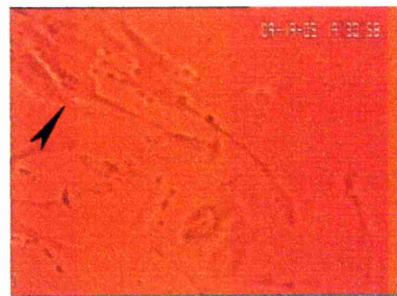
Figure 3-33: Appearances of BMEC and primary endothelial cells on different substrates

- a) BMEC cultured on tissue culture plastic
- b) primary human bone marrow endothelial cells on tissue culture plastic
- c) BMEC cultured on Thermanox
- d) primary human bone marrow endothelial cells on Thermanox
- e) BMEC cultured on glass
- f) primary human bone marrow endothelial cells cultured on glass

Both cell types produced a flattened spindle shaped morphology on all substrates, and produced an organised monolayer on Thermanox compared to the disorganised layer with overlapping cells seen on glass. Primary bone marrow endothelial cells did not achieve full confluence in all cultures. Cells were cultured on fibronectin coated substrates in BMSCM. Phase contrast photographs taken using a Zeiss Axiovert 35M. Scale bar represents 200 μ m.



00:00

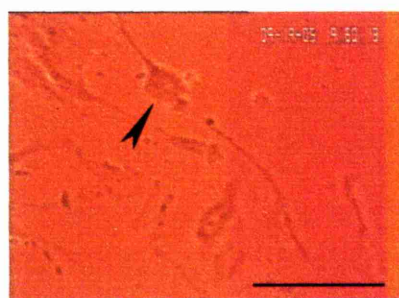


02:56

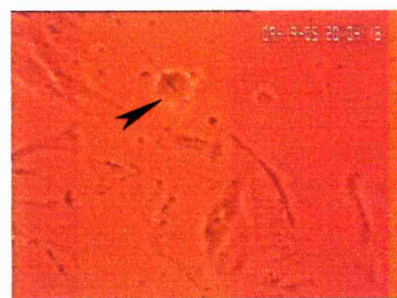
Figure 3-34: Primary human bone marrow endothelial cells cultured in BMSCM

A cell (arrowhead) shows very slow fibroblastic movement across the substrate. Times are shown as hours and minutes after the first image at 00:00. Scale bar represents 100 μ m.

See also video clip 28



00:00



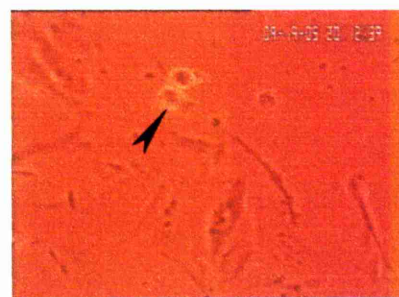
00:14



00:17



00:18



00:22



00:37

Figure 3-35: Primary human bone marrow endothelial cell undergoing mitosis

A cell (arrowhead) divides parallel to the substrate and spreads rapidly on the substrate. Times are shown as hours and minutes after the first image at 00:00. Scale bar represents 100 μ m.

See also video clip 28

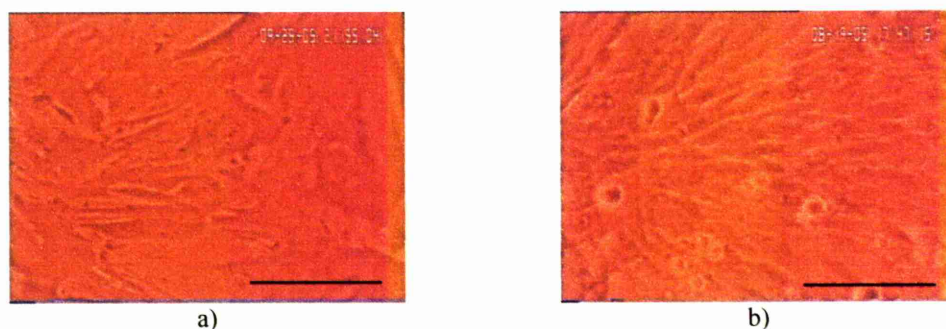


Figure 3-36: Primary human bone marrow endothelial cells

a) primary human bone marrow endothelial cells. The cells show very little movement and form a layer composed of flattened spindle shaped cells. Cells did not achieve full confluence in culture. b) BMEC for comparison showing confluent culture.

Scale bars represents 100µm.

See also video clip 29

3.3.2.3 Immunofluorescence

Cells cultured on fibronectin or attachment factor coated coverslips were used for immunofluorescent staining. Primary human bone marrow cells were used at passage 3-5 but did not achieve confluence in culture.

Initial experiments using BMEC stained by the three step technique (section 2.2.6.2.2.1) produced excessive background staining and a two step method (section 2.2.6.2.2.2) produced better results. This method was used for single antibody staining of isolated cultures. The high level of background staining made labelling difficult to assess. Positive labelling was judged to be present when there was fluorescence above the background level seen on the negative control, and/or when staining occurred consistently at the expected location (e.g. cell-cell junctions). Where labelling was judged to be positive, virtually all cells were positive and no scoring system was used. The phenotypes expressed are summarised in Table 3-5 for BMEC and Table 3-6 for primary human bone marrow endothelial cells. Staining is also shown in Figure 3-37 for BMEC and Figure 3-38 for primary cells.

Not all tight junction proteins could be detected in both types of endothelial cell. ZO-1 produced irregular linear staining at the cell-cell junctions of both BMEC and primary cells. ZO-2 staining was non-specific in primary cells and showed focal, weak staining of some cell-cell junctions in BMEC. Claudin-12 did not stain cell-cell junctions but showed prominent staining of the Golgi body, seen as a perinuclear membranous structure in BMEC; it did not stain primary cells. Occludin produced a dot-like staining pattern on both cell types, which was difficult to interpret but

seemed to be present on the surface of cell processes. Claudin-5 expression could not be demonstrated on either cell type.

Table 3-5: Immunophenotype of BMEC when cultured in BMSCM

MARKER	STAINING	EXPECTED STAINING
Occludin	Negative	Unknown (major component of tight junctions)
ZO-1	Prominent background staining in intracytoplasmic vesicles with patchy and sometimes poorly staining cell-cell junctions showing irregular linear staining	Unknown (major component of tight junctions)
ZO-2	Weak staining of some cell-cell junctions is present, with staining of nuclei which may be non-specific	Unknown (major component of tight junctions)
ZO-3	Dot-like staining of the nucleus with vague cytoplasmic staining. No edge staining	Unknown (major component of tight junctions)
Claudin-5	Negative (even in confluent cultures)	Unknown (previously demonstrated in mouse and thought to be endothelial specific [135])
Claudin-12	Staining of Golgi body but no edge staining	Unknown
β_1 -integrin	Positive (after formalin, but not methanol, fixation)	Positive* [130]
β_4 -integrin	Negative	Unknown (variable in human BME ** [136])
α_2 -integrin	Negative	Positive ** [137]
α_4 -integrin	Negative	Positive** [136]
α_5 -integrin	Negative	Positive** [136]
P-Selectin	Negative	Unknown** (variable in human EC [136])
VCAM-1	Membrane staining (cultured in BMSCM but not in M199)	Positive [138]
E-Cadherin	Negative	Negative ***
N-Cadherin	Negative	Cell-cell junctions ***
VE-cadherin	Negative	Cell-cell junctions*** [139]
CD31	Negative	Cell-cell junctions ** [136]

* BMEC cell line has previously been shown to express the marker

** Other human bone marrow endothelial cell lines have previously been shown to express/not express this marker

*** Other human endothelial cell lines have been shown to express/not express this marker

Both BMEC and primary cells expressed VCAM-1 when cultured in BMSCM but BMEC did not when cultured in M199 (results not shown). BMEC did not express any of the integrins tested except β_1 , although the primary cells did express α_5 and β_1 integrin. BMEC were negative for both E and N-cadherin. Due to the limited numbers of primary cells available, staining for all markers was not possible.

Table 3-6: Immunophenotype of primary human bone marrow endothelial cells in BMSCM

MARKER	STAINING	EXPECTED STAINING
Occludin	Dot-like staining over cell surface	Unknown (major component of tight junctions)
ZO-1	Irregular linear staining of cell peripheries is seen	Unknown (major component of tight junctions)
ZO-2	Negative	Unknown (major component of tight junctions)
ZO-3	Negative	Unknown (major component of tight junctions)
Claudin-5	Negative	Unknown
β_1 -integrin	Linear and dot-like staining of cell membranes	Unknown
β_4 -integrin	Negative	Unknown
α_2 -integrin	Negative	Unknown
α_4 -integrin	Negative	Unknown
α_5 -integrin	Linear and dot-like staining of cell membranes	Unknown
VCAM-1	Membrane staining	Positive [138]
VE-cadherin	Negative	Positive
CD31	Negative	Positive

As immunofluorescent staining was to be used to examine the roles of junctional proteins and cell surface receptors during endothelial transmigration, it was decided to optimise staining by attempting to reduce background and non-specific staining. A variety of different blocking techniques were used (see Table 3-7) as well as staining after fixation with formalin and Triton X100 or paraformaldehyde alone. In order to reduce the effects of autofluorescence, far red fluorophores were also used with both 2 step and Zenon labelled primary antibody techniques. Representative images of the results of some of these experiments are shown in Figure 3-39.

Although non-specific antibody binding did seem to contribute to the high background levels, autofluorescence was also a problem. Autofluorescence is less pronounced in the far red part of the spectrum, and in cells cultured in phenol red free medium. Unfortunately the powdered Iscove's medium required to make the medium used is unavailable in a phenol red free form. Staining using secondary antibodies labelled with far red fluorophores was still disappointing with high levels of non-specific binding. To check that the staining protocol itself was working, PNT2-C2 prostate epithelial cells, which also form a confluent monolayer, were stained using the same techniques and antibodies. The results of this staining were satisfactory, shown in Figure 3-40.

Table 3-7: Blocking techniques used with immunofluorescent staining

<i>BLOCK</i>	<i>STAINING TECHNIQUE</i>
Mouse serum	Zenon labelled mouse primary antibodies
Mouse IgG (non-specific)	Zenon labelled mouse primary antibodies
Image IT FX	Zenon labelled mouse primary antibodies
BSA in PBS (1%, 5%, 10%, 20%)	2 step
1% BSA + 10% rabbit serum	2 step with rabbit secondary antibody
1% BSA + 10% goat serum	2 step with goat secondary antibody
Casein in PBS (5%, 10%)	2 step
Milk in PBS (0.1%, 0.5%, 1%, 3%, 5%, 10%)	2 step
2% fish gelatin in PBS	2 step
1%BSA + 1% milk + 2% fish gelatin in PBS	2 step
FCS in PBS (5%, 10%)	2 step
5% FCS + 5% BSA in PBS	2 step
Human normal immunoglobulin	2 step
10% horse serum	2 step

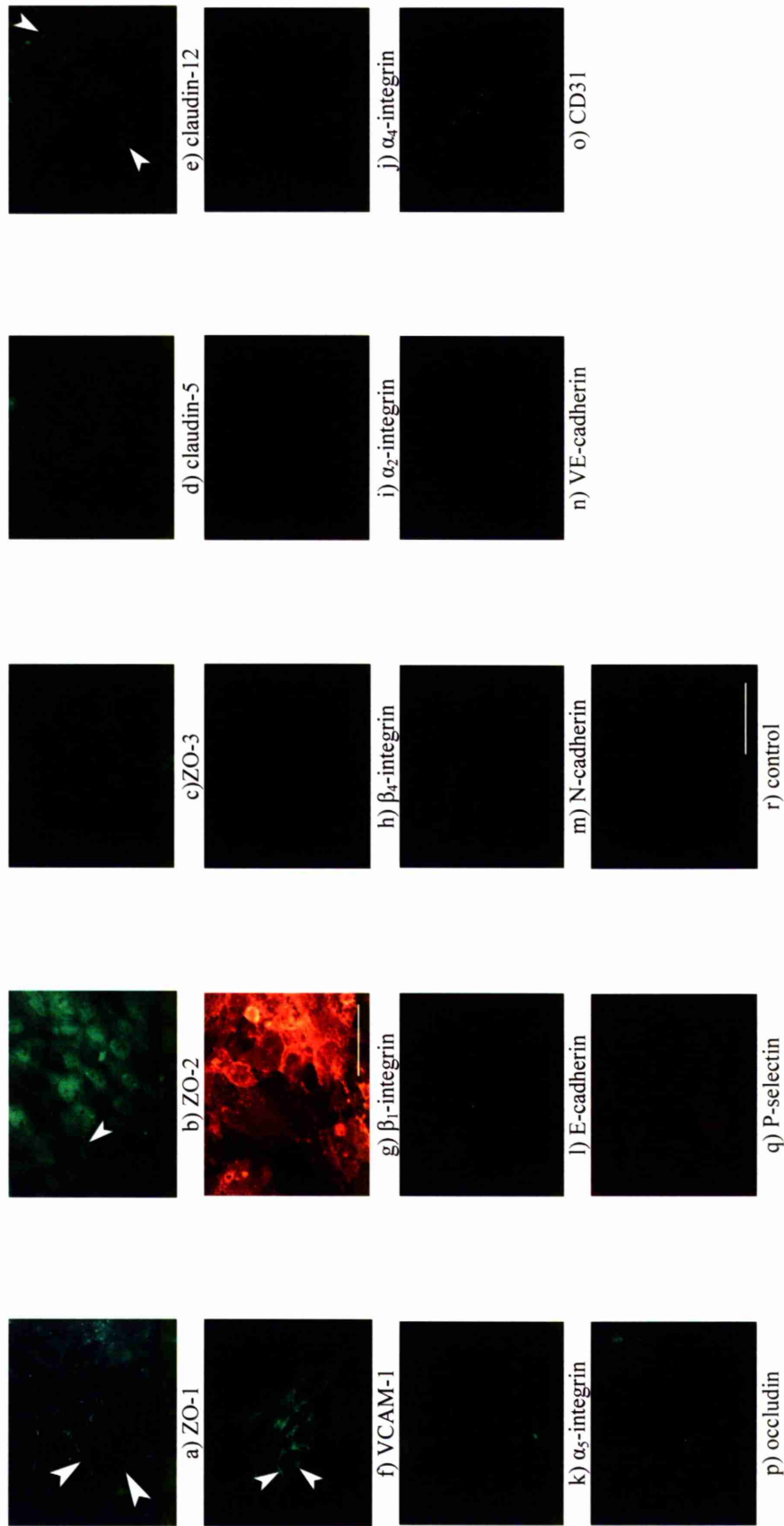


Figure 3-37: Immunophenotype of BMEC cultured in BMSCM

Methanol fixed cells on glass coverslips were stained using a 2 step method with a secondary antibody conjugated to Alexa Fluor 555 (images g and q) or FITC (all other images) and examined using an Olympus BX51 fluorescence microscope. Positive labelling was seen with a) ZO-1 (cell-cell junctions arrowed), b) ZO-2 (cell-cell junctions arrowed), c) ZO-3, e) claudin-12 (positive labelling of Golgi body arrowed), f) VCAM-1 (positive labelling of cell membrane arrowed) and g) β_1 -integrin. Scale bars represent 50 μ m.

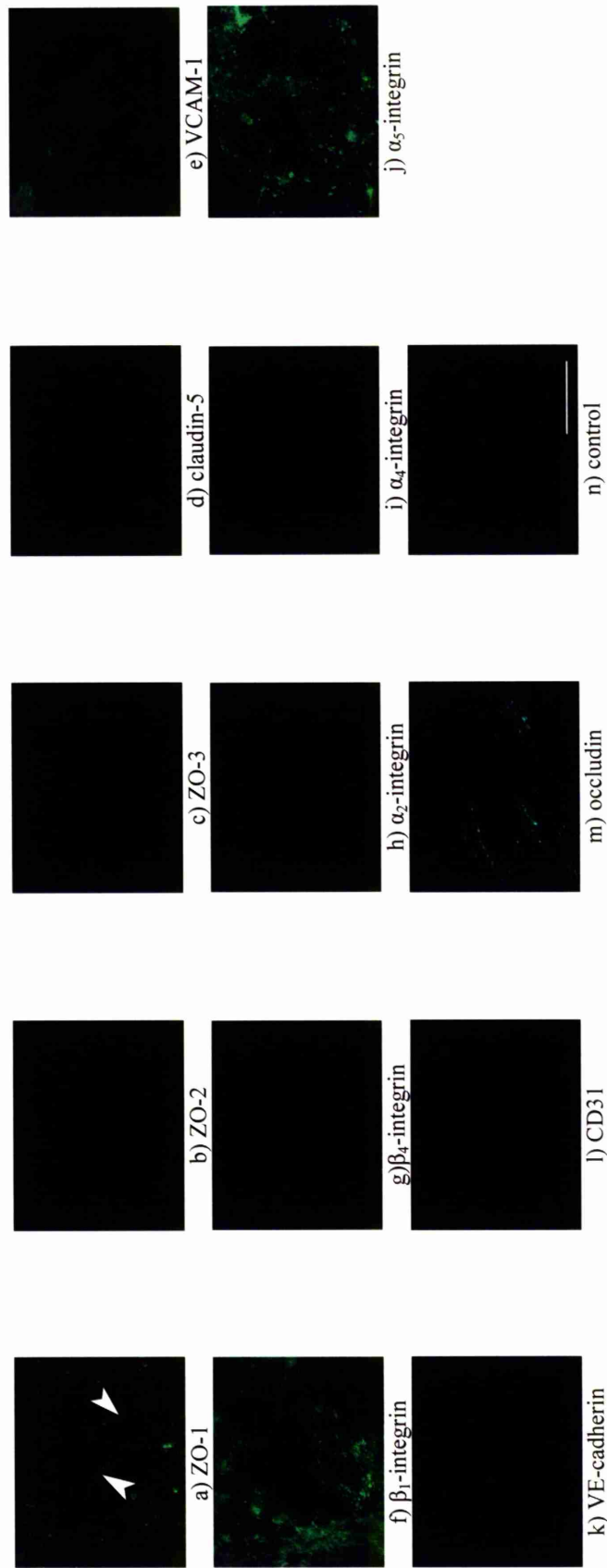


Figure 3-38: Immunophenotype of primary human bone marrow endothelial cells cultured in BMSCM
Methanol fixed cells on glass coverslips were stained using a 2 step method with a FITC conjugated secondary antibody and examined using an Olympus BX51 fluorescence microscope. Positive labelling was seen with a) ZO-1 (cell-cell junctions arrowed), e) VCAM-1, f) β_1 -integrin, j) α_5 -integrin and m) occludin. Scale bar represents 50 μ m.

Since the problems of non-specific staining and autofluorescence were so troublesome, it was decided not to continue with this aspect of the project.

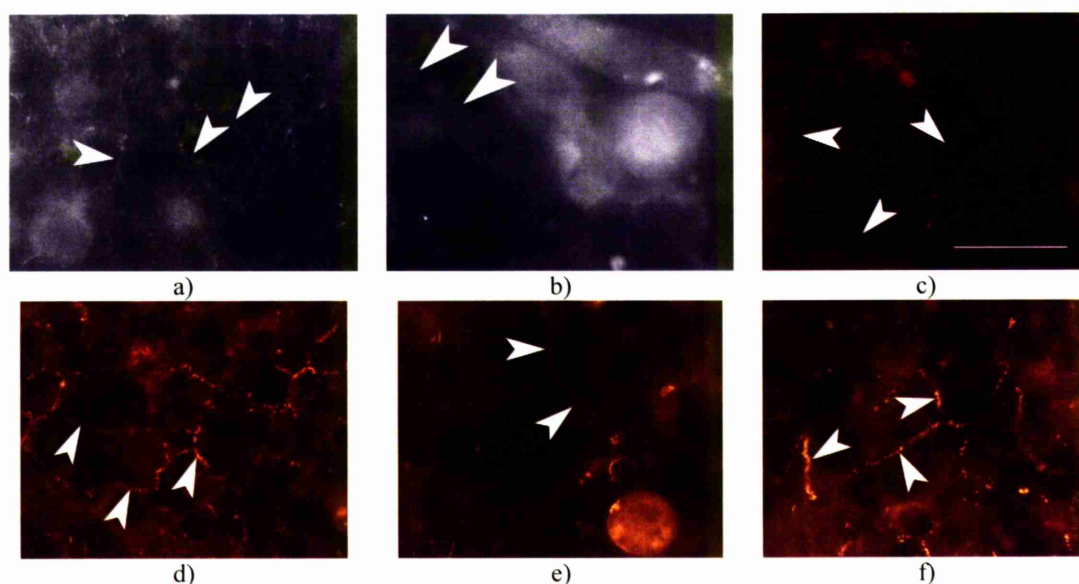


Figure 3-39: Results of labelling with antibody to ZO-1 using different techniques to reduce non-specific staining

- a) far red fluorophore with 5% BSA block
- b) far red fluorophore with 10% horse serum block
- c) mouse IgG block with Zenon labelled primary antibody
- d) milk 0.1% block
- e) Marvel 1% block
- f) 1%BSA + 1% milk + 2% fish gelatin in PBS

ZO-1 labelling of tight junctions is visible as irregular linear fluorescence at cell-cell junctions (arrowheads). Background staining in the form of ill-defined cytoplasmic fluorescence and occasional positive rounded intracytoplasmic structures is present. Scale bar represents 50µm

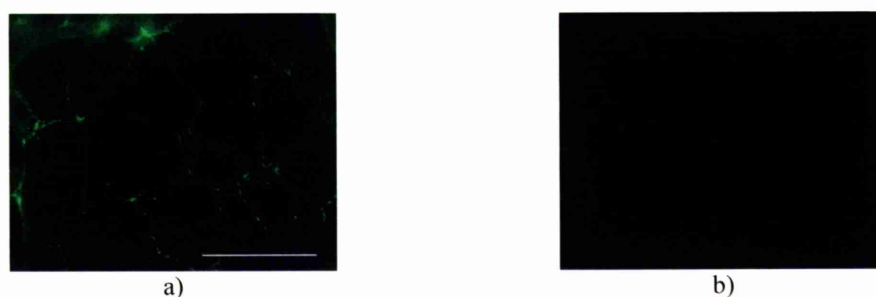


Figure 3-40: Results of immunofluorescent staining of PNT2-C2 cells

- a) ZO-1 b) E-cadherin

Cell-cell junctions are labelled by both antibodies, with minimal non-specific background fluorescence.

Scale bar represents 50µm

3.4 Co-culture studies

3.4.1 Time lapse video microscopy live invasion studies

To visualise invasion in real time, cells were observed by time lapse video microscopy. PC-3 or PC-3-GFP cells (6.25×10^5) in BMSCM were added to a confluent monolayer of BMEC in a 12.5cm^2 tissue culture flask and observed in the time lapse video microscopy unit for 24 hours. Prostate cells quickly settled on the endothelium in a rounded state before beginning to invade through the endothelial layer. Cells were observed and time to complete invasion was noted. This was judged to be when cells were seen to flatten into the endothelial layer or migrate underneath endothelial cells. The time at which cells initiated invasion could not be determined. Results are shown in Table 3-8, Figure 3-41 and Figure 3-42. The corresponding video clips can be found on the accompanying DVD in presentation 3.4.

	BLEBBING PRIOR TO INVASION	NUMBER OF CELLS OBSERVED	NUMBER OF CELLS INVADING	EARLIEST COMPLETE INVASION	LATEST COMPLETE INVASION	MEAN TIME TO COMPLETE INVASION
PC-3	7 (39%) showed prominent blebbing	19	18	35 minutes	13h 15 minutes	4h 9 minutes (249 minutes)
PC-3- GFP	8 (32%) showed prominent blebbing	25	25	50 minutes	16h 50 minutes	4h 51 minutes (291 minutes)

Table 3-8: Results of live invasion study using time lapse video microscopy

PC-3 or PC-3-GFP cells were added to a confluent monolayer of BMEC and observed in the time lapse video microscopy unit for 24 hours. Only cells which could be observed continuously from initial settling on the endothelium to complete invasion or the end of the 24h period are included. Results are from two experiments with a single field of view for each experiment.

All of the 25 PC-3-GFP cells observed completed invasion within 24 hours, as did 18 of the 19 PC-3 cells observed. Not every cell which settled on the endothelium could be followed through to either completed invasion or the end of the 24 hour period as some cells moved out of the field of view or were obscured by adjacent cells. Three PC-3-GFP cells and two PC-3 cells produced lamellipodia and actively migrated short distances over the surface of the BMEC monolayer before invading through it. Around a third of cells showed prominent blebbing prior to invasion. The mean time to complete invasion was similar (T-test $p=0.6$) for both cell lines: 249 ± 48 minutes for PC-3 and 291 ± 52 minutes for PC-3-GFP cells, shown in

Figure 3-41, although there was a wide variation between individual cells in time taken to complete invasion. Most cells could not be followed once they had spread on the substrate after invasion but occasional cells could be followed for a short distance as they migrated under the BMEC (see Figure 3-44 and video clip 33). As more cells invaded, the BMEC monolayer became increasingly disrupted and cells with large nucleoli, likely to be PC-3/PC-3-GFP cells, could be seen moving across the substrate underneath other cells. At the end of the 24 hour period the BMEC monolayer was completely disrupted and there were possible colonies of malignant cells forming (see Figure 3-46b and video clip 36).

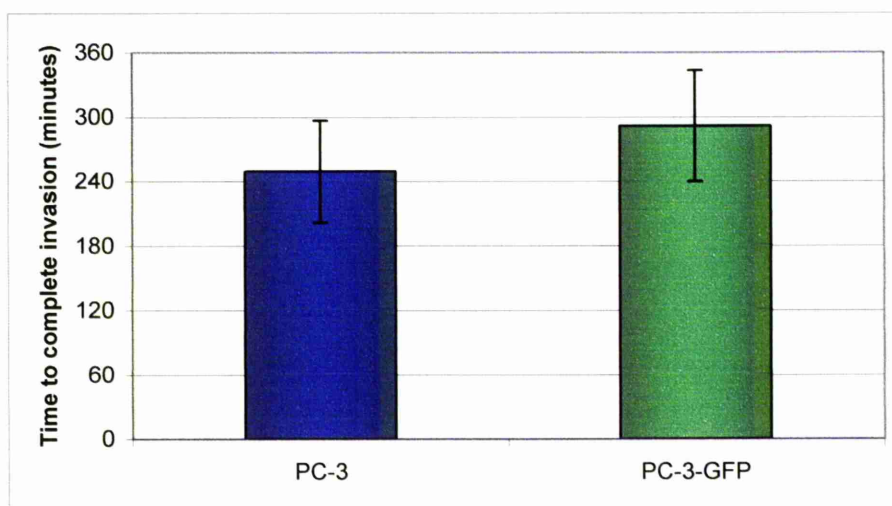


Figure 3-41: Time taken for PC-3 and PC-3-GFP cells to complete invasion across a BMEC monolayer

PC-3 or PC-3-GFP cells were seeded onto a confluent BMEC monolayer and observed in the time lapse video microscopy unit. A total of 18 PC-3 and 25 PC-3-GFP cells were observed. The mean time to complete invasion in minutes is shown. Bars show standard error.

As shown in Figure 3-42, PC-3 and PC-3-GFP cells invaded through the BMEC monolayer at a similar rate: 60% of PC-3 and PC-3-GFP cells completed invasion through the BMEC monolayer within the first 4 hours (240 minutes), and 80% had completed invasion after 8 hours (480 minutes).

Frames from the video time lapse invasion study using PC-3 cells are shown in Figure 3-43 to Figure 3-45. Figure 3-43 a) and video clip 30 show the confluent BMEC monolayer before the addition of PC-3 cells. In Figure 3-43 b) and video clip 31, PC-3 cells have been added to the monolayer and settle onto the surface.

After settling on the BMEC monolayer, cells begin to show blebbing, which could be very pronounced, and begin to invade through the monolayer. Invading cells are shown in Figure 3-44 and video clips 32 to 34.

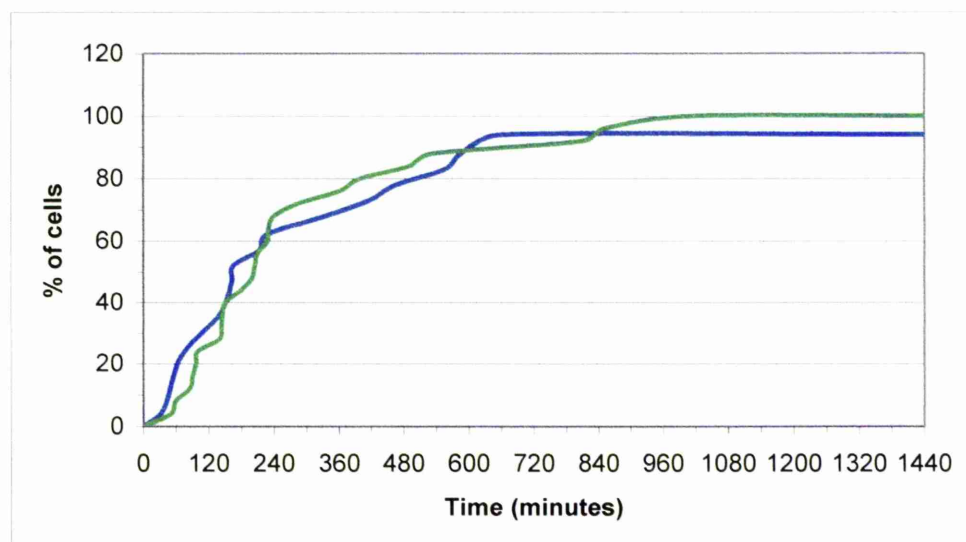


Figure 3-42: Percentage of PC-3 and PC-3-GFP cells completing invasion at different time points

PC-3 or PC-3-GFP cells were seeded onto a confluent BMEC monolayer and observed in the time lapse video microscopy unit. The cumulative percentage of cells completing invasion plotted against time is shown. Each experiment performed twice using a single field of view. A total of 18 PC-3 and 25 PC-3-GFP cells were observed. Blue: PC-3 cells. Green: PC-3-GFP cells.

In video clip 32 a PC-3 cell shows prominent blebbing and produces a lamellipodium before it flattens into the endothelial layer. However not all cells showed such prominent blebbing; the invading PC-3 cell seen in Figure 3-44 and video clip 33 does not show this. The visible portion of the cell body above the BMEC layer reduces in size as the cell invades and spreads on the substrate. The cell remains identifiable and can be seen to extend a long process and migrate across the substrate underneath BMEC. The cell seen in video clip 34 also invades through the endothelial layer in a similar way.

PC-3 cells are visible migrating across the substrate under the endothelial cells and in video clip 35 an area of the BMEC monolayer (indicated in Figure 3-45 a) can be seen to move. After 18 hours of co-culture, the BMEC monolayer is disrupted and PC-3 cells can be seen spread on the substrate (circled areas in Figure 3-45 b) and migrating underneath BMEC (see video clip 36).

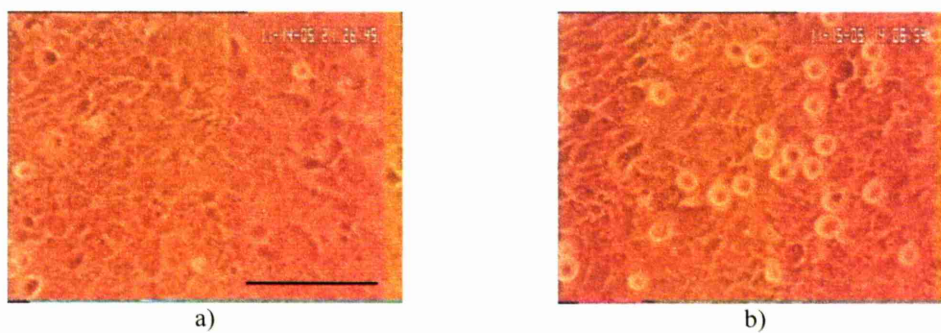


Figure 3-43: Live cell invasion study using time lapse video microscopy

a) confluent BMEC monolayer before addition of PC-3 cells. **b)** confluent BMEC monolayer with PC-3 cells present as rounded cells on top of BMEC. Image taken 20 minutes after addition of PC-3 cells. Scale bar represents 100µm.

See also video clips 30 and 31

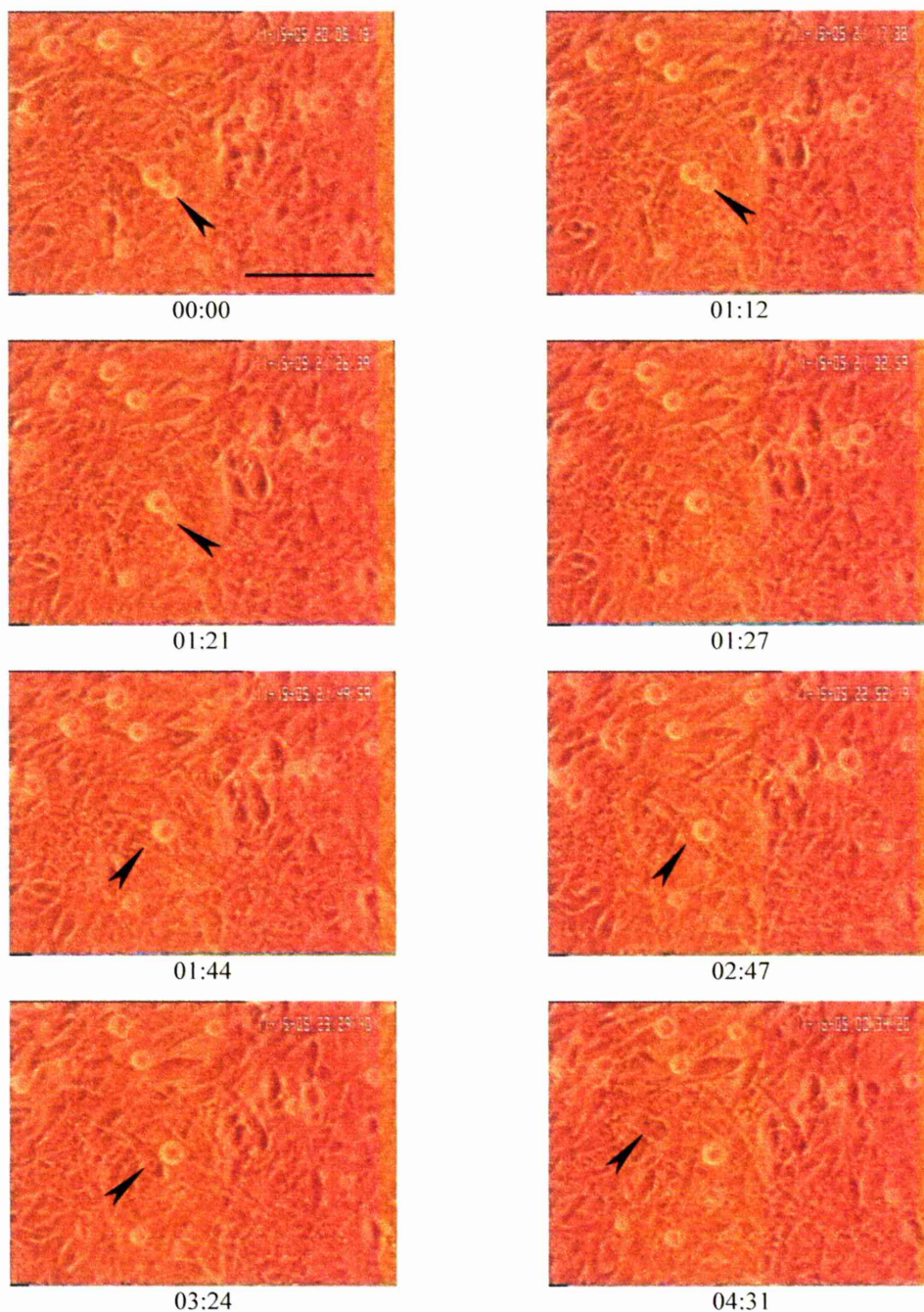


Figure 3-44: PC-3 cell invading through a BMEC monolayer

The cell (arrowhead) migrates through the endothelial monolayer. In the images from 01:44 to 04:31 the cell can be seen migrating across the substrate underneath BMEC.

Times are shown as hours and minutes after the first image at 00:00. Scale bar represents 100 μ m.

See also video clip 33

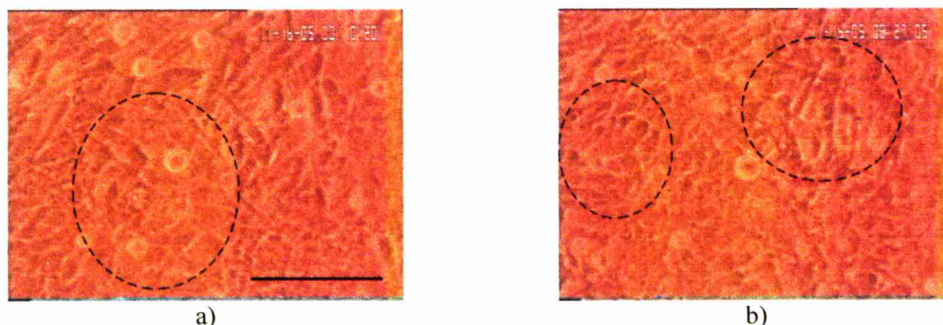


Figure 3-45: BMEC monolayer after invasion of PC-3 cells

a) shows an area (circled) where the BMEC monolayer can be seen to move as PC-3 cells migrate under BMEC. **b)** co-culture approximately 18 hours after addition of PC-3 cells: most cells have invaded through the endothelium and there are areas (circled) where small colonies of PC-3 cells appear to have formed. Scale bar represents 100 μ m.

See also video clips 35 and 36

Frames from the video time lapse invasion study using PC-3-GFP cells are shown in Figure 3-46 to Figure 3-48 and video clips 37 to 41.

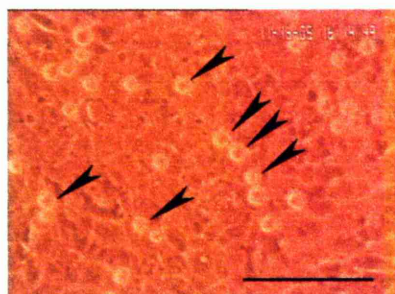


Figure 3-46: BMEC monolayer with PC-3-GFP cells

Confluent BMEC monolayer approximately 25 minutes after addition of PC-3-GFP cells which are present as rounded cells (some indicated by arrowheads) on top of the BMEC layer. Scale bar represents 100 μ m.

See also video clip 38

A PC-3-GFP cell is shown migrating across the endothelial layer in Figure 3-47 and video clip 39. The cell produces a lamellipodium and migrates a short distance over the monolayer towards a BMEC cell-cell junction.

Figure 3-48 and video clip 40 show a PC-3-GFP cell invading through the BMEC monolayer. The cell initially appears to float across the monolayer, blebbing, before making contact with a BMEC that undergoes apoptosis (white arrowhead in images 00:10 to 00:19). The PC-3-GFP cell then settles on the endothelium a short distance away and invades through the monolayer. A second BMEC in contact with the prostate cell then appears to undergo apoptosis (white arrowhead in image

01:30). Video clip 41 shows the co-culture 15 hours after addition of PC-3-GFP cells which have disrupted the BMEC monolayer.

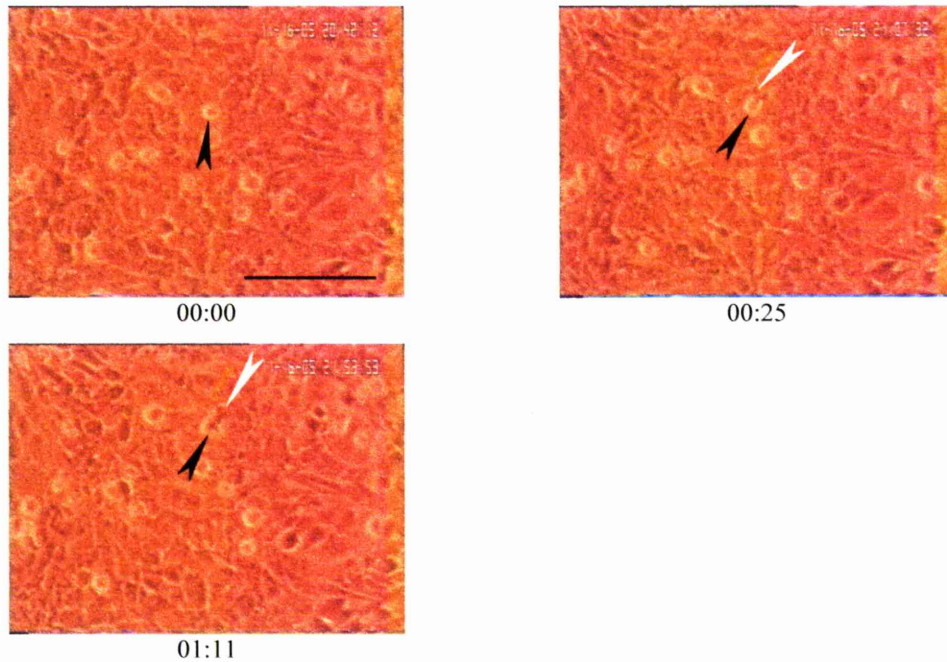


Figure 3-47: PC-3-GFP cell migrating over a BMEC monolayer

The cell (black arrowhead) produces a lamellipodium (white arrowhead) and migrates over the BMEC monolayer, including over BMEC cell-cell junctions.

Times are shown as hours and minutes after the first image at 00:00. Scale bar represents 100 μ m.

See also video clip 39

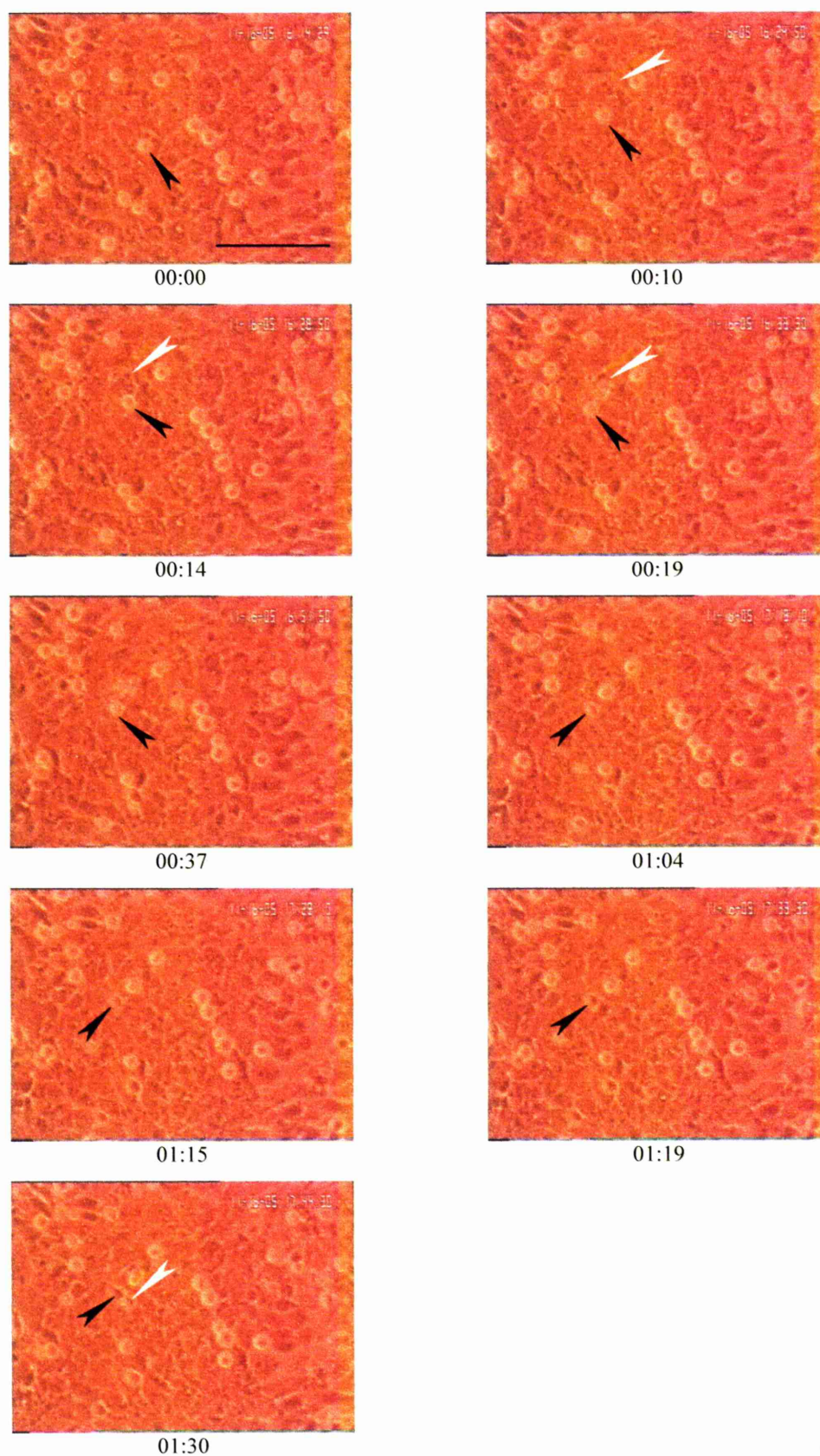


Figure 3-48: PC-3-GFP cell invading through a BMEC monolayer

The PC-3-GFP cell (black arrowhead) floats across the BMEC. A BMEC undergoes apoptosis adjacent to the PC-3-GFP cell (white arrowhead in images at 00:10 to 00:19). The PC-3-GFP cell then migrates through the monolayer and a second BMEC appears to undergo apoptosis (white arrowhead in image 01:30). Times are shown as hours and minutes after the first image at 00:00. Scale bar represents 100 μ m. *See also video clip 40*

As a comparison, the non-tumourigenic transformed benign prostate epithelial cell line PNT2-C2 was used in a co-culture study. On addition to a BMEC monolayer (shown in video clip 42) PNT2-C2 cells quickly settled on the endothelium. They did not remain rounded, like the malignant prostate cells, but spread on top of the endothelial cells. Some PNT2-C2 cells moved short distances laterally over the BMEC layer to form small groups of PNT2-C2 cells (see Figure 3-49 and video clip 43). Over the course of the experiment PNT2-C2 cells were not observed to invade and did not alter the BMEC monolayer.

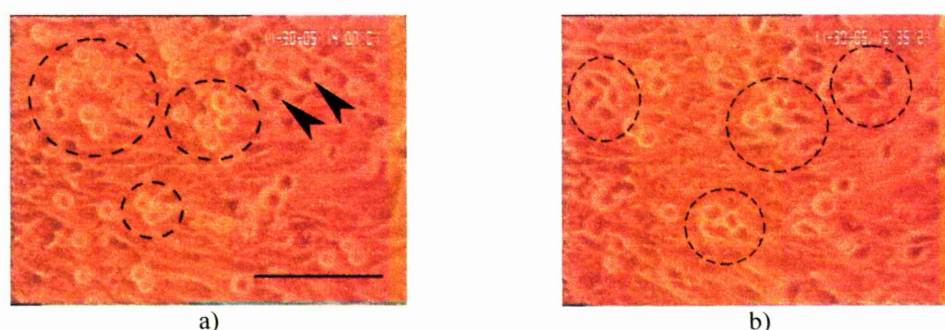


Figure 3-49: BMEC monolayer with PNT2-C2 cells

a) 22 minutes after addition of PNT2-C2 cells. Some of the PNT2-C2 cells are rounded (circled) but others (arrowheads) appear to have spread on top of the BMEC layer. **b)** 110 minutes after addition of PNT2-C2 cells, several groups of PNT2-C2 cells (circled) appear to have spread on top of the BMEC monolayer rather than invading it. Scale bar represents 100µm. See also video clip 43

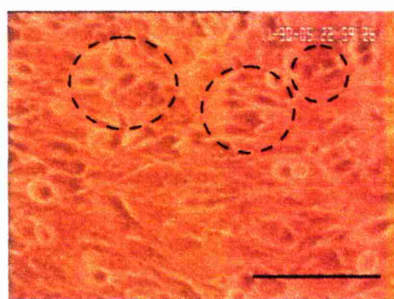


Figure 3-50: BMEC monolayer with PNT2-C2 cells

The BMEC monolayer 9 hours 14 minutes after addition of PNT2-C2 cells. Flattened PNT2-C2 cells are still present in groups (circled) on top of the endothelial monolayer. Scale bar represents 100µm.

As PC-3 cells were routinely cultured in medium based on HAMS F12 and PNT2-C2 cells were routinely cultured in medium based on RPMI 1640, a quantitative invasion assay was used to assess any effects of the medium on the invasiveness of the prostate cells. The results are shown in Figure 3-51. PNT2-C2 cells showed more invasion towards BMS than TCP, but there was no significant difference between PNT2-C2 cells cultured in RPMI or HAMS F12 (T-test $p=0.5$, Mann-Whitney U test $p=0.48$) for invasion towards BMS. PC-3 cells showed

significantly greater invasion through Matrigel towards BMS than PNT2-C2 cells cultured in HAMS F12 (T-test $p=0.0001$, Mann-Whitney U test $p=0.002$).

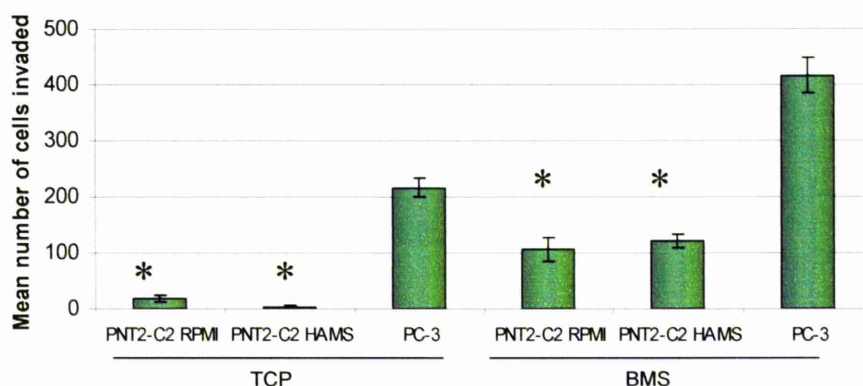


Figure 3-51: Effect of cell culture medium on invasiveness of PNT2-C2 cells through Matrigel
 1×10^5 PNT2-C2 or PC-3 cells invading towards either tissue culture plastic (TCP) or bone marrow stroma (BMS). PNT2-C2 cells were cultured in either RPMI based medium (see section 2.2.1.3.2) or HAMS F12 based medium without hygromycin B (see section 2.2.1.3.1) for a minimum of 7 days prior to invasion. PC-3 cells were cultured in HAMS F12 based medium. PNT2-C2 cells showed less invasion than PC-3 cells when cultured in either RPMI or HAMS F12. Bars show standard error (results shown as mean of 3 experiments, each experiment performed in duplicate). Asterisks indicate significance at $p < 0.05$ for both T-test and Mann-Whitney U test.

3.4.2 Confocal live invasion studies

Confocal laser scanning microscopy was used to image cells during live invasion studies. This method enabled 4 dimensional brightfield and fluorescence images to be collected allowing visualisation of cellular interactions and identification of PC-3-GFP cells by their fluorescence. Vertical (z) plane images were collected to follow cells as they invaded, and images were collected over a period of 24 hours to allow cells time to invade. Invasion studies were set up as shown in Figure 3-52. BMEC were cultured until confluent on a fibronectin coated quartz glass bottomed dish, before PC-3-GFP cells were added.

In initial experiments a brightfield image and a fluorescence image were collected at 30 minute intervals for 24 hours with 10 stage positions. Vertical (z) plane images were recorded at $3\mu\text{m}$ intervals over a distance of $30\mu\text{m}$. Results are shown in Figure 3-53 to Figure 3-55 and video clips 44 to 48.

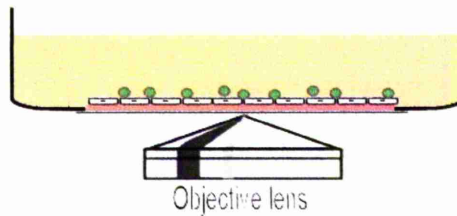


Figure 3-52: Live cell invasion study using confocal microscope

BMEC (white) were cultured on fibronectin (pink) in a quartz glass bottomed dish until confluent. 5×10^5 PC-3-GFP cells (green) were added and invasion observed using an inverted confocal microscope.

A series of images showing a PC-3-GFP cell invading through the BMEC monolayer is shown in Figure 3-53 and video clips 44 and 45. The PC-3-GFP cell is initially rounded on top of the endothelium and over time the rounded part of the cell body visible above the endothelium reduces in size, through successive images, as the cell invades through the endothelial layer. In the image at 03:30 there is a GFP signal present outside the rounded part of the cell body, indicating a cell process extending under the endothelial cells. In the image at 05:30 the cell is spreading on the substrate under the endothelium. In the images at 04:30 to 05:30 there is retraction of an endothelial cell adjacent to the invading cell. Video clip 46 shows a PC-3-GFP cell invading through a BMEC monolayer. The cell is initially present on top of the monolayer and shows membrane blebbing. A GFP signal is present to the left of the cell body which is likely to be a pseudopodium extending underneath the BMEC layer. Endothelial retraction is not seen in this sequence. Figure 3-54 and Figure 3-55 (video clips 47 and 48) show the same PC-3-GFP cell as it migrates a short distance across the BMEC monolayer in Figure 3-54 before invading through the BMEC in Figure 3-55. The cell is blebbing as it migrates slowly across the BMEC and a lamellipodium is visible in Figure 3-54 15:30.. The cell then invades the endothelium and is no longer distinguishable in the brightfield image in Figure 3-55 19:30 but is still visible using the GFP signal, indicating that it has invaded through the BMEC layer. Endothelial cell retraction is not seen in this sequence.

Figure 3-53: PC-3-GFP cell invading a BMEC monolayer

PC-3-GFP cell invading through a BMEC monolayer. Images were recorded at 30 minute intervals. The upper images are 3D projections of the brightfield and GFP images combined, including all vertical plane (z) images. The lower images are flat projections showing brightfield with or without GFP including all vertical plane (z) images. Times are shown as hours and minutes after addition of PC-3-GFP cells. Scale bar represents 50 μ m.

The PC-3-GFP cell is initially rounded on top of the BMEC monolayer, but the rounded portion of the cell body visible reduces in size between 02:00 and 05:00 hours as seen on the brightfield images. In the image at 03:30 the GFP signal shows that part of the cell body is present under the BMEC monolayer, invisible in the brightfield image but identifiable by the GFP signal which extends outside the region of the rounded part of the cell body in this image. At 05:30 no part of the cell body is visible above the BMEC monolayer in the brightfield image but the GFP signal shows that the PC-3-GFP cell is still present, now below the BMEC monolayer.

See also video clips 44 and 45

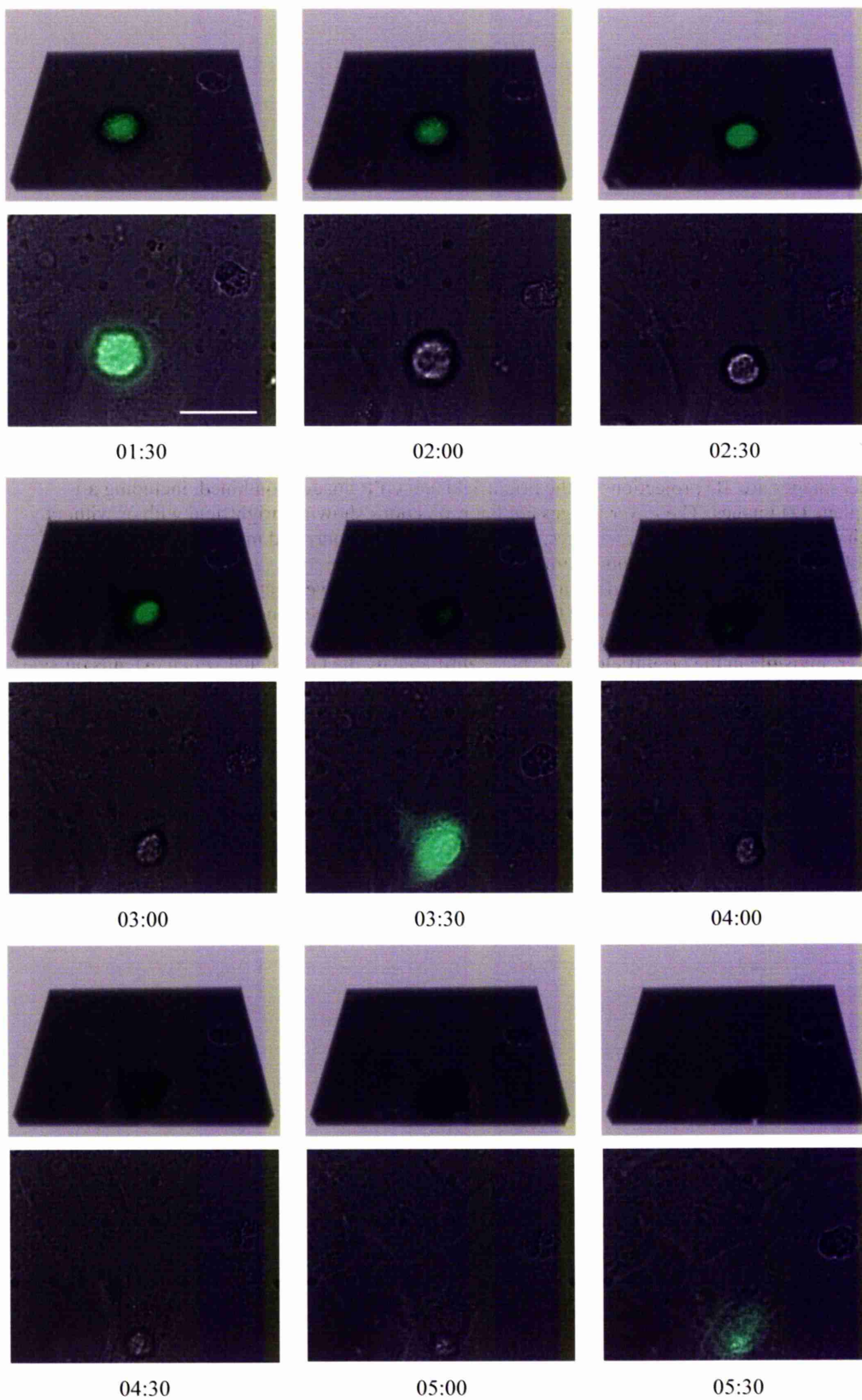
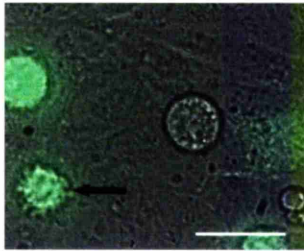


Figure 3-54: PC-3-GFP cell migrating across a BMEC monolayer

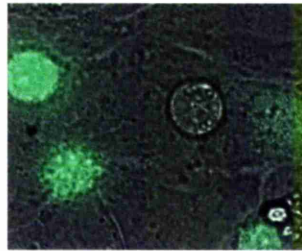
PC-3-GFP cell invading through a BMEC monolayer. Images shown are at 60 minute intervals. The upper images are 3D projections of the brightfield and GFP images combined, including all vertical plane (z) images. The lower images are flat projections showing brightfield and GFP including all vertical plane (z) images. Times are shown as hours and minutes after addition of PC-3-GFP cells. Scale bar represents 50µm.

PC-3-GFP cell (arrow) migrating over a BMEC monolayer prior to invasion. The cell shows membrane blebbing, visible as small, smooth rounded projections from the plasma membrane throughout the sequence. The cell migrates over several BMEC cell-cell junctions before migrating through the monolayer (shown in Figure 3-55).

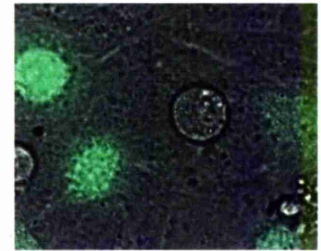
See also video clips 47 and 48



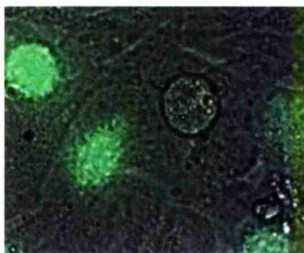
07:30



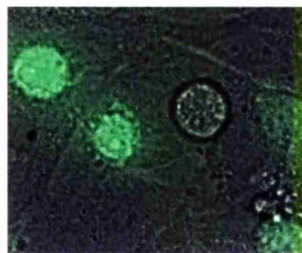
08:30



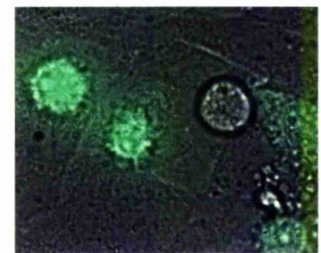
09:30



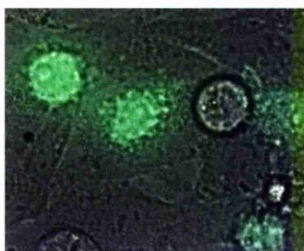
10:30



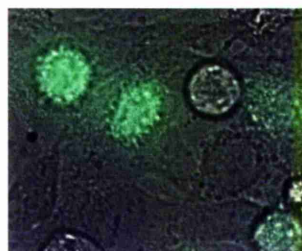
11:30



12:30



13:30



14:30

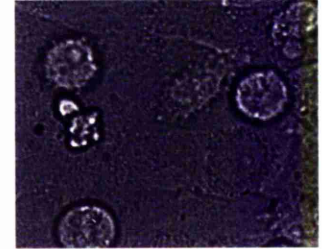
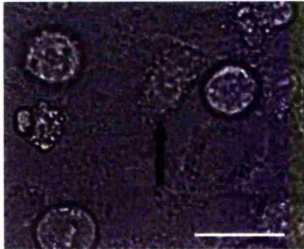


15:30

Figure 3-55: PC-3-GFP cell invading a BMEC monolayer

PC-3-GFP cell (arrow) invading through a BMEC monolayer. This is the same cell shown in Figure 3-54 but this sequence of images begins 90 minutes after the last image in Figure 3-54. The cell is visible on the surface of the monolayer in the brightfield image until 18:30, after which it becomes less distinct as it migrates through the endothelial layer. The GFP image shows it is still present within the field of view but has flattened onto the substrate. Images were recorded at 30 minute intervals. The upper images are 3D projections of the brightfield and GFP images combined, including all vertical plane (z) images. The lower images are flat projections showing brightfield without GFP including all vertical plane (z) images. Times are shown as hours and minutes after addition of PC-3-GFP cells. Scale bar represents 50 μ m.

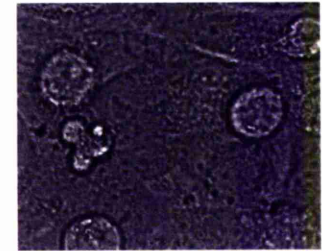
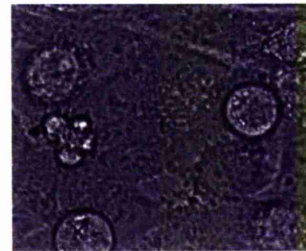
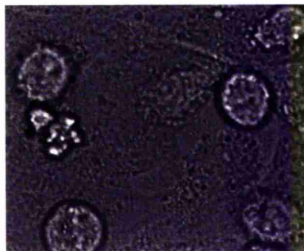
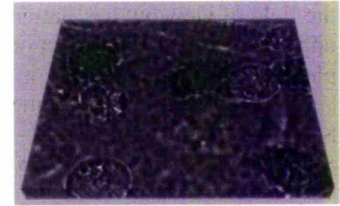
See also video clips 47 and 48



17:00

17:30

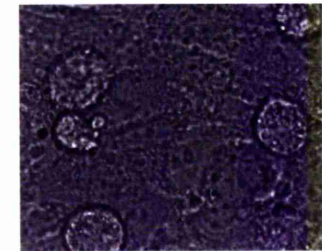
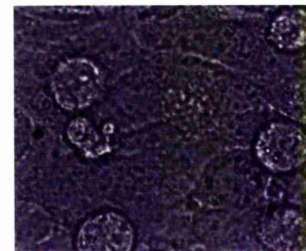
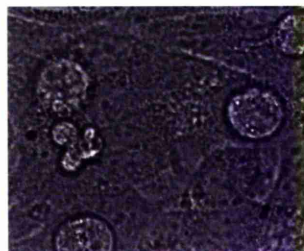
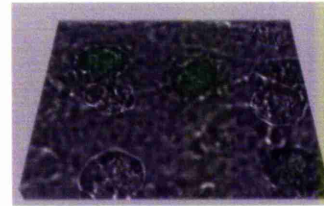
18:00



18:30

19:00

19:30



20:00

20:30

21:00

3.4.2.1 Confocal invasion studies using 24 well plate insert and Transwell chambers

As cellular morphology offered clues as to which mode of motility the invading cells were using, we wanted to visualise the migration of prostate cells through Matrigel and combined Matrigel/BMEC barriers which more closely mimicked the process of migration through the vessel wall. A convenient way of constructing these barriers was to use Transwell chambers. This enabled data from invasion assays to be linked to morphological information gained by visualisation and allowed the identification of definite invasion by the passage of the cells through the pores in the chamber membrane.

3.4.2.1.1 Development of the plate insert

Initial experiments used standard plastic 24-well plates with Transwell chambers but the results were very poor due to the optical quality of the plastic and the effects of heating and cooling of the plastic shifting the field of view over time. 24-well plates with thin borosilicate glass bottoms, which have superior optical quality, are available but they are not the same height as the plastic plates, unfortunately the Transwell chambers are too tall to fit into them, as shown in Figure 3-56. This would prevent free migration of cells through and across the underside of the Transwell membrane and could exclude cell culture medium from under the Transwell. Since there was no ready-made solution to this problem a way of using the Transwells in the glass-bottomed plates had to be devised.

The first method tried was to build up plastic cable ties to the right height by sticking them together with glue. Once dried, these could be rinsed in 100% ethanol to clean them and then stuck onto the 24-well plate with adhesive tape, along the edges of the experimental wells, so that the Transwells could be suspended from the cable ties, as shown in Figure 3-57 image a). The lid of the plate could then be placed on top and sealed with adhesive tape. Although the images obtained using this technique were better, there was still some shift of the field of view due to the Transwells moving within the wells, and the experiment was difficult to set up.

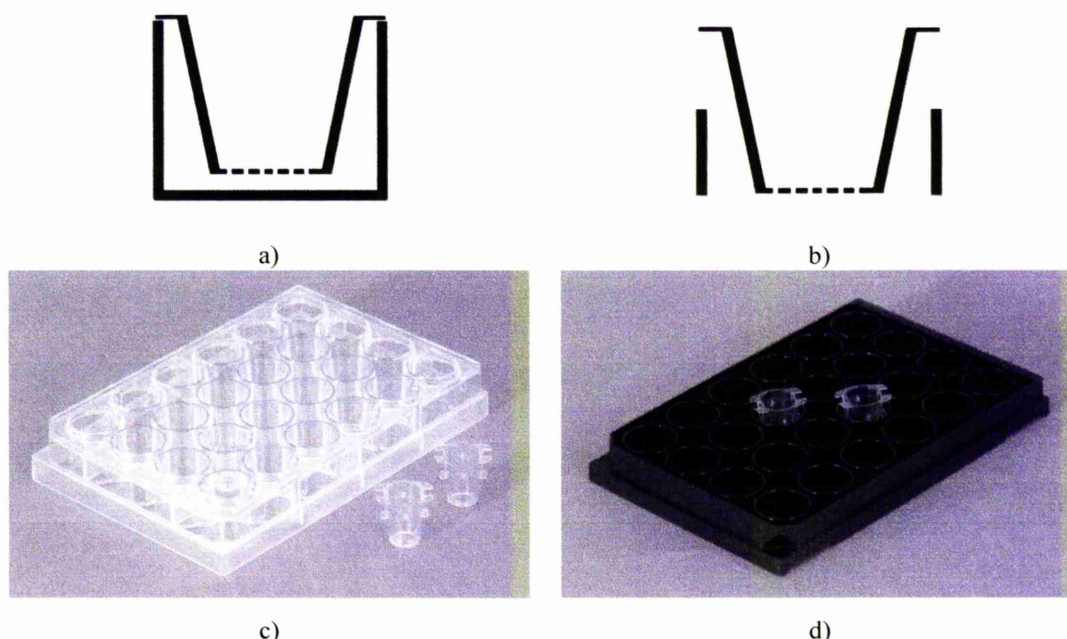


Figure 3-56: Transwell chambers with plastic and glass bottomed 24 well plates

Transwell chambers and 24 well plates are shown diagrammatically in image **a)** of a chamber in a plastic plate and image **b)** of a chamber in a glass bottomed plate. Image **c)** shows Transwells and a plastic plate and image **d)** shows them in a glass bottomed plate.

We then asked the Christie Hospital workshop to make an insert for the glass-bottomed 24-well plate using measurements taken from the plate, Transwells and cable ties. This proved more successful in reducing Transwell movement and was easier to set up. The Perspex used for the insert meant that it could be cleaned in ethanol and re-used. This system is shown in Figure 3-57 image **b)**. In order to visualise invasion with this system, an objective lens with a long working distance was needed and a x20 objective was the highest magnification that was available on our microscope.

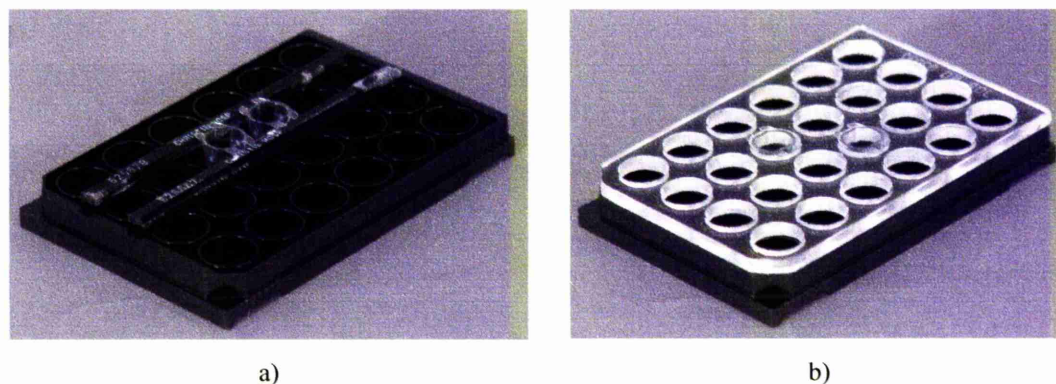


Figure 3-57: Methods of holding Transwells in a glass bottomed 24 well plate

Image **a)** shows Transwells held in place by cable ties and image **b)** shows the custom made insert holding Transwells in the 24 well plate.

3.4.2.1.2 Invasion studies using the plate insert

These invasion studies were initially set up using 1×10^5 PC-3-GFP cells per Transwell chamber, as used in the invasion assay for quantitative analysis, but this was too many to allow individual cells to be identified and followed over time. A range of lower numbers of cells was tried and 2×10^4 was found to be the optimum number. During initial studies using a layer of Matrigel with BMEC as a barrier, the total vertical height of the invasion barrier was around $70 \mu\text{m}$. Even using the glass bottomed plate and custom made insert there could still be a vertical shift in the apparent height of the Transwell membrane above the microscope objective by $5\text{--}10 \mu\text{m}$ during the experiment. In order to allow for these factors images were acquired over a minimum vertical distance of $100 \mu\text{m}$, with a step size of $4\text{--}10 \mu\text{m}$. This meant that cells were exposed to high levels of light during the experiment and therefore BMSCM was used as the culture medium (unlike the serum-free medium used for quantitative invasion assays) to keep cells in good condition. Experiments were set up as shown in Figure 3-58.

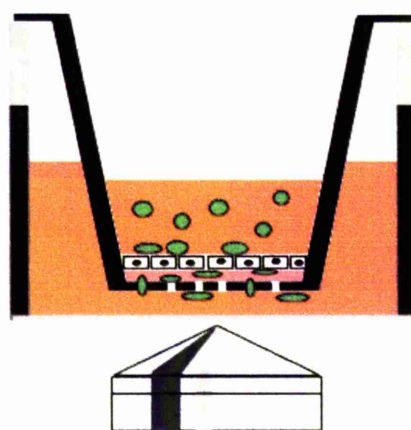


Figure 3-58: Confocal invasion study using Transwell chamber and glass bottomed 24 well plate
The Transwell chamber is suspended from the plate insert (shown in grey) which raises the height of the well. PC-3-GFP cells (green) are able to migrate from the Transwell chamber, through a barrier composed of BMEC (white) and/or basement membrane (pink) and through pores onto the underside of the Transwell chamber membrane. Invasion is observed with an inverted microscope through the glass bottom of the well.

A series of images from an invasion study are shown in Figure 3-59. Only a single $10 \mu\text{m}$ slice (z-plane) is shown as the detail in each slice is obscured when the full 3D volume is used.

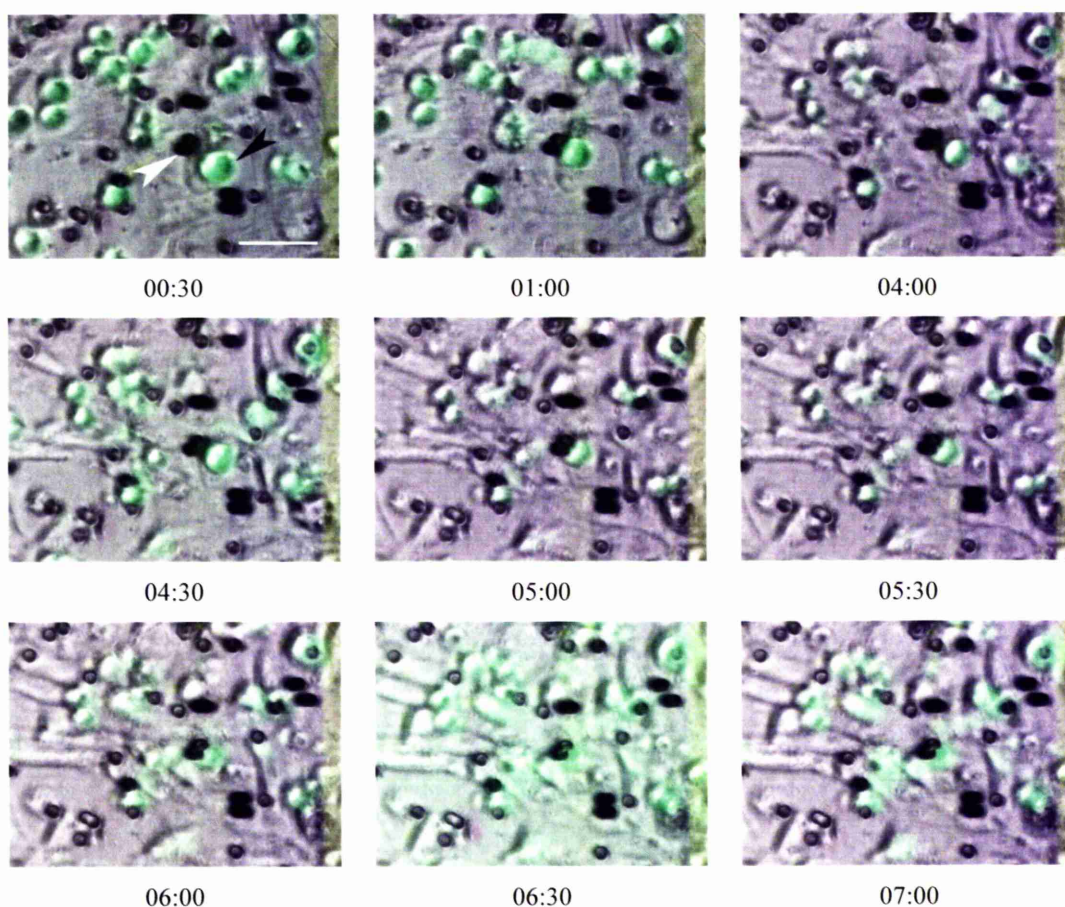


Figure 3-59: PC-3-GFP cell invading through Matrigel and Transwell membrane pore
 PC-3-GFP cell (black arrowhead) invading through a layer of Matrigel (with subconfluent BMEC seen as elongated non-GFP cells) and a Transwell membrane pore (white arrowhead). The images are flat projections of a single 10 μ m vertical (z) slice at the level of the Transwell chamber membrane. Times are shown as hours and minutes after addition of PC-3-GFP cells. Scale bar represents 50 μ m. *See video clip 49.*

In these images a PC-3-GFP cell can be seen migrating towards and then through a pore in the Transwell membrane, which is covered by a layer of Matrigel and a subconfluent layer of BMEC. The PC-3-GFP cell has a rounded morphology during this process.

3.4.3 SEM invasion studies

In an initial study BMEC were cultured until confluent on fibronectin coated Thermanox pieces in separate wells of a 6 well plate. PC-3 cells in BMSCM were added and cultures fixed after 3 hours and 5 hours. Monocultures of BMEC were also fixed and all specimens were prepared for SEM by critical point drying and platinum-palladium coating. Although cultures appeared confluent on light microscopy before fixation, there appeared to be gaps between cells visible on SEM as seen previously in Figure 3-32. On examination of the BMEC monocultures and comparison with co-cultures with PC-3 it was noted that PC-3 cells could not always be distinguished from rounded and blebbing BMEC and that this was a source of potential artefacts, as were the gaps between cells which could be mistaken for endothelial retraction during invasion. Typical appearances of morphologically similar cells from BMEC mono and co-culture specimens are shown in Figure 3-60. Images a) to d) both show rounded cells with membrane blebs but in images a) and c) these cells are BMEC in monoculture. Images b) and d) shows co-cultures and the rounded cells could be BMEC or PC-3 cells. Images e) and f) show rounded cells with fine microvillous projections; in image e) the cell is a BMEC in monoculture but in image f) it could be either a BMEC or a PC-3 cell.

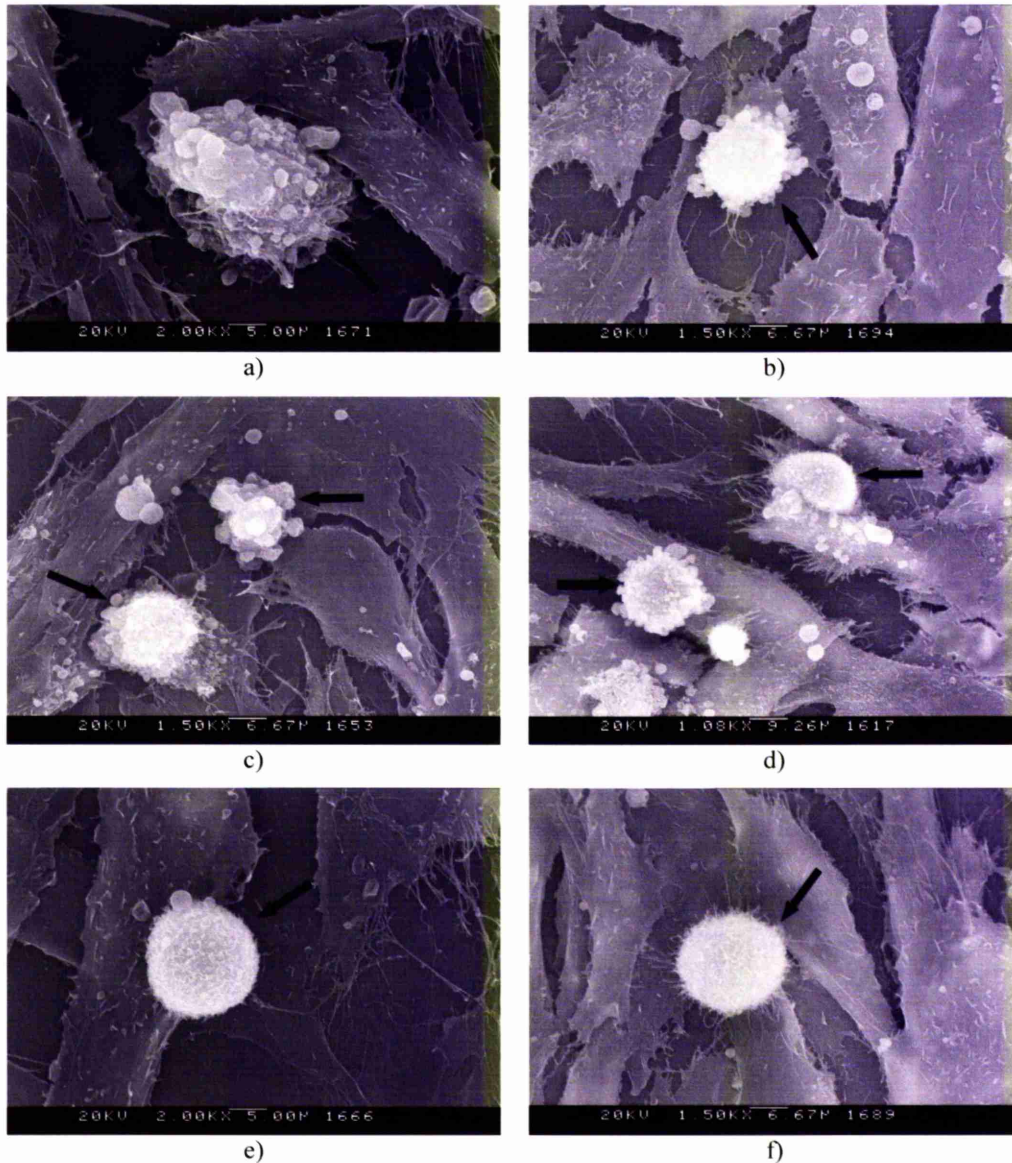


Figure 3-60: SEM images of BMEC monocultures and BMEC + PC-3 co-cultures showing potential artefacts

In all images blebbing and/or rounded cells (arrows) are present which cannot be readily distinguished morphologically. In images a), c) and e) no PC-3 cells had been added to the culture but the morphology of some of the BMEC makes them difficult to distinguish from the cells seen in images b), d) and f). These images are from co-cultures and these cells could be either BMEC or PC-3.

a), c) and e) isolated BMEC (a) x2000, c) x1500, e) x2000)

b), d) and f) BMEC monolayer with PC-3 cells added either 3 hours (b and f) or 5 hours (d) before fixation (b) x1500, d) x1000, f) x1500)

Due to the difficulty of distinguishing BMEC and PC-3 cells, immunogold labelling was used to identify cells. Several antibodies were tried and α_5 -integrin was found to label BMEC only and be compatible with the paraformaldehyde fixation without permeabilisation needed to prepare the specimens for SEM. Cells were identified by looking for the presence of gold particles on the plasma membrane at a

magnification of 80,000x. The presence of one or fewer gold particles in a single field was taken to indicate a PC-3 cell, three or more gold particles in a single field indicated a BMEC. At least five separate fields on each cell surface were examined. These results also enabled more confident identification of cells based on morphology in unlabelled specimens. The typical morphological features of the cells are shown in Table 3-9. Morphological identification was useful because gold particles cannot be identified in platinum/palladium coated samples. Samples need to be coated with chromium and examined at 30kV for optimum identification of gold, but this led to problems with specimen charging. The immunolabelling procedure also increased the risk of air-drying artefacts in the specimen. Both of these problems meant that the secondary electron images from these specimens tended to be of poorer quality than those from platinum/palladium coated specimens.

Table 3-9: Morphological characteristics of PC-3 cells and BMEC on SEM

<i>PC-3 cells</i>	<i>BMEC</i>
Specimens fixed at up to 8 hours Rounded morphology Rounded surface blebs Blebs have smooth surface Blebs all similar sizes on the same cell Presence of pseudopodia Long, complex, thick microvilli on cell surface	At all time points Flattened polygonal or flattened elongated morphology Cell surface smooth or with sparse, short, fine microvilli Cell-cell junctions visible with arching arrangement of cell processes onto adjacent cell Occasional cells with irregularly shaped and variably sized blebs
Specimens fixed at 16 hours or more Spindle shaped or rounded cells Lamellipodium with ruffled leading edge Long, complex, thick microvilli on cell body	

Figure 3-61 shows images taken from specimens labelled with 10nm gold particles. In images a) to e) the specimen was fixed 8 hours after addition of PC-3 cells to the BMEC monolayer. A rounded, blebbing cell which does not label with α_5 -integrin is present on top of the BMEC monolayer. This is a PC-3 cell. In a similar specimen fixed 16 hours after addition of PC-3 cells, shown in images f) to j), the unlabelled PC-3 cell has adopted an elongated, fibroblastic morphology. Gold particles can be seen in the backscatter images of the plasma membranes as small bright spots.

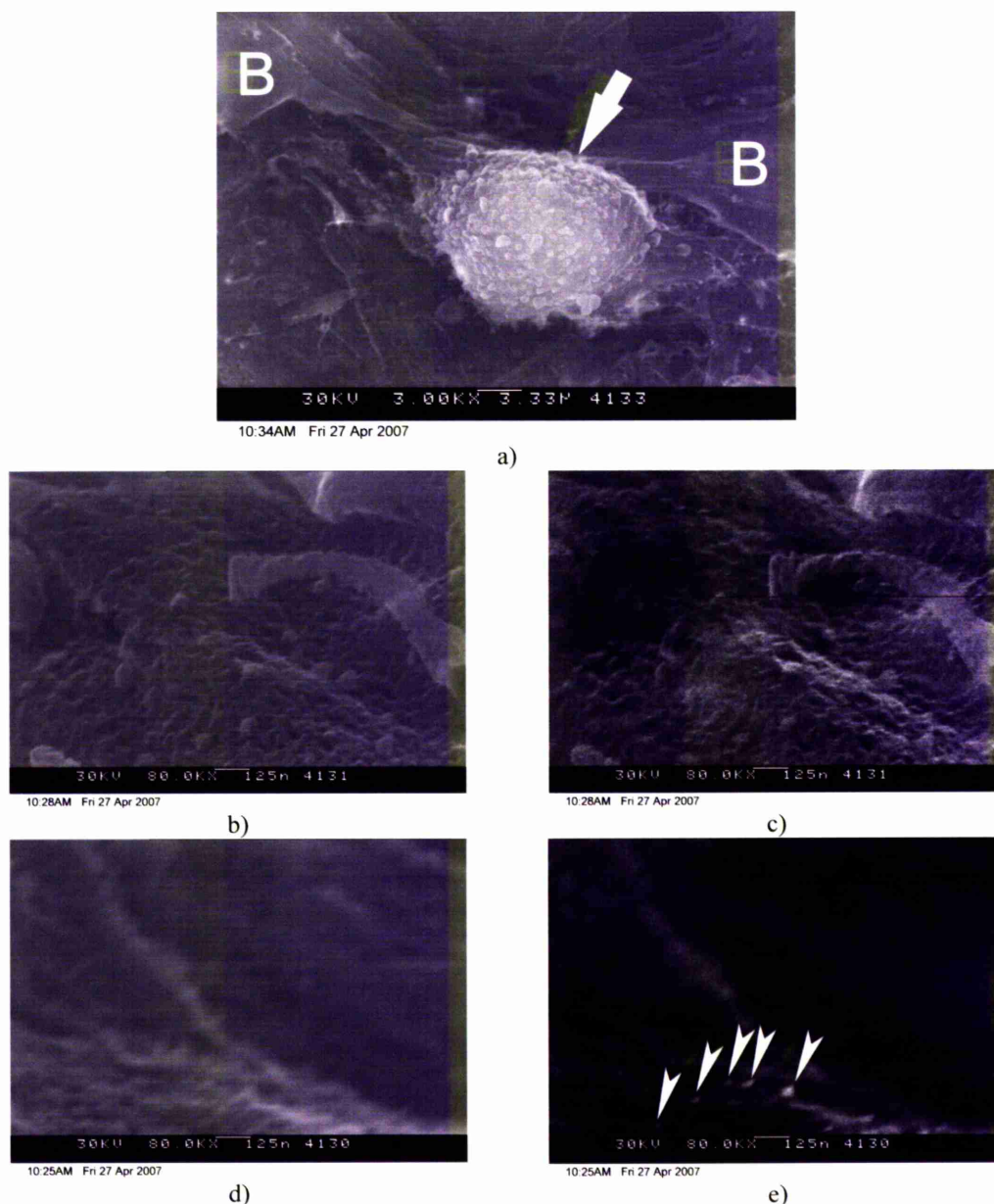
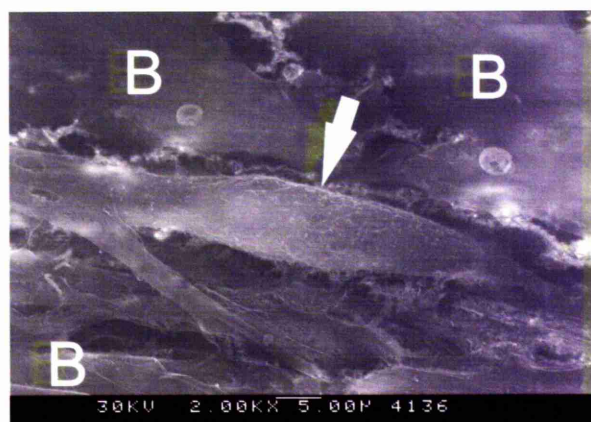


Figure 3-61: SEM images of 10nm gold labelled BMEC/PC-3 cell co-culture specimens
a) to e) co-culture fixed at 8 hours
f) to j) co-culture fixed at 16 hours
a) rounded, blebbing cell (arrow) on a layer of flattened cells (B)
b) secondary electron and **c)** backscatter images of the surface of the rounded blebbing cell in **a)** showing no gold labelling **d)** secondary electron and **e)** backscatter images of the surface of a flattened cell in **a)** showing the presence of gold particles, visible as bright spots (arrowheads)
f) elongated fibroblastic cell (arrow) among flattened cells (B)
g) secondary electron and **h)** backscatter images of the surface of the fibroblastic cell seen in **f)** showing no gold labelling **i)** secondary electron and **j)** backscatter images of the surface of a flattened cell seen in **f)** showing gold labelling (arrowheads)
a) x3000 **f)** x2000 **b) to e)** and **g) to j)** x80,000

f) to j) see next page



10:46AM Fri 27 Apr 2007

f)



10:44AM Fri 27 Apr 2007

g)



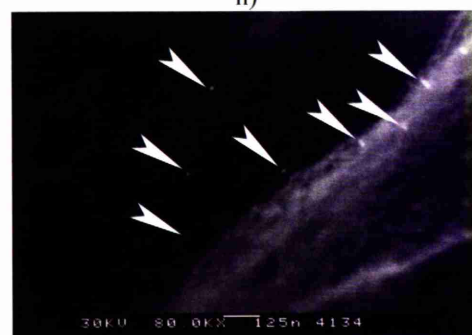
10:44AM Fri 27 Apr 2007

h)



10:41AM Fri 27 Apr 2007

i)



10:41AM Fri 27 Apr 2007

j)

SEM images of 10nm gold labelled BMEC/PC-3 cell co-culture specimens

a) to e) co-culture fixed at 8 hours

f) to j) co-culture fixed at 16 hours

a) rounded, blebbing cell (arrow) on a layer of flattened cells (B)

b) secondary electron and **c)** backscatter images of the surface of the rounded blebbing cell in a)

showing no gold labelling **d)** secondary electron and **e)** backscatter images of the surface of a flattened cell in a) showing the presence of gold particles, visible as bright spots (arrowheads)

f) elongated fibroblastic cell (arrow) among flattened cells (B)

g) secondary electron and **h)** backscatter images of the surface of the fibroblastic cell seen in f)

showing no gold labelling **i)** secondary electron and **j)** backscatter images of the surface of a flattened cell seen in f) showing gold labelling (arrowheads)

a) x3000 **f)** x2000 **b) to e)** and **g) to j)** x80,000

a) to e) see previous page

In the unlabelled co-culture specimens, cells could be identified which seemed very likely to be invading PC-3 cells. These cells were identified based on their morphology and behaviour. Figure 3-62 shows a cell extending a pseudopodium from under adjacent flattened BMEC. BMEC had not been observed underlapping each other on light microscopy, time lapse, or SEM of isolated cultures. PC-3 cells had been seen to migrate underneath BMEC on time lapse video microscopy, and underlap them on confocal imaging of invasion studies; therefore the underlapping cell seen in Figure 3-62 shows an invading PC-3 cell (short arrow). There is also a rounded and blebbing cell present which may also be a PC-3 cell (long arrow).

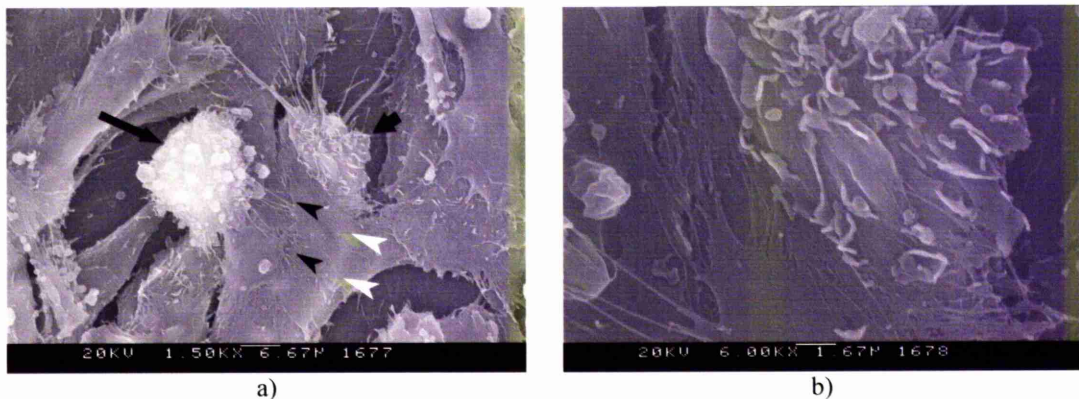


Figure 3-62: SEM images of a PC-3 cell invading a BMEC monolayer

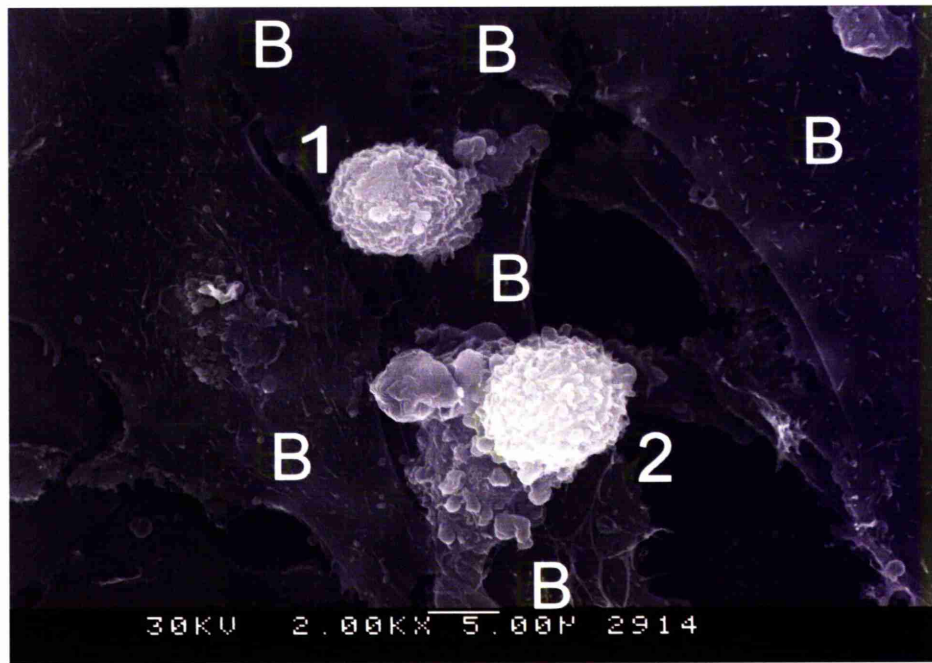
SEM images of a BMEC monolayer 5 hours after addition of PC-3 cells.

a) a rounded and blebbing cell (long arrow), and part of a pseudopodium (short arrow) which appears to be extending from underneath flattened BMEC in the area of a BMEC cell-cell junction (arrowheads). The edges of the underlapping cell can be seen as an area where BMEC appear lifted (white arrowheads).

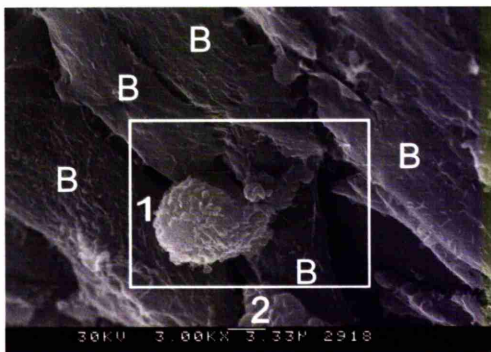
b) a higher magnification view of the pseudopodium which does not appear to be part of either of the flattened cells. These cells are likely to be invading PC-3 cells.

a) x1500

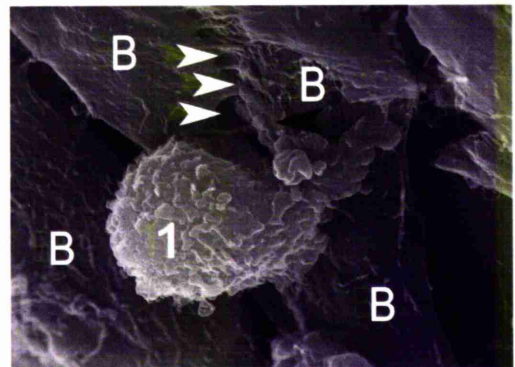
b) x6000



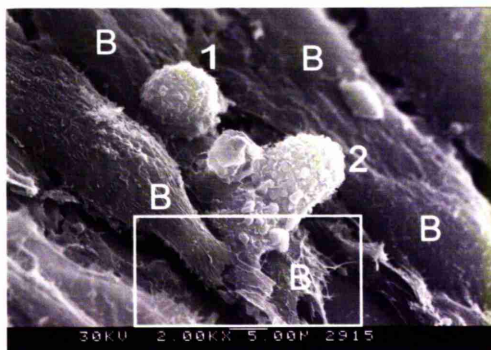
a)



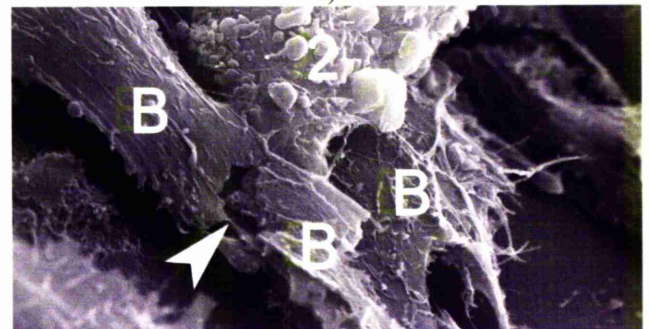
b)



c)



d)



e)

Figure 3-63: Tilted SEM images of PC-3 cells invading a BMEC monolayer

SEM images of a BMEC monolayer 5 hours after addition of PC-3 cells. BMEC are labelled B and PC-3 cells are labelled 1 and 2.

a) flat view of the specimen from above showing both PC-3 cells

b) the same specimen tilted to around 60° showing an improved view of the PC-3 cell pseudopodium

c) the area indicated by the box in image b). The PC-3 cell pseudopodium (black arrowhead) can be seen extending into the BMEC cell-cell junction (white arrowheads)

d) the specimen tilted to around 60° in the opposite direction showing the second PC-3 cell

e) the area indicated by the box in image d). The PC-3 cell (labelled 2) pseudopodium can be seen extending underneath a BMEC. The white arrowhead indicates an artefactual crack in the BMEC process, probably caused by drying. a) x2000 b) x3000 d) x2000

The use of a tilting sample holder in the SEM allows specimens to be viewed from different angles, giving views which cannot be seen when the sample is viewed from above. The sample holder allows tilting of the specimen to around 60° in two opposite directions. A series of images produced using this sample holder can be seen in Figure 3-63. Image a) shows a flat view of the specimen with two rounded and blebbing PC-3 cells on a layer of flattened BMEC. Both the PC-3 cells can be seen extending pseudopodia across the surface of the BMEC. The tilted views shown in images b) to e) show that much more information can be obtained by examining the specimen using this technique. In the tilted views shown in images b) and c), the first PC-3 cell can be seen extending a pseudopodium into a BMEC cell-cell junction. Images d) and e) show the second PC-3 cell extending a pseudopodium under a BMEC process.

3.5 Inhibitor studies

The changing morphology of the prostate carcinoma cells during endothelial transmigration and subsequent migration across the substrate suggested that they were using both mesenchymal and amoeboid motility. In order to study this, four inhibitors were used to block different aspects of cell motility. Inhibitors that were chosen had been previously used with malignant cells by other investigators and had been shown to inhibit cell motility or enzyme action at concentrations that were not toxic to the cells (see section 3.5.2). These inhibitors are described in Table 3-10 on page 145.

3.5.1 Invasion through basement membrane

Initial experiments with motility inhibitors were carried out using Transwell chambers to assess invasion through Matrigel as these assays were relatively simple and multiple assays could be set up at the same time. This allowed assessment of whether there was any inhibitory effect on invasion and facilitated the assessment of appropriate concentrations of inhibitor for use in further experiments. Invasion through basement membrane was assessed using the invasion chamber method using a layer of Matrigel in the bottom of the chamber (section 2.2.3). Inhibitors were added to the PC-3 or PC-3-GFP cell suspension and mixed thoroughly before addition to the upper chamber. After 18 hours of invasion the chambers were fixed and stained with crystal violet. Cells in the centre of the insert were counted. As this

was the simplest quantitative invasion assay a range of inhibitor doses were initially used to assess the effects of different doses on the prostate cells.

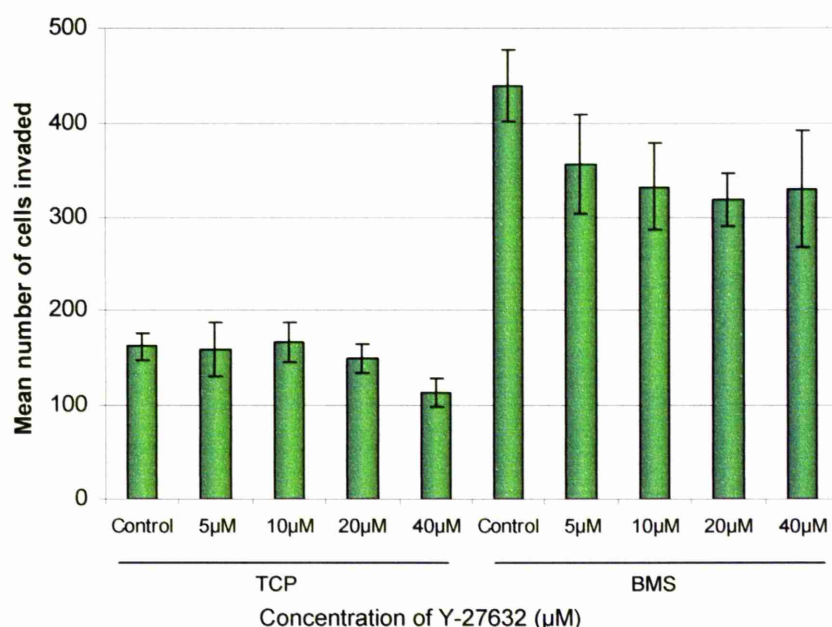


Figure 3-64: Effect of the ROCK inhibitor Y-27632 on PC-3-GFP invasion through Matrigel
 1×10^5 PC-3-GFP cells invading towards either tissue culture plastic (TCP) or bone marrow stroma (BMS) in the presence of Y-27632. PC-3-GFP cells were seeded onto Matrigel coated Transwell chambers. Bars show standard error (results shown as mean of 3 experiments, each experiment performed in duplicate). Asterisks indicate significance at $p < 0.05$ for both T-test and Mann-Whitney U test. No results were significant on both tests.

Figure 3-64 shows the effects of Y-27632 on invasion of PC-3-GFP cells through Matrigel. There appeared to be some reduction in invasion with increasing concentrations of Y-27632. This was significant on T-test for invasion towards BMS at 20µM Y-27632 ($p=0.04$) and towards TCP at 40µM Y-27632 ($p=0.05$), but no results were significant on Mann-Whitney U test.

Figure 3-65 shows the effects of blebbistatin on invasion of PC-3-GFP cells through Matrigel. There appeared to be some reduction in invasion with increasing concentrations of blebbistatin, with the largest inhibition of invasion seen with 75µM blebbistatin towards BMS which approached statistical significance ($p=0.07$) on T-test but no results were significant on Mann-Whitney U test.

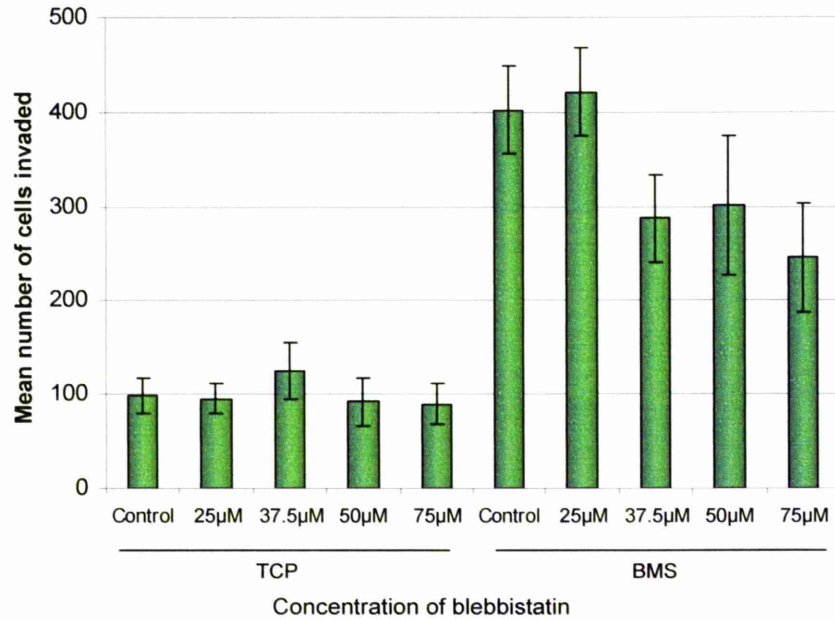


Figure 3-65: Effect of blebbistatin on PC-3-GFP invasion through Matrigel

1×10^5 PC-3-GFP cells invading towards either tissue culture plastic (TCP) or bone marrow stroma (BMS) in the presence of blebbistatin. PC-3-GFP cells were seeded onto Matrigel coated Transwell chambers. Bars show standard error (results shown as mean of 3 experiments, each experiment performed in duplicate). Asterisks indicate significance at $p < 0.05$ for both T-test and Mann-Whitney U test. No results were significant on both tests.

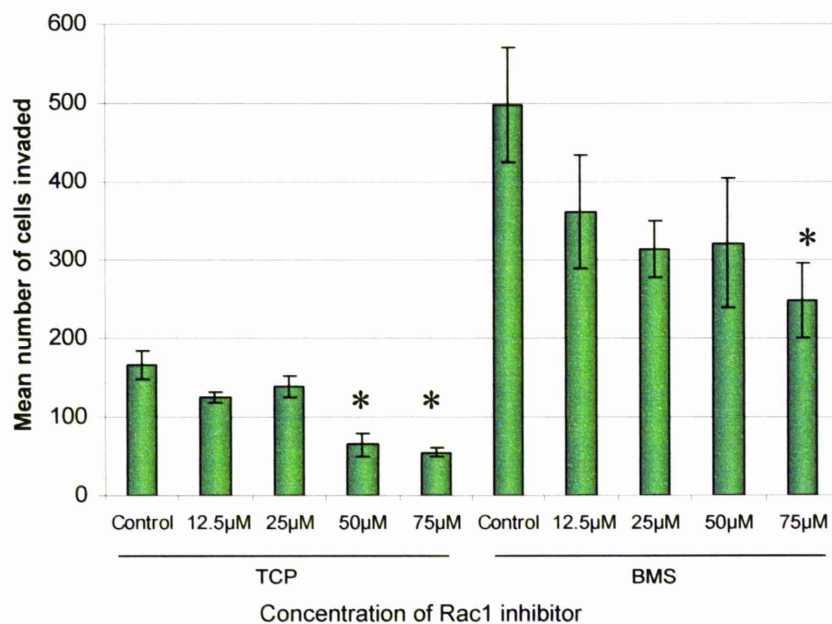


Figure 3-66: Effect of Rac1 inhibitor on PC-3-GFP invasion through Matrigel

1×10^5 PC-3-GFP cells invading towards either tissue culture plastic (TCP) or bone marrow stroma (BMS) in the presence of Rac1 inhibitor. PC-3-GFP cells were seeded onto Matrigel coated Transwell chambers. Bars show standard error (results shown as mean of 3 experiments, each experiment performed in duplicate). Asterisks indicate significance at $p < 0.05$ for both T-test and Mann-Whitney U test.

Figure 3-66 shows the effects of Rac1 inhibitor on invasion of PC-3-GFP cells through Matrigel. There was a significant reduction in invasion towards both TCP and BMS with Rac1 inhibitor at a concentration of 75 μ M (T-test $p=0.002$ for TCP and $p=0.03$ for BMS. Mann-Whitney U test $p=0.0043$ for TCP and $p=0.038$ for BMS). There was also a significant reduction in invasion towards TCP at 50 μ M (T-test $p=0.002$, Mann-Whitney U test $p=0.0043$).

Figure 3-67 shows the effects of the matrix metalloproteinase inhibitor GM6001 on invasion of PC-3-GFP cells through Matrigel. There was a significant reduction in invasion towards BMS in the presence of 20 μ M GM6001 (T-test $p=0.0007$, Mann-Whitney U test $p=0.002$) but the results were not significant for the other conditions.

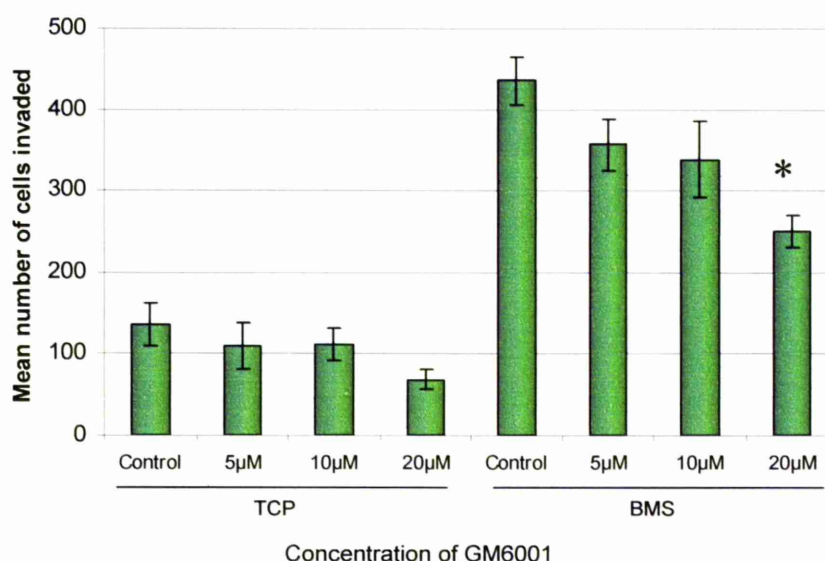


Figure 3-67: Effect of GM6001 on PC-3-GFP invasion through Matrigel

1 X 10⁵ PC-3-GFP cells invading towards either tissue culture plastic (TCP) or bone marrow stroma (BMS) in the presence of GM6001. PC-3-GFP cells were seeded onto Matrigel coated Transwell chambers. Bars show standard error (results shown as mean of 3 experiments, each experiment performed in duplicate). Asterisks indicate significance at $p<0.05$ for both T-test and Mann-Whitney U test.

After titration of inhibitor doses using PC-3-GFP cells, the inhibitor concentrations decided on for further experiments were used in assays with PC-3 cells. Figure 3-68 shows the effects of different inhibitors on PC-3 cells as they invade through Matrigel. All of the inhibitors produced a reduction in invasion ($p<0.05$ for both T-test and Mann-Whitney U test) except for invasion towards TCP

in the presence of Y-27632 which was not significant (T-test $p=0.5$). In this series the two mesenchymal motility inhibitors, Rac1 inhibitor and GM6001, produced a reduction in invasion that was similar to each other (T-test $p=0.4$ for both TCP and BMS). GM6001 lead to a larger reduction in invasion than blebbistatin (T-test $p=0.001$ for TCP and $p=0.01$ for BMS. Mann-Whitney U test $p=0.002$ for TCP and $p=0.0087$ for BMS).

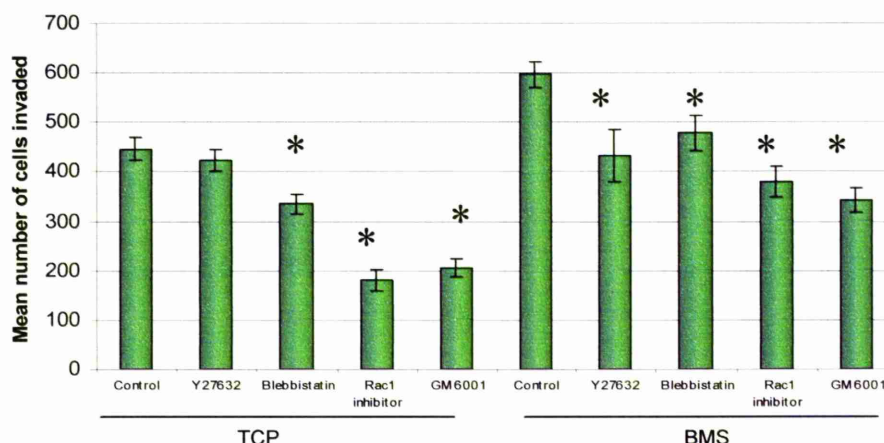


Figure 3-68: Effect of inhibitors on PC-3 cells invading through Matrigel

1×10^5 PC-3 cells invading towards either tissue culture plastic (TCP) or bone marrow stroma (BMS) in the presence of different inhibitors. PC-3 cells were seeded onto Matrigel coated Transwell chambers. Inhibitors were used at the following concentrations: Y-27632 $40\mu\text{M}$, blebbistatin $75\mu\text{M}$, Rac1 inhibitor $75\mu\text{M}$ and GM6001 $20\mu\text{M}$. Bars show standard error (results shown as mean of 3 experiments, each experiment performed in duplicate). Asterisks indicate significance at $p < 0.05$ for both T-test and Mann-Whitney U test.

Although the results were slightly different between PC-3 and PC-3-GFP cells, overall the inhibitors of mesenchymal motility showed a greater ability to inhibit invasion of both cell lines across a Matrigel layer.

Table 3-10: Cell motility inhibitors

INHIBITOR	MOTILITY AFFECTED	ACTION	CONCENTRATION
Y-27632	Amoeboid	Inhibits ROCK I and ROCK II (Rho kinase)	$40\mu\text{M}$
Blebbistatin	Amoeboid	Inhibits non-muscle myosin II	$75\mu\text{M}$
Rac1 inhibitor	Mesenchymal	Blocks Rac1	$75\mu\text{M}$
GM6001	Mesenchymal	Broad spectrum inhibitor of matrix metalloproteinases	$20\mu\text{M}$

The doses shown in Table 3-10 were chosen for use in further experiments as they were at the higher end of the concentrations used and showed the maximum effect in invasion. Inhibitors were used at the concentrations given in Table 3-10 unless stated otherwise. These concentrations were at the higher end of the range of concentrations used in the literature.

3.5.2 Cell motility in 2D monoculture

PC-3 and PC-3-GFP cells are spontaneously motile in culture so the effect of the different inhibitors was first assessed by adding them to the culture medium of cells in tissue culture treated plastic flasks and using time lapse video microscopy to look at cell motility. Cells were filmed for two to three hours in growth medium before addition of the appropriate inhibitor at the concentration given in Table 3-10 and then filmed for a further 24 hours. In all experiments there was no increase in the number of cells undergoing apoptosis compared to cells cultured in PC-3 or PC-3-GFP growth medium without inhibitors. Video clips of time lapse video microscopy studies with inhibitors can be found on the DVD in presentation 3.5.

3.5.2.1 Amoeboid motility inhibitors

3.5.2.1.1 Y-27632

When cultured in the presence of Y-27632, both PC-3 and PC-3-GFP cells showed similar changes in morphology and motility. All PC-3 cells and over 90% of PC-3-GFP cells observed within the culture were affected. Cells took on an elongated morphology and became more static, shown in Figure 3-69. Some cells were able to migrate over short distances with a broad leading edge and broad trailing edge giving them a crescentic shape, shown in Figure 3-70. Other cells were unable to retract their trailing edge, as seen in Figure 3-71 which shows a PC-3 cell with a very elongated shape. This cell seemed unable to retract its trailing edge and had to detach most of its cell body from the substrate in order to round up and divide. Mitosis occurred normally in the presence of Y-27632, as shown in Figure 3-71 and Figure 3-73. Occasional PC-3-GFP cells were able to continue to migrate using amoeboid movement, shown in Figure 3-72.

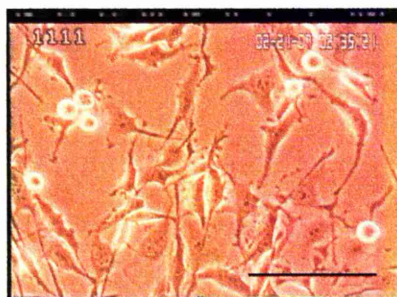
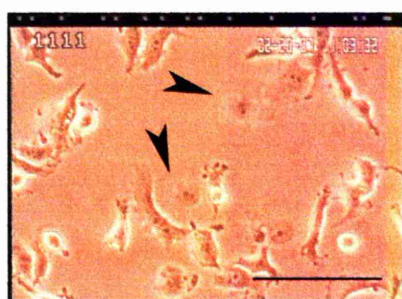


Figure 3-69: PC-3 cells cultured on tissue culture plastic in the presence of Y-27632
Cells have an elongated morphology with long processes, occasional rounded cells are seen. Cells were cultured in HAMS F12. Scale bar represents 100 μ m.
See video clip 50.



00:00



00:48



01:11



01:38



02:01

Figure 3-70: PC-3 cells cultured on tissue culture plastic in the presence of Y-27632
Some cells are able to move short distances with a broad leading edge (black arrows) and a broad retracting edge (white arrows) giving them a crescentic shape. Cells were cultured in HAMS F12. Times are shown as hours and minutes after the first image at 00:00. Scale bar represents 100 μ m.
See video clip 51

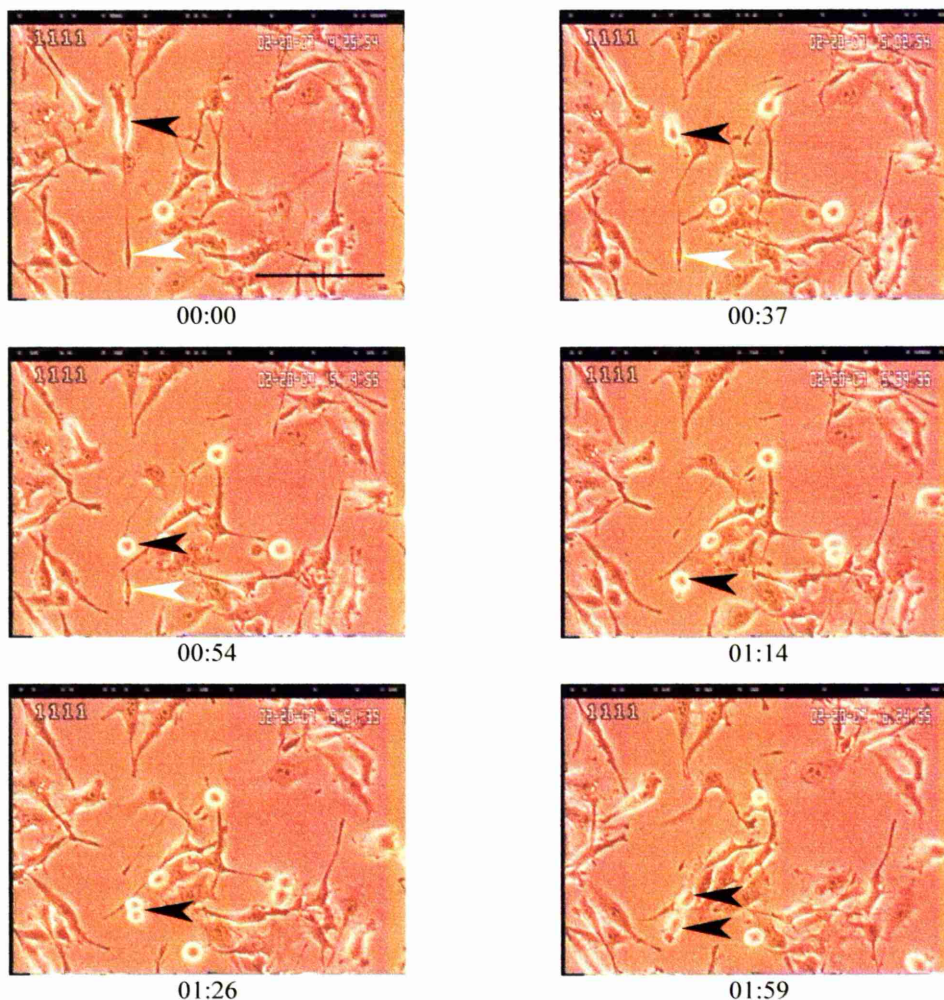


Figure 3-71: PC-3 cells cultured on tissue culture plastic in the presence of Y-27632

A cell (cell body, black arrow) showing inability to retract its trailing edge (white arrow). The cell is able to detach its leading edge before undergoing mitosis. Cells were cultured in Hams F12. Times are shown as hours and minutes after the first image at 00:00. Scale bar represents 100 μ m.

See video clip 52.

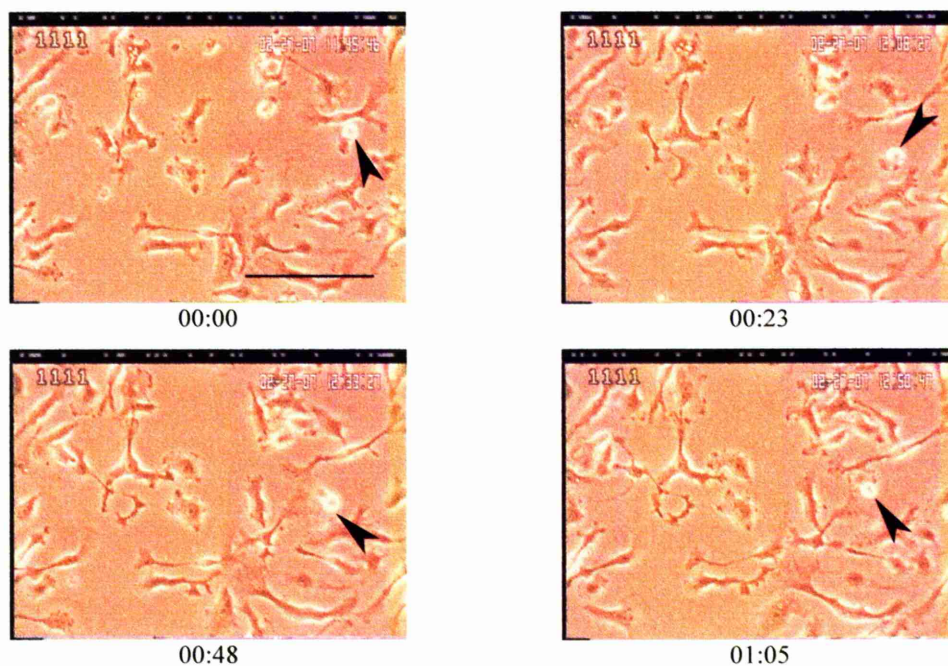


Figure 3-72: PC-3-GFP cells cultured on tissue culture plastic in the presence of Y-27632
 Most PC-3-GFP cells show an elongated morphology and reduced migration but some (arrow) continued to move using amoeboid motility. Cells were cultured in Hams F12. Times are shown as hours and minutes after the first image at 00:00. Scale bar represents 100 μ m.
 See video clip 53.

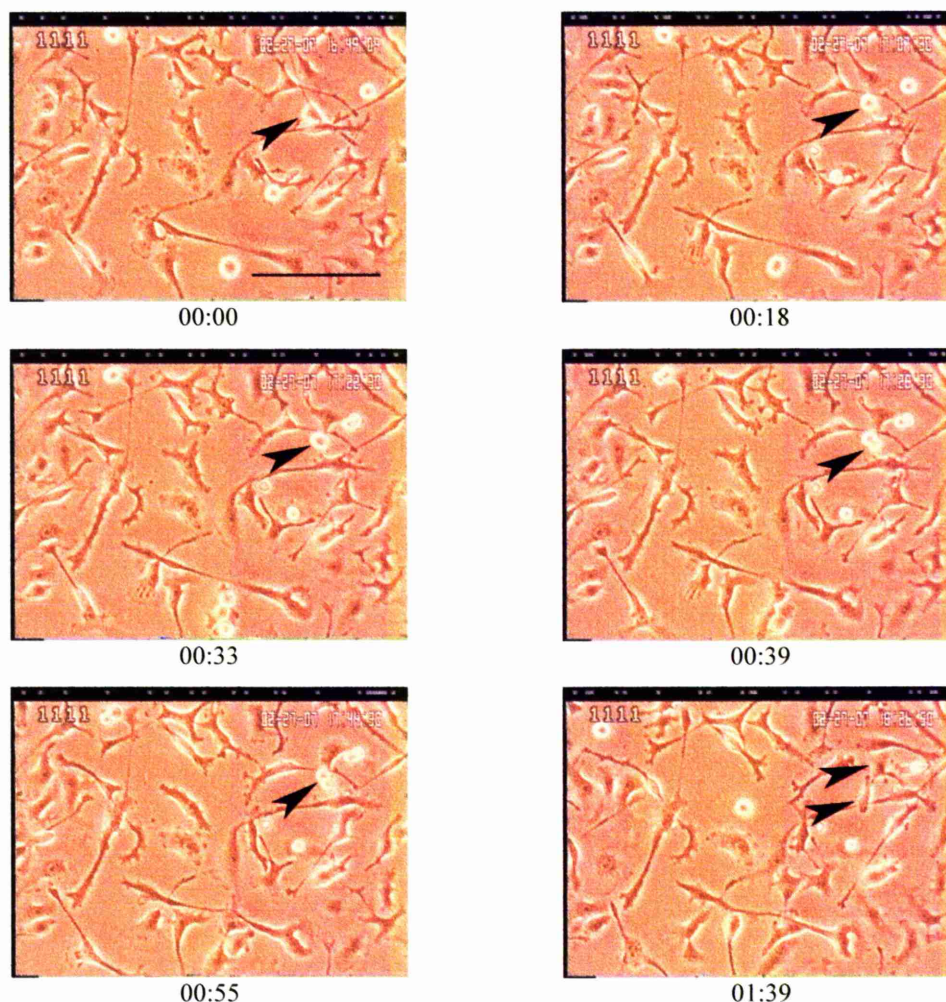


Figure 3-73: PC-3-GFP cells cultured on tissue culture plastic in the presence of Y-27632
Cells are able to complete mitosis. The cell (arrow) divides and the two daughter cells (arrowed) spread on the substrate. Cells were cultured in Hams F12. Times are shown as hours and minutes after the first image at 00:00. Scale bar represents 100 μ m.
See video clip 54.

3.5.2.1.2 *Blebbistatin*

PC-3 and PC-3-GFP cells cultured in the presence of blebbistatin showed similar changes to those seen with Y-27632, with elongated shapes and an overall reduction in migration across the substrate. All cells observed were affected. Figure 3-74 shows two frames taken 1 hour 13 minutes apart showing that many of the PC-3 cells had not moved and showed little shape change. PC-3-GFP cells were also more static, shown in Figure 3-76. Cells cultured with blebbistatin were unable to complete cytokinesis, shown in Figure 3-75 for PC-3 cells and Figure 3-77 for PC-3-GFP cells. In Figure 3-75 the PC-3 cell attempted to divide but could not complete

cytokinesis, leaving a strand of cytoplasm connecting the daughter cells. The two cells were unable to separate and became a single large cell with two nuclei.

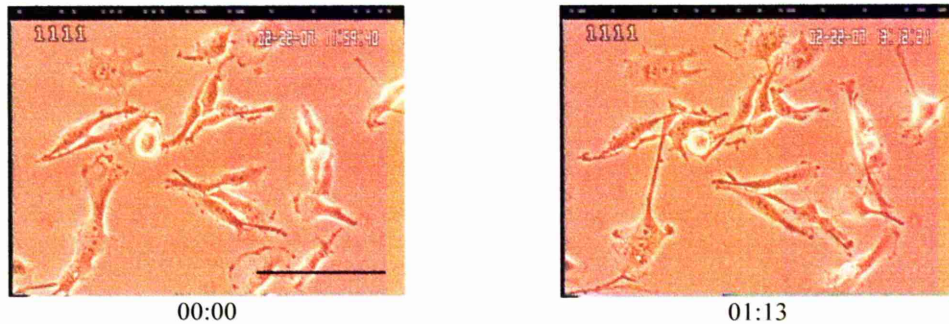
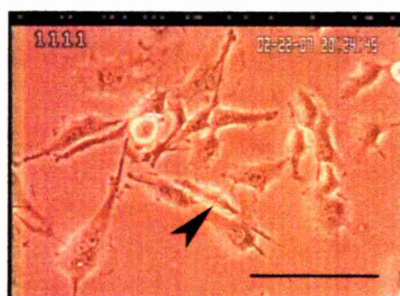


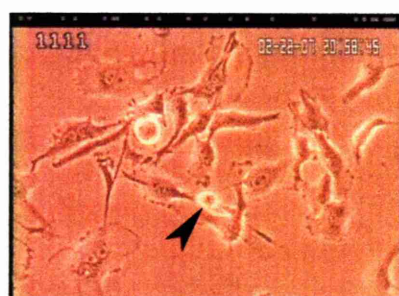
Figure 3-74: PC-3 cells cultured on tissue culture plastic in the presence of blebbistatin

Cells show reduced motility, little cell movement occurs between these images 1 hour 13 minutes apart. Cells were cultured in Hams F12. Times are shown as hours and minutes after the first image at 00:00. Scale bar represents 100 μ m.

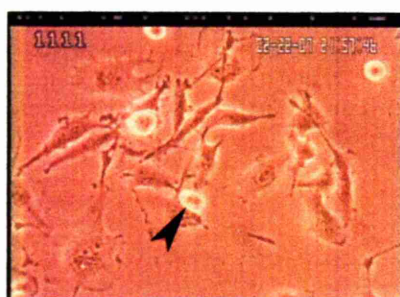
See video clip 55.



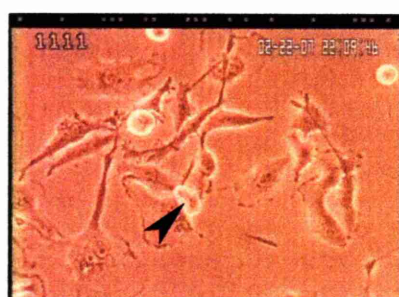
00:00



00:34



00:59



01:12



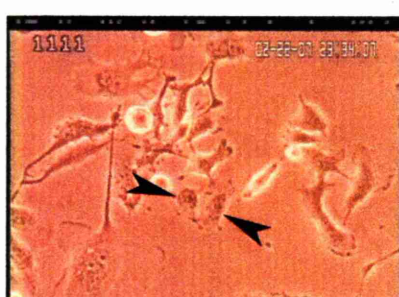
01:38



01:53



02:12



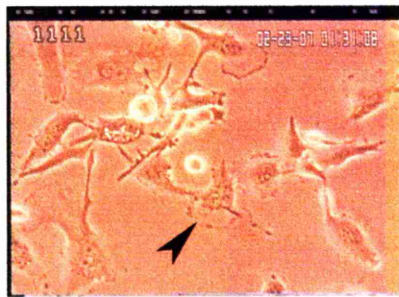
02:41



03:17



03:43



04:38

Figure 3-75: PC-3 cells cultured on tissue culture plastic in the presence of blebbistatin

Cells are unable to complete cytokinesis. A cell (black arrow in frame 00:00) attempts to divide but cannot complete cytokinesis. A strand of cytoplasm (white arrow) connects the two daughter cells and eventually a single cell with two nuclei is formed (black arrow in frame 03:17). Cells were cultured in Hams F12. Times are shown as hours and minutes after the first image at 00:00. Scale bar represents 100µm.

See video clip 56.



00:00



00:38

Figure 3-76: PC-3-GFP cells cultured on tissue culture plastic in the presence of blebbistatin

Cells show reduced migration, little cell movement occurs between these images 38 minutes apart. Cells were cultured in Hams F12. Times are shown as hours and minutes after the first image at 00:00. Scale bar represents 100µm.

See video clip 57.

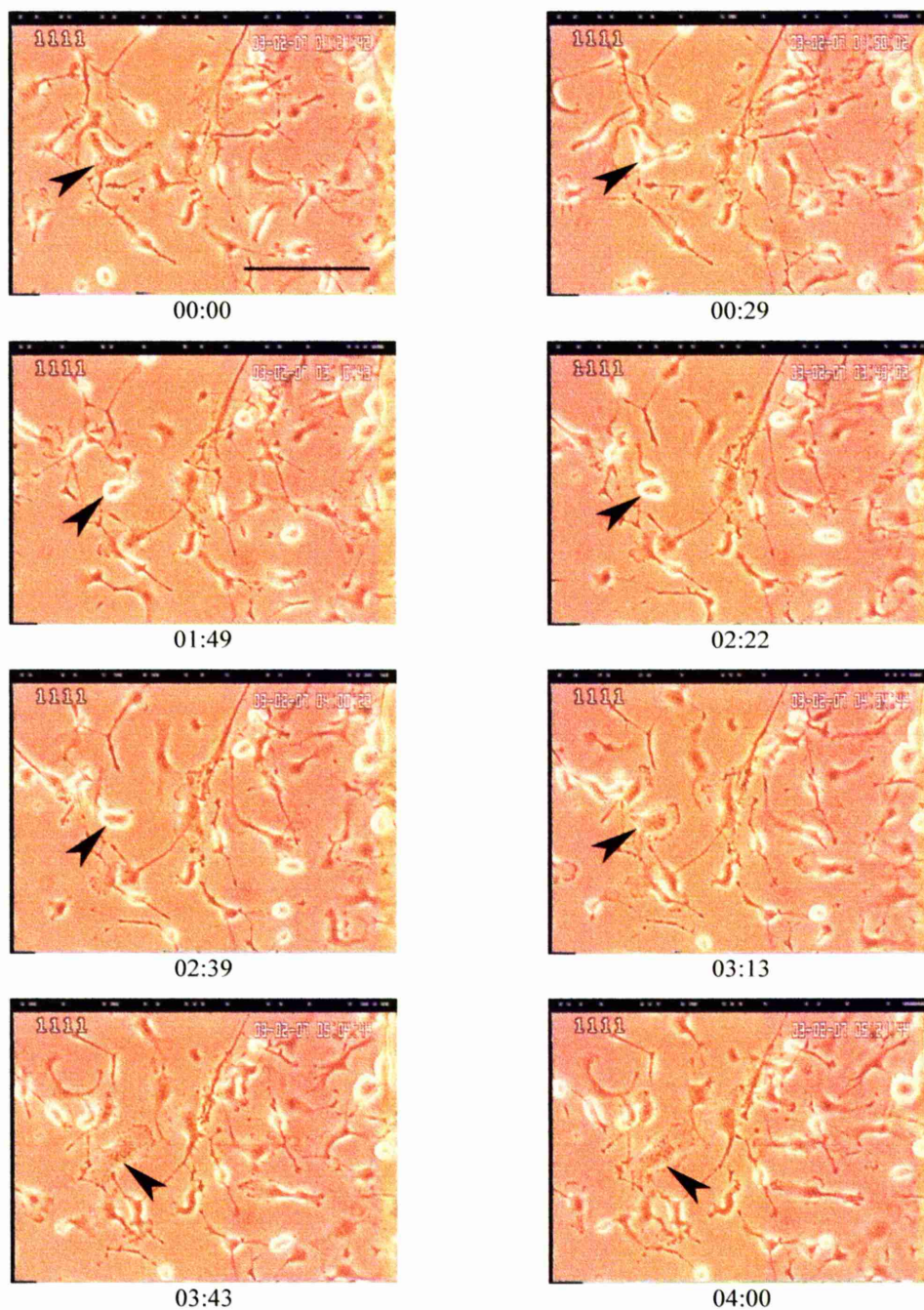


Figure 3-77: PC-3-GFP cells cultured on tissue culture plastic in the presence of blebbistatin
Cells are unable to complete cytokinesis. A cell (arrow) attempts to divide but cannot complete cytokinesis and becomes a large binucleate cell. Cells were cultured in Hams F12. Times are shown as hours and minutes after the first image at 00:00. Scale bar represents 100 μ m.
See video clip 58.

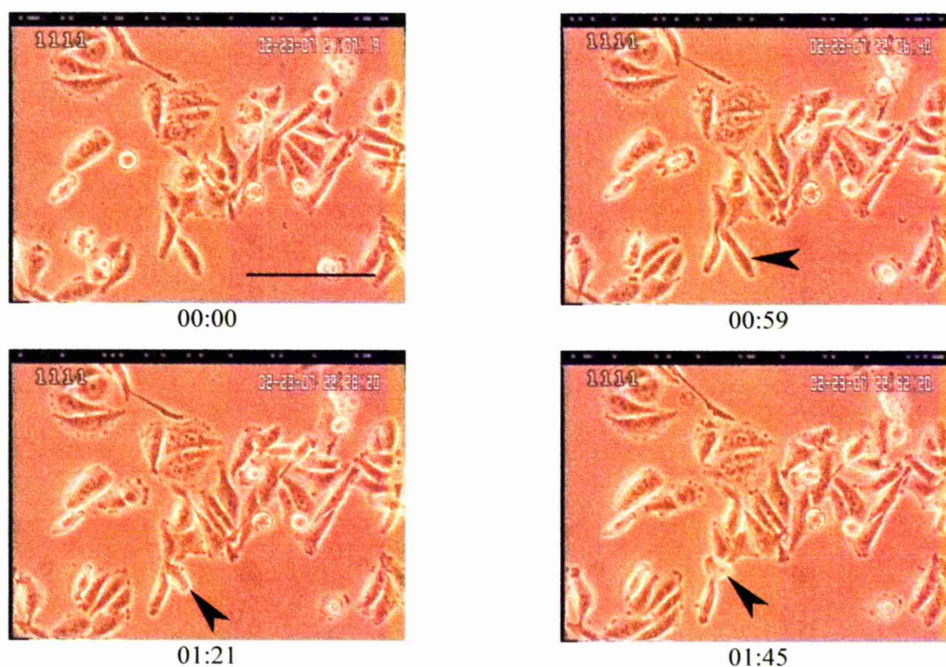


Figure 3-78: PC-3 cells cultured on tissue culture plastic in the presence of Rac1 inhibitor
Cells show reduced movement but one cell (arrowed) is able to switch to amoeboid movement. Cells were cultured in Hams F12. Times are shown as hours and minutes after the first image at 00:00. Scale bar represents 100 μ m.
See video clip 59.

3.5.2.2 Mesenchymal movement inhibitors

3.5.2.2.1 *Rac1* inhibitor

Rac1 inhibitor affected PC-3 and PC-3-GFP cells differently. It reduced the motility of all PC-3 cells observed and increased the proportion of cells with a flattened epithelioid morphology, as shown in Figure 3-78, although occasional cells did continue to migrate using amoeboid motility. Mitosis and membrane ruffling were not affected.

PC-3-GFP cells did not show any change in their morphology or motility in the presence of Rac1 inhibitor, with many cells able to migrate using amoeboid movement and occasional cells able to use mesenchymal movement (Figure 3-79).

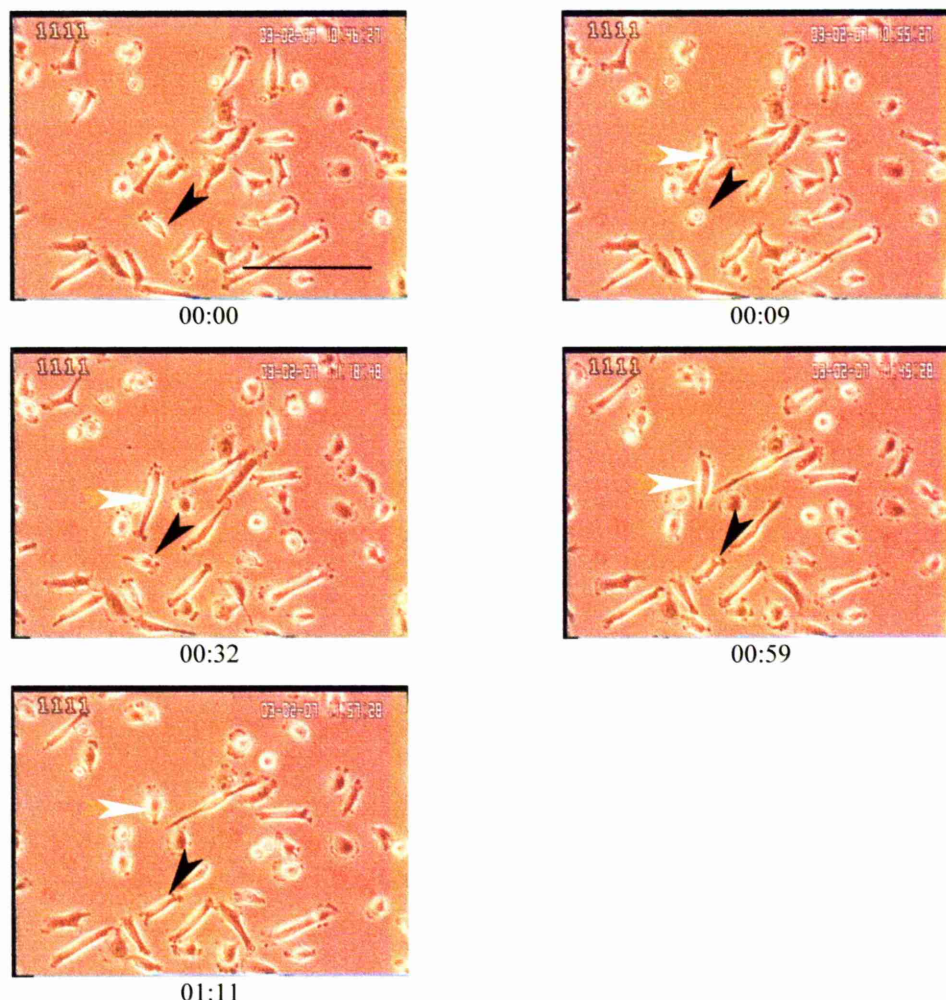


Figure 3-79: PC-3-GFP cell cultured on tissue culture plastic in the presence of Rac1 inhibitor Cells show their normal morphology and motility. A cell (black arrowhead) shows amoeboid movement and another (white arrowhead) shows mesenchymal movement. Cells were cultured in Hams F12. Times are shown as hours and minutes after the first image at 00:00. Scale bar represents 100µm.

See video clip 60.

3.5.2.2.2 *GM6001*

The matrix metalloproteinase inhibitor GM6001 had no effect on the motility, morphology, mitosis or behaviour of PC-3 and PC-3-GFP cells cultured on a 2D tissue culture plastic substrate without extracellular matrix. Prostate cells can be seen moving and behaving normally in video clips 61 (PC-3 cells) and 62 (PC-3-GFP cells).

3.5.2.3 Inhibitor washout studies

Because of the potential effect of inhibitors on the BMEC, the duration of action of inhibitors on PC-3 and PC-3-GFP cells was assessed in the hope of being

able to pre-treat the prostate cells with inhibitors before addition to the BMEC monolayer. PC-3 or PC-3-GFP cells were seeded into a tissue culture flask and allowed to spread on the substrate overnight. They were then incubated with inhibitors for 24 hours. Two hours before the end of the incubation period the cells were put onto the microscope to be filmed. After the medium containing inhibitors was removed, the cells were washed twice in PBS and fresh medium free of inhibitors was added before they were replaced on the microscope and filmed for a further 24 hours. The time at which cells could be seen to return to their typical morphology and behaviour was noted. Cells incubated with Rac1 inhibitor or blebbistatin returned to normal within 1 hour of the inhibitor being removed. After removal of Y-27632, PC-3 cells returned to normal after 4.5 hours and PC-3-GFP cells after 4 hours. Since GM6001 had no effect on the morphology and behaviour of PC-3 or PC-3-GFP cells in culture on plastic, it could not be assessed. Due to the speed with which the inhibitors lost their effects after washout it was not practical to use pre-treated PC-3 or PC-3-GFP cells in co-culture experiments.

3.5.3 Effect of inhibitors on the BMEC monolayer

Since the inhibitors would need to be added to co-cultures of BMEC with prostate epithelial cells it was necessary to examine any effects of the inhibitors on the BMEC. As inhibitors would only be added to monolayers that were already confluent, BMEC were grown to confluence before being used for these experiments.

3.5.3.1 Time lapse video microscopy studies

BMEC were cultured in BMSCM in a fibronectin coated flask until they were confluent before filming them in the time lapse video microscopy unit for 2-3 hours. The appropriate inhibitor, mixed with BMSCM, was added and the flask was returned to the unit for a further 24 hours. BMEC showed no change in morphology or behaviour during incubation with any of the inhibitors and the monolayer appeared intact. Representative video clips (clips 63-66) are shown in presentation 3.5.

3.5.3.2 Immunofluorescent staining of tight junctions

Confluent monolayers of BMEC were cultured on coverslips coated with fibronectin before being incubated with inhibitors for 24 hours. They were then fixed in methanol and stained for the tight junction protein ZO-1 using the 2-step method

(section 2.2.6.2.2.2) in order to assess the effect of the inhibitors on tight junctions. ZO-1 was chosen as it was the most reliable junctional marker of the antibodies used for immunophenotyping of these cells. Irregular linear staining was seen at the cell-cell junctions and there was no difference in the amount or distribution of staining in BMEC incubated with the inhibitors compared to that seen in control cells. Representative images are shown in Figure 3-80.

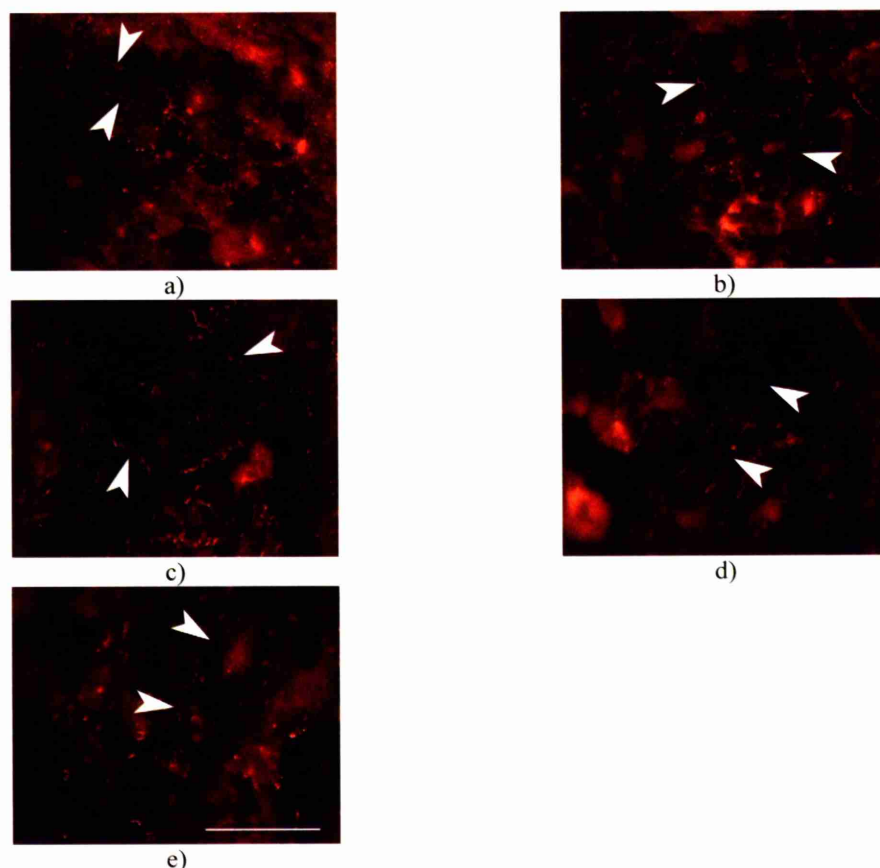


Figure 3-80: ZO-1 staining in BMEC after 24 hours incubation with inhibitors
 Confluent monolayers of BMEC were incubated with inhibitors for 24 hours before staining for ZO-1. ZO-1 staining can be seen as irregular linear labelling of cell-cell junctions (arrows). Scale bar represents 50µm.
a) Y-27632 **b)** blebbistatin **c)** Rac1 inhibitor **d)** GM6001 **e)** control

3.5.3.3 Permeability studies

Confluent monolayers of BMEC were cultured on fibronectin coated Transwell chambers with 1µm diameter pores. PC-3 cells at 1×10^5 cells per well or inhibitors at the concentrations shown in Table 3-10 were added to the culture medium in the Transwell chamber and incubated for 6 or 24 hours. After incubation with inhibitors or PC-3 cells, FITC labelled dextran was added to the Transwell chamber and allowed 30 minutes to diffuse through the BMEC monolayer into the

lower chamber before the level of fluorescence in the lower chamber was read. A series of standard dilutions of FITC-dextran in medium were made to allow the amount of diffusion through the BMEC monolayer to be calculated. An example of a standard curve is shown in Figure 3-81, the results of a 6 hour incubation study are shown in Figure 3-82 and a 24 hour study in Figure 3-83.

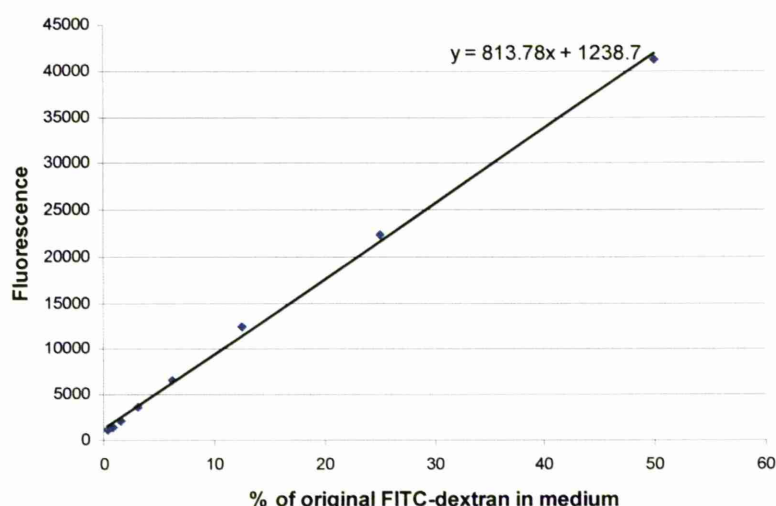


Figure 3-81: A typical standard curve for FITC-dextran dilutions

A serial dilution of FITC labelled dextran in culture medium (BMSCM) was performed, the level of fluorescence read and the results plotted to produce a standard curve.

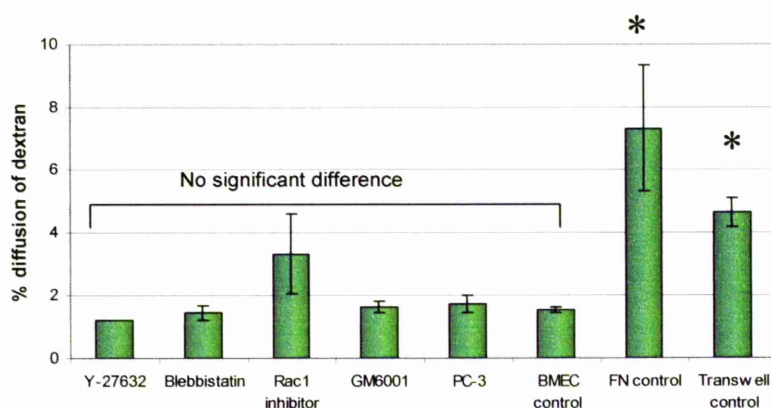


Figure 3-82: Permeability of the BMEC monolayer to FITC-dextran in the presence of inhibitors or PC-3 cells after 6 hours incubation

BMEC monolayers were cultured on fibronectin coated Transwell chambers and incubated with inhibitors for 6 hours before permeability was assessed. The presence of a BMEC monolayer significantly reduced diffusion of FITC-dextran through a Transwell chamber. None of the inhibitors, or the presence of PC-3 cells, altered the permeability of the BMEC monolayer. BMEC control = BMEC monolayer, no inhibitors. FN control = fibronectin coated Transwell insert without BMEC or inhibitors. Transwell control = Transwell insert without fibronectin, BMEC or inhibitors. Bars show standard error (results shown as mean of 3 experiments, each experiment performed in duplicate).

The results of permeability studies were similar at both 6 and 24 hours. Figure 3-82 shows that, at 6 hours, a plain Transwell insert without fibronectin or BMEC allowed 4.6% of the dextran to diffuse into the lower well, while a fibronectin coated Transwell chamber allowed 7.3% to diffuse; both results were significantly higher than diffusion through the BMEC monolayer (T-test and Mann-Whitney U test $p < 0.05$ for both results). The results for Transwells and fibronectin coated Transwells were not significantly different from each other (T-test $p = 0.3$). Once a BMEC monolayer was present, diffusion of dextran was reduced to 1.5% and the presence of PC-3 cells or inhibitors did not significantly affect BMEC monolayer permeability (T-test and Mann-Whitney U test $p > 0.2$ for PC-3 cells and all inhibitors).

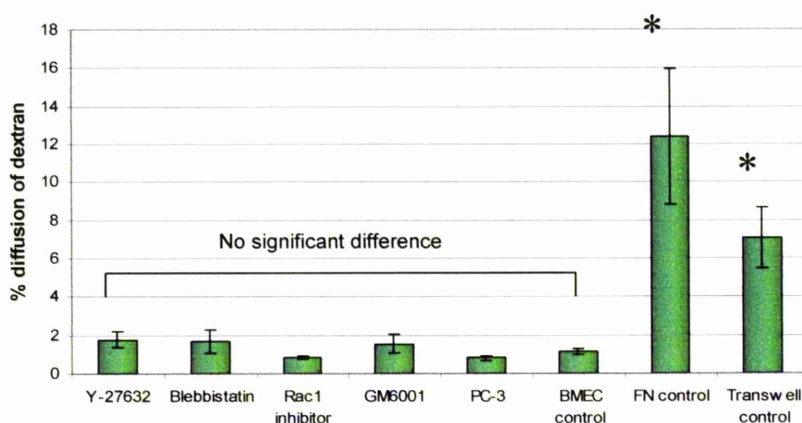


Figure 3-83: Permeability of the BMEC monolayer to FITC-dextran in the presence of inhibitors or PC-3 cells after 24 hours incubation

BMEC monolayers were cultured on fibronectin coated Transwell chambers and incubated with inhibitors for 24 hours before permeability was assessed. The presence of a BMEC monolayer significantly reduced diffusion of FITC-dextran through a Transwell chamber. None of the inhibitors, or the presence of PC-3 cells, altered the permeability of the BMEC monolayer. BMEC control = BMEC monolayer, no inhibitors. FN control = fibronectin coated Transwell insert without BMEC or inhibitors. Transwell control = Transwell insert without fibronectin, BMEC or inhibitors. Bars show standard error (results shown as mean of 3 experiments, each experiment performed in duplicate).

Figure 3-83 shows that a plain Transwell insert without fibronectin or BMEC allowed 7.1% of the dextran to diffuse across the pores, while a fibronectin coated Transwell chamber allowed 12.4% to diffuse. These results both indicated significantly higher diffusion through Transwells without a BMEC monolayer (T-test and Mann-Whitney U test $p < 0.05$) than through a BMEC monolayer. Inhibitors or PC-3 cells did not significantly increase diffusion through the BMEC monolayer (T-

test and Mann-Whitney U test $p>0.2$ for PC-3 cells and all inhibitors). Again the results for Transwells and fibronectin coated Transwells were not significantly different (T-test $p=0.2$).

3.5.4 Invasion through endothelial cells

Time lapse video microscopy invasion studies were set up in the same way as detailed in section 3.4.1, with a confluent monolayer of BMEC, but with the addition of the appropriate inhibitor to the suspension of 6.25×10^5 PC-3 or PC-3-GFP cells before addition to the flask of BMEC. The co-culture was filmed for 24 hours in the time lapse video microscopy unit. Two experiments were done with a single field of view used for each.

3.5.4.1 Amoeboid motility inhibitors

3.5.4.1.1 Y-27632

The ROCK inhibitor Y-27632 was added to a suspension of PC-3 or PC-3-GFP cells before they were added to a confluent BMEC monolayer and filmed in the time lapse video microscopy unit for 24 hours. Representative frames are shown in Figure 3-84 and Figure 3-85 for PC-3 cells and Figure 3-86 and Figure 3-87 for PC-3-GFP cells.

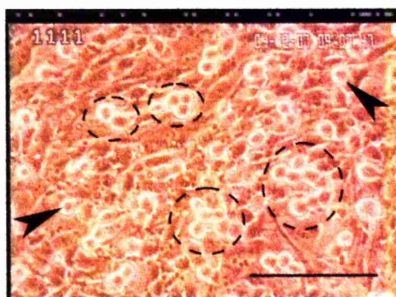


Figure 3-84: BMEC monolayer with PC-3 cells in the presence of Y-27632

The BMEC monolayer 50 minutes after the addition of PC-3 cells and Y-27632. Groups (circled) and single (arrowed) PC-3 cells are present on top of the monolayer. Cells were cultured in BMSCM. Scale bar represents 100 μ m.

See video clip 67.

Both prostate cell lines showed a change in behaviour in the presence of Y-27632: no blebbing occurred and cells flattened on top of the BMEC monolayer, often in small groups, instead of migrating through it. This behaviour was similar to that of PNT2-C2 cells, shown in Figure 3-49. Of the 52 PC-3 cells followed, 20 did not invade and for the remaining 32 it was uncertain. Only one of the 37 PC-3-GFP

cells appeared to migrate through the BMEC monolayer, 20 showed no invasion and 16 were uncertain.

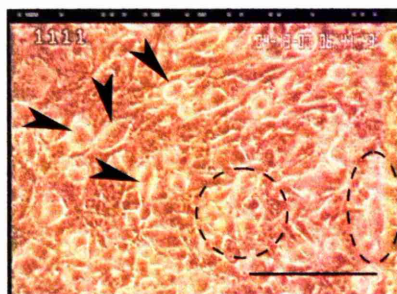
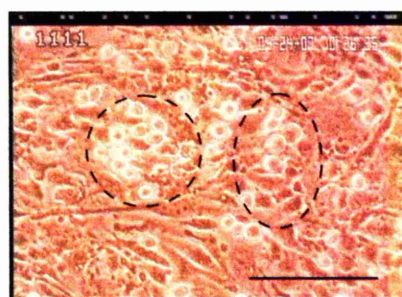


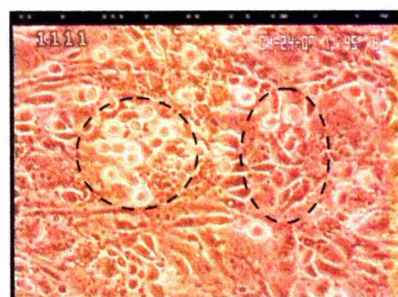
Figure 3-85: BMEC monolayer with PC-3 cells in the presence of Y-27632

The BMEC monolayer 20 hours 24 minutes after the addition of PC-3 cells and Y-27632. Groups (circled) and single (arrowed) PC-3 cells are still present on top of the monolayer. Cells were cultured in BMSCM. Scale bar represents 100 μ m.

See video clip 68.



00:36



02:00

Figure 3-86: BMEC monolayer with PC-3-GFP cells in the presence of Y-27632

The BMEC monolayer after the addition of PC-3-GFP cells and Y-27632. Groups of PC-3-GFP cells (circled) are present and start to flatten on top of the BMEC monolayer. Cells were cultured in BMSCM. Times are shown as hours and minutes after the addition of PC-3-GFP cells. Scale bar represents 100 μ m.

See video clip 69.

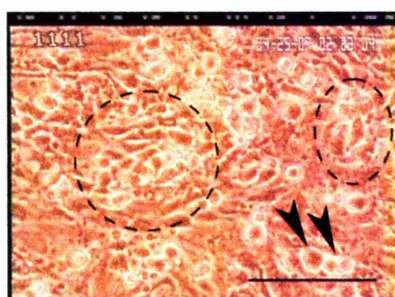


Figure 3-87: BMEC monolayer with PC-3-GFP cells in the presence of Y-27632

The BMEC monolayer 15 hours 38 minutes after the addition of PC-3-GFP cells and Y-27632. Groups (circled) and single (arrowed) PC-3-GFP cells are still present on top of the monolayer. Cells were cultured in BMSCM. Scale bar represents 100 μ m.

See video clip 70.

3.5.4.1.2 *Blebbistatin*

Blebbistatin produced similar effects on both prostate cell lines to those seen with Y-27632. No blebbing occurred and most cells either flattened or remained rounded on top of the BMEC monolayer, often in small groups. Figure 3-88 to Figure 3-90 show images of PC-3 cells and Figure 3-91 and Figure 3-92 show PC-3-GFP cells. Of the 32 PC-3 cells followed, four migrated through the monolayer, 13 did not migrate and 15 were uncertain; a PC-3 cell is shown invading in Figure 3-89. Three of the 28 PC-3-GFP cells migrated through the monolayer, 16 did not migrate and 9 were uncertain.

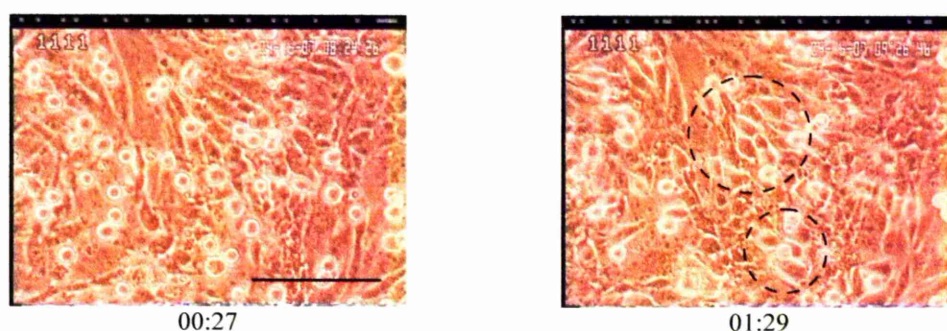


Figure 3-88: BMEC monolayer with PC-3 cells in the presence of blebbistatin

The BMEC monolayer after the addition of PC-3 cells and blebbistatin. PC-3 cells start to flatten on top of the BMEC monolayer and form groups (circled). Cells were cultured in BMSCM. Times are shown as hours and minutes after the addition of PC-3 cells. Scale bar represents 100 μ m.

See video clip 71.

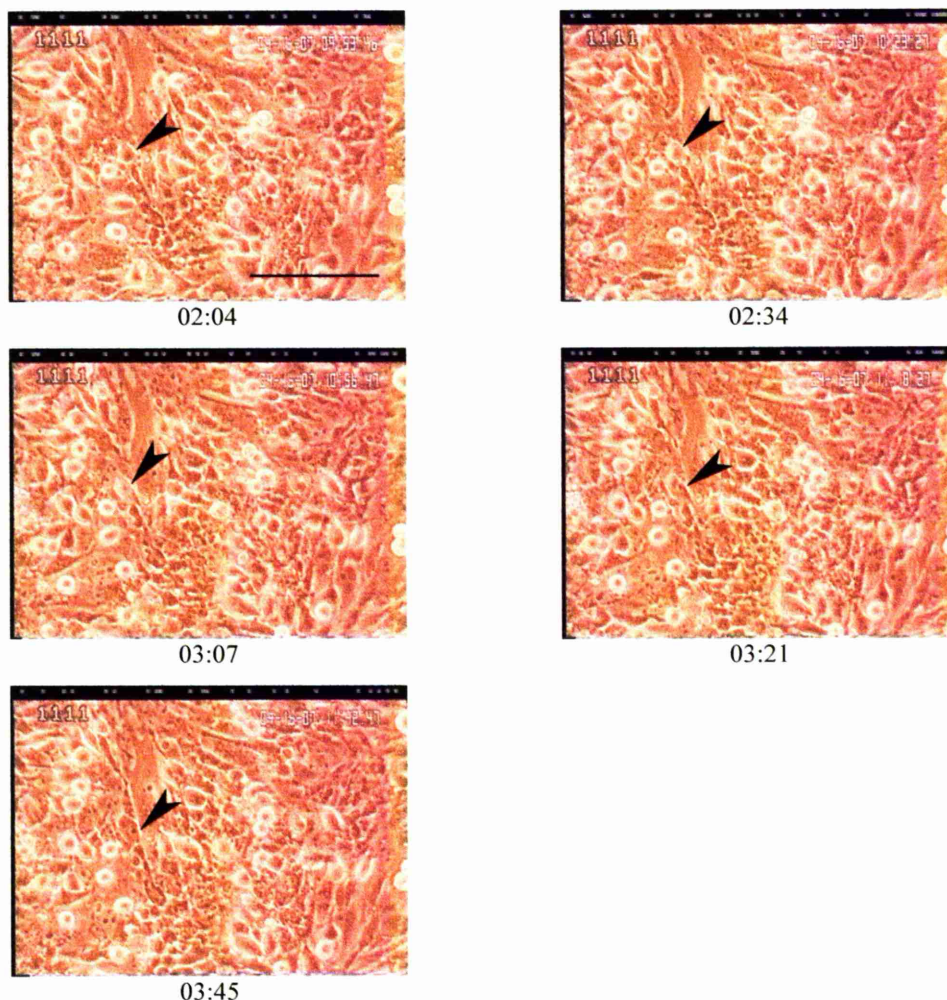


Figure 3-89: BMEC monolayer with PC-3 cells in the presence of blebbistatin

The BMEC monolayer after the addition of PC-3 cells and blebbistatin. A PC-3 cell (arrowed) can be seen migrating between BMEC onto the underlying substrate. Cells were cultured in BMSCM. Times are shown as hours and minutes after the addition of PC-3 cells. Scale bar represents 100 μ m.

See video clip 72.

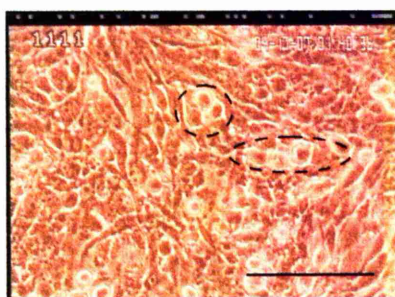


Figure 3-90: BMEC monolayer with PC-3 cells in the presence of blebbistatin

The BMEC monolayer 16 hours 43 minutes after the addition of PC-3 cells and blebbistatin. Groups of flattened PC-3 cells (circled) are still present on top of the BMEC monolayer. Cells were cultured in BMSCM. Scale bar represents 100 μ m.

See video clip 73.

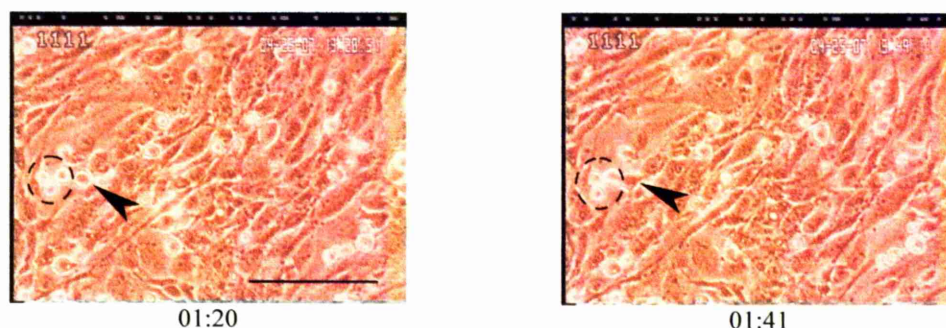


Figure 3-91: BMEC monolayer with PC-3-GFP cells in the presence of blebbistatin
 The BMEC monolayer after the addition of PC-3-GFP cells and blebbistatin. Some cells (circled) remain rounded while another (arrowed) flattens on top of the BMEC. Cells were cultured in BMSCM. Times are shown as hours and minutes after the addition of PC-3 cells. Scale bar represents 100µm.
 See video clip 74.

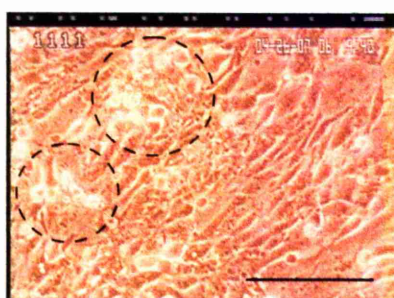


Figure 3-92: BMEC monolayer with PC-3-GFP cells in the presence of blebbistatin
 The BMEC monolayer 17 hours 11 minutes after the addition of PC-3-GFP cells and blebbistatin. Groups of flattened PC-3-GFP cells (circled) are still present on top of the BMEC monolayer. Cells were cultured in BMSCM. Scale bar represents 100µm.
 See video clip 75.

3.5.4.2 Mesenchymal motility inhibitors

3.5.4.2.1 *Rac1* inhibitor

Migration of both PC-3 and PC-3-GFP cells across the BMEC monolayer in the presence of Rac1 inhibitor occurred in the same way as that seen in the controls, and at the same rate as shown in Figure 3-97 and Figure 3-98. It was difficult to follow cells once they had completed endothelial transmigration and their behaviour once they had reached the substrate could not be assessed in most cases, although a PC-3-GFP cell could be seen to migrate across the substrate. Representative images from time lapse films of prostate carcinoma cells completing endothelial transmigration in the presence of Rac1 inhibitor are shown in Figure 3-93 for PC-3 cells and Figure 3-94 for PC-3-GFP cells. A total of 39 PC-3 cells were followed, of which one underwent apoptosis and the remainder completed migration through the

BMEC monolayer. All but one of the 29 PC-3-GFP cells completed migration through the BMEC monolayer.

In Figure 3-93 a PC-3 cell is shown which remained rounded as it moved a short distance over the BMEC monolayer before flattening onto the substrate. Figure 3-94 shows a PC-3-GFP cell which completed transmigration and was then able to migrate a short distance across the substrate before it could no longer be identified.

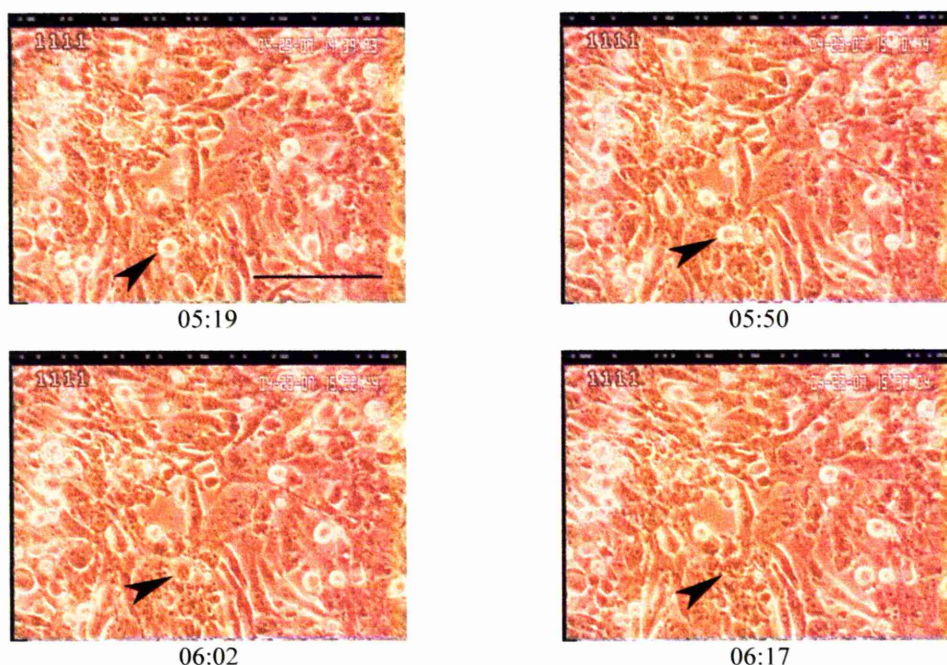


Figure 3-93: BMEC monolayer with PC-3 cells in the presence of Rac1 inhibitor

The BMEC monolayer after the addition of PC-3 cells and Rac1 inhibitor. A PC-3 cell (arrowed) migrates through the BMEC monolayer. Cells were cultured in BMSCM. Times are shown as hours and minutes after the addition of PC-3 cells. Scale bar represents 100 μ m.

See video clip 76.

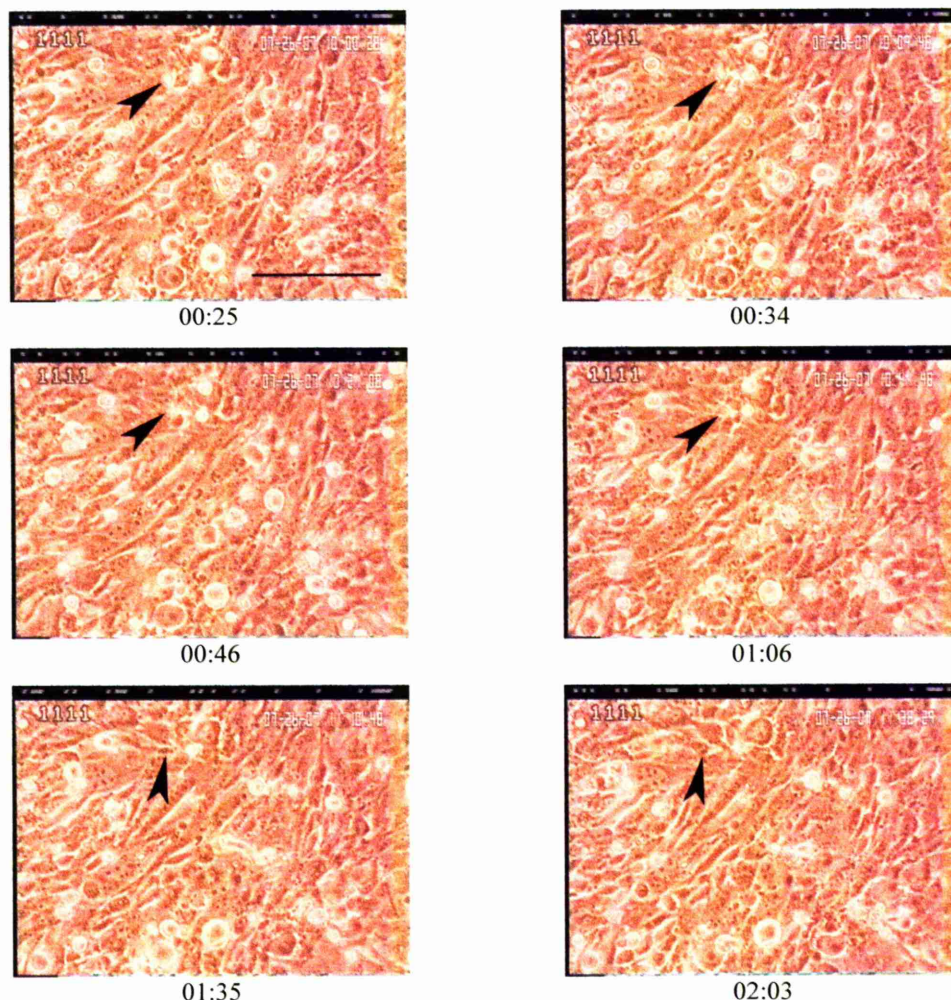


Figure 3-94: BMEC monolayer with PC-3-GFP cells in the presence of Rac1 inhibitor
The BMEC monolayer after the addition of PC-3-GFP cells and Rac1 inhibitor. A PC-3-GFP cell (arrowed) migrates through the BMEC monolayer and across the substrate. Cells were cultured in BMSCM. Times are shown as hours and minutes after the addition of PC-3-GFP cells. Scale bar represents 100 μ m.
See video clip 77.

3.5.4.2.2 *GM6001*

Migration of both PC-3 and PC-3-GFP cells across the BMEC monolayer in the presence of GM6001 occurred in the same way as that seen in the controls, and at the same rate as shown in Figure 3-97 and Figure 3-98. All but one of the 19 PC-3 cells, and all of the 22 PC-3-GFP cells completed migration through the BMEC monolayer. A PC-3 cell, shown in Figure 3-95 produced a lamellipodium and migrated a short distance over the BMEC before invading through the monolayer

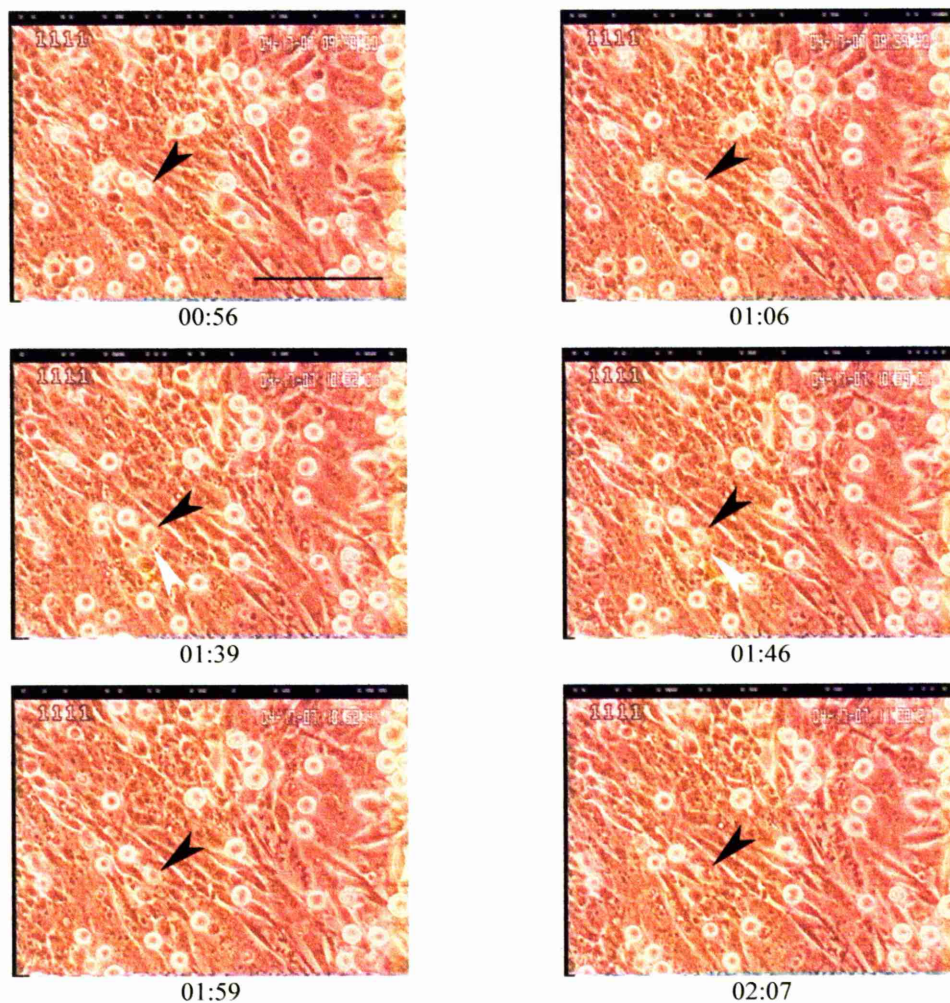


Figure 3-95: BMEC monolayer with PC-3 cells in the presence of GM6001

The BMEC monolayer after the addition of PC-3 cells and GM6001. A PC-3 cell (black arrow) produces a lamellipodium (white arrow) and migrates a sort distance across the BMEC monolayer before invading through it. Cells were cultured in BMSCM. Times are shown as hours and minutes after the addition of PC-3 cells. Scale bar represents 100 μ m.

See video clip 78.

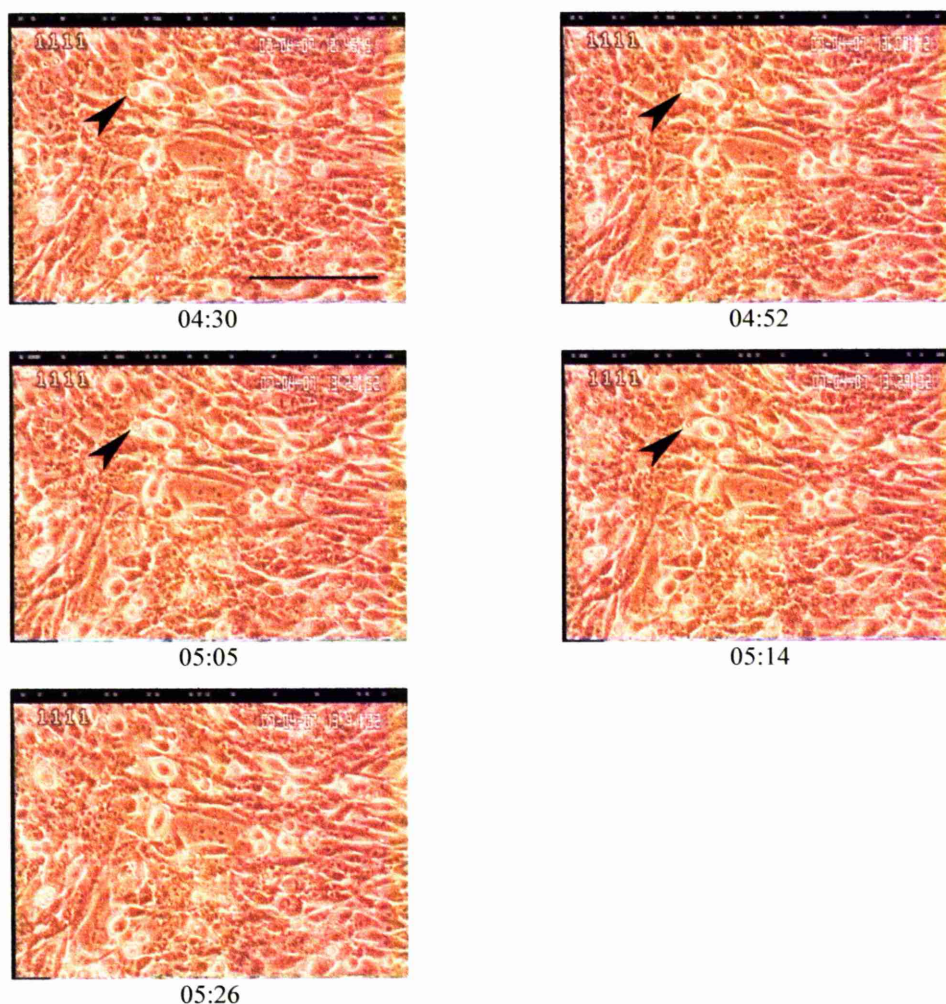


Figure 3-96: BMEC monolayer with PC-3-GFP cells in the presence of GM6001

The BMEC monolayer after the addition of PC-3-GFP cells and GM6001. A PC-3-GFP cell (arrowed) migrates through the endothelial monolayer. Cells were cultured in BMSCM. Times are shown as hours and minutes after the addition of PC-3-GFP cells. Scale bar represents 100 μ m.

See video clip 79.

For all the transmigration studies, the cells were observed and time to complete invasion was noted. This was judged to be when cells were seen to flatten into the endothelial layer or migrate underneath endothelial cells. Although it was normally possible to determine which cells had completed invasion, in the presence of amoeboid motility inhibitors there were prostate carcinoma cells which seemed to flatten on top of the endothelial layer and it was not always possible to be sure if an individual cell had flattened on top of the monolayer or invaded through it. In these cases the cells were recorded as having invaded after 24 hours (the end of the experiment) in order to avoid overestimating the effect of the inhibitor in blocking migration through the endothelial layer. Cells that migrated out of the field of view were not counted. The results given in Figure 3-97 and Figure 3-98 have been

produced using this method. These results show that the inhibitors of mesenchymal motility (Rac1 inhibitor and GM6001) did not inhibit migration of PC-3 and PC-3-GFP cells through the BMEC monolayer. The amoeboid motility inhibitors (Y-27632 and blebbistatin) both reduced migration through the BMEC monolayer to 62% of cells or less compared to 94% or more in the controls.

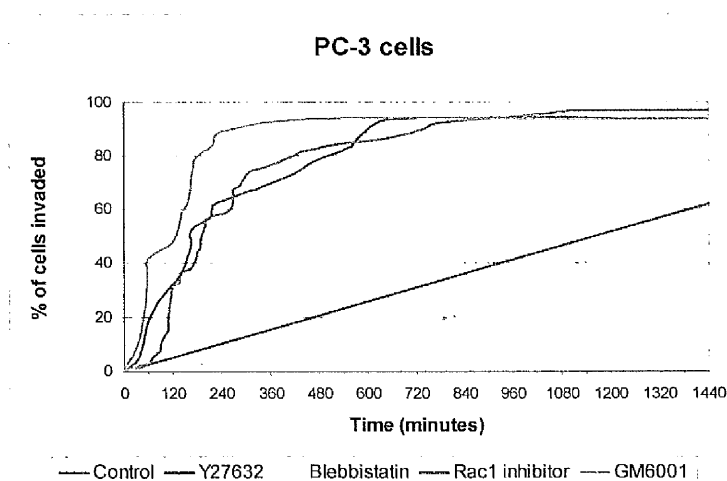


Figure 3-97: Invasion of PC-3 cells through a BMEC monolayer in the presence of motility inhibitors

PC-3 cells were seeded onto a confluent monolayer of BMEC and observed for 24 hours in the time lapse video microscopy unit. In the control experiment 19 cells were followed, 52 in the Y-27632 experiment, 32 for blebbistatin, 39 for Rac1 inhibitor and 19 for GM6001. Inhibitors were used at the following concentrations: Y-27632 40 μ M, blebbistatin 75 μ M, Rac1 inhibitor 75 μ M and GM6001 20 μ M.

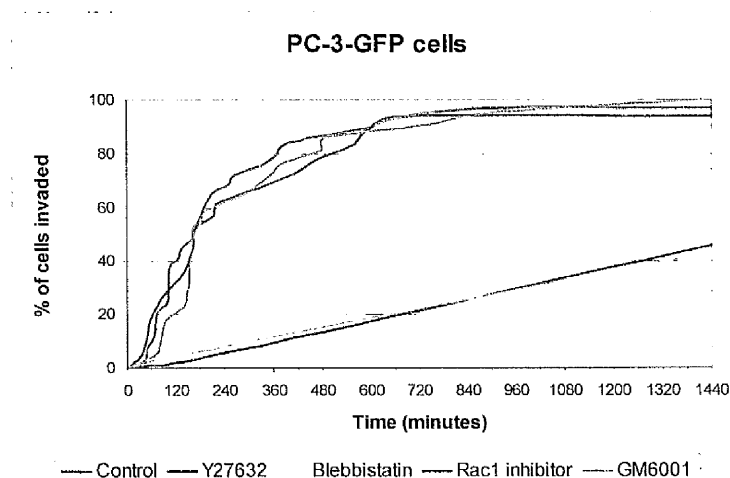


Figure 3-98: Invasion of PC-3-GFP cells through a BMEC monolayer in the presence of motility inhibitors

PC-3-GFP cells were seeded onto a confluent monolayer of BMEC and observed for 24 hours in the time lapse video microscopy unit. In the control experiment 25 cells were followed, 37 in the Y-27632 experiment, 28 for blebbistatin, 29 for Rac1 inhibitor and 22 for GM6001. Inhibitors were used at the following concentrations: Y-27632 40 μ M, blebbistatin 75 μ M, Rac1 inhibitor 75 μ M and GM6001 20 μ M.

3.5.5 Invasion through BMEC monolayer

The effect of inhibitors on invasion through BMEC monolayers was also assessed using Transwell chambers. BMEC would not adhere to the Transwell membrane alone so it had to be coated with fibronectin before BMEC were seeded into the chamber and cultured for two days until they were confluent. PC-3 or PC-3-GFP cells mixed with inhibitors were added to the chamber as described in section 2.2.3.2. After 18 hours of invasion the chambers were fixed and stained using an immunocytochemical method for cytokeratins (section 2.2.3.1.1) in order to identify the prostate epithelial cells.

Figure 3-99 shows the effects of inhibitors on PC-3 cells invading through a BMEC monolayer cultured on fibronectin. All the inhibitors produced a significant reduction in invasion towards both TCP and BMS (T-test and Mann-Whitney U test $p < 0.05$).

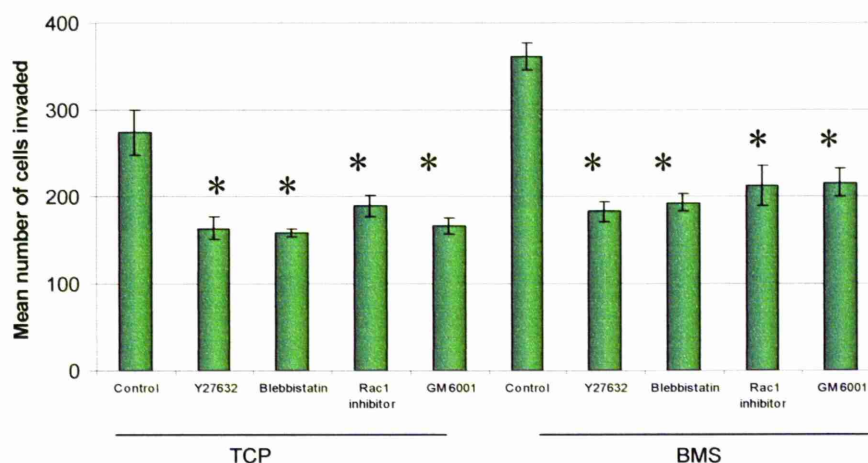


Figure 3-99: Effect of inhibitors on invasion of PC-3 cells through a BMEC monolayer
 1×10^5 PC-3 cells invading towards either tissue culture plastic (TCP) or bone marrow stroma (BMS) in the presence of inhibitors. PC-3 cells were seeded onto BMEC monolayers cultured on fibronectin coated Transwell chambers. Inhibitors were used at the following concentrations: Y-27632 40 μ M, blebbistatin 75 μ M, Rac1 inhibitor 75 μ M and GM6001 20 μ M. Bars show standard error (results shown as mean of 3 experiments, each experiment performed in duplicate). Asterisks indicate significance at $p < 0.05$ for both T-test and Mann-Whitney U test.

Figure 3-100 shows the effect of inhibitors on invasion of PC-3-GFP cells invading through a BMEC monolayer cultured on fibronectin. Y-27632 and GM6001 both lead to a significant (T-test and Mann-Whitney U test $p < 0.05$) reduction in invasion towards both TCP and BMS but Rac1 inhibitor did not have a significant effect (T-test $p = 0.6$ for TCP and $p = 0.1$ for BMS). Blebbistatin only significantly reduced

invasion towards BMS (T-test $p=0.001$, Mann-Whitney U test $p=0.008$), although its effect in reducing invasion towards TCP approached significance (Mann-Whitney U test $p=0.055$).

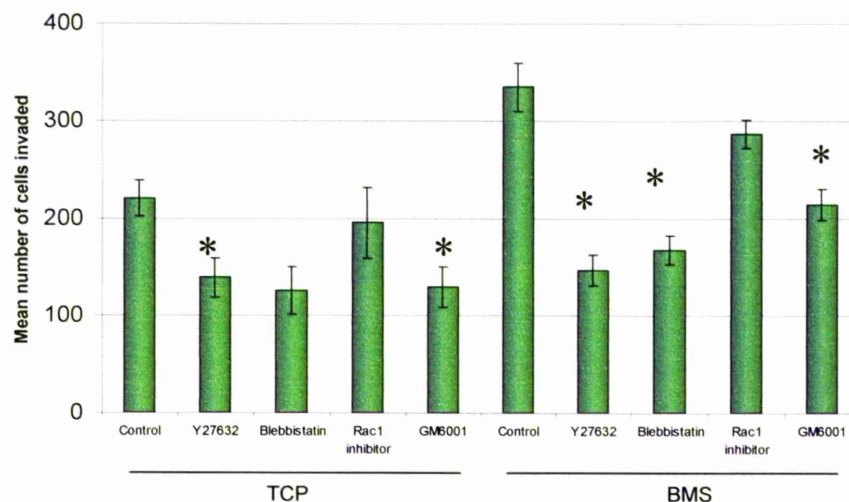


Figure 3-100: Effect of inhibitors on invasion of PC-3-GFP cells through a BMEC monolayer
 1×10^5 PC-3-GFP cells invading towards either tissue culture plastic (TCP) or bone marrow stroma (BMS) in the presence of inhibitors. PC-3 cells were seeded onto BMEC monolayers cultured on fibronectin coated Transwell chambers. Inhibitors were used at the following concentrations: Y-27632 40 μ M, blebbistatin 75 μ M, Rac1 inhibitor 75 μ M and GM6001 20 μ M. Bars show standard error (results shown as mean of 3 experiments, each experiment performed in duplicate). Asterisks indicate significance at $p < 0.05$ for both T-test and Mann-Whitney U test.

Overall the effect of all the inhibitors was to reduce migration of both PC-3 and PC-3-GFP cells through the BMEC monolayer, except for Rac 1 inhibitor which was only effective in inhibiting PC-3 cells and did not significantly inhibit PC-3-GFP cells.

3.5.6 Invasion through BMEC monolayer and basement membrane

In order to provide a more realistic simulation of cancer cell migration through the vessel wall, Transwell chambers containing a monolayer of BMEC on a layer of Matrigel were used for invasion assays. The Transwell membrane was coated with Matrigel before BMEC were seeded into the chamber and cultured for two days until they were confluent. PC-3 or PC-3-GFP cells mixed with inhibitors were added to the chamber as described in section 2.2.3.2. After 18 hours of invasion the chambers were fixed and stained using an immunocytochemical method for cytokeratins in order to identify the prostate epithelial cells.

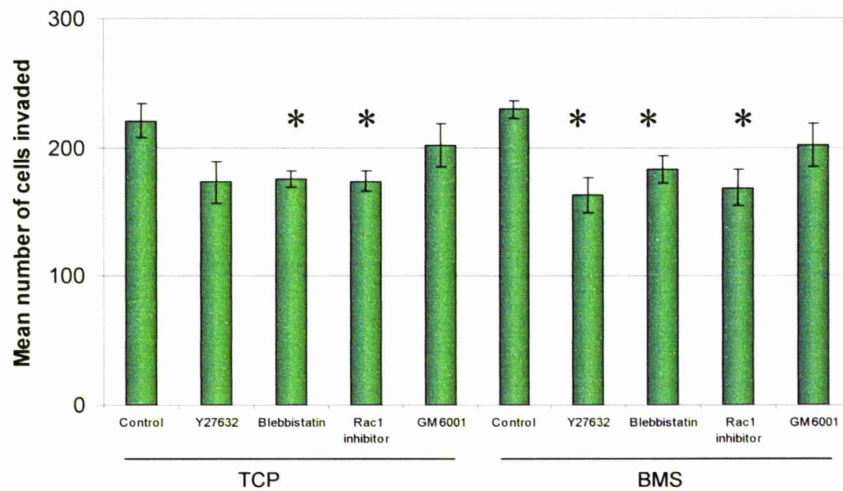


Figure 3-101: Effect of inhibitors on invasion of PC-3 cells through a confluent BMEC monolayer with an underlying Matrigel layer

1×10^5 PC-3 cells invading towards either tissue culture plastic (TCP) or bone marrow stroma (BMS) in the presence of inhibitors. PC-3 cells were seeded onto BMEC monolayers on top of Matrigel coated Transwell chambers. Inhibitors were used at the following concentrations: Y-27632 $40\mu\text{M}$, blebbistatin $75\mu\text{M}$, Rac1 inhibitor $75\mu\text{M}$ and GM6001 $20\mu\text{M}$. Bars show standard error (results shown as mean of 3 experiments, each experiment performed in duplicate). Asterisks indicate significance at $p < 0.05$ for both T-test and Mann-Whitney U test.

Figure 3-101 shows the effect of inhibitors on invasion of PC-3 cells through a barrier composed of a layer of Matrigel with a confluent monolayer of BMEC on top. Blebbistatin and Rac1 inhibitor both produced a significant inhibition in invasion (T-test and Mann-Whitney U test $p < 0.05$) towards both TCP and BMS but GM6001 did not (T-test $p = 0.4$ for TCP and $p = 0.2$ for BMS). Y-27632 significantly inhibited invasion towards BMS (T-test and Mann-Whitney U test $p < 0.05$) but not towards TCP.

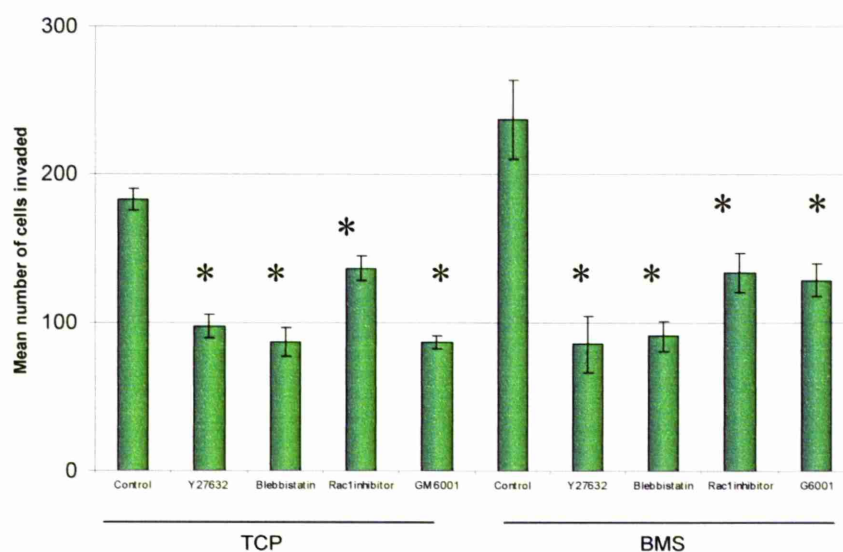


Figure 3-102: Effect of inhibitors on invasion of PC-3-GFP cells through a confluent BMEC monolayer with an underlying Matrigel layer

1×10^5 PC-3-GFP cells invading towards either tissue culture plastic (TCP) or bone marrow stroma (BMS) in the presence of inhibitors. PC-3-GFP cells were seeded onto BMEC monolayers on top of Matrigel coated Transwell chambers. Inhibitors were used at the following concentrations: Y-27632 $40\mu\text{M}$, blebbistatin $75\mu\text{M}$, Rac1 inhibitor $75\mu\text{M}$ and GM6001 $20\mu\text{M}$. Bars show standard error (results shown as mean of 3 experiments, each experiment performed in duplicate). Asterisks indicate significance at $p < 0.05$ for both T-test and Mann-Whitney U test.

Figure 3-102 shows the effect of inhibitors on invasion of PC-3-GFP cells through a barrier composed of a layer of Matrigel with a confluent monolayer of BMEC on top. All the inhibitors significantly (T-test and Mann-Whitney U test $p < 0.05$) reduced invasion towards both TCP and BMS. Compared to the mesenchymal motility inhibitors (Rac1 inhibitor and GM6001), invasion towards BMS was also reduced by the inhibitor of amoeboid motility, blebbistatin (T-test and Mann-Whitney U test $p < 0.05$).

4 Discussion

Prostate cancer is very common worldwide and the UK has one of the highest rates of mortality from this disease in the world. The main cause of morbidity and mortality among patients is metastasis and the most common site for prostate cancer metastasis is the bone marrow. Previous *in vitro* work has shown that benign prostate cells are incapable of migrating across the bone marrow endothelium, but will grow in bone marrow stromal cultures; whereas malignant prostate cells are able to cross the endothelial barrier. The mechanism of endothelial transmigration is very poorly understood. In this project we sought to develop an *in vitro* model of prostate carcinoma migration across the bone marrow endothelial barrier and to investigate this important step in prostate carcinoma metastasis to bone.

4.1 Development of the *in vitro* model

Various model systems have been described for studying cancer invasion and metastasis. Some systems assess single elements of the process such as the ability of cells to migrate using simple techniques such as the wound healing assay [111] but these techniques following migration on a 2D surface are not representative of motility and behaviour in a 3D environment [140]. While these methods are useful for assessing cell motility, they are not very representative of the *in vivo* environment and a more complex system was required. Many systems use *in vitro* invasion through basement membrane or ECM components, such as the Boyden or Transwell chamber assay in which cells migrate through a relatively thin layer of matrix. This system is useful for simulating invasion through basement membranes and/or cell monolayers. The technique is especially useful due to the ability to quantify invasion by counting the number of cells invading, and the ability to use chemoattractants in the system. A problem with the chemoattractants in this system is that, depending on the speed of diffusion, the chemoattractant concentration gradient between the two chambers may be lost within a few hours, before the end of the migration period [140]. This series of experiments were concerned with the ability of the cells to migrate in the presence of different inhibitors rather than assessing their response to different chemoattractants so this issue did not constitute a major disadvantage. Matrigel is an ECM preparation commonly used in cell invasion and migration studies. It is derived from the ECM produced by a mouse sarcoma cell line and is mainly composed of collagen type IV and laminins [140, 141]. It contains growth

factors, although its complex composition has not been fully defined [140]. These factors mean it may have effects on the behaviour of experimental cells but because of its composition it provides a good simulation of the basement membrane which made it useful for this work. Some model systems use migration through a thicker matrix which mimics the environment in solid tissues [113]. These systems are useful for studying cell behaviour in the primary tumour or in a metastasis, but do not simulate the process of migration between these sites.

The study of endothelial transmigration and interactions between endothelial and malignant cells can be done *in vitro* using co-culture model systems. The interactions between prostate carcinoma and bone marrow endothelial cells have been studied using a co-culture system in which the cells are grown in adjacent layers of collagen gel [114]. This technique has the advantage of providing the 3D environment important for simulating *in vivo* conditions and is very useful for examining angiogenesis and cell interactions in solid tumours. However, it is less useful for studying the process of endothelial transmigration. The Boyden/Transwell chamber system can be used for studying endothelial transmigration as well as basement membrane invasion, by culturing a monolayer of endothelial cells in the chamber and studying the ability of malignant cells to migrate across this layer [142]. The ability to quantify transmigration using this technique is another advantage, as is the fact that the endothelial cells would be adherent to a substrate with liquid medium on the other side, as they would be in a blood vessel *in vivo*. Other techniques involving culturing an endothelial monolayer on a substrate *in vitro* have been used by many investigators [40, 81, 143] using various techniques to study malignant cell migration across the endothelial monolayer, including real time light microscopy [143], electron microscopy [126], fixation and immunolabelling [40]. These methods can be adapted to examine endothelial transmigration under flow conditions [47]. The main advantage of these methods is the high degree of control over the experimental environment including the ability to control culture conditions and the relative ease of observing transmigration. In addition the endothelial monolayer technique provides a good *in vitro* simulation of transmigration. Some investigators have used a system that utilises umbilical vein and saphenous vein segments pinned out in perfusion chambers [116]. Although this method is useful for simulating flow conditions and also provides the endothelial cells with their native basement membrane, other supporting structures and associated cells, it uses vessels

larger than those where most transmigration would be expected to occur. It has also been shown that there are critical differences between HUVEC and bone marrow endothelial cells [13]. *Ex vivo* perfusion of the dura mater vessels allowed Glinskii *et al* (2003) [46] to visualise transmigration of DU-145 prostate carcinoma cells within the microvasculature. This technique allowed the study of migration in the small vessels through which metastasis is likely to occur, while keeping the endothelial cells within their native tissue. The thin nature of the dura mater allowed visualisation of events using fluorescent labelling and light microscopy. This method was used to good effect to study malignant cell rolling and adhesion to the endothelium. Although this technique has several advantages, it could not be easily applied to bone marrow which is a friable tissue containing small vessels which would be difficult to cannulate. In addition the relative thickness of a piece of tissue such as the dura could make high resolution imaging of the events of endothelial transmigration difficult.

A major technique for the study of metastasis is the use of animal models. Very few animals spontaneously develop prostate carcinoma, but rats and dogs both do and both have been used as models for human prostate cancer. The tumours that develop in both species are different to human disease. In dogs the tumours are androgen independent; in rats the tumours are non-metastatic, although modifications have produced rats with metastatic tumours the major sites of metastasis are the lungs and lymph nodes, rather than the bones [118]. Although mice do not spontaneously develop prostate cancer, mouse models of prostate carcinoma have been developed such as the transgenic adenocarcinoma of the mouse prostate (TRAMP) model. These mice develop locally invasive carcinoma that becomes metastatic but metastases are predominantly in the lymph nodes and lungs, in contrast to the predominant bone metastases seen in human disease. Despite this, the TRAMP model is widely used. The development of other models is still continuing but a mouse model of prostate carcinoma with bone metastases is still awaited. Although mouse models have proved very useful in studying many aspects of prostate carcinoma development and metastasis, they are not currently ideal for studying prostate carcinoma metastasis to bone. [118]. Due to the difference between these models and human disease, they are not suitable for our study. Other models use a transplantable cancer system. For studies on prostate carcinoma this most commonly utilises immunocompromised animals, often mice, and malignant human

cells that are injected into them. The host animal needs to be immunocompromised to prevent rejection and destruction of the transplanted malignant cells by the animal's immune system. Malignant cells can be injected directly into the circulation, simulating haematogenous dissemination. This approach can produce bone metastases using prostate carcinoma cells [119]; a related technique is to implant the malignant cells directly into the organ which would usually form the primary site for the tumour. One of the problems with these techniques is the lack of the tumour-stromal interactions that would occur in a spontaneous tumour [119]. These models are useful for studying metastasis but are not a suitable setting for the visualisation of endothelial transmigration of malignant cells

The technique we therefore chose for studying endothelial transmigration was the Transwell chamber system to allow quantification of transmigration, in conjunction with the endothelial monolayer system to simulate an *in vivo* endothelial barrier. Many current models of endothelial transmigration use human umbilical vein endothelial cells but these are unlikely to be representative of endothelial cells in small vessels within the bone marrow [13]. Therefore, the model used immortalised human bone marrow derived endothelial cells in conjunction with human prostate carcinoma cells derived from a bony metastasis in order to produce a more realistic *in vitro* model. The cells chosen for the model were first characterised by light and electron microscopy, immunophenotyping, and time lapse video microscopy to assess movement and behaviour.

The PC-3 cell line was originally isolated from a vertebral metastasis from a poorly differentiated prostate adenocarcinoma in a 62 year old man. They have been previously shown to bind to, and invade across a layer of bone marrow endothelium [13], as well as to grow in co-culture with bone marrow stroma [9]. They show increased invasion through a layer of Matrigel in response to bone marrow stroma compared to tissue culture plastic. They are therefore suitable for the study of metastasis to bone in tissue culture models. These cells show anchorage independent growth and are tumourigenic in mice. When originally characterised, the morphology of the cells was epithelioid and they formed loosely attached clusters of rounded cells. On SEM there were numerous microvilli on the cell membrane [127]. These morphological features are still apparent in our cells as seen by light microscopy and SEM.

The PC-3-GFP cell line is a GFP transfected variant of the prostate adenocarcinoma cell line PC-3. PC-3-GFP cells were created by transfection with a vector containing EGFP linked to a gene for Hygromycin resistance [128]. PC-3 and PC-3-GFP cells show very similar morphology and identical immunophenotypes. Our cells have an immunophenotype very similar to that reported by other investigators: published studies indicate that PC-3 cells express α_2 , α_5 , β_1 and β_4 integrins and do not express α_4 integrin. Our cells did not express α_5 -integrin, but showed the same pattern of expression of α_2 , β_1 , β_4 and α_4 integrin. Integrin expression can be affected by the confluence of cultured cells [61] which may be the reason for this discrepancy. Although PC-3 cells are reported to express both E and N-cadherins [144], our cells expressed N-cadherin but did not appear to express E-cadherin on immunofluorescent staining. N-cadherin expression in prostate epithelial cells is associated with partial or complete loss of E-cadherin expression and epithelial-mesenchymal transition. This loss of epithelial phenotype and a transition to a more invasive mesenchymal phenotype [144] is consistent with the metastatic nature of PC-3 cells. The loss of E-cadherin and expression of N-cadherin has been thought of as characteristic of cells that have undergone an EMT, however the situation appears to be more complex. The EMT may only be a transient phase in cancer invasion and metastasis, and cells which exhibit both epithelial and mesenchymal markers are known to have the ability to metastasize [110]. Culture in a 2D environment without ECM may alter the phenotype of cells compared to the phenotype exhibited by the same cells in a 3D environment or *in vivo* [145] and the differences in phenotype observed *in vitro* may be due to a combination of factors including substrate, culture media and confluence. The good agreement between expression of markers by our cells and that reported by other authors suggests that our cells are very similar in phenotype to those used in other studies.

The behaviour of the prostate cells was assessed by time lapse video microscopy. PC-3 cells form a heterogeneous population with some cells remaining relatively static and others showing almost constant migration; PC-3-GFP cells are more homogeneous and are likely to be derived from the selection of transfected PC-3 cells which were of the more motile type. Both cell lines show characteristics such as prominent membrane ruffling and numerous microvillous processes on the cell surface which have been associated with motility and invasiveness [146]. On time lapse video microscopy both cell lines were observed migrating across the substrate

and cells were able to show different modes of movement: amoeboid and fibroblastic (mesenchymal). Amoeboid movement is integrin independent and is seen in cells with weak cell-substrate adhesion. These cells have a rounded shape and are able to migrate through 3D extracellular matrices by squeezing their cell body through the matrix rather than degrading it. Mesenchymal movement is integrin dependent and cells are more firmly adherent to the substrate. They adopt a more elongated morphology and degrade the ECM when moving through it in this manner. The same PC-3 or PC-3-GFP cell could switch between modes of movement but amoeboid movement, as well as detachment from the substrate, was seen more frequently when cells were cultured in BMSCM. The proportion of cells that were motile showed little difference when cells were cultured in BMSCM compared to HAMS F12, but more of the motile cells showed amoeboid movement in BMSCM. This medium contains a higher concentration of serum plus a variety of cytokines produced by bone marrow stroma and one or more of these factors are a likely cause of the increased amoeboid movement seen by leading to altered intracellular signalling. The balance of Rac and Rho signalling is important for cell motility [147, 148] and factors in the medium may have altered this balance. Malignant cells can also be induced to switch from mesenchymal to amoeboid movement when migrating in 3D matrices by protease inhibitors that block the matrix degradation required [149]; but in these experiments cells were migrating on tissue culture plastic without a 3D matrix so factors in the medium other than protease inhibitors seem likely to have induced this change.

Synchronisation of the cell cycle of PC-3 and PC-3-GFP cells was initially attempted in the hope of achieving synchronised invasion of malignant cells through the endothelial layer. There is evidence that haematopoietic progenitor cells migrate across endothelia when in G₀/G₁ phase [150] and if this was similar for malignant cells then use of synchronised cells would enable co-culture invasion studies to be stopped at defined points in the invasion process more easily.

Unfortunately, attempts to synchronise cells by starvation or FACS sorting rendered them significantly less invasive than unsynchronised cells. The relatively harsh conditions of the starvation protocol deprived cells of serum which is essential for PC-3 cell growth, with cell survival declining after 24 hours in serum-free conditions [151]. Lipids such as the arachidonic acid precursor linoleic acid, contained in HAMS F12 medium, also seem to be important for cell survival [151].

Metabolites of arachidonic acid have been linked to invasiveness in PC-3 cells [148] and lack of these may also contribute to their lack of invasive ability following starvation. Starvation affected the ability of cells to invade through a layer of Matrigel even after 48 hours recovery in HAMS F12 with serum. Hoechst staining and FACS sorting was then used to sort cells by cell cycle phase. This avoided subjecting cells to serum starvation conditions but did require the use of the stain Hoechst 33342, which binds to nucleic acids. Although this can be used on live cells, which remain viable after staining, it produced cells with reduced invasive ability in these experiments. This was most likely to be due to toxicity of the Hoechst stain. Other methods of synchronisation involve the use of drug treatments or irradiation which may be even harsher. Mitotic shake-off techniques would allow cells to be synchronised without adverse effects but yields are low and PC-3 cells are often poorly adherent to the substrate, in addition they frequently remain rounded and poorly adherent for several hours after mitosis, reducing the accuracy of the procedure.

Although synchronisation of the cell cycle may have produced synchronised invasion, the effects of synchronisation procedures seemed to be detrimental to the cells. Therefore it was decided to use unsynchronised cells as they retained their invasive ability and the lack of pre-treatment would avoid the possibility of unwanted effects on the motility or behaviour of the cells. The variability of timing of invasion would allow cells at different points during invasion to be examined in the same fixed co-culture and the use of multiple stage positions during live invasion studies would allow multiple cells to be followed during the same experiment.

The invasive ability of PC-3 and PC-3-GFP cells, their origin from a bone metastasis and their proven ability to bind to and invade endothelium, as well as their expression of surface markers including integrins, makes them a good cell line for use in the *in vitro* endothelial transmigration model.

The second cell type needed for this model was an endothelial cell. In many studies of endothelial transmigration, endothelial cells such as HUVEC have been used, but these may not be ideal for the study of malignant transmigration. The umbilical vein is a relatively large vessel whereas transmigration is likely to occur in smaller vessels [53], and, due to the differences between endothelial cells from different sites [30], may not be representative of events during metastasis to specific organs. It is known that epithelial cells bind to endothelia from different sites with

different affinities [13], another factor which may be important in metastasis. The bone marrow endothelium is also specialised to allow the cell trafficking needed for newly formed blood cells to exit the marrow [152]. The characteristics of bone marrow endothelial cells are unlikely to be adequately replicated by HUVEC. Prostate carcinoma shows a strong tendency to spread to bone and since prostate epithelial cells adhere to bone marrow endothelial cells more avidly than to endothelial cells from other sites such as lung or HUVEC [13], this process may be better studied using bone marrow endothelial cells. BMEC [130], a cell line produced by SV40 transfection of normal primary human bone marrow endothelial cells was therefore used. These cells had been shown to have no apparent differences in morphology and phenotype from primary bone marrow endothelial cells [130].

An important first step in working with the BMEC was to provide an in vitro environment that would support their growth, but also promote the expression of the bone marrow endothelial phenotype. Initial culture of BMEC in the endothelial medium EGM-2 produced disappointing results with a high rate of cell death and reluctance to form a monolayer. Despite containing substances thought to be essential for endothelial cells in culture, such as heparin [153], as well as 15% FCS and several growth factors including VEGF (vascular endothelial growth factor), this medium appeared to be unsuitable for BMEC. These cells had been successfully cultured by other groups in a medium based on M199, with the addition of 15% FCS, heparin and endothelial cell growth supplement. Endothelial cell growth supplement is derived from bovine pituitary gland and contains a partially characterised mitogen which appears to be the active component in promoting endothelial growth [154, 155]. This medium produced good morphology and cells formed a monolayer more readily than in EGM-2, but growth was slow and unpredictable possibly due to batch to batch variation in the endothelial cell growth supplement.

It is known that endothelial cells respond and adapt to their environment; HUVEC cultured in astrocyte conditioned medium develop more extensive tight junctions than typical HUVEC [156]. Schweitzer *et al* [138] found that long term culture medium designed for bone marrow stromal cultures supported the growth of primary human bone marrow endothelial cells better than specific endothelial cell culture medium, and ascribed this effect to the higher concentration of growth factors in the long term culture medium more closely mimicking the bone marrow microenvironment. It was therefore decided to culture BMEC in medium conditioned

by cultures of normal primary human bone marrow, with the aim of providing the cells with an environment similar to that experienced by them *in vivo*, thus encouraging BMEC to express a phenotype as close as possible to normal bone marrow endothelial cells. BMEC showed good growth and morphology in this medium, appearing more spindle-shaped than in M199; similar to the spindle-shaped morphology previously reported for primary bone marrow endothelial cells [157].

This medium contained 20% serum and hydrocortisone but no additional growth factors were added before it was fed to bone marrow stromal cultures. Bone marrow is known to produce a large range of growth factors and cytokines such as macrophage colony stimulating factor, stem cell factor, interleukin-1 β (IL-1 β), IL-6, IL-7, tumour necrosis factor α (TNF- α) and transforming growth factor β [158]. A potential problem with this medium is that it was produced from bone marrow stromal cultures from several different donors. Variations in the age and health of the donor, as well as the length of time in culture, could produce variations in the types and quantities of growth factors secreted into the medium. There was likely to be variation in the BMSCM between batches and this could have affected the growth and phenotype of the BMEC. However, the BMSCM still produced the most consistent BMEC growth of all the media tested. This medium also showed evidence that it supported the phenotype of the cells as BMEC grown in BMSCM expressed VCAM-1. This is an adhesion molecule constitutively expressed by bone marrow endothelium *in vivo*, but not always expressed *in vitro* [138]. BMEC cultured in M199 did not express VCAM-1. In studies by other investigators using other immortalised human bone marrow endothelial lines, cells did not express VCAM-1 in the culture conditions used, but it could be induced by treating cells with IL-1 β [136] or TNF- α [159], both of which are produced by bone marrow stroma. The use of BMSCM for BMEC culture was therefore continued throughout the study as it produced good growth and appeared to support a similar phenotype to that seen *in vivo*.

Finding substrates for culture of BMEC which would produce good cellular morphology and be suitable for experimental work proved difficult. Although BMEC could be cultured easily in tissue culture treated plastic flasks coated with either fibronectin, an extracellular matrix glycoprotein, or attachment factor, a gelatine-based matrix, flasks were not suitable for most experimental work. BMEC could not be cultured on tissue culture treated glass or silicon wafers, and grew poorly on plain

glass coverslips; all of which were potential substrates for imaging of co-cultures. Coating these substrates with fibronectin or attachment factor did not improve growth or morphology. After testing various substrates it was found that BMEC formed a confluent monolayer on fibronectin coated quartz glass and also grew readily on Thermanox tissue culture treated plastic coated with either fibronectin or attachment factor. Primary bone marrow endothelial cells showed a similar substrate preference; with growth on tissue culture plastic and Thermanox, disorganised growth on plain glass and almost no growth on silicon wafers. Both cell types seem to be sensitive to the surface properties of their substrate. It has been shown that the adsorption of fibronectin onto substrates affects the attachment and growth of other types of endothelial cells as shown in studies using HUVEC [160]. The ability of HUVEC to attach to the substrate was affected by the availability of fibronectin cell adhesion domains. The availability of these domains was determined by the nature of the underlying surface. In this study tissue culture plastic was shown to have a high concentration of available cell binding domains on adsorbed fibronectin. Another factor found to be important was the presence of serum in the culture medium, which promoted cell attachment, probably because it contains soluble ECM components including vitronectin and fibronectin [160]. Our cells were always cultured in medium containing 20% serum, so the variation in the amount of adsorbed fibronectin and availability of binding domains is likely to be the reason for the substrate preference of these cells. Further work with these cells was done using tissue culture treated plastic, quartz glass dishes and tissue culture treated Thermanox plastic, with some immunofluorescence work done using glass coverslips. Quartz glass dishes have good optical properties and are useful culture vessels for high resolution light microscopy of either fixed or live cells. They cannot be used for electron microscopy and as BMEC did not grow on silicon wafers, the usual substrate for this, an alternative had to be found. Thermanox plastic is resistant to the chemical processing required for scanning electron microscopy, can easily be cut to the 5x5mm size required, and is suitable for BMEC culture. Therefore it was decided to use quartz glass for light microscopy and Thermanox for SEM.

Although the quartz glass bottomed dishes proved successful for light microscopy, Thermanox produced problems when used for SEM. Initial attempts to use chromium coated Thermanox held in copper sample holders in the SEM, in the same way as for silicon wafers, produced images which were severely affected by

charging artefacts. These are caused by the build up of negative charge on a specimen which is non-conductive. Areas of the specimen with a high negative charge can produce many more secondary electrons than other areas leading to abnormally high contrast; their high negative charge can also cause deflection of secondary electrons leading to the appearance of lines on the image. There are several possible solutions to these problems, including increasing the conductivity of the sample and reducing the number of electrons in the electron beam (by reducing the accelerating voltage) [134]. A combination of these methods was needed to reduce the severe charging we experienced. It was necessary to increase the sample conductivity in two ways: by mounting the Thermanox onto an aluminium stub using electrically conductive adhesive as well as coating the sample with a thicker layer of metal (8nm platinum-palladium vs 4nm chromium). The accelerating voltage was also reduced by 10 kV. These measures removed almost all of the charging artefact. While the potential resolution of the images was also reduced, this should not have had an effect at the relatively low magnification levels needed to examine the cell-cell interactions being studied.

After finding suitable culture media and substrates for the cells, BMEC were compared with primary cells to further assess their suitability as a model for the bone marrow endothelium. Although there were some differences in morphology, both cell types showed a similar substrate preference, similar immunophenotype and behaviour on time lapse video microscopy. When cultured in M199, BMEC formed a disorganised monolayer as they became more confluent, and showed relatively fast movement across the substrate. When cultured in BMSCM they formed an organised monolayer and showed only slow movement which was similar to the almost totally static primary cells. Immunophenotype has been shown to vary between endothelial cell lines in culture and primary cells [161]. Primary cells can be difficult to culture and in these experiments, cells did not achieve confluence. So cell-cell junctional proteins may not have been expressed as they would in a confluent culture, making this comparison less useful. However, the expression of VCAM-1 by both primary cells and BMEC when cultured in BMSCM supports the hypothesis that this medium encourages cells to express a phenotype similar to that seen *in vivo*. Of the cell-cell junction proteins tested, ZO-1 appeared to be the most reliable tight junction marker in our system. It produced irregular linear staining of cell-cell junctions, which may be due to the overlapping cell-cell junctions of endothelial cells previously reported,

and also seen on SEM. Claudin-5 has been reported as being specific to endothelial cells [28], but it could not be demonstrated on either endothelial cell type in this study. Although it is known to be expressed in endothelia of the brain, lung and kidney, it is not expressed in all segments of blood vessels and expression by bone marrow endothelial cells has not been previously investigated [135]. It may be the case that bone marrow endothelial cells do not express claudin-5. N-cadherin could not be demonstrated on BMEC in this study, although it is expressed by other endothelial cells. There were also differences in integrin expression with primary cells expressing integrins α_5 and β_1 but BMEC showing no expression of these markers; however this may be due to the BMEC forming confluent monolayers while the primary cells did not. This may also explain why BMEC expressed ZO-2 at some cell-cell junctions while primary cells did not express it. Variations in marker expression can be demonstrated between different cell lines, cell lines and primary cells, and between the same cells in different culture conditions [161]. These factors may explain the discrepancies in labelling between BMEC and primary cells. However, the difficulties encountered in labelling may mean that low levels of marker expression could not be accurately detected or localised. In the current studies, endothelial cells proved difficult to label using immunofluorescent techniques. This appeared to be due to a combination of autofluorescence and non-specific labelling. It was thought that the presence of phenol red in the medium used to culture these cells contributed to the autofluorescence, but a phenol red free version of this medium was not available. Autofluorescence was most intense in the red and green parts of the spectrum, but even after using far red or blue fluorophores to label the cells, the results were still disappointing with prominent non-specific staining, particularly within what appeared to be intracytoplasmic vesicles. The labelling protocols used had been used successfully with other adherent cells but despite trialling numerous different blocking methods, antibody concentrations and labelling protocols, immunofluorescent labelling of endothelial cells continued to be problematic. It was decided therefore to concentrate on prostate cell motility during endothelial transmigration, rather than the fate of endothelial junctional proteins during the process. For this reason the assessment of endothelial cell movement and behaviour became more important

Both BMEC and primary cells exhibited similar behaviour when observed by time lapse video microscopy; both were mostly static, with any cell movement being

slow and over short distances. Cells spread on the substrate rapidly after division. As confluence increased, cells formed a monolayer of flattened, spindle-shaped cells orientated alongside each other. Both cell types showed variable membrane blebbing, with blebs sometimes detaching from cells and floating in the medium or attaching to the substrate. This blebbing was rarely a prelude to apoptosis, although occasional cells were seen to undergo apoptosis in culture. The reason for the blebbing shown by these cells is unknown, although the use of detached membrane blebs as a method of paracrine signalling between endothelial cells has been described [162] so blebbing may be a normal function of these endothelial cells.

On SEM BMEC formed a discontinuous monolayer with smooth-edged gaps between cells, these were not due to cracking during the drying process but were more likely to be due to exaggeration of pre-existing gaps by shrinkage during drying. These gaps may be due to cells being fixed before achieving full confluence, or due to the ability of cells to open and close their cell-cell junctions as noted on time lapse video microscopy. The cell-cell junctions observed by SEM showed overlapping of the cell edges and short processes extending from one cell onto the plasma membrane of the adjacent cell, giving the junction a "saw-toothed" appearance which is consistent with the irregular linear labelling of ZO-1 seen in confluent BMEC cultures.

The similarity between the primary cells and BMEC supports the use of this cell line as a model for the bone marrow endothelium *in vivo*. The good growth, morphology and expression of appropriate markers in BMSCM show that this medium is suitable for maintaining a phenotype similar to that seen *in vivo*, thus providing a good model system for endothelial transmigration studies.

Co-cultures of human bone marrow endothelial cells and human prostate carcinoma cells derived from a vertebral metastasis were used with culture medium conditioned by bone marrow stroma to support the bone marrow phenotype of the endothelial cells. Although these studies sought to mimic the process of endothelial transmigration that occurs *in vivo* they could not completely mimic the environment *in vivo* as endothelial binding and invasion occur under flow conditions. There are pericytes associated with the endothelium, and the extracellular matrix and microenvironment are more complex in a living patient [66]. However, in the model used the conditions provided a controllable and convenient simulation utilising human cells. Having chosen and characterised cell lines, determined conditions for

endothelial cell growth and decided on the most appropriate techniques for modelling endothelial transmigration, co-culture experiments were initiated. For the first studies, invasion was observed in the time lapse video microscopy unit. The time lapse video microscopy unit allowed capture of images every 20 seconds across a relatively wide field of view, so numerous cells could be followed and timing of events accurately judged. The microscope in this unit was not confocal and had no fluorescence facilities so z plane images could not be collected and cells could not be identified by fluorescence. The stage was not motorised so only one field of view could be observed per experiment. However, the advantages of this system were its wide field of view, frequent image capture, lack of damaging effects on cells and the relatively small file sizes of the data generated, making data analysis rapid, even for acquisition periods of up to 7 days. Initial experiments showed that over 90% of PC-3 and PC-3-GFP cells completed endothelial transmigration within 24 hours and mean time to invade through the endothelial monolayer was 4 hours 9 minutes for PC-3 cells and 4 hours 51 minutes for PC-3-GFP cells. These times were similar to those found previously showing PC-3-GFP cells migrated through an endothelial layer in 3 hours 52 minutes [17] and melanoma cells in a median time of 5 hours [73]. These results suggested that our model provided a realistic and practical *in vitro* environment in which to study transmigration.

4.2 Migration of prostate carcinoma cells through bone marrow endothelium

Further investigation of endothelial transmigration continued using time lapse video microscopy as well as confocal microscopy. Studies using the confocal microscope allowed collection of fluorescence and 3 dimensional data over time, but damaging effects of UV radiation on the cells limited the number of time points that could be captured and the large data files generated were difficult to process. The two techniques were complementary, with video time lapse giving a broad overview and allowing confocal studies to be refined and targeted to examine in detail the events occurring during particular parts of the invasion process.

The behaviour of the malignant prostate cell lines PC-3 and PC-3-GFP was compared with that of the non-tumourigenic benign prostate cell line PNT2-C2. When PNT2-C2 cells were added to a BMEC monolayer they flattened rapidly on top of the endothelium and did not appear to invade. This is in agreement with

previous work showing that PNT2-C2 cells bind to, but do not invade through, a layer of endothelial cells [13]. PNT2-C2 cells also show very low levels of invasion through Matrigel compared to PC-3 cells. The two cell lines were cultured in different media, with PNT2-C2 cells cultured in medium based on RPMI which does not contain fatty acids and PC-3 cells cultured in medium based on HAMS F12 which contains fatty acids. Fatty acids seem to be important for the invasive ability of PC-3 cells [148] but culturing PNT2-C2 cells in HAMS F12 did not lead to an increase in their invasion through Matrigel towards BMS. This is also consistent with the observed non-invasive phenotype of PNT2-C2 cells. PC-3 and PC-3-GFP cells were both able to invade through the endothelial monolayer. PC-3 cells completed invasion across the BMEC layer in a mean time of 249 minutes and PC-3-GFP cells in 291 minutes. However the range of times taken by different cells to complete invasion suggests that at least some of the cells are able to complete the invasion process more quickly than previously thought; PC-3 cells were able to complete invasion in as little as 35 minutes and PC-3-GFP cells in 50 minutes. Studies using melanoma cells have shown that around 15% of melanoma cells seeded on an endothelial layer have migrated and spread on the substrate after 1 hour [72], increasing to around 60% after 6 hours. The time taken may include a variable phase between binding to the endothelium and initiating invasion, as well as differences in the time taken for the actual invasion process. It is known that the time taken for transmigration of malignant cells can vary from minutes up to 48 hours depending on the organ-specific endothelium being traversed and the tumour cell type; this may be due to the affinity of the malignant cell for the secondary site [163].

Previous work using prostate cells has shown that benign cells are able to bind to endothelial monolayers but are not able to invade through them [13, 126]. Other investigators have shown that non-metastatic tumour cells show little to no ability to migrate through endothelial layers compared to metastatic tumour cells [72] and this suggests that the ability to undergo endothelial transmigration is acquired after the initial malignant transformation for at least some tumour types.

Malignant cells appear to bind to the endothelium preferentially at endothelial cell-cell junctions [17, 45, 82], a phenomenon also observed in neutrophils [164]. This preferential binding may facilitate transmigration as malignant cells have so far been observed almost exclusively using the paracellular route (between adjacent endothelial cells), although there is evidence that leukocytes can also use the

transcellular route [43]. A single study, using electron microscopy, has suggested that melanoma cells may be able to use the transcellular route [165], although the results in this paper are less convincing for melanoma cells than for the leukaemia cells also studied. We did not observe any prostate carcinoma cells apparently using the transcellular route, although we did not specifically search for this. In our experiments many prostate carcinoma cells migrated through the endothelium in the location where they first bound to it but some migrated across the surface of the endothelium, over several endothelial junctions, before undergoing transmigration. The reason for this is unknown but may relate to surface markers expressed by endothelial or prostate cells allowing prostate cells to recognise junctional areas or signal to endothelial cells. It has been shown that contact with the endothelium induced an increase in N-cadherin expression by melanoma cells, as well as a change in its distribution on the cell surface, and that these changes facilitated endothelial transmigration [166]. Lung cancer cells can induce endothelial expression of E-selectin [167]. Contact with the endothelium may stimulate the prostate cell or endothelial cell to express surface markers or genes necessary for transmigration which may be why the cells do not undergo transmigration immediately. Under flow conditions these interactions may occur during rolling.

In previous reports of the endothelial transmigration process [17, 73], an early event is blebbing of the malignant cell. This was observed in around one third of invading cells on time lapse video microscopy, but because of the resolution of the technique, the presence of blebbing could not be excluded in other invading cells. It was also seen frequently on confocal microscopy transmigration studies. Non-invasive PNT2-C2 cells did not show any evidence of blebbing. Blebbing was also observed on SEM and confocal invasion studies, both in cells during the process of transmigration, and in some cells as they migrated across the surface of the endothelium prior to invasion. Some cells exhibited prominent blebbing for several hours prior to invasion through the endothelium. Blebbing can be a sign of impending apoptosis but had also been previously associated with cell spreading and locomotion [168]. In this case it is more likely to reflect the adoption of amoeboid motility requiring rapid membrane protrusion [101] and re-organisation of the cytoskeleton [169] due to the shape changes required as the cell invades through the endothelium. Blebbing has been observed in transmigrating melanoma cells

previously [72, 73] but had not been associated with amoeboid motility in this context.

The next stage of transmigration includes extension of a pseudopodium through the endothelial layer with associated endothelial retraction. Confocal imaging demonstrated cells extending pseudopodia under the endothelial layer and the rounded portion of the cell body above the monolayer reducing in size as the cell migrated through and spread on the substrate. Pseudopodia were well demonstrated by SEM, where they could clearly be seen extending into BMEC cell-cell junctions and underneath BMEC. Pseudopodial extension has been observed as an early stage of transmigration in melanoma cells [72, 73] and prostate cancer cells [18]. A feature of transmigration observed in many cell types seems to be that malignant cells maintain membrane contact with endothelial cells during transmigration, suggesting that there is some communication between the cells during the process [17, 72, 84]. In a study of transmigrating colon cancer cells, electron microscopy showed areas of cell-cell adhesion between malignant and endothelial cells, although specialised junctional structures were not identified [170]. During melanoma transmigration through HUVEC, melanoma cells showed blebbing, which was prominent on the basal surface of the cell where it was in contact with the endothelial cell and endothelial actin filament bundles frequently terminated near the site of these blebs suggesting active interactions between the cells [72]. This study also noted continued membrane contact between melanoma and HUVEC during transmigration. A study using PC-3 cells and human lung microvascular cells also showed that endothelial actin filaments concentrated around migrating PC-3 cells and that contact was maintained between the two cell types during transmigration [18]. We observed continued membrane contact between BMEC and prostate carcinoma cells during transmigration, even where there was some endothelial cell retraction, in agreement with other authors [18, 72]. Endothelial retraction was not always seen; this may be related to the confluence of the BMEC monolayer prior to addition of malignant cells, with tightly confluent BMEC monolayers unable to show prominent retraction even when malignant cells were migrating through. Endothelial retraction has been observed during transmigration of breast, lung and colon carcinoma cells [163] but it does not seem to be necessary for a visible gap to be present for transmigration to occur.

In the final stage of transmigration, after invasion, malignant cells could be observed spreading and migrating on the substrate underneath the endothelial cells and causing both single and sheets of endothelial cells to move. The elongated morphology of the prostate carcinoma cells during this phase of transmigration suggests a switch to a mesenchymal mode of motility. A similar morphological change from rounded to flattened and elongated has been observed in transmigrating melanoma cells [72] and suggests these cells are using similar mechanisms. A spindle like shape was also observed in a variety of different malignant cells by Bauer *et al* (2007) [84] when these cells were migrating through a collagen gel underlying an endothelial monolayer which the malignant cells had just crossed. Ovarian carcinoma cells used integrins and proteinase enzymes including MMP2 to migrate through an endothelial basement membrane [171], suggesting that they were using mesenchymal motility. These results suggest that many tumour cell types use mesenchymal motility during the later stages of transmigration, when interacting with the vascular basement membrane.

Although there have been previous reports of solid tumour cells inducing endothelial apoptosis on contact [172], an extensive study with 45 malignant cell types did not observe this effect with any of the cells tested [84]. In the current study endothelial apoptosis did not seem to play a major role in the transmigration of prostate carcinoma cells across the bone marrow endothelium. Only one PC-3-GFP cell appeared to induce apoptosis on contact with BMEC, and this may have been a coincidence since BMEC show spontaneous apoptosis in culture. The lack of an increase in endothelial permeability to dextran in the presence of PC-3 cells also suggests that endothelial apoptosis and disruption does not play a major role in transmigration. It is possible that endothelial apoptosis occurs as a result of endothelial retraction with loss of cell-cell contact and detachment from the ECM leading to apoptosis, as suggested by Heyder *et al* (2002) [143]. Their study showed that endothelial cell apoptosis could be induced by the transmigration of bladder carcinoma spheroids composed of several malignant cells [143]. It is possible that single malignant cells migrating through an endothelium rarely induce apoptosis, while a larger malignant spheroid causes more endothelial disruption and detachment.

The observations on the morphology of endothelial transmigration of prostate carcinoma cells are in agreement with those described by Wang *et al* (2005) [18] on

the transmigration of PC-3 cells through a monolayer of human lung microvascular endothelial cells. These findings are also very similar to those described by Voura *et al* [73] for melanoma transmigration. This suggests that different types of malignant cell can use common mechanisms for endothelial transmigration and shows that the different stages of transmigration described by Voura *et al* [73] can be observed in more than one malignant cell type. The observation that endothelial intracellular calcium rises during transmigration of prostate cancer, melanoma [87] and breast cancer cells [81] also supports the theory that common mechanisms are being used, as well as supporting the idea of tumour cell-endothelial interactions. The fact that leukocytes also induce rises in endothelial calcium [39, 69] suggests that some of these mechanisms may be shared with them.

The techniques used in these studies allowed the observation of morphology and behaviour during endothelial transmigration using microscopy, or quantification of transmigration using Transwell chamber assays. Transwell membranes fixed during migration assays have been used for electron microscopy [142] and fluorescence [173] studies. Being able to observe cells as they migrated through Transwell chambers, combined with quantifying cell invasion, would allow better correlation of morphological changes with invasive ability. Transwell chambers are designed to be used in plastic 24 well plates where the Transwell is suspended in the well and there is space for culture medium with or without chemoattractants under the base of the Transwell. Experiments were set up in plastic plates and cells observed using time lapse confocal microscopy but results were very poor due to heating and cooling of the plastic causing shifts in the field of view. Glass bottomed 24 well plates provided superior optical qualities but the wells were a different height to those in the equivalent plastic plate necessitating the development of an adaptor to raise the height of the 24 well plate so that Transwells would fit.

The use of this adaptor allowed images of cells migrating through Transwell chambers to be obtained. Unfortunately the distance between the objective and the Transwell chamber membrane meant that a x20 objective was the highest power that could be used, as the higher power objectives could not focus at the distance required. This meant that fine details could not be obtained. The large vertical distance needed to image the whole barrier also meant that high resolution in the vertical plane was not possible as the large number of vertical planes would have exposed the cells to high levels of light which would have damaged them. Despite

these problems, PC-3-GFP cells were observed invading through a Transwell chamber. With further work on the system to improve light sensitivity, allowing less light to be used for imaging, and higher magnification, this system could provide more detailed information on morphology as well as quantification of invasion.

The ability of cells to migrate is essential for cancer metastasis. During time lapse video microscopy studies PC-3 and PC-3-GFP cells had been observed using both mesenchymal and amoeboid motility during endothelial transmigration and migration on tissue culture plastic. Although the use of mesenchymal motility to invade tissues by malignant epithelial cells has been studied for several decades, it is only more recently that amoeboid motility has been studied in this cell type. Plasma membrane blebbing and cortical distribution of actin was described by Voura *et al* [72] during melanoma cell migration across endothelial monolayers, but this was not at the time linked with amoeboid type motility. The current studies aimed to learn more about cell motility during endothelial transmigration by observing the effects of motility inhibitors on PC-3 and PC-3-GFP cells and their ability to migrate through the endothelial layer and a simulated basement membrane.

As the PC-3 and PC-3-GFP cells were spontaneously motile in culture, initial experiments studied the effects of different inhibitors on their motility and behaviour on a 2D substrate. Cells migrated on tissue culture plastic in the absence of an extracellular matrix. In this environment the enzyme inhibitor GM6001 had no visible effect on cell behaviour or motility. The amoeboid motility inhibitor Y-27632 had similar effects on both PC-3 and PC-3-GFP cells, reducing motility overall and leading to the apparent inability of cells to retract their tails. ROCK [97] and Myosin II [98] are involved in the mechanism of rear detachment, which would explain the inability of treated cells to detach their tails. Cells developed an elongated morphology more like that seen in mesenchymal motility than the rounded appearance associated with amoeboid motility. This elongated morphology with Y-27632 treatment of PC-3 cells was also noted by Somlyo *et al* [174]. Some prostate carcinoma cells continued to attempt to migrate and adopted a morphology with a broad, crescentic leading edge; this morphology was also observed in studies with the highly invasive MDA-MB231 breast carcinoma cells treated with Y-27632 [105]; untreated MDA-MB231 cells were observed using both amoeboid and mesenchymal motility in this study [105]. The balance between Rac and ROCK activity has been suggested to be important in determining cell motility [92] and the use of the ROCK

inhibitor Y-27632 may produce a shift towards mesenchymal motility and morphology in these cells. It has previously been shown that PC-3 cells with inactive RhoC (an upstream signalling molecule activating ROCK) showed an increase in Rac1 expression and activity [175]. This may manifest as the morphological changes seen in these cells. The second amoeboid motility inhibitor, blebbistatin, produced similar changes to those seen with Y-27632; cells showed a more mesenchymal morphology and reduced migration. Blebbistatin, unlike Y-27632, had an effect on the ability of the cells to divide. Both PC-3 and PC-3-GFP cells were unable to complete cytokinesis and attempts at mitosis usually produced a single large binucleate cell. This inhibition of cytokinesis is a known effect of blebbistatin [176]. Although the majority of spontaneously motile PC-3 and PC-3-GFP cells appeared to be using mesenchymal motility when migrating on a 2D substrate in the absence of an extracellular matrix, the effect of Y-27632 and blebbistatin indicate that pathways associated with amoeboid motility are active in these cells.

The mesenchymal motility inhibitor Rac1 inhibitor had different effects on PC-3 and PC-3-GFP cells. PC-3 cells showed reduced motility and adopted a flattened, epithelioid morphology. In contrast, PC-3-GFP cells continued to migrate in the same way as they had in the absence of any inhibitors, with cells showing amoeboid and what appeared to be mesenchymal motility. This suggests that PC-3-GFP cells are less dependent on Rac1 in order to be motile, and may be able to produce mesenchymal movement in the presence of Rac1 inhibitor. The inhibition of movement of PC-3 cells with both amoeboid and mesenchymal motility inhibitors shows that pathways involved in both types of motility are active in these cells and contribute to their ability to migrate. It also shows that under these experimental conditions, cells will not necessarily continue to migrate by altering their pattern of motility in the presence of an inhibitor, although under different environmental conditions this can occur [99].

The signalling pathways associated with cell motility are complex and ROCK and myosin II do have a role in mesenchymal motility. The intrinsic activity of different pathways within the cells is also important; in more aggressive breast carcinoma cell lines Rac1 inhibition leads to increased Rho activity and increased migration while Rac1 inhibition of less aggressive breast carcinoma cells leads to a reduction in migration [106]. PC-3-GFP cells were more motile than PC-3 cells when cultured in HAMS F12 and a greater proportion of cells showed amoeboid

movement, suggesting that in the production of the PC-3-GFP cell line, a population of cells with a different balance of motility related signalling pathways was produced. The difference in response to Rac1 inhibitor supports this.

Although the ability of cells to migrate across substrates in 2D systems is a poor predictor of their ability to invade in 3D systems [105], these studies allowed an assessment of the possible effects of the inhibitors in 3D systems, the speed of onset of inhibitors, the effects on mitosis and cell survival/apoptosis, and the duration of inhibitor action after washout. Washout studies indicated that cells rapidly recovered from the effects of inhibitors after washout and that pre-treatment of PC-3 and PC-3-GFP cells before adding them to BMEC would not be feasible. Although this would reduce the ability of the system to study the effects of the inhibitors on the prostate cells' motility and invasiveness without affecting the BMEC, it would more closely replicate an *in vivo* system where both malignant cells and endothelial cells would be exposed to a putative anti-metastatic drug.

The effects of inhibitors on the BMEC monolayer were studied; there was no effect on morphology or behaviour with any of the inhibitors and tight junctions did not show any changes in ZO-1 labelling. Although some studies have found that ROCK inhibitors such as Y-27632 may enhance the barrier function of cell layers [108], none of the inhibitors had any effect on the permeability of a BMEC monolayer to dextran.

The Transwell chamber system was used to provide a quantitative system for studying invasion of malignant prostate cells through a simulated basement membrane (Matrigel). Overall the mesenchymal motility inhibitors produced the greatest inhibition of invasion through the Matrigel layer for both PC-3 and PC-3-GFP cells. PC-3 cells are known to have high Rac1 activity compared to non-tumourigenic prostate cell lines [177] and this is likely to contribute to their tumourigenicity by increasing proliferation and migration. Rac1 inhibitor reduced invasion through Matrigel by both cell lines, in agreement with previous findings for PC-3 cells [177].

Both amoeboid motility inhibitors showed some ability to inhibit invasion at higher concentrations, although PC-3 cells seemed to be slightly more vulnerable to their effects than PC-3-GFP cells did. Other studies have shown that blebbistatin (a highly specific inhibitor of myosin II activity) treated pancreatic adenocarcinoma cells also showed reduced invasion through Matrigel. This appeared to be due to an

effect on the cytoskeleton rather than any alterations in adhesiveness to the substrate or matrix metalloproteinase activity [176]. Myosin II is important for force generation during cell motility as is ROCK [100] and force generation is an important factor in allowing invasion into and through the ECM. When ROCK was inhibited in breast carcinoma cells they were able to adhere to collagen and spread on the surface, but did not invade into it. These cells were shown to secrete only low levels of protease and invade a collagen gel in the presence of broad spectrum proteinase inhibitors, suggesting that ROCK dependent motility was being used [100].

Although some malignant cells are able to use amoeboid motility to migrate through an extracellular matrix [100], our experiments using PC-3 and PC-3-GFP cells showed that these cells seemed to use mesenchymal motility preferentially for this process. The interaction between the cell and the surrounding matrix may influence the type of motility used and this may provide an explanation. There is evidence that other malignant epithelial cells preferentially use mesenchymal motility to migrate through extracellular matrices. Human breast cancer cells MDA-MB231 invading through collagen I gels were inhibited by a cocktail of MMP inhibitors but not by Y-27632. These cells had been observed showing both mesenchymal and amoeboid movement when invading collagen gels in the absence of any inhibitors [105]. Human ovarian carcinoma cells also appeared to use mesenchymal motility to invade endothelial ECM as this process could be inhibited by MMP inhibitors and integrin α_v blockers [171]. However, in other experiments, some cells preferentially use amoeboid motility to invade through Matrigel [178]. Some of these differences may be due to the intrinsic balance between signalling pathways within the cells but the nature of the matrix may also play a role in determining the type of cell motility. Matrigel has important differences from connective tissue matrix *in vivo*, endogenous matrix is crosslinked but the extracted Matrigel used *in vitro* is not [107].

Endothelial transmigration was studied by culturing a monolayer of BMEC on fibronectin, adding prostate cells and observing events using time lapse microscopy. In the absence of inhibitors, PC-3 and PC-3-GFP cells remained rounded on top of the BMEC layer until invasion through the monolayer occurred. Around a third of prostate cells showed prominent blebbing prior to transmigration. Migration of PC-3 and PC-3-GFP cells across the BMEC monolayer was inhibited

by the amoeboid motility inhibitors Y-27632 and blebbistatin. Blebbing of prostate cells was not seen and instead of remaining rounded, prostate cells flattened on top of the BMEC layer and formed small groups. This behaviour was very similar to that exhibited by the non-tumourigenic PNT2-C2 prostate epithelial cell line which does not invade through BMEC monolayers.

Previous studies have shown that malignant cells with high levels of ROCK activity show increased aggressiveness and ability to metastasize [103, 108] and the current results are in line with this, showing that in vitro assessment of metastatic ability, as assessed by migration across an endothelial barrier, can be reduced by inhibition of ROCK using Y-27632. Blebbistatin, another inhibitor of amoeboid motility which acts by inhibiting myosin II, also shows the same effect on endothelial transmigration suggesting that ROCK activity is not the only determinant of ability to migrate through an endothelial monolayer.

It has been shown that cells using amoeboid motility can move through extracellular matrices by pushing matrix fibres such as collagen aside and squeezing through the gaps [100]. ROCK activity has been shown to be important for force generation during this process [100] and this may also be important for the ability of malignant cells to migrate between endothelial cells. Another possibility is that enhancement of the endothelial barrier function by Y-27632 [179] is involved in preventing endothelial transmigration, even though an effect was not seen with dextran. Effects of inhibitors on the endothelial cell layer may be important. Using brain microvascular endothelial cells, Li et al (2006) [180] showed that using endothelial cells lacking active ROCK prevented transmigration of small cell lung carcinoma cells and that prevention of disassembly of endothelial tight junctions was an important factor. It was thought that lack of ROCK prevented cytoskeletal alterations associated with tight junction opening. A newer ROCK inhibitor, Wf-536, has been shown to inhibit migration of HT1080 sarcoma cells across a monolayer of ECV304 cells (a spontaneously transformed HUVEC cell line). Wf-536 inhibited spontaneous motility of HT1080 cells at a concentration of 10 μ M; invasion through Matrigel at 1 μ M and migration across ECV304 monolayer at 0.3 μ M. It reduced dextran leakage through the ECV304 monolayer induced by HGF (hepatocyte growth factor/scatter factor) and HT1080 conditioned medium. Wf-536 therefore, enhanced the barrier function of the ECV304 monolayer as well as reducing migration of HT1080 cells. This was interpreted as showing that the effects of

ROCK inhibitor on both endothelial cells and HT1080 cells contributed to the reduction in transmigration [179]. Although it is not possible to be certain if the inhibition of endothelial transmigration in the current study is due to an effect on malignant prostate cells, BMEC or both cell lines, demonstration of this inhibition could be important for future development of antimetastatic therapy. The reduction in transmigration with blebbistatin may be due to a similar effect arising from the action of blebbistatin on a different part of the same pathway. There is evidence that ROCK signalling in endothelial cells is needed for leukocyte migration [163] and it may be that active ROCK is required in both endothelial and migrating cells for transmigration to occur. Inhibitors of amoeboid motility have a marked effect on PC-3 and PC-3-GFP cell motility in a 2D system and although this is not predictive of their response in other environments, it shows the potential of the inhibitors to affect the cells.

Mesenchymal motility inhibitors showed no ability to reduce endothelial transmigration by PC-3 and PC-3-GFP cells, suggesting that matrix metalloproteinases and Rac1 activity are not needed for this process. Despite the fact that Rac1 inhibitor was able to reduce movement and promote the development of an epithelioid morphology and behaviour in PC-3 cells on a 2D substrate, it appeared to have no effect on them in the 3D system and environment provided by a BMEC monolayer. These results suggest that factors in the environment of the BMEC transmigration experiment promote Rac1 independent motility in PC-3 cells.

The lack of activity of GM6001 in reducing endothelial transmigration of the prostate cells is consistent with previous findings that a broad spectrum MMP inhibitor did not affect the extravasation of melanoma cells in a mouse model [181]. In a study also using PC-3 cells and the BMEC cell line, Sequeira *et al* (2008) [178] used interfering shRNA to downregulate Rac and Rho GTPases in PC-3 cells and assess their ability to migrate through Matrigel or BMEC layers. These experiments avoided the potential effects of inhibitors on the BMEC layer. They found that downregulation of Rac1 GTPase had little effect on PC-3 cell invasion through Matrigel and thought that the cells had switched to amoeboid motility to continue invading. Downregulation of Rac1 GTPase did reduce migration through the BMEC layer. In contrast, downregulation of RhoC GTPase reduced migration through Matrigel but not through the BMEC monolayer. In an endothelial transmigration experiment, C3 exotransferase, an inhibitor of RhoA, RhoB and RhoC was not found

to inhibit transmigration. These results show effects which are the opposite of ours, with inhibition of mesenchymal motility reducing endothelial transmigration and inhibition of amoeboid motility reducing invasion through Matrigel. However, the situation is more complex: in our experiments we used a ROCK inhibitor which would be expected to reduce downstream signalling of RhoA and RhoC simultaneously, whereas Sequeira *et al* used shRNA to inhibit RhoA and RhoC separately. They found that inhibition of RhoA alone caused an increase in the ability of PC-3 cells to invade Matrigel but had no effect on endothelial transmigration. They also found that inhibition of RhoC was associated with upregulation of RhoA by 1.6 fold and Rac1 by 4 fold, which may represent a mechanism used by the PC-3 cells to continue migration in the presence of RhoC inhibition. An increase in RhoA after RhoC siRNA knockdown was also observed by Wang *et al* in hepatocellular carcinoma cells [182]. From experiments by Sequeira *et al* [178] it seems that Rac1 is essential for endothelial transmigration but Rho is not, and RhoA inhibits Matrigel invasion. Although RhoC appears to promote Matrigel invasion as its inhibition caused a reduction in invasion, this may also be due to the upregulation of RhoA seen after RhoC inhibition. These experiments again show the importance of the balance between different pathways in the regulation of motility.

The reasons for the discrepancy between our results and those of Sequeira *et al* [178] are uncertain. In our experiments the use of inhibitors in the culture medium would have lead to potential effects on the BMEC monolayer, and although no changes were shown in morphology, behaviour, tight junction staining and permeability to dextran in the presence of inhibitors or PC-3 cells, the presence of an effect on transmigration independent of monolayer permeability to dextran cannot be ruled out. As the endothelial layer seems to re-form over migrated PC-3 cells in our current system and that of Voura *et al* [73], there may be no significant increased permeability. We also used bone marrow stroma as a chemoattractant while Sequeira *et al* did not use a chemoattractant. It is possible that the growth factors or fats produced by the BMS produced an alteration in the mode of motility in the PC-3 cells, or in the behaviour of the BMEC leading to different behaviour in the presence of inhibitors. The results from the Matrigel experiments are also subject to the potential effects of BMS on the PC-3 cells. Although the current invasion and transmigration experiments in Transwell chambers were carried out in serum-free medium, BMSCM appeared to promote amoeboid motility in PC-3 and PC-3-GFP

cells in 2D culture and the BMS may have had a similar effect. We also used Transwell chambers which we coated using diluted Matrigel and this may have lead to slightly different matrix properties which could affect cell motility. Another source of differences could be the effects of Y-27632. The mechanism of action of this inhibitor has not been fully characterised and it seems to inhibit ROCK I and ROCK II to different degrees depending on the cell type and the environment the cell is in [183].

Transwell experiments using BMEC monolayers presented additional problems, as in this system, BMEC did not grow on uncoated Transwell chamber membranes so these experiments had to be performed using fibronectin or Matrigel to coat the membrane before BMEC could be cultured. This meant that some form of ECM was always present and it was not possible to quantify the effect of inhibitors on migration through BMEC alone. It was also difficult to be sure that the BMEC monolayer was confluent in the Transwell due to the difficulty of seeing the monolayer, and the fact that only the centre of the chamber was visible using the microscope. In experiments using Matrigel, BMEC also migrated through the Matrigel, possibly due to its known effects of promoting tube formation in endothelial cells [141], and could be seen as unstained cells on the underside of the Transwell membrane after staining. These problems may contribute to a relatively low level of inhibition by amoeboid motility inhibitors compared to what might be expected based on the results of the time lapse video microscopy experiments. Further problems with experiments involving BMEC and inhibitors could derive from the effect of inhibitors on BMEC; Rho and Rac are both involved in endothelial cell migration and angiogenesis, and Rac is important in regulation of the capillary endothelial barrier function [184].

4.2.1.1 Overview of migration

Observation of endothelial transmigration showed that PC-3 and PC-3-GFP cells appeared to switch between mesenchymal and amoeboid motility during the migration process. Switching between types of motility can be induced by blocking one mode, for example, blocking proteolysis can cause cells to switch to amoeboid motility [93, 149]. Conditions within the microenvironment, including interactions with endothelial cells, could also induce changes in the type of motility and could be responsible for the observed alterations in cellular morphology and movement. A

model of invasion, based on the development of tumour microenvironments that induce transient gene expression patterns favouring invasion and metastasis in the adjacent cells, has been proposed by Wang et al (2005) [95]. This 'tumour microenvironment invasion model' could also be useful in understanding the changes occurring during endothelial transmigration as the cell encounters different microenvironments during endothelial binding, transmigration and invasion through the basement membrane. Interactions with endothelial cells and basement membrane may promote different types of cell behaviour and motility.

It is known that leukocytes use amoeboid motility [92] and they also migrate through the endothelium *in vivo*. Although relatively few studies have been done into malignant endothelial transmigration compared to the number into leukocyte transmigration, there are various similarities and differences apparent between the two.

Malignant cells have only been observed using the paracellular route, which seems to be the predominant route used by leukocytes. Both cell types require active interactions with endothelial cells in order for transmigration to occur. There is evidence that cell signalling leads to an increase in endothelial intracellular Ca^{2+} levels which are associated with cytoskeletal alterations that seem to be essential for transmigration. VE-cadherin also disappears from endothelial cell junctions in the region of the transmigrating cell. There is evidence of interactions between the cells via more than one adhesion system during the process.

Differences include the relatively long time it takes for malignant cells to cross the endothelium compared to leukocytes, although some malignant cells have been shown to be capable of transmigration within minutes [163]. The adhesive interactions used may be different, for example leukocyte migration involves PECAM-1, which is not required for melanoma transmigration. Malignant cells produce pronounced endothelial retraction during transmigration in contrast to the minimal endothelial disruption caused by leukocytes. ROCK activity in both leukocytes and endothelial cells is required for transmigration [185] and active Rac1 within endothelial cells is needed for leukocyte transmigration as it promotes cell-cell junction disassembly [186]. Blocking endothelial Rac1 activity prevents leukocyte transmigration [186], but in our system, prostate carcinoma cells continued to migrate through BMEC monolayers in the presence of Rac1 inhibitor.

There appear to be some common mechanisms operating when malignant cells migrate across endothelial monolayers, and there may be some overlap with mechanisms used by migrating leukocytes.

4.3 Summary and future work

The aim of this project was to understand the process of endothelial transmigration with particular reference to malignant prostate cells migrating across the bone marrow endothelium. We have developed an *in vitro* model of prostate carcinoma migration across the bone marrow endothelium and used this to show that prostate carcinoma cells migrate across the endothelial monolayer in a similar way to that observed for melanoma [73], suggesting that there are common mechanisms used by malignant cells to cross endothelial barriers. We have shown that prostate carcinoma cells preferentially use mesenchymal motility to migrate through extracellular matrices, similar to other investigators' findings with breast carcinoma cells [105], and have shown that they preferentially use amoeboid motility to migrate across an endothelial monolayer. This is a new finding. We have also shown that inhibitors of ROCK and myosin II can reduce transmigration through the endothelial cell layer, in agreement with other investigators findings using other malignant cells.

Future work in this area could take several directions. The model system allows the assessment of potential antimetastatic agents by exposing both malignant cells and endothelial cells to them. This simulates the *in vivo* environment in which both cell types would be exposed to a therapeutic drug. This would allow the effectiveness and effective concentration of an agent to be determined and lead to further experiments in more complex systems. The use of a mouse model in conjunction with optical imaging of fluorescent tumour cells would allow the assessment of metastases and potential therapies *in vivo* [120]. Other types of malignant cell could be assessed as it is likely that antimetastatic agents would be effective for more than one tumour given the likelihood that the transmigration process shares common features across tumour types. The inhibitor Y-27632 has shown promise as an antimetastatic agent in animal studies, inhibiting intrahepatic metastasis [187] and transperitoneal dissemination [188] of hepatocellular carcinoma cells and metastasis of PC-3 cells [174]. Other ROCK inhibitors have been developed and are also being used in animal experiments [189] and the comparison of different inhibitors may help to establish the characteristics of the most successful

type of inhibitor. Rho pathways are involved in vascular smooth muscle contraction and Rho-kinase inhibitors have already been investigated for treating cardiovascular disorders [190, 191] such as hypertension and angina, and these drugs may also prove useful as antimetastatic agents. There is a ROCK inhibitor, fasudil, used in humans in Japan to prevent cerebral vasospasm in patients with intracranial haemorrhage [190]. Although no long term studies in humans have yet been carried out, the drug was well tolerated by patients who took it for 4 weeks [190], suggesting that ROCK inhibitors may be potentially useful agents to investigate in the search for antimetastatic therapies. An important aspect of these studies would be the investigation of possible resistance to antimetastatic therapy. Malignant cells have demonstrated their ability to switch between different modes of motility in response to inhibitors and it is thought that this is partly responsible for the disappointing results of mesenchymal motility inhibitors in clinical trials [192]. It may be necessary to use a combination of amoeboid and mesenchymal motility inhibitors to achieve effective long-term reduction in metastasis.

Although this would be a useful technique for developing treatments it is less useful for understanding the factors involved in cell motility and metastasis. In order to learn more about this area, inhibition of pathways in malignant and endothelial cells separately is necessary. This could be done using a siRNA approach similar to that of Sequeira *et al* [178], with inhibition of Rac and Rho in malignant cells, endothelial cells or both. This would assess the contribution of the signalling pathways in endothelial cells to the transmigration process. Inhibition of the different forms of Rho separately would also aid in understanding more about the signalling pathways. The use of blocking antibodies to various cell surface markers would enable the study of the molecules involved in prostate cell binding and signalling to endothelial cells. Endothelial intracellular calcium alterations are important in the transmigration process and the signalling leading to these alterations, as well as the potential inhibition of this process by blocking the Rho pathway would be useful areas for further study. Further work to overcome the problems associated with fluorescent labelling of endothelial cells would enable the fate of endothelial cell-cell junctional proteins during transmigration to be studied. Quantum dots [193, 194], which are nanocrystals with a narrow band, intense fluorescence emission spectrum, may be useful for overcoming these problems by providing a brighter signal. They can be conjugated to antibodies and used in the same way as conventional

fluorophores. All of these techniques could be applied to our *in vitro* system. Animal models could be used in conjunction with a system of conditional ROCK activation in tumour cells such as that used by Croft *et al* [108] to investigate ROCK activity and local invasion in colon carcinoma cells. This system allowed the activation of ROCK in tumour cells by administration of tamoxifen, after the initial establishment of the tumour. A system such as this could be used to assess metastasis formation under conditions of ROCK activation or ROCK knockdown in tumour cells to examine the contribution of tumour cell ROCK to metastasis formation.

Investigating the fate of endothelial junctional proteins during the transmigration process proved unsuccessful due to problems with non-specific antibody staining and autofluorescence of BMEC. It is possible that the use of fluorescent conjugates of junctional proteins such as those used by Shaw *et al* [63] to image leukocyte transmigration would provide more specific fluorescence and allow further study in this area using our cell lines.

5 References

1. CRUK. [cited 2008 19/12/08]; Available from: <http://info.cancerresearchuk.org/cancerstats/types/prostate/incidence/>.
2. CRUK. Feb 2005 [cited 2005 26/04/05]; Available from: <http://info.cancerresearchuk.org/cancerstats/prostate>.
3. Gronberg, H., Prostate cancer epidemiology. *Lancet*, 2003. **361**(9360): p. 859-64.
4. Allaf, M.E. and H.B. Carter, Update on watchful waiting for prostate cancer. *Curr Opin Urol*, 2004. **14**(3): p. 171-5.
5. George, N.J., Natural history of localised prostatic cancer managed by conservative therapy alone. *Lancet*, 1988. **1**(8584): p. 494-7.
6. Carlin, B.I. and G.L. Andriole, The natural history, skeletal complications, and management of bone metastases in patients with prostate carcinoma. *Cancer*, 2000. **88**(12 Suppl): p. 2989-94.
7. Frankel, S., et al., Screening for prostate cancer. *Lancet*, 2003. **361**(9363): p. 1122-8.
8. Tantivejkul, K., L.M. Kalikin, and K.J. Pienta, Dynamic process of prostate cancer metastasis to bone. *J Cell Biochem*, 2004. **91**(4): p. 706-17.
9. Lang, S.H., et al., Interaction of prostate epithelial cells from benign and malignant tumor tissue with bone-marrow stroma. *Prostate*, 1998. **34**(3): p. 203-13.
10. Mundy, G.R., Metastasis to bone: causes, consequences and therapeutic opportunities. *Nat Rev Cancer*, 2002. **2**(8): p. 584-93.
11. Eschwege, P., et al., Haematogenous dissemination of prostatic epithelial cells during radical prostatectomy. *Lancet*, 1995. **346**(8989): p. 1528-30.
12. Arcangeli, G., et al., Prognostic impact of transurethral resection on patients irradiated for localized prostate cancer. *Radiother Oncol*, 1995. **35**(2): p. 123-8.
13. Scott, L.J., et al., Interactions of human prostatic epithelial cells with bone marrow endothelium: binding and invasion. *Br J Cancer*, 2001. **84**(10): p. 1417-23.
14. Romanov, V.I., et al., Prostate cancer cell adhesion to bone marrow endothelium: the role of prostate-specific antigen. *Cancer Res*, 2004. **64**(6): p. 2083-9.
15. Lehr, J.E. and K.J. Pienta, Preferential adhesion of prostate cancer cells to a human bone marrow endothelial cell line. *J Natl Cancer Inst*, 1998. **90**(2): p. 118-23.
16. Lang, S.H., et al., Primary prostatic epithelial cell binding to human bone marrow stroma and the role of alpha2beta1 integrin. *Clin Exp Metastasis*, 1997. **15**(3): p. 218-27.
17. Hart, C.A., et al., Invasive characteristics of human prostatic epithelial cells: understanding the metastatic process. *Br J Cancer*, 2005. **92**(3): p. 503-12.
18. Wang, X., et al., Beta3 integrins facilitate matrix interactions during transendothelial migration of PC3 prostate tumor cells. *Prostate*, 2005. **63**(1): p. 65-80.
19. Sun, Y.X., et al., Expression of CXCR4 and CXCL12 (SDF-1) in human prostate cancers (PCa) in vivo. *J Cell Biochem*, 2003. **89**(3): p. 462-73.
20. Taichman, R.S., et al., Use of the stromal cell-derived factor-1/CXCR4 pathway in prostate cancer metastasis to bone. *Cancer Res*, 2002. **62**(6): p. 1832-7.
21. Engl, T., et al., CXCR4 chemokine receptor mediates prostate tumor cell adhesion through alpha5 and beta3 integrins. *Neoplasia*, 2006. **8**(4): p. 290-301.
22. Burger, M., et al., Functional expression of CXCR4 (CD184) on small-cell lung cancer cells mediates migration, integrin activation, and adhesion to stromal cells. *Oncogene*, 2003. **22**(50): p. 8093-101.
23. Muller, A., et al., Involvement of chemokine receptors in breast cancer metastasis. *Nature*, 2001. **410**(6824): p. 50-6.
24. Sumpio, B.E., J.T. Riley, and A. Dardik, Cells in focus: endothelial cell. *Int J Biochem Cell Biol*, 2002. **34**(12): p. 1508-12.
25. Aird, W.C., Endothelium as an organ system. *Crit Care Med*, 2004. **32**(5 Suppl): p. S271-9.

26. Aird, W.C., Endothelial cell heterogeneity. *Crit Care Med*, 2003. **31**(4 Suppl): p. S221-30.
27. Bazzoni, G. and E. Dejana, Endothelial cell-to-cell junctions: molecular organization and role in vascular homeostasis. *Physiol Rev*, 2004. **84**(3): p. 869-901.
28. Dejana, E., Endothelial cell-cell junctions: happy together. *Nat Rev Mol Cell Biol*, 2004. **5**(4): p. 261-70.
29. Ruffer, C., et al., Cell-cell junctions of dermal microvascular endothelial cells contain tight and adherens junction proteins in spatial proximity. *Biochemistry*, 2004. **43**(18): p. 5360-9.
30. Auerbach, R., et al., Expression of organ-specific antigens on capillary endothelial cells. *Microvasc Res*, 1985. **29**(3): p. 401-11.
31. Springer, T.A., Traffic signals for lymphocyte recirculation and leukocyte emigration: the multistep paradigm. *Cell*, 1994. **76**(2): p. 301-14.
32. McCarthy, S.A., et al., Heterogeneity of the endothelial cell and its role in organ preference of tumour metastasis. *Trends Pharmacol Sci*, 1991. **12**(12): p. 462-7.
33. Ebnet, K., et al., Junctional adhesion molecules (JAMs): more molecules with dual functions? *J Cell Sci*, 2004. **117**(Pt 1): p. 19-29.
34. van Buul, J.D. and P.L. Hordijk, Signaling in leukocyte transendothelial migration. *Arterioscler Thromb Vasc Biol*, 2004. **24**(5): p. 824-33.
35. Stevens, T., et al., Mechanisms regulating endothelial cell barrier function. *Am J Physiol Lung Cell Mol Physiol*, 2000. **279**(3): p. L419-22.
36. Mason, M.D., G. Davies, and W.G. Jiang, Cell adhesion molecules and adhesion abnormalities in prostate cancer. *Crit Rev Oncol Hematol*, 2002. **41**(1): p. 11-28.
37. Mehta, D., p120: the guardian of endothelial junctional integrity. *Am J Physiol Lung Cell Mol Physiol*, 2004. **286**(6): p. L1140-2.
38. Vestweber, D., Regulation of endothelial cell contacts during leukocyte extravasation. *Curr Opin Cell Biol*, 2002. **14**(5): p. 587-93.
39. Muller, W.A., Leukocyte-endothelial-cell interactions in leukocyte transmigration and the inflammatory response. *Trends Immunol*, 2003. **24**(6): p. 327-34.
40. Sandig, M., et al., Role of cadherins in the transendothelial migration of melanoma cells in culture. *Cell Motil Cytoskeleton*, 1997. **38**(4): p. 351-64.
41. Hallmann, R., et al., Expression and function of laminins in the embryonic and mature vasculature. *Physiol Rev*, 2005. **85**(3): p. 979-1000.
42. Inoue, S. and D.G. Osmond, Basement membrane of mouse bone marrow sinusoids shows distinctive structure and proteoglycan composition: a high resolution ultrastructural study. *Anat Rec*, 2001. **264**(3): p. 294-304.
43. Feng, D., et al., Neutrophils emigrate from venules by a transendothelial cell pathway in response to FMLP. *J Exp Med*, 1998. **187**(6): p. 903-15.
44. Rosen, S.D., Ligands for L-selectin: homing, inflammation, and beyond. *Annu Rev Immunol*, 2004. **22**: p. 129-56.
45. Price, E.A., D.R. Coombe, and J.C. Murray, beta-1 Integrins mediate tumour cell adhesion to quiescent endothelial cells in vitro. *Br J Cancer*, 1996. **74**(11): p. 1762-6.
46. Glinskii, O.V., et al., Continuous real time ex vivo epifluorescent video microscopy for the study of metastatic cancer cell interactions with microvascular endothelium. *Clin Exp Metastasis*, 2003. **20**(5): p. 451-8.
47. Dimitroff, C.J., et al., Rolling of human bone-metastatic prostate tumor cells on human bone marrow endothelium under shear flow is mediated by E-selectin. *Cancer Res*, 2004. **64**(15): p. 5261-9.
48. Cooper, C.R., et al., Preferential adhesion of prostate cancer cells to bone is mediated by binding to bone marrow endothelial cells as compared to extracellular matrix components in vitro. *Clin Cancer Res*, 2000. **6**(12): p. 4839-47.

49. Haq, M., et al., Rat prostate adenocarcinoma cells disseminate to bone and adhere preferentially to bone marrow-derived endothelial cells. *Cancer Res*, 1992. **52**(17): p. 4613-9.
50. Cooper, C.R., et al., Stromal factors involved in prostate carcinoma metastasis to bone. *Cancer*, 2003. **97**(3 Suppl): p. 739-47.
51. Romanov, V.I. and M.S. Goligorsky, RGD-recognizing integrins mediate interactions of human prostate carcinoma cells with endothelial cells in vitro. *Prostate*, 1999. **39**(2): p. 108-18.
52. Cooper, C.R., et al., The regulation of prostate cancer cell adhesion to human bone marrow endothelial cell monolayers by androgen dihydrotestosterone and cytokines. *Clin Exp Metastasis*, 2002. **19**(1): p. 25-33.
53. Orr, F.W., et al., Interactions between cancer cells and the endothelium in metastasis. *J Pathol*, 2000. **190**(3): p. 310-29.
54. Fornaro, M., T. Manes, and L.R. Languino, Integrins and prostate cancer metastases. *Cancer Metastasis Rev*, 2001. **20**(3-4): p. 321-31.
55. Friedl, P. and K. Wolf, Tumour-cell invasion and migration: diversity and escape mechanisms. *Nat Rev Cancer*, 2003. **3**(5): p. 362-74.
56. Hood, J.D. and D.A. Cheresh, Role of integrins in cell invasion and migration. *Nat Rev Cancer*, 2002. **2**(2): p. 91-100.
57. Yao, E.S., et al., Increased beta1 integrin is associated with decreased survival in invasive breast cancer. *Cancer Res*, 2007. **67**(2): p. 659-64.
58. Slack-Davis, J.K. and J.T. Parsons, Emerging views of integrin signaling: implications for prostate cancer. *J Cell Biochem*, 2004. **91**(1): p. 41-6.
59. Seftor, R.E., et al., Role of the alpha v beta 3 integrin in human melanoma cell invasion. *Proc Natl Acad Sci U S A*, 1992. **89**(5): p. 1557-61.
60. Mizejewski, G.J., Role of integrins in cancer: survey of expression patterns. *Proc Soc Exp Biol Med*, 1999. **222**(2): p. 124-38.
61. Haywood-Reid, P.L., D.R. Zipf, and W.R. Springer, Quantification of integrin subunits on human prostatic cell lines--comparison of nontumorigenic and tumorigenic lines. *Prostate*, 1997. **31**(1): p. 1-8.
62. Sobel, R.E. and M.D. Sadar, Cell lines used in prostate cancer research: a compendium of old and new lines--part 1. *J Urol*, 2005. **173**(2): p. 342-59.
63. Shaw, S.K., et al., Real-time imaging of vascular endothelial-cadherin during leukocyte transmigration across endothelium. *J Immunol*, 2001. **167**(4): p. 2323-30.
64. Engelhardt, B. and H. Wolburg, Mini-review: Transendothelial migration of leukocytes: through the front door or around the side of the house? *Eur J Immunol*, 2004. **34**(11): p. 2955-63.
65. Sandig, M., E. Negrou, and K.A. Rogers, Changes in the distribution of LFA-1, catenins, and F-actin during transendothelial migration of monocytes in culture. *J Cell Sci*, 1997. **110** (Pt 22): p. 2807-18.
66. Yadav, R., et al., Migration of leukocytes through the vessel wall and beyond. *Thromb Haemost*, 2003. **90**(4): p. 598-606.
67. Del Maschio, A., et al., Polymorphonuclear leukocyte adhesion triggers the disorganization of endothelial cell-to-cell adherens junctions. *J Cell Biol*, 1996. **135**(2): p. 497-510.
68. Lorenzon, P., et al., Endothelial cell E- and P-selectin and vascular cell adhesion molecule-1 function as signaling receptors. *J Cell Biol*, 1998. **142**(5): p. 1381-91.
69. Huang, A.J., et al., Endothelial cell cytosolic free calcium regulates neutrophil migration across monolayers of endothelial cells. *J Cell Biol*, 1993. **120**(6): p. 1371-80.
70. Hixenbaugh, E.A., et al., Stimulated neutrophils induce myosin light chain phosphorylation and isometric tension in endothelial cells. *Am J Physiol*, 1997. **273**(2 Pt 2): p. H981-8.

71. Saito, H., et al., Endothelial myosin light chain kinase regulates neutrophil migration across human umbilical vein endothelial cell monolayer. *J Immunol*, 1998. **161**(3): p. 1533-40.
72. Voura, E.B., et al., Cell shape changes and cytoskeleton reorganization during transendothelial migration of human melanoma cells. *Cell Tissue Res*, 1998. **293**(3): p. 375-87.
73. Voura, E.B., M. Sandig, and C.H. Siu, Cell-cell interactions during transendothelial migration of tumor cells. *Microsc Res Tech*, 1998. **43**(3): p. 265-75.
74. Ito, A., et al., A role for heterologous gap junctions between melanoma and endothelial cells in metastasis. *J Clin Invest*, 2000. **105**(9): p. 1189-97.
75. el-Sabban, M.E. and B.U. Pauli, Cytoplasmic dye transfer between metastatic tumor cells and vascular endothelium. *J Cell Biol*, 1991. **115**(5): p. 1375-82.
76. Voura, E.B., N. Chen, and C.H. Siu, Platelet-endothelial cell adhesion molecule-1 (CD31) redistributes from the endothelial junction and is not required for the transendothelial migration of melanoma cells. *Clin Exp Metastasis*, 2000. **18**(6): p. 527-32.
77. Bogenrieder, T. and M. Herlyn, Axis of evil: molecular mechanisms of cancer metastasis. *Oncogene*, 2003. **22**(42): p. 6524-36.
78. Mareel, M. and A. Leroy, Clinical, cellular, and molecular aspects of cancer invasion. *Physiol Rev*, 2003. **83**(2): p. 337-76.
79. Voura, E.B., et al., Involvement of integrin $\alpha(v)\beta(3)$ and cell adhesion molecule L1 in transendothelial migration of melanoma cells. *Mol Biol Cell*, 2001. **12**(9): p. 2699-710.
80. Gavert, N., et al., L1, a novel target of beta-catenin signaling, transforms cells and is expressed at the invasive front of colon cancers. *J Cell Biol*, 2005. **168**(4): p. 633-42.
81. Lewalle, J.M., et al., Endothelial cell intracellular Ca^{2+} concentration is increased upon breast tumor cell contact and mediates tumor cell transendothelial migration. *Clin Exp Metastasis*, 1998. **16**(1): p. 21-9.
82. Lewalle, J.M., et al., Alteration of interendothelial adherens junctions following tumor cell-endothelial cell interaction in vitro. *Exp Cell Res*, 1997. **237**(2): p. 347-56.
83. Saiki, I., et al., Functional role of sialyl Lewis X and fibronectin-derived RGDS peptide analogue on tumor-cell arrest in lungs followed by extravasation. *Int J Cancer*, 1996. **65**(6): p. 833-9.
84. Bauer, K., C. Mierke, and J. Behrens, Expression profiling reveals genes associated with transendothelial migration of tumor cells: a functional role for $\alpha v \beta 3$ integrin. *Int J Cancer*, 2007. **121**(9): p. 1910-8.
85. Nakamori, S., et al., Increased endothelial cell retraction and tumor cell invasion by soluble factors derived from pancreatic cancer cells. *Ann Surg Oncol*, 1997. **4**(4): p. 361-8.
86. Tremblay, P.L., F.A. Auger, and J. Huot, Regulation of transendothelial migration of colon cancer cells by E-selectin-mediated activation of p38 and ERK MAP kinases. *Oncogene*, 2006. **25**(50): p. 6563-73.
87. Pili, R., et al., Endothelial cell Ca^{2+} increases upon tumor cell contact and modulates cell-cell adhesion. *J Clin Invest*, 1993. **92**(6): p. 3017-22.
88. Sikes, R.A., et al., Cellular interactions in the tropism of prostate cancer to bone. *Int J Cancer*, 2004. **110**(4): p. 497-503.
89. Edlund, M., S.Y. Sung, and L.W. Chung, Modulation of prostate cancer growth in bone microenvironments. *J Cell Biochem*, 2004. **91**(4): p. 686-705.
90. Hart, C.A., et al., Role of proteolytic enzymes in human prostate bone metastasis formation: in vivo and in vitro studies. *Br J Cancer*, 2002. **86**(7): p. 1136-42.
91. Wolf, K., Friedl, P., Molecular mechanisms of cancer cell invasion and plasticity. *Br J Dermatol*, 2006. **154**(Suppl 1): p. 11-15.

92. Friedl, P., *Prespecification and plasticity: shifting mechanisms of cell migration.* *Curr Opin Cell Biol*, 2004. **16**(1): p. 14-23.
93. Niggemann, B., et al., *Tumor cell locomotion: differential dynamics of spontaneous and induced migration in a 3D collagen matrix.* *Exp Cell Res*, 2004. **298**(1): p. 178-87.
94. Charras, G.T., et al., *Reassembly of contractile actin cortex in cell blebs.* *J Cell Biol*, 2006. **175**(3): p. 477-90.
95. Wang, W., et al., *Tumor cells caught in the act of invading: their strategy for enhanced cell motility.* *Trends Cell Biol*, 2005. **15**(3): p. 138-45.
96. Hegerfeldt, Y., et al., *Collective cell movement in primary melanoma explants: plasticity of cell-cell interaction, beta1-integrin function, and migration strategies.* *Cancer Res*, 2002. **62**(7): p. 2125-30.
97. Sahai, E., *Mechanisms of cancer cell invasion.* *Curr Opin Genet Dev*, 2005. **15**(1): p. 87-96.
98. Kirfel, G., Rigort, A., Borm, B., Herzog, V., *Cell migration: mechanisms of rear detachment and the formation of migration tracks.* *Eur J Cell Biol*, 2004. **83**: p. 717-724.
99. Sahai, E. and C.J. Marshall, *Differing modes of tumour cell invasion have distinct requirements for Rho/ROCK signalling and extracellular proteolysis.* *Nat Cell Biol*, 2003. **5**(8): p. 711-9.
100. Wyckoff, J.B., et al., *ROCK- and myosin-dependent matrix deformation enables protease-independent tumor-cell invasion in vivo.* *Curr Biol*, 2006. **16**(15): p. 1515-23.
101. Yoshida, K. and T. Soldati, *Dissection of amoeboid movement into two mechanically distinct modes.* *J Cell Sci*, 2006. **119**(Pt 18): p. 3833-44.
102. Coleman, M.L., et al., *Membrane blebbing during apoptosis results from caspase-mediated activation of ROCK I.* *Nat Cell Biol*, 2001. **3**(4): p. 339-45.
103. Kamai, T., et al., *Significant association of Rho/ROCK pathway with invasion and metastasis of bladder cancer.* *Clin Cancer Res*, 2003. **9**(7): p. 2632-41.
104. Carragher, N.O., et al., *Calpain 2 and Src dependence distinguishes mesenchymal and amoeboid modes of tumour cell invasion: a link to integrin function.* *Oncogene*, 2006. **25**(42): p. 5726-40.
105. Torka, R., et al., *ROCK signaling mediates the adoption of different modes of migration and invasion in human mammary epithelial tumor cells.* *Exp Cell Res*, 2006. **312**(19): p. 3857-71.
106. Zuo, Y., S.K. Shields, and C. Chakraborty, *Enhanced intrinsic migration of aggressive breast cancer cells by inhibition of Rac1 GTPase.* *Biochem Biophys Res Commun*, 2006. **351**(2): p. 361-7.
107. Sherwood, D.R., *Cell invasion through basement membranes: an anchor of understanding.* *Trends Cell Biol*, 2006. **16**(5): p. 250-6.
108. Croft, D.R., et al., *Conditional ROCK activation in vivo induces tumor cell dissemination and angiogenesis.* *Cancer Res*, 2004. **64**(24): p. 8994-9001.
109. Yang, J. and R.A. Weinberg, *Epithelial-mesenchymal transition: at the crossroads of development and tumor metastasis.* *Dev Cell*, 2008. **14**(6): p. 818-29.
110. Lou, Y., et al., *Epithelial-mesenchymal transition (EMT) is not sufficient for spontaneous murine breast cancer metastasis.* *Dev Dyn*, 2008. **237**(10): p. 2755-68.
111. Entschladen, F., et al., *Analysis methods of human cell migration.* *Exp Cell Res*, 2005. **307**(2): p. 418-26.
112. Pinner, S. and E. Sahai, *Imaging amoeboid cancer cell motility in vivo.* *J Microsc*, 2008. **231**(3): p. 441-5.
113. Ghajar, C.M., et al., *A novel three-dimensional model to quantify metastatic melanoma invasion.* *Mol Cancer Ther*, 2007. **6**(2): p. 552-61.
114. Barrett, J.M., et al., *Bi-directional interactions of prostate cancer cells and bone marrow endothelial cells in three-dimensional culture.* *Prostate*, 2005.

115. Kim, J.B., *Three-dimensional tissue culture models in cancer biology*. *Semin Cancer Biol*, 2005. **15**: p. 365-377.
116. Sehgal, L.R., et al., *Novel in vitro perfusion model to study the interaction between coagulation and blood-borne metastasis*. *J Cell Biochem*, 2005. **96**(4): p. 700-8.
117. Nitz, M.D., Harding, M.A., Theodorescu, D., *Invasion and metastasis models for studying RhoGDI2 in bladder cancer*. *Methods in Enzymology*, 2008. **439**: p. 219-233.
118. Ahmad, I., O.J. Sansom, and H.Y. Leung, *Advances in mouse models of prostate cancer*. *Expert Rev Mol Med*, 2008. **10**: p. e16.
119. Khanna, C. and K. Hunter, *Modeling metastasis in vivo*. *Carcinogenesis*, 2005. **26**(3): p. 513-23.
120. Henriquez, N.V., et al., *Advances in optical imaging and novel model systems for cancer metastasis research*. *Clin Exp Metastasis*, 2007. **24**(8): p. 699-705.
121. Kaijzel, E.L., Snoeks, T. A. J., Buijs, J. T., van der Pluijm, G., Lowick, C. W. G. M., *Multimodal imaging and treatment of bone metastasis*. *Clin Exp Metastasis*, 2008 E-Pub ahead of print.
122. Wetterwald, A., van der Pluijm, G., Que, I., Sijmons, B., Buijs, J., Karperien, M., Lowick, C. W. G. M., Gautschi, E., Thalmann, G. N., Cecchini, M. G., *Optical imaging of cancer metastases to bone marrow: a mouse model of minimal residual disease*. *Am J Pathol*, 2002. **160**: p. 1143-1153.
123. Hell, S.W., *Toward fluorescence nanoscopy*. *Nat Biotechnol*, 2003. **21**(11): p. 1347-1355.
124. Allen, T.D. and M.W. Goldberg, *High-resolution SEM in cell biology*. *Trends Cell Biol*, 1993. **3**(6): p. 205-8.
125. Erlandsen, S.L., S.R. Hasslen, and R.D. Nelson, *Detection and spatial distribution of the beta 2 integrin (Mac-1) and L-selectin (LECAM-1) adherence receptors on human neutrophils by high-resolution field emission SEM*. *J Histochem Cytochem*, 1993. **41**(3): p. 327-33.
126. Kramer, R.H. and G.L. Nicolson, *Interactions of tumor cells with vascular endothelial cell monolayers: a model for metastatic invasion*. *Proc Natl Acad Sci U S A*, 1979. **76**(11): p. 5704-8.
127. Kaighn, M.E., et al., *Establishment and characterization of a human prostatic carcinoma cell line (PC-3)*. *Invest Urol*, 1979. **17**: p. 16-23.
128. Sharrard, R.M. and N.J. Maitland, *Phenotypic effects of overexpression of the MMAC1 gene in prostate epithelial cells*. *Br J Cancer*, 2000. **83**(8): p. 1102-1109.
129. Berthon, P., et al., *Functional expression of SV40 in normal prostatic epithelial and fibroblastic cells: differentiation pattern of non-tumourigenic cell lines*. *Int J Oncol*, 1995. **6**: p. 333-343.
130. Almeida-Porada, G. and J.L. Ascensao, *Isolation, characterization, and biologic features of bone marrow endothelial cells*. *J Lab Clin Med*, 1996. **128**: p. 399-407.
131. Coutinho, L.H., et al., *Clonal and long-term cultures using human bone marrow, in Haemopoiesis: a practical approach*, N.G. Testa and G. Molineux, Editors. 1993, Oxford University Press: Oxford.
132. Masek, L.C. and J.W. Sweetenham, *Isolation and culture of endothelial cells from human bone marrow*. *Br J Haematol*, 1994. **88**(4): p. 855-65.
133. Allen, T.D., *Time lapse video microscopy using an animation control unit*. *J Microsc*, 1987. **147** (Pt 2): p. 129-35.
134. Flegler, S.L., J.W. Heckman Jr, and K.L. Klomparens, *Scanning and transmission electron microscopy: an introduction*. 1993, New York: Oxford University Press.
135. Morita, K., et al., *Endothelial claudin: claudin-5/TMVCF constitutes tight junction strands in endothelial cells*. *J Cell Biol*, 1999. **147**(1): p. 185-94.
136. Rood, P.M., et al., *Immortalisation of human bone marrow endothelial cells: characterisation of new cell lines*. *Eur J Clin Invest*, 2000. **30**(7): p. 618-29.

137. Candal, F.J., Rafii, S., Parker, J. T., Ades, E. W., Ferris, B., Nachman, R. L., Kellar, K. L., *BMEC-1: a human bone marrow microvascular endothelial cell line with primary cell characteristics. Microvasc Res*, 1996. **52**: p. 221-234.
138. Schweitzer, C.M., et al., Isolation and culture of human bone marrow endothelial cells. *Exp Hematol*, 1995. **23**(1): p. 41-8.
139. Kieda, C., Paprocka, M., Krawczyński, A., Zalecki, P., Dupuis, P., Monsigny, M., Radzikowski, C., Dus, D., New human microvascular endothelial cell lines with specific adhesion molecules phenotypes. *Endothelium*, 2002. **9**: p. 247-261.
140. Hooper, S., J.F. Marshall, and E. Sahai, Tumor cell migration in three dimensions. *Methods Enzymol*, 2006. **406**: p. 625-43.
141. Kleinman, H.K., Martin, G.R., Matrigel: basement membrane matrix with biological activity. *Semin Cancer Biol*, 2005. **15**: p. 378-386.
142. Okada, T., H. Okuno, and Y. Mitsui, A novel in vitro assay system for transendothelial tumor cell invasion: significance of E-selectin and alpha 3 integrin in the transendothelial invasion by HT1080 fibrosarcoma cells. *Clin Exp Metastasis*, 1994. **12**(4): p. 305-14.
143. Heyder, C., et al., Realtime visualization of tumor cell/endothelial cell interactions during transmigration across the endothelial barrier. *J Cancer Res Clin Oncol*, 2002. **128**(10): p. 533-8.
144. Tran, N.L., et al., N-Cadherin expression in human prostate carcinoma cell lines. An epithelial-mesenchymal transformation mediating adhesion with Stromal cells. *Am J Pathol*, 1999. **155**(3): p. 787-98.
145. Birgersdotter, A., R. Sandberg, and I. Ernberg, Gene expression perturbation in vitro--a growing case for three-dimensional (3D) culture systems. *Semin Cancer Biol*, 2005. **15**(5): p. 405-12.
146. Yu, D., et al., c-erbB-2/neu overexpression enhances metastatic potential of human lung cancer cells by induction of metastasis-associated properties. *Cancer Res*, 1994. **54**(12): p. 3260-6.
147. Malliri, A. and J.G. Collard, Role of Rho-family proteins in cell adhesion and cancer. *Curr Opin Cell Biol*, 2003. **15**: p. 583-589.
148. Yamazaki, D., S. Kurisu, and T. Takenawa, Regulation of cancer cell motility through actin reorganization. *Cancer Sci*, 2005. **96**(7): p. 379-86.
149. Wolf, K., et al., Compensation mechanism in tumor cell migration: mesenchymal-amoeboid transition after blocking of pericellular proteolysis. *J Cell Biol*, 2003. **160**(2): p. 267-77.
150. Yong, K.L., et al., Influence of cell cycling and cell division on transendothelial migration of CD34+ cells. *Br J Haematol*, 2002. **119**(2): p. 500-9.
151. Pidgeon, G.P., et al., Overexpression of platelet-type 12-lipoxygenase promotes tumor cell survival by enhancing alpha(v)beta(3) and alpha(v)beta(5) integrin expression. *Cancer Res*, 2003. **63**(14): p. 4258-67.
152. Garlanda, C. and E. Dejana, Heterogeneity of endothelial cells. Specific markers. *Arterioscler Thromb Vasc Biol*, 1997. **17**(7): p. 1193-202.
153. Terramani, T.T., et al., Human macrovascular endothelial cells: optimization of culture conditions. *In Vitro Cell Dev Biol Anim*, 2000. **36**(2): p. 125-32.
154. Maciag, T., G.A. Hoover, and R. Weinstein, High and low molecular weight forms of endothelial cell growth factor. *J Biol Chem*, 1982. **257**(10): p. 5333-5336.
155. Maciag, T., et al., An endothelial cell growth factor from bovine hypothalamus: identification and partial characterization. *Proc Natl Acad Sci U S A*, 1979. **76**(11): p. 5674-5678.
156. Burns, A.R., et al., Analysis of tight junctions during neutrophil transendothelial migration. *J Cell Sci*, 2000. **113** (Pt 1): p. 45-57.
157. Rafii, S., et al., Isolation and characterization of human bone marrow microvascular endothelial cells: haematopoietic progenitor cell adhesion. *Blood*, 1994. **84**(1): p. 10-19.

158. Chuitmans, F.H.M., et al., Constitutive in vivo cytokine and hematopoietic growth factor gene expression in the bone marrow and peripheral blood of healthy individuals. *Blood*, 1995. **85**(8): p. 2038-2044.
159. Schweitzer, K.M., et al., Characterization of a newly established human bone marrow endothelial cell line: distinct adhesive properties for hematopoietic progenitors compared with human umbilical vein endothelial cells. *Lab Invest*, 1997. **76**(1): p. 25-36.
160. Koenig, A.L., V. Gambillara, and D.W. Grainger, Correlating fibronectin adsorption with endothelial cell adhesion and signaling on polymer substrates. *J Biomed Mater Res A*, 2003. **64**(1): p. 20-37.
161. Unger, R.E., et al., In vitro expression of the endothelial phenotype: comparative study of primary isolated cells and cell lines, including the novel cell line HPMEC-ST1.6R. *Microvasc Res*, 2002. **64**(3): p. 384-97.
162. van Gorp, R.M.A., et al., Glutathione oxidation in calcium and p38 MAPK-dependent membrane blebbing of endothelial cells. *Biochim Biophys Acta*, 2002. **1591**: p. 129-138.
163. Miles, F.L., et al., Stepping out of the flow: capillary extravasation in cancer metastasis. *Clin Exp Metastasis*, 2008. **25**(4): p. 305-24.
164. Shaw, S.K., et al., Coordinated redistribution of leukocyte LFA-1 and endothelial cell ICAM-1 accompany neutrophil transmigration. *J Exp Med*, 2004. **200**(12): p. 1571-80.
165. De Bruyn, P.P. and Y. Cho, Vascular endothelial invasion via transcellular passage by malignant cells in the primary stage of metastases formation. *J Ultrastruct Res*, 1982. **81**(2): p. 189-201.
166. Qi, J., et al., Transendothelial Migration of Melanoma Cells Involves N-Cadherin-mediated Adhesion and Activation of the {beta}-Catenin Signaling Pathway. *Mol Biol Cell*, 2005. **16**(9): p. 4386-97.
167. Khatib, A.M., et al., Rapid induction of cytokine and E-selectin expression in the liver in response to metastatic tumor cells. *Cancer Res*, 1999. **59**(6): p. 1356-61.
168. Cunningham, C.C., Actin polymerization and intracellular solvent flow in cell surface blebbing. *J Cell Biol*, 1995. **129**(6): p. 1589-99.
169. Paluch, E., et al., Dynamic modes of the cortical actomyosin gel during cell locomotion and division. *Trends Cell Biol*, 2006. **16**(1): p. 5-10.
170. Di Bella, M.A., et al., Different phenotypes of colon carcinoma cells interacting with endothelial cells: role of E-selectin and ultrastructural data. *Cell Tissue Res*, 2003. **312**(1): p. 55-64.
171. Leroy-Dudal, J., et al., Transmigration of human ovarian adenocarcinoma cells through endothelial extracellular matrix involves alphav integrins and the participation of MMP2. *Int J Cancer*, 2005. **114**(4): p. 531-43.
172. Kebers, F., et al., Induction of endothelial cell apoptosis by solid tumor cells. *Exp Cell Res*, 1998. **240**(2): p. 197-205.
173. Brandt, B., et al., 3D-extravasation model -- selection of highly motile and metastatic cancer cells. *Semin Cancer Biol*, 2005. **15**(5): p. 387-95.
174. Somlyo, A.V., et al., Rho-kinase inhibitor retards migration and in vivo dissemination of human prostate cancer cells. *Biochem Biophys Res Commun*, 2000. **269**(3): p. 652-9.
175. Yao, H., et al., RhoC GTPase is required for PC-3 prostate cancer cell invasion but not motility. *Oncogene*, 2006. **25**(16): p. 2285-96.
176. Duxbury, M.S., S.W. Ashley, and E.E. Whang, Inhibition of pancreatic adenocarcinoma cellular invasiveness by blebbistatin: a novel myosin II inhibitor. *Biochem Biophys Res Commun*, 2004. **313**(4): p. 992-7.
177. Gao, Y., et al., Rational design and characterization of a Rac GTPase-specific small molecule inhibitor. *Proc Natl Acad Sci U S A*, 2004. **101**(20): p. 7618-23.
178. Sequeira, L., et al., Rho GTPases in PC-3 prostate cancer cell morphology, invasion and tumor cell diapedesis. *Clin Exp Metastasis*, 2008. **25**(5): p. 569-79.

179. Nakajima, M., Katayama, K., Tamechika, I., Hayashi, K., Amano, Y., Uehata, M., Goto, N., Kondo, T., *WF-536 inhibits metastatic invasion by enhancing the host cell barrier and inhibiting tumour cell motility. Clin Exp Metastasis*, 2003. **30**: p. 457-463.
180. Li, B., et al., *Involvement of Rho/ROCK signalling in small cell lung cancer migration through human brain microvascular endothelial cells. FEBS Lett*, 2006. **580**(17): p. 4252-60.
181. Deryugina, E.I. and J.P. Quigley, *Matrix metalloproteinases and tumor metastasis. Cancer Metastasis Rev*, 2006. **25**(1): p. 9-34.
182. Wang, W., et al., *Inhibition of invasion and metastasis of hepatocellular carcinoma cells via targeting RhoC in vitro and in vivo. Clin Cancer Res*, 2008. **14**(21): p. 6804-12.
183. Darenfed, H., et al., *Molecular characterization of the effects of Y-27632. Cell Motil Cytoskeleton*, 2007. **64**(2): p. 97-109.
184. Fryer, B.H., Field, J., *Rho, Rac, Pak and angiogenesis: old roles and newly identified responsibilities in endothelial cells. Cancer Lett*, 2005. **229**: p. 13-23.
185. Sahai, E. and C.J. Marshall, *RHO-GTPases and cancer. Nat Rev Cancer*, 2002. **2**(2): p. 133-42.
186. Wittchen, E.S., et al., *Trading spaces: Rap, Rac, and Rho as architects of transendothelial migration. Curr Opin Hematol*, 2005. **12**(1): p. 14-21.
187. Takamura, M., et al., *Inhibition of intrahepatic metastasis of human hepatocellular carcinoma by Rho-associated protein kinase inhibitor Y-27632. Hepatology*, 2001. **33**(3): p. 577-81.
188. Itoh, K., et al., *An essential part for Rho-associated kinase in the transcellular invasion of tumor cells. Nat Med*, 1999. **5**(2): p. 221-5.
189. Nakajima, M., et al., *Effect of Wf-536, a novel ROCK inhibitor, against metastasis of B16 melanoma. Cancer Chemother Pharmacol*, 2003. **52**(4): p. 319-24.
190. Hirooka, Y. and H. Shimokawa, *Therapeutic potential of rho-kinase inhibitors in cardiovascular diseases. Am J Cardiovasc Drugs*, 2005. **5**(1): p. 31-9.
191. Kast, R., et al., *Cardiovascular effects of a novel potent and highly selective azaindole-based inhibitor of Rho-kinase. Br J Pharmacol*, 2007. **152**(7): p. 1070-80.
192. Zucker, S., Cao, J., Chen, W-T., *Critical appraisal of the use of matrix metalloproteinase inhibitors in cancer treatment. Oncogene*, 2000. **19**: p. 6642-6650.
193. Voura, E.B., et al., *Tracking metastatic tumor cell extravasation with quantum dot nanocrystals and fluorescence emission-scanning microscopy. Nat Med*, 2004. **10**(9): p. 993-8.
194. Nisman, R., et al., *Application of quantum dots as probes for correlative fluorescence, conventional, and energy-filtered transmission electron microscopy. J Histochem Cytochem*, 2004. **52**(1): p. 13-8.

6 Appendix: video clips and animations

Video clips and animations are supplied as PowerPoint presentations and as mpg or avi files on the DVD. Clips within PowerPoint will start playing when the picture is clicked. Video clip files are all within the same folder and can also be played in Windows media player, Apple QuickTime player etc. Section numbers associated with clips refer to the corresponding sections in the report and still frames from the clips and animations are also in the corresponding sections.

Section 3.2. Characterisation of cell lines

- Clips 1-5 PC-3 cells cultured in HAMS F12
- Clips 6-9 PC-3-GFP cells cultured in HAMS F12
- Clips 10-16 PC-3 cells cultured in BMSCM
- Clips 17-20 PC-3-GFP cells cultured in BMSCM

Section 3.3. BMEC culture optimisation and characterisation

- Clips 21-23 BMEC cultured in M199
- Clips 24-27 BMEC cultured in BMSCM
- Clips 28-29 Primary human bone marrow endothelial cells cultured in BMSCM

Section 3.4. Co-culture studies

- Clips 30-36 Time lapse invasion study using PC-3 cells
- Clips 37-41 Time lapse invasion study using PC-3-GFP cells
- Clips 42-43 Time lapse study using PNT2-C2 cells
- Clips 44-48 Confocal invasion study using PC-3-GFP cells
- Clip 49 Transwell chamber confocal invasion using PC-3-GFP cells

Section 3.5. Inhibitor studies

- Clips 50-54 PC-3 and PC-3-GFP cells with Y-27632
- Clips 55-58 PC-3 and PC-3-GFP cells with blebbistatin
- Clips 59-60 PC-3 and PC-3-GFP cells with Rac1 inhibitor
- Clips 61-62 PC-3 and PC-3-GFP cells with GM6001
- Clips 63-66 BMEC with all inhibitors
- Clips 67-70 BMEC with Y-27632 and PC-3 or PC-3-GFP cells
- Clips 71-75 BMEC with blebbistatin and PC-3 or PC-3-GFP cells
- Clips 76-77 BMEC with Rac1 inhibitor and PC-3 or PC-3-GFP cells
- Clips 78-79 BMEC with GM6001 and PC-3 or PC-3-GFP cells